Non-alcoholic steatohepatitis with fibrosis in diabetes: clinical exploration and targeting CCN family members in a pre-clinical rodent model

Sarah Nicole Parry

BSc (Hons I) MBBS FRACP

A thesis submitted in fulfilment of the requirements for the degree of Doctor of Philosophy

Sydney Medical School

Faculty of Medicine and Health

The University of Sydney

2023

CULTURAL CARE WARNING NOTICE

Cultural advice
This item may contain culturally sensitive information.

All users are advised that this item may contain images, voices and/or names of people who have died.

Indigenous Cultural and Intellectual Property
This item may contain Indigenous Cultural and Intellectual Property. Please consult with the relevant communities if you wish to use any of the content in this item.

Copyright

Table of Contents

Declaration

This is to certify that to the best of my knowledge, the content of this thesis is my own work. This thesis has not been submitted for any degree or other purposes.

I certify that the intellectual content of this thesis is the product of my own work and that all the assistance received in preparing this thesis and sources have been acknowledged.

Sarah N Parry

Author Attribution Statement

Data from Chapter 3 of this thesis was submitted as an RACP Advanced Training research project.

I assisted with the design of the study, I retrieved and analysed the data, and I wrote the drafts of the MS.

As supervisor for the candidature upon which this thesis is based, I can confirm that the authorship attribution statements above are correct.

Professor Stephen M Twigg

18th July 2023

Acknowledgements

For John and Senthil

Firstly, thank you to Professor Stephen Twigg, my primary supervisor and mentor, for the support and encouragement that he has provided me during my PhD years and more broadly as an Endocrinology Advanced Trainee and then Consultant Endocrinologist. His vast knowledge, expertise, and dedication to patient care, inspire me to become a better researcher and a better clinician. Thank you to my two associate supervisors: thank you to Dr Xiaoyu Wang for her invaluable support inside the laboratory, and for her friendship and kindness outside of it; thank you to Associate Professor Paul Williams, for his astute feedback and insightful ideas. I am very grateful for the great deal of time that each supervisor has dedicated to providing guidance and direction, assisting with troubleshooting, and reviewing and editing my thesis.

I also acknowledge the rest of the staff and students from the Greg Brown Diabetes and Endocrinology Research Laboratory, and especially Dr Danqing Min for her hard work as the Laboratory Manager. I am grateful to Professor Andrew Leask, for his generous donation of the CCN2/CCN1 floxed mice, from which Dr Wang skilfully generated the knockout mice used in this thesis.

I thank others who have contributed to this thesis including Dr Min Li Huang, who assisted with analysis of the mouse liver histology, Associate Professor Kathryn Williams, the original researcher of The DaSH Study, and Mr Kyle Lloyd, who performed some laboratory analyses within The DaSH Study. I thank the staff and patients who were involved in The DLC Audit and The DaSH Study. I am also grateful for the use of the following facilities within The University of Sydney: the CPC Laboratory Animal Services, the CPC histology laboratory, the Sydney Microscopy & Microanalysis facility, the CPC Pre-Clinical Imaging Facility, and the Sydney University Glycaemic Index Research Service.

Finally, thank you to my family and friends for always being there for me, for celebrating my achievements, and for laughing with me over my failures. I am especially grateful to my parents, Ruby and Norman, for always encouraging me to follow my dreams, and to my sister, Susan, for being my number one supporter.

Conference Presentations

Parry SN*, Wang X, Min D, Huang M, Williams PF, Leask A and Twigg SM. Hepatocyte-specific CCN1 gene deletion exacerbates the severity of NASH fibrosis in an established mouse model of high fat feeding and diabetes.
Conference: 58th Annual Meeting, European Association for the Study of Diabetes. Stockholm, Sweden, 2022. Short oral presentation.

Parry SN*, Wang X, Min D, Williams PF, Leask A and Twigg SM. Hepatocyte-specific CCN1 gene deletion worsens NASH fibrosis in a mouse model of high fat feeding and diabetes. (Finalist, Pincus Taft Young Investigator Award)
Conference: Australasian Diabetes Congress. Virtual meeting, 2021. Oral presentation.

Parry SN*, Wang X, Lloyd KWW, Gorrell MD, Williams KH and Twigg SM. Circulating CCN proteins as potential biomarkers in diabetes-related complications.
Conference: Australasian Diabetes Congress. Virtual meeting, 2021. Poster presentation.

Parry SN*, Wang X, Min D, Lourdesamy JS, Williams PF, Leask A and Twigg SM. Hepatocyte-specific CCN2 gene deletion prevents NASH fibrosis in a mouse model of high fat feeding and diabetes.
Conference: 81st Scientific Sessions, American Diabetes Association. Virtual meeting, 2021. Oral presentation.

Parry SN*, Wang X, Min D, Lourdesamy JS, Leask A, Williams PF and Twigg SM. Effects of hepatocyte specific CCN2 gene deletion on NASH fibrosis in a mouse model of high fat feeding and diabetes. (Finalist, Pincus Taft Young Investigator Award)
Conference: Australasian Diabetes Congress. Virtual meeting, 2020. Oral presentation.

Parry SN*, Fernandes AR, Gauld A, Strasser SI, Twigg SM, Majumdar A and Hocking SL. Prediction and clinical correlates of NASH fibrosis in patients with diabetes: can clinical factors help in the process?
Conference: Australasian Diabetes Congress. Virtual meeting, 2020. Poster presentation.

Gauld A*, Fernandes AR, **Parry SN**, Williams KH, Wu T, Majumdar A, Hocking SL, Strasser SI and Twigg SM. Can a dedicated diabetes and liver clinic enrich the population with NAFLD fibrosis?
Conference: Australasian Diabetes Congress. Virtual meeting, 2020. Poster presentation.

Parry SN, Wang X, Lloyd KWW, Gorrell MD, Williams KH and Twigg SM*. Circulating CCNs as potential biomarkers in diabetes-related complications.
Conference: The 10th International Workshop on the CCN Family of Genes. Niagara, Canada, 2019. Oral presentation.

* presenting author

Awards Related to this Thesis

Research Training Program Scholarship (Australian Government) 2019 - 2022

Postgraduate Research Supplementary Scholarship in Diabetes and Liver Disease 2019 - 2022

The University of Sydney Completion Stipend Scholarship 2022

Charles Perkins Centre EMCR Travel Grant 2022

European Association for the Study of Diabetes (EASD) Travel Grant 2022

Finalist, Pincus Taft Young Investigator Award, Australasian Diabetes Congress 2021

Australian Diabetes Society - Abbott ADC Registration Grant 2021

Finalist, Pincus Taft Young Investigator Award, Australasian Diabetes Congress 2020

Australian Diabetes Society - Abbott ADC Registration Grant 2020

List of Tables

Chapter 1

Chapter 2

Chapter 4

Chapter 5

Chapter 6

List of Figures

Chapter 1

Chapter 2

Chapter 4

Chapter 5

Chapter 6

List of Abbreviations

4-AAP	4-aminoantipyrine
4-PL	4-parameter logistic
7T	7 tesla
AACE	American Association of Clinical Endocrinology
AASLD	American Association for the Study of Liver Diseases
AAV	adeno-associated virus
ACE	angiotensin-converting enzyme
ACTA2	α smooth muscle actin
ADA	American Diabetes Association
ADP	adenosine diphosphate
AEC	Animal Ethics Committee
AER	albumin excretion rate
AIHW	Australian Institute of Health and Welfare
AlbCre	AlbuminCre mouse
ALP	alkaline phosphatase
ALT	alanine aminotransferase
AMT	abnormal monofilament test
ANOVA	analysis of variance
APRI	AST to platelet ratio index
ARB	angiotensin receptor blocker
AST	aspartate aminotransferase
AST:ALT	AST to ALT ratio
ATF-2	activating transcription factor-2
ATP	adenosine triphosphate
AUC	area under the curve
AUROC	area under the receiver operating characteristic curve
AUSDRISK	Australian type 2 diabetes risk assessment tool
BA	bone area
BARD	calculated from BMI, AST:ALT and diabetes presence
BGL	blood glucose level
BMC	bone mineral content
BMD	bone mineral density
BMI	body mass index
BMP	bone morphogenic protein
BNP	brain natriuretic peptide
bp	base pair
°C	degrees Celsius
C/EBP	CCAAT/enhancer binding protein
CAP	controlled attenuation parameter
CCL2	C-C motif chemokine ligand 2
CCl_4	carbon tetrachloride
CCN	cellular communication network
CCN1	cellular communication network factor 1
$CCN1^{fl/fl}$	homozygous CCN1 floxed mouse
CCN1-KO	hepatocyte-specific CCN1 gene knockout mouse
CCN2	cellular communication network factor 2
$CCN2^{fl/fl}$	homozygous CCN2 floxed mouse
CCN2-KO	hepatocyte-specific CCN2 gene knockout mouse
CCN3	cellular communication network factor 3

CCN4	cellular communication network factor 4
CCN5	cellular communication network factor 5
CCN6	cellular communication network factor 6
CDAA	choline-deficient, L-amino acid-defined
cDNA	complementary DNA
ChREBP	carbohydrate response element binding protein
CK-18	cytokeratin-18
CKD	chronic kidney disease
COL1	collagen-I
COL3	collagen-III
COL4a1	collagen-IVα1
COL4a2	collagen-IVα2
COL6	collagen-VI
CPC	Charles Perkins Centre
CRP	c-reactive protein
CT domain	C-terminal domain
CT	computed tomography
CTGF	connective tissue growth factor
CV	central vein
CYR61	cysteine rich angiogenic inducer 61
DAMP	damage-associated molecular pattern
DAP	dihydroxyacetone phosphate
DaSH Study	Diabetes and Steatohepatitis Study
DBP	diastolic blood pressure
DEN	diethylnitrosamine
DHBS	3,5-dichloro-2-hydroxybenzene sulfonate
DIAMOND	diet-induced animal model of non-alcoholic fatty liver disease
DKD	diabetic kidney disease
DLC	Diabetes and Liver Clinic
DMN	dimethylnitrosamine
DNA	deoxyribonucleic acid
DNL	*de novo* lipogenesis
DPP4	dipeptidyl-peptidase 4
DPX	dibutylphthalate polystyrene xylene
DXA	dual energy x-ray absorptiometry
EASD	European Association for the Study of Diabetes
EASL	European Association for the Study of Liver
EASO	European Association for the Study of Obesity
ECG	electrocardiogram
ECM	extracellular matrix
eGFR	estimated glomerular filtration rate
ELF	Enhanced Liver Fibrosis
ELISA	enzyme-linked immunosorbent assay
ER	endoplasmic reticulum
ERK	extracellular signal-regulated kinase
FaD model	Fat and Diabetes model
FAP	fibroblast activation protein
FFA	free fatty acids
FIB-4	fibrosis-4 index
FNI	fibrotic NASH index
FPG	fasting plasma glucose
GGT	gamma-glutamyl transferase

GIP	glucose-dependent insulinotropic polypeptide
GLP-1	glucagon-like peptide-1
GLP-1RA	glucagon-like peptide-1 receptor agonist
H&E	haematoxylin and eosin
H_2O_2	hydrogen peroxide
HA	hyaluronic acid
HbA1c	haemoglobin A1c
HCC	hepatocellular carcinoma
HDL-c	high-density lipoprotein cholesterol
HFD	high fat diet
HFD+DM	high fat diet with diabetes
HIV	human immunodeficiency virus
HOMA-IR	homeostatic model assessment for insulin resistance
HOMA-β	homeostatic model assessment for β cell function
HREC	Human Research Ethics Committee
HRI	hepatorenal index
HRP	horseradish peroxidase
HSC	hepatic stellate cell
hsCRP	high sensitivity c-reactive protein
HSPG	heparin sulphate proteoglycan
IDF	International Diabetes Federation
IFG	impaired fasting glucose
IGF	insulin-like growth factor 1
IGFBP	IGF binding protein
IL1B	interleukin-1β
IL-6	interleukin-6
IL-8	interleukin-8
IL-10	interleukin-10
IFN-γ	interferon γ
INR	international normalised ratio
IPF	idiopathic pulmonary fibrosis
IQR	interquartile range
ITT	insulin tolerance test
JNK	c-jun N-Terminal kinase
LDL-c	low-density lipoprotein cholesterol
LRP1	LDL receptor-related protein 1
LSM	liver stiffness measurement
MAFLD	metabolic (dysfunction) associated fatty liver disease
MAPK	mitogen-activated protein kinase
MCD	methionine- and choline-deficient
MEK-1/-2	MAPK kinase-1/-2
MMP	matrix metalloproteinase
MMP-2	matrix metalloproteinase 2
MRE	magnetic resonance elastography
MRI	magnetic resonance imaging
mRNA	messenger ribonucleic acid
MRS	magnetic resonance spectroscopy
NADPH	nicotinamide adenine dinucleotide phosphate
NAFLD	non-alcoholic fatty liver disease
NAS	NAFLD activity score
NASH	non-alcoholic steatohepatitis
NCEP ATP3	National Cholesterol Education Program Adult Treatment Panel 3

NF-κB	nuclear factor κB
NFS	NAFLD fibrosis score
NLR	NOD-like receptor
NOV	nephroblastoma overexpressed gene
NPV	negative predictive value
OGTT	oral glucose tolerance test
OR	odds ratio
OSA	obstructive sleep apnoea
PCR	polymerase chain reaction
PDGF	platelet-derived growth factor
PIIINP	procollagen III amino-terminal peptide
PN	peripheral neuropathy
PPAR-α	peroxisome proliferator-activated receptor α
PPAR-γ	peroxisome proliferator-activated receptor γ
PPV	positive predictive value
Pro-C3	neo-epitope-specific competitive ELISA for PIIINP
PRR	pattern recognition receptor
PSR	Picro Sirius Red
PT	portal tract
PVD	peripheral vascular disease
qPCR	real-time quantitative polymerase chain reaction
QUICKI	quantitative insulin check index of insulin sensitivity
RARE	rapid acquisition with relaxation enhancement
RCT	randomised controlled trial
RN18S	18S ribosomal RNA
ROI	region of interest
ROS	reactive oxygen species
RPAH	Royal Prince Alfred Hospital
RPLP0	ribosomal protein, large, P0
rpm	revolutions per minute
SASP	senescence-associated secretory phenotype
SBP	systolic blood pressure
SD	standard deviation
SDS-PAGE	sodium dodecyl-sulphate polyacrylamide gel electrophoresis
SEM	standard error of the mean
SGLT2	sodium-glucose co-transporter-2
siRNA	small interfering ribonucleic acid
SREBP-1c	sterol regulatory element-binding protein-1c
STAM™	Stelic Animal Model
STZ	streptozotocin
T1DM	type 1 diabetes mellitus
T2DM	type 2 diabetes mellitus
TAA	thioacetamide
TBW	total body weight
TGFβ1	transforming growth factor β1
TIMP1	tissue inhibitor of metalloproteinase 1
TLR	Toll-like receptor
TMB	3,3',5,5'-tetramethylbenzidine
TNF	tumour necrosis factor α
TSH	thyroid stimulating hormone
TSP	Talented Student Program
TSP1	thrombospondin 1

UACr	urine albumin to creatinine ratio
VEGF	vascular endothelial growth factor
VLDL	very-low-density lipoprotein
vWC	von Willebrand Factor C
WC	waist circumference
WHO	World Health Organisation
WHR	waist to hip ratio
WISP	Wnt induced secreted protein

Abstract

Introduction: Type 2 diabetes mellitus (T2DM) is a risk factor for the development of non-alcoholic fatty liver disease (NAFLD) and its progression to the severe phenotype of non-alcoholic steatohepatitis (NASH) fibrosis. The profibrotic protein, CCN2 and the antifibrotic protein, CCN1 have been implicated in the development of NASH fibrosis, but their exact roles are currently unknown.

Aims:
(i) To evaluate the prevalence of advanced liver fibrosis in individuals attending a dedicated diabetes and liver clinic.
(ii) To explore the role of CCN2 and CCN1 in the development and progression of NASH fibrosis.
(iii) To investigate the utility of circulating CCNs as potential blood biomarkers for NASH fibrosis.

Methods: Four studies were conducted. Firstly, a retrospective audit of the CPC RPAH Diabetes and Liver Clinic was performed. Next, two animal studies were performed using a pre-clinical model of NASH fibrosis induced by high fat feeding and diabetes (FaD model) in mice with hepatocyte gene deletion of CCN2 and CCN1. Finally, circulating CCNs were measured in blood samples from humans and mice with diabetes +/- NASH fibrosis.

Results: Advanced liver fibrosis was common in adults with T2DM. Mice with hepatocyte CCN2 deletion developed less liver fibrosis, whilst mice with hepatocyte CCN1 deletion developed more liver fibrosis, when compared with control mice in the FaD model. These histological results by quantitative image analysis as the main study endpoint were supported by concordant changes in mRNA levels of fibrosis markers. Circulating CCNs did not perform well as biomarkers of NASH fibrosis, but this may be due to the relatively small study group size.

Conclusions: The growing burden of disease posed by NASH fibrosis in individuals with T2DM highlights the need for increasing clinical and pre-clinical research into this area. The results of this thesis indicate that CCN2 and CCN1 may be potential therapeutic targets, and further studies in this area are needed.

Chapter 1: Literature Review, Hypotheses, and Aims

1.1 Type 2 Diabetes Mellitus

1.1.1 Definition and pathogenesis of T2DM

Type 2 diabetes mellitus (T2DM) is a chronic metabolic disease characterised by hyperglycaemia[1]. Insulin resistance is a key early stage that often precedes the development of T2DM by some years[2]. In response to insulin resistance, the pancreatic β cells are required to produce more insulin to maintain normoglycaemia, and a progressive failure to achieve this results in a relative insulin deficiency and subsequent hyperglycaemia into the diabetes range in those who develop T2DM. Obesity and other metabolic derangements such as hypertension and dyslipidaemia, often co-exist in people with T2DM.

1.1.2 Diagnostic criteria for T2DM

The World Health Organisation (WHO) currently recommends four diagnostic tests for diabetes[3], as outlined in *Table 1.1*. In people who are asymptomatic of hyperglycaemia with a positive diagnostic test, a second test (preferably the same one) should be repeated for concordance.

Table 1.1: Diagnostic criteria for diabetes[3].

Test	Criteria for diagnosis	Notes
FPG	≥ 7.0 mmol/L	After an 8 h fast
75 g OGTT	≥ 11.1 mmol/L at 2 hrs	After an 8 h fast prior to the OGTT
HbA1c	≥ 6.5%	
Random BGL	≥ 11.1 mmol/L	With symptomatic hyperglycaemia

BGL, blood glucose level; FPG, fasting plasma glucose; HbA1c, haemoglobin A1c; OGTT, oral glucose tolerance test.

1.1.3 National and global prevalence

According to the Australian Institute of Health and Welfare (AIHW) there were ~1.2 million Australians living with T2DM in 2020, an increase of almost three-fold over the previous 20 years[4]. A further 500 000 Australians are estimated to have undiagnosed T2DM, giving a national total of ~1.7 million people. Depending on the data source, overall prevalence lies at approximately 4-5% and has plateaued, or even slightly decreased over the past five years[4]. However, diabetes mellitus still remains the seventh most common cause of death in Australia[5] and costs the Australian economy $16 billion each year[6].

In 2021, the International Diabetes Federation (IDF) estimated that there were more than half a billion adults (aged 20-79 years) living with diabetes worldwide (*Figure 1.1*), representing a prevalence of 10.5%[7,8]. The majority of cases exist in adulthood, but diagnosis in childhood is increasingly common[9]. Concerningly, the overall prevalence is expected to continue to rise by almost 50% by 2045 and data shows that whilst rates of diabetes are higher in high-income countries, it is low- and middle-income countries that have had the fastest increase in the past decade[7,10]. Although these global estimates were not able to differentiate between the different subtypes of diabetes, T2DM is by far the most common form of diabetes, accounting for over 90% of cases[8]. The rise in prevalence of T2DM is predominantly attributed to an increased prevalence of obesity and unhealthy lifestyles, with improved detection and people living longer with T2DM only explaining a small fraction of the global increase.

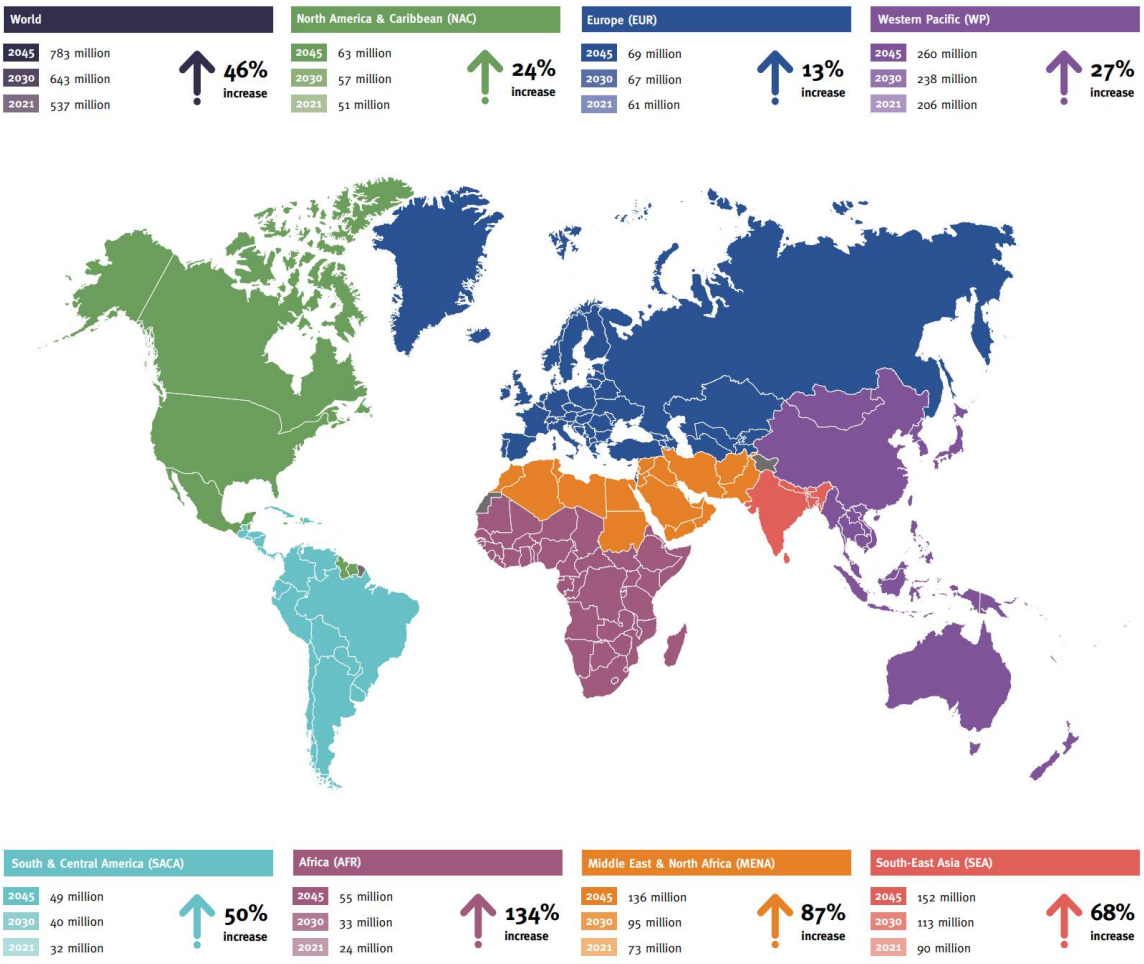

Figure 1.1: Number of people estimated to have diabetes worldwide and per IDF Region in 2021-2045 (20-79 years). Image from IDF Diabetes Atlas[8].

1.1.4 Risk factors for developing T2DM

Several non-modifiable and modifiable risk factors for developing T2DM have been identified. Non-modifiable risk factors include increasing age, male gender, family history of T2DM and high risk ethnicity. Modifiable risk factors include overweight and obesity (discussed in detail in *Section 1.2*), sedentary lifestyle, unhealthy diet, and smoking. The Australian type 2 diabetes risk assessment tool (AUSDRISK) was developed to identify Australian adults at high risk of developing T2DM, using demographic, lifestyle and simple anthropometric measures[11]. The risk calculator uses the above-mentioned risk factors (or surrogates of these), as well as medication for hypertension or previously elevated blood glucose (e.g., prediabetes or history of gestational diabetes). A risk score of 12 predicts that one person in every 14 will develop T2DM over the next five years, whereas a score of 20+ carries a one in three risk. The sensitivity and specificity of the AUSDRISK has been reported to be fair for population screening, at 74% and 68%, respectively[11].

1.1.5 Management of T2DM

T2DM is usually a progressive disease that often requires more intensive therapy with time. In addition to lifestyle measures that include healthy diet, physical activity and weight management, there are several classes of medications available in Australia for treatment of T2DM. The Australian type 2 diabetes glycaemic management algorithm is an easy-to-follow resource for clinicians to aid in choosing the next most appropriate medication for their patient[12]. The mechanism of action of each class is described briefly below[12]:

A) Biguanides: reduce hepatic glucose output and lower fasting glucose levels.
B) Sulfonylureas: trigger insulin release in a glucose-independent manner.
C) Dipeptidyl-peptidase 4 (DPP4) inhibitors: decrease inactivation of glucagon-like peptide (GLP-1) thereby increasing its availability. GLP-1 stimulates β cell insulin release in a glucose-dependent manner.
D) Thiazolidinediones: transcription factor peroxisome proliferator-activated receptor γ (PPAR-γ) agonists lower glucose levels through insulin sensitisation.
E) Alpha 1 glucosidase inhibitors: slow intestinal carbohydrate absorption and reduce post-prandial glucose levels.
F) Sodium-glucose co-transporter-2 (SGLT2) inhibitors: inhibit SGLT2 in the kidney to induce urinary glucose loss and decrease blood glucose levels. They

also have non-glycaemic benefits in heart failure and chronic kidney disease (CKD).

G) Glucagon-like peptide-1 receptor agonists (GLP-1RA): stimulate pancreatic β cell insulin release and slow gastric emptying. Benefits include increased satiety and weight loss.
H) Insulins: directly activate the insulin receptor to potentiate cellular glucose uptake and suppress endogenous glucose production.

Contraindications, potential adverse effects, and precautions for these classes of medications are beyond the scope of this thesis.

1.1.6 Chronic diabetes-related complications

People with long-standing T2DM are at risk of developing diabetes-related complications. Traditionally, complications have been divided into macro- or micro-vascular complications, with glucose toxicity driving oxidative stress, inflammation, and production of advanced glycation end products. However, links with non-vascular-related disease states are increasingly being recognised.

1.1.6.1 Macrovascular diabetes complications

Atherosclerotic cardiovascular disease, which encompasses coronary heart disease, cerebrovascular disease, and peripheral arterial disease, is the leading cause of morbidity and mortality in people with diabetes[13]. In recent years, heart failure has also been recognised as a major cardiovascular complication. Regular assessment and aggressive management of risk factors has led to decreased morbidity and mortality from cardiovascular disease in people with diabetes[14,15]. A multifactorial approach to risk reduction includes glycaemic management, blood pressure management, lipid management, prescription of medications with cardiovascular and/or kidney benefit, in addition to lifestyle modifications, including smoking cessation, optimising physical activity and improving diet quality[13]. Epidemiological studies have established correlations between chronic hyperglycaemia and cardiovascular disease, but the outcomes of randomised controlled trials (RCTs) have not consistently demonstrated a beneficial effect of intensive glycaemic treatment on macrovascular diabetes complications. Multiple studies of people with longstanding T2DM (8 - 12 years) did not show any benefit from intensive (haemoglobin A1c (HbA1c) 6.5%) versus

conventional (HbA1c 7.5 - 8.5%), and in fact, the ACCORD study showed increased harm[16-21]. However, the UKPDS and its 10-year post-trial monitoring study, did show long-term benefits of initial intensive glycaemic control (HbA1c 7.0%) on rates of cardiovascular disease (myocardial infarction, diabetes-related death, and overall death) in people with newly diagnosed T2DM[22,23]. Meta-analyses of these and other studies have been impacted by study heterogeneity, however, they have shown a modest reduction in coronary heart disease and nonfatal myocardial infarction, but not in stroke or mortality[24-26].

1.1.6.2 Microvascular diabetes complications

Microvascular complications include diabetic retinopathy, diabetic kidney disease and peripheral neuropathy[27].

Diabetic retinopathy is a leading cause of working age vision loss worldwide. It is strongly linked to duration of diabetes and the level of glycaemic control, with almost 60% of individuals with T2DM developing some degree of retinopathy by 20 years of diabetes duration[28]. The main pathology involves abnormal permeability of retinal blood vessels, with occlusion, ischaemia, and neovascularisation[29]. It is categorised into non-proliferative and proliferative disease, based on the absence or presence of retinal neovascularisation. Macular oedema, where there is vascular leakage of proteins into the retina, can occur at any stage of diabetic retinopathy and is the leading cause of vision loss in people with diabetes[30,31]. Other eye conditions such as cataract and glaucoma are also more common in people with diabetes. Current recommendations for screening include a dilated eye examination at the time of diagnosis of T2DM, and generally every 1 - 2 years thereafter[32]. Specific treatment for diabetic retinopathy will not be discussed here, however strategies for primary prevention and to slow progression include optimising glycaemic control, blood pressure and lipids[29].

Diabetic kidney disease (DKD) is defined as the persistent presence of albuminuria and/or low estimated glomerular filtration rate (eGFR <60 mL/min per 1.73 m^2)[33]. It is the leading cause of CKD and end-stage kidney disease worldwide[34]. It globally affects ~40% of people with T2DM[35], although rates in Australia are closer to 27%[36]. Pathological changes include glomerular hypertrophy and hyperfiltration,

glomerulosclerosis and tubulointerstitial inflammation and fibrosis[34]. Screening with a urine albumin to creatinine ratio (UACr) and measurement of eGFR should occur from time of diagnosis of T2DM, and annually thereafter. Management strategies for primary prevention and to slow progression include optimising glycaemic control, blood pressure and lipids, in addition to the use of angiotensin-converting enzyme (ACE) inhibitors or angiotensin receptor blockers (ARB) and SGLT2 inhibitors[33]. Finerenone, a non-selective mineralocorticoid receptor antagonist, has been shown to improve renal outcomes in people with T2DM, but is not yet widely available in Australia[37].

Diabetic neuropathy is a common diabetes-related complication, affecting ~50% of people with diabetes. It frequently occurs as a symmetrical length dependent peripheral neuropathy, resulting from progressive injury to distal axons[38]. Symptoms include alterations in sensation, with numbness, burning and paraesthesia commonly described. It can result in loss of protective sensation in the feet, thereby increasing the risk of foot ulcers, subsequent infection, and amputation. Painful neuropathy may also occur. Charcot neuroarthropathy is another associated condition that also carries high morbidity. Other manifestations of diabetic neuropathy include diabetic autonomic neuropathies affecting the cardiac (e.g., resting tachycardia, orthostatic hypotension), gastrointestinal (e.g., gastroparesis, oesophageal dysmotility, constipation/diarrhoea) or genitourinary (e.g., erectile dysfunction, bladder dysfunction) systems[29]. Screening by history taking and physical examination should take place at diagnosis and annually thereafter. As there are no known effective therapies to reverse diabetic neuropathy, the mainstay of care focuses on optimising glycaemic control, and providing symptomatic pain relief when needed.

Unlike the data for macrovascular complications, good quality RCTs have consistently shown that improved glycaemic control reduces the risk of microvascular complications in people with T2DM, primarily in eye and kidney complications[16,17,22]. In addition, the 10-year post-trial monitoring study of the UKPDS indicated that good glycaemic control in newly diagnosed people with T2DM had a legacy effect in reducing microvascular disease some years later[23]. Each 1% reduction in HbA1c translated to a 37% reduction in risk of developing a microvascular complication[39].

1.1.6.3 Non-classical diabetes complications

Non-alcoholic fatty liver disease (NAFLD) is increasingly recognised as a non-classical complication of T2DM. It will be discussed in detail in *Sections 1.4* and *1.5*.

Other comorbidities that are linked with T2DM but not discussed in detail here, include: malignancy (such as bowel, breast, pancreatic, hepatoma), cognitive impairment, hepatitis C infection, pancreatitis, osteoporosis, hearing impairment, male hypogonadism, obstructive sleep apnoea (OSA) and periodontal disease[40].

1.2 Obesity and The Metabolic Syndrome

1.2.1 Definition of obesity

Obesity is a chronic disease characterised by an excessive accumulation of fat that presents a risk to health. The WHO defines a body mass index (BMI) in adults of greater than or equal to 25 kg/m^2 as overweight and a BMI of greater than or equal to 30 kg/m^2 as obesity[41]. It should be noted that these cut-offs were validated in a Caucasian population, and lower cut-offs are frequently applied in Asian populations as the risk of obesity-related harm is evident from a lower BMI[42]. There also remains controversy around the use of BMI as a measure of fatness, as the same BMI may not correspond to the same degree of fatness in different individuals. However, BMI remains useful as a population-level assessment of overweight and obesity[41].

1.2.2 Prevalence and burden of obesity

The worldwide prevalence of obesity almost tripled between 1975 and 2016, at which point there were an estimated 650 million adults living with obesity[41]. Projected targets suggest that by 2030 more than 1 billion adults globally will have a BMI in the obese range, with the greatest number of people living in low- and middle-income countries[43]. Concerningly, childhood weight problems are also rapidly increasing, with a four-fold increase in overweight and obesity over the past 40 years[41]. In 2016, overweight and obesity cost the United States of America more than $1.7 trillion[44].

Australia is no exception to the rising prevalence of overweight and obesity. The latest data from the 2017-18 Australian Bureau of Statistics National Health Survey indicated that two out of three adults (36% overweight and 31% obese), and one in four children

(17% overweight and 8% obese), had a weight problem[45,46]. Whilst rates of weight problems in children have plateaued or even slightly decreased in recent years, rates continue to climb in adults, predominantly driven by increased obesity rather than overweight; with this comes an enormous financial burden on Australia: $5.4 billion in direct health costs from disability and hospitalisation and $6.4 billion in indirect costs from reduced quality of life, premature death and lost productivity[47].

1.2.3 Obesity-related complications

Obesity has profound effects on morbidity and mortality. There is a J-shaped relationship between BMI and all-cause mortality, including cardiovascular and cancer mortality[48]. Over 2.4 million deaths globally were attributed to being overweight or obese in 2017[49] and there are now more deaths linked to overweight and obesity compared with underweight each year[43]. On average, all grades of obesity were estimated to reduce life expectancy by 3.5 years in women and 4.2 years in men, but those with the highest BMIs (≥ 40.0 kg/m^2) had the most number of years lost (7.7 years in women and 9.1 years in men)[50].

The morbidity of obesity should not be underestimated: obesity affects every organ system in the body and there are over 230 recognised weight-related complications[51]. The main disease states are summarised in *Figure 1.2*[52], many of which can be improved with weight reduction[53]. Diseases of particular interest to this thesis included T2DM, of which 80% of cases can be attributed to obesity, and NAFLD, both of which are strongly linked to insulin resistance.

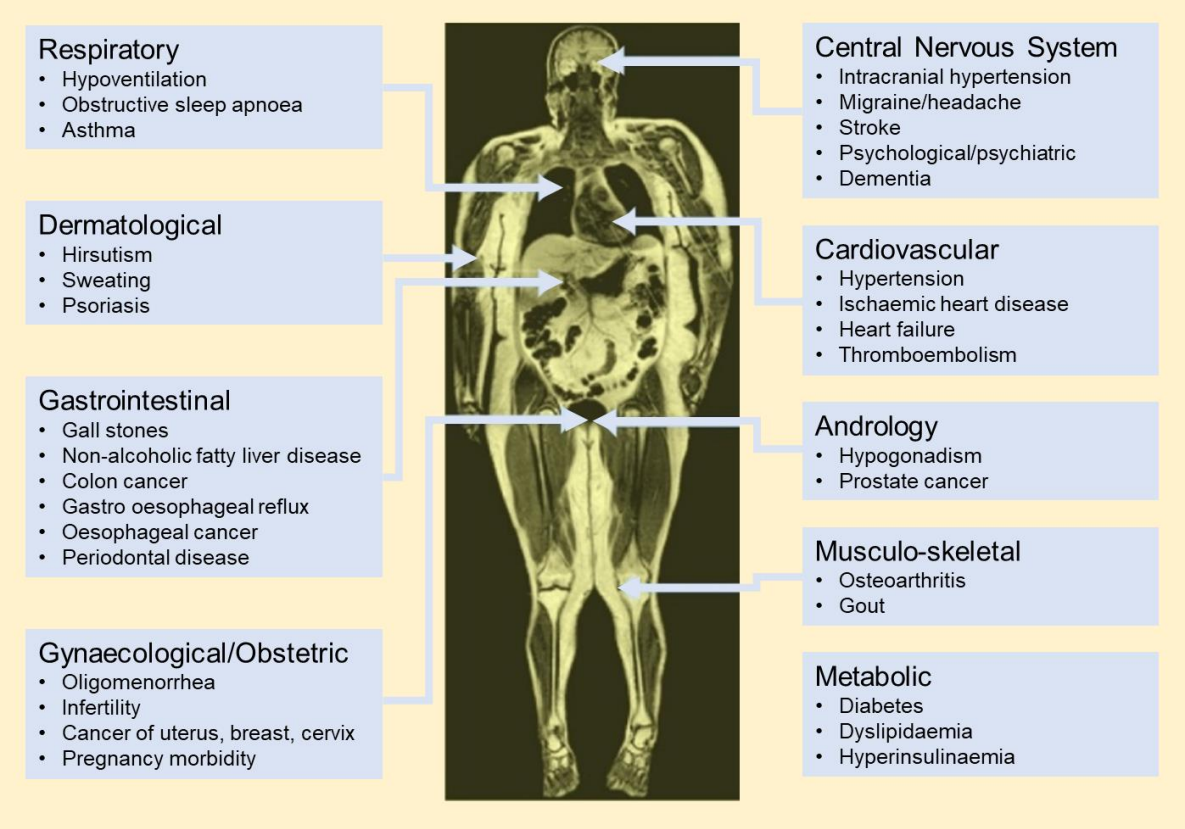

Figure 1.2: Summary of the major medical complications of obesity. Image from Finer, 2015[52].

1.2.4 Pathogenesis of obesity

Obesity is a complex disease, but in its most simplest form, represents a long-term imbalance of energy intake versus energy expenditure[54]. This is influenced by many genetic, metabolic, behavioural, and environmental factors that promote excessive fat deposition. Whilst monogenetic causes of obesity are rare, twin studies estimate that heritable factors account for up to 75% of the variation in adiposity[55]. In addition, environmental factors, such as prolonged exposure to an obesogenic environment, can modify the genetic effects[56]. It is also acknowledged that signals from adipose tissue, the gut and the liver, act upon the brain to influence satiety and appetite, and it is these hormonal, metabolic and neurochemical adaptations that not only defend against weight reduction, but also promote weight regain[54]. Despite increased research occurring into understanding the biology of obesity, the main proponent of the obesity epidemic is the "Westernisation" of lifestyles: the rising prevalence of obesity over the past 50 years has coincided with reduced home cooking, increased availability of convenience foods, reduced physical activity and more sedentary occupations[54].

1.2.5 The metabolic syndrome

The metabolic syndrome refers to the clustering of several metabolic risk factors that share underlying mechanisms and pathways that are strongly linked to insulin resistance. Each individual component on its own carries a risk for cardiovascular disease and/or T2DM, and combination of these factors may increase the magnitude of the risk. There is no international consensus on the definition of metabolic syndrome, and as such, there are multiple diagnostic criteria (*Table 1.2*) which use different thresholds for each of the risk factors of hyperglycaemia, obesity, hypertension, and atherosclerotic dyslipidaemia. The key clinical implication of diagnosing the metabolic syndrome is the identification of people at elevated risk of cardiovascular disease and T2DM, to subsequently promote aggressive lifestyle changes, such as weight reduction and increased physical activity, to then help to prevent or delay the onset of disease.

The metabolic syndrome has associations with other obesity-related diseases, including NAFLD (discussed in detail in *Section 1.4*), CKD, polycystic ovary syndrome, OSA, and gout. Apart from the WHO definition, which includes markers of kidney disease in their criteria, surrogates of these other conditions are not part of the diagnostic criteria despite being linked to the same metabolic milieu.

Table 1.2: Criteria for the metabolic syndrome by three commonly used definitions.

	NCEP ATP3 2005[57]	IDF 2009[58]	WHO 1999[59]
Diagnostic criteria	≥ 3 components	≥ 3 components	Hyperglycaemia and ≥ 2 other components
Glucose	Fasting glucose ≥ 5.6 mmol/L or drug treatment for elevated blood glucose	Fasting glucose ≥ 5.6 mmol/L or diagnosed diabetes	Fasting glucose ≥ 6.1 mmol/L or 2 h OGTT glucose ≥ 7.8 mmol/L or diagnosed diabetes or insulin resistance[#]
Obesity	WC ≥ 102 cm (men) or ≥ 88 cm (women) or ethnic specific cut-offs	WC ≥ 94 cm (men) or ≥ 80 cm (women)	WHR > 0.90 (men) or > 0.85 (women) or BMI > 30 kg/m^2
Hypertension	≥ 130/85 mmHg or treated hypertension	≥ 130/85 mmHg or treated hypertension	≥ 140/90 mmHg or treated hypertension
Triglycerides	≥ 1.7 mmol/L or treatment for high triglycerides	≥ 1.7 mmol/L or treatment for high triglycerides	≥ 1.7mmol/L
HDL-c	< 1.0 mmol/L (men) or < 1.3 mmol/L (women) or treatment for low HDL-c	< 1.0 mmol/L (men) or < 1.3 mmol/L (women) or treatment for low HDL-c	< 0.9 mmol/L (men) or < 1.0 mmol/L (women)
Other			Urinary AER ≥ 20 µg/min or UACr ≥ 30 mg/g

AER, albumin excretion rate; BMI, body mass index; HDL-c, high-density lipoprotein cholesterol; IDF, International Diabetes Federation; NCEP ATP3, National Cholesterol Education Program Adult Treatment Panel 3; OGTT, oral glucose tolerance test; UACr, urine albumin to creatinine ratio; WHO, World Health Organisation; WC, waist circumference; WHR, waist to hip ratio. [#] insulin resistance measured by insulin clamp.

1.3 The Liver

1.3.1 Function of the liver

The liver is the largest internal organ of the body and is the main interface between the digestive system and the systemic circulation. It has a diverse range of metabolic, exocrine, and endocrine functions, as summarised below[60,61]:

- Production of bile which is required for the emulsification, hydrolysis, and uptake of fats in the duodenum;
- Production and secretion of plasma proteins into the blood (including albumin, carrier proteins, coagulation factors, hormonal and growth factors);

- Metabolism, detoxification and/or conjugation of toxins for excretion;
- Regulation of nutrients (including glucose, glycogen, lipids, cholesterol, amino acids, fat-soluble vitamins);
- Removal of old red blood cells.

1.3.2 Structure of the liver

The liver is unique in that it has two blood supplies: 20% is oxygen-rich from the hepatic artery and 80% is nutrient-rich from the portal vein[61]. Structurally, the liver is organised in lobules, with central veins in the centre and portal tracts (bile duct, portal vein and hepatic artery) at the periphery of each lobule (*Figure 1.3*). But functionally, the liver is organised into acini, with both hepatic arterial and portal venous blood entering the acinus from the portal areas (zone 1) and then flowing through the sinusoids (zone 2) to the central veins (zone 3). Bile flows in the opposite direction, from zone 3 to zone 1. Zone 1 is at highest risk of damage from toxins entering via the portal vein, whilst zone 3 is at highest risk of damage from ischaemia due to its position furthest from arterial blood supply.

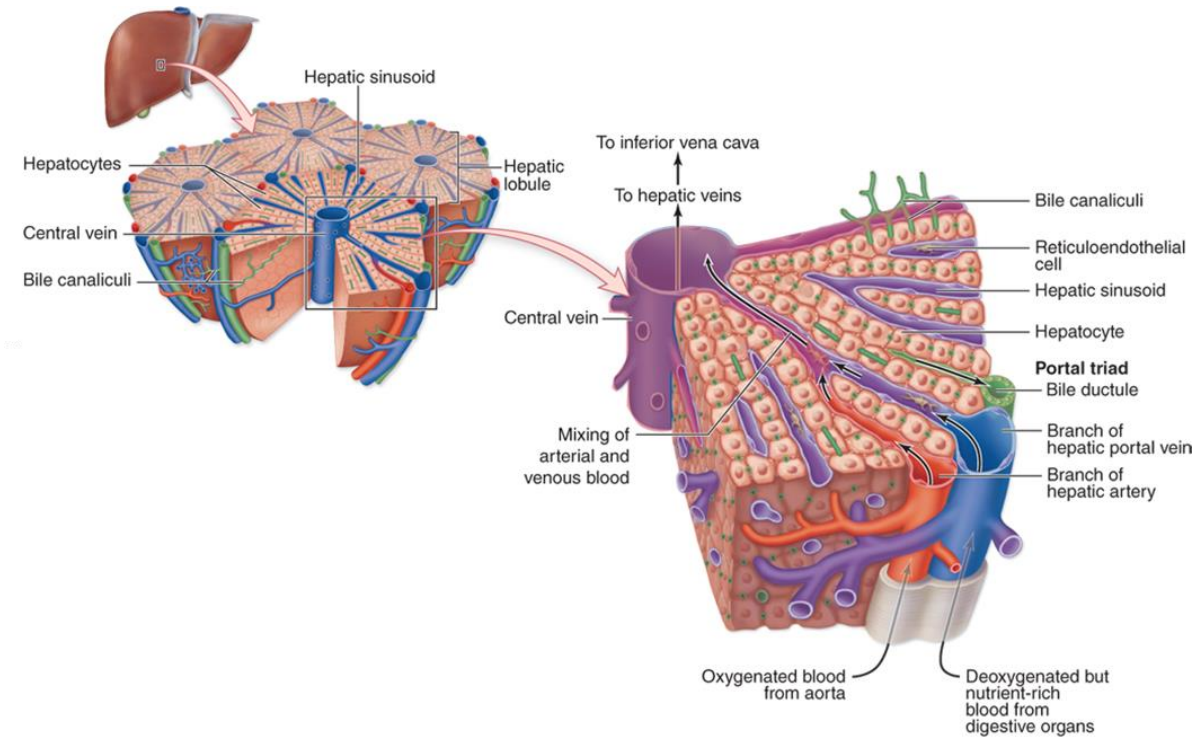

Figure 1.3: The structure of the liver. Image from Mescher, 2021[60].

1.3.3 Cell types of the liver

The liver is formed from parenchymal and non-parenchymal cells. The parenchyma is comprised of hepatocytes, the main cell type in the liver, accounting for up to 80% of liver volume[60]. The hepatocytes form plates aligned radially around a central vein and the sinusoids are the space between the plates where nutrient-rich and oxygen-rich blood mix (*Figure 1.3*). There are discontinuations and fenestrations along the plates, forming a narrow perisinusoidal space (space of Disse) where plasma can flow, allowing uptake and release of nutrients, proteins, and other molecules. The bile canaliculi form on the opposite (apical) side of the hepatocyte, where bile passes.

Non-parenchymal cells include sinusoidal endothelial cells, Kupffer cells and the hepatic stellate cells, which in total constitute 5 - 10% of liver volume[60]. The sinusoidal endothelial cells line the sinusoids and have important functions in filtration and transport of nutrients, modulating vascular tone and inflammation. Kupffer cells are specialised macrophages that reside in the sinusoidal lumen. They are involved in cytokine production, phagocytosis of old erythrocytes, act as antigen-presenting cells and can remove bacteria from the portal circulation. Hepatic stellate cells (HSCs; also called Ito cells) are found in the space of Disse. They are mesenchymal cells that produce extracellular matrix (ECM) components in response to injury and repair. They also store fat and vitamin A and produce cytokines and chemokines to regulate the activity of Kupffer cells.

1.4 Non-alcoholic Fatty Liver Disease

1.4.1 Definition of NALFD

Non-alcoholic fatty liver disease (NAFLD) is defined as the presence of an excessive amount (> 5%) of liver fat[62]. Importantly, other causes of liver disease need to be excluded, such as hepatitis B or C infection, autoimmune diseases, genetic diseases, drug toxicities or excess alcohol consumption. Although it is a spectrum of disease, it can be subdivided into two main histological categories: simple steatosis or non-alcoholic steatohepatitis (NASH). Simple steatosis, as its name suggests, is the accumulation of fat inside the hepatocytes without any other adverse histological features, whereas NASH constitutes the presence of fat in addition to hepatocyte damage and inflammation, with or without the presence of fibrosis. Individuals with

NASH are at risk of progressing to cirrhosis, the latter where there is extensive fibrosis and adverse effects on liver function. Further complications include decompensated cirrhosis and hepatocellular carcinoma (HCC). *Figure 1.4* shows the spectrum of NAFLD progression[63].

1.4.1.1 Metabolic associated fatty liver disease

In recent years, the term metabolic (dysfunction) associated fatty liver disease (MAFLD) has been proposed to replace NAFLD[64]. There are many constructive reasons behind this, including a greater appreciation of the heterogeneity of the disease, and its frequent co-existence with other liver diseases. However, for the purposes of this thesis, the term MAFLD and its sub-categories have not been utilised for reasons listed below:

- This thesis was commenced before the release of the International Consensus Panel in 2020[64];
- The bulk of the literature has used NAFLD and early literature indicates that whilst NAFLD and MAFLD have great overlap, they do not specifically refer to the same populations, and the clinical implications of this is not yet clear[65];
- The term MAFLD has not yet been universally adopted by all international bodies.

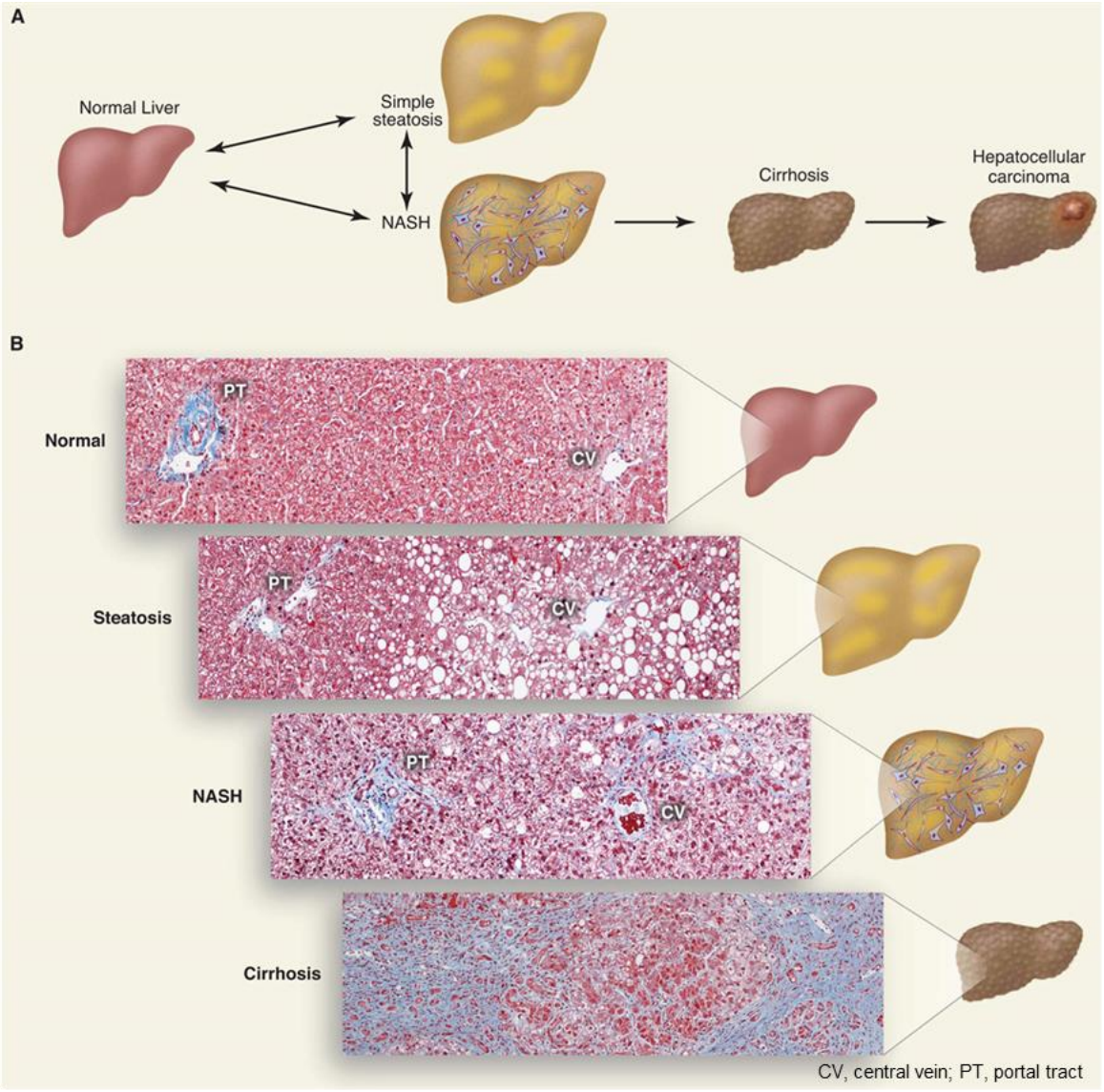

Figure 1.4: The spectrum of NAFLD. (A) Schematic of the progression of NAFLD, from simple steatosis to NASH, cirrhosis, and hepatocellular carcinoma. (B) Histological sections of normal liver, steatosis (with macro- and micro-vesicular lipid accumulation), NASH (with inflammatory cell infiltration and fibrosis), and cirrhosis (with deranged liver architecture, extensive fibrosis, and nodular change). Image from Cohen et al., 2011[63].

1.4.2 Prevalence and natural history of NAFLD

NAFLD has become the leading cause of chronic liver disease worldwide[66]. The increase in prevalence of NAFLD is driven by its epidemiologic and pathophysiologic links to obesity, insulin resistance, T2DM, dyslipidaemia, and the metabolic syndrome[67]. Approximately 25% of the general population has NAFLD[68]. Of those, ~80% have simple steatosis, whilst ~20% have NASH. While extensive population studies of NAFLD natural history are relatively few, progression to advanced fibrosis

is reported to occur in ~4% of individuals with NAFLD (*Figure 1.5*). Whilst progression of NAFLD to the more severe subtypes generally occurs over years to decades[69], it should be noted that this may be somewhat heterogenous, with some individuals remaining stable for years, others progressing rapidly, and a small minority even reversing their pathology[70].

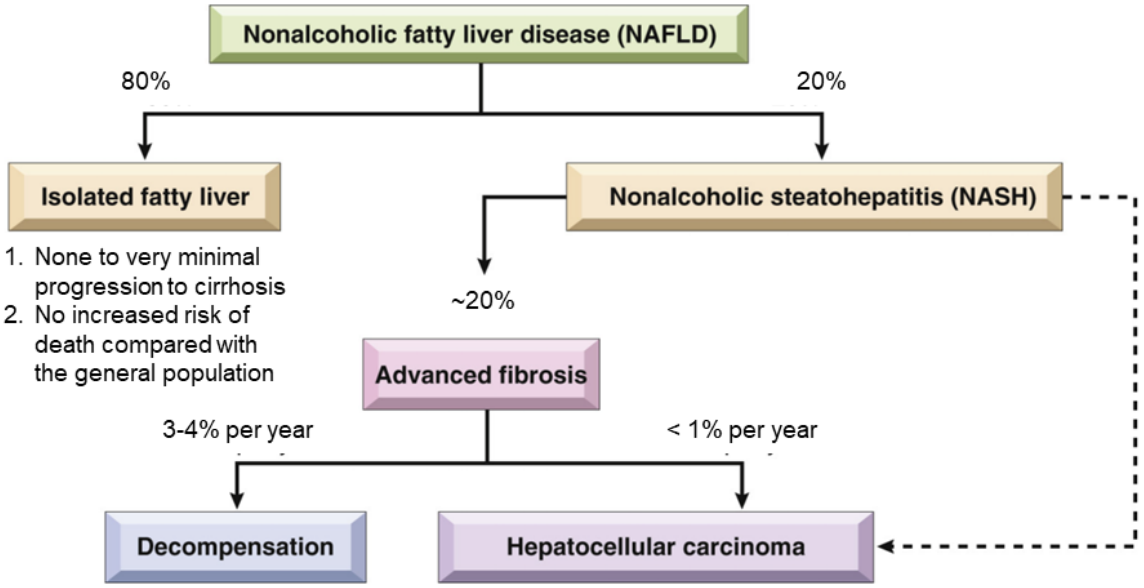

Figure 1.5: The natural history of NAFLD. Image from Gill and Kakar, 2021[71].

Despite only a relatively small percentage of individuals developing decompensated liver failure or HCC, the rates of liver transplantation for NAFLD/NASH as the underlying aetiology are increasing[72]. In the past two decades NASH has overtaken alcoholic liver disease as the second most common indication for transplant in the United States[73]. In Australia, it has increased more than five-fold since 2003[74]. The change in trends is partially explained by improved prevention and treatments for chronic liver disease caused by hepatitis infections[75]. However, the absolute increased prevalence of NAFLD cannot be ignored. In fact, it is expected that by 2030 the prevalence of all stages of NAFLD will have increased by more than 20%, but the prevalence of the most severe stages of fibrosis (F3 and F4), will have more than doubled[76]. Projections from Australian data indicate a similar trend, that is, an 85% increase in both advanced liver disease and liver deaths by 2030, unless effective strategies for prevention and treatment can be instituted[77].

Individuals with NAFLD have increased mortality compared with the general population. Cardiovascular disease is the leading cause of death, likely driven by insulin resistance and related cardiometabolic diseases, pro-inflammatory factors and vasoactive and thrombogenic molecules[78]. This is followed by extra-hepatic malignancies and liver-related complications[62].

1.4.3 Diagnosis and evaluation of NAFLD and NASH

1.4.3.1 Histological assessment

A liver biopsy is the gold standard method for assessing NAFLD, diagnosing NASH, grading activity and staging severity of fibrosis, in clinical practice and in clinical trials[79]. Liver biopsies are reported according to the Brunt and Kleiner criteria for NAFLD (*Table 1.3*), which reflects both the location and extent of liver fibrosis[80]. Using these criteria, NASH is defined by the presence of: grade 1 or higher fibrosis, or grade 2 or higher necroinflammation. As this scoring system indicates, although fibrosis is a major component of the score, it is possible to make a NASH diagnosis without the presence of fibrosis.

Table 1.3: Brunt and Kleiner criteria for NAFLD[80].

Criteria	Grade	Definition
Steatosis	0	< 5%
	1	5 - 33%
	2	34 - 66%
	3	> 66%
Fibrosis	0	Absent
	1	Perisinusoidal/pericellular
	2	Periportal
	3	Bridging
	4	Cirrhosis
Necroinflammation	0	Absent
	1	Occasional ballooned hepatocytes and no or very mild inflammation
	2	Ballooning of hepatocytes and mild to moderate portal inflammation
	3	Intra-acinar inflammation and portal inflammation

Limitations of the Brunt and Kleiner criteria led to the development of the NAFLD activity score (NAS) by the NASH Clinical Research Network (NASH CRN)[81]. This validated scoring system addresses the full spectrum of NAFLD histology, performs

well in adults and children, and can be used to grade disease activity which is particularly useful in clinical trials. It is derived from the sum of scores allocated for steatosis (0 - 3), lobular inflammation (0 - 3), and hepatocyte ballooning (0 - 2). The specific criteria are listed in *Table 1.4*. Unlike the Brunt and Kleiner criteria, fibrosis is not a component of the NAS. A NAS of 0 to 2 is unlikely to be NASH, whilst a score of 5 to 8 is considered diagnostic of NASH and a score of 3 to 4 is indeterminate[81].

Table 1.4: The NASH CRN NAFLD activity score[81].

NASH CRN NAS	Score	Criteria
Steatosis	0	< 5%
	1	5 - 33%
	2	34 - 66%
	3	> 66%
Lobular inflammation	0	Absent
	1	1 focus per 200x field
	2	2 - 4 foci per 200x field
	3	> 4 foci per 200x field
Hepatocyte ballooning	0	Absent
	1	Few ballooned cells
	2	Many cells/prominent ballooning

1.4.3.2 Non-histological assessment

The gold standard for assessing NAFLD remains liver biopsy, but in most cases, this is unnecessary, highly invasive, and carries inherent risk[82]. Therefore, other methods of assessing the liver non-invasively have been developed, which can be implemented in the clinical setting[83]. This includes use of clinical risk scores, blood tests, including biomarkers, and radiological assessment.

1.4.3.2.1 Biochemical assessment

a) Liver enzymes and other measures of liver function

The liver enzymes, alanine aminotransferase (ALT), aspartate aminotransferase (AST), alkaline phosphatase (ALP) and gamma-glutamyl transferase (GGT) are non-specific markers of liver damage. An isolated mildly elevated ALT is frequently the primary abnormality in individuals with NAFLD. The AST and ALT are generally only mildly elevated, much less than ~5 times the upper reference range, however the

degree of elevation does not predict the severity of hepatic inflammation or fibrosis. An AST to ALT ratio (AST:ALT) of less than one is consistent with NAFLD. Less commonly, there may also be mild elevations in GGT and/or ALP in NAFLD. Confusingly, liver enzymes may be within the normal range even in the presence of severe liver disease.

Other blood test results that are more useful indicators of liver dysfunction include hypoalbuminaemia, prolonged prothrombin time, thrombocytopaenia and hyperbilirubinaemia. The latter reflects abnormalities in hepatic conjugation and excretion, whilst the others reflect reduced protein synthesis of albumin, coagulation factors and thrombopoietin, respectively.

b) Novel blood biomarkers

There is much interest in the development of blood biomarkers, which may overcome the need for liver biopsy to diagnose and/or monitor progression of NAFLD and NASH. This topic has been extensively reviewed by Wong and colleagues[84]. The most promising individual biomarker of NASH is cytokeratin-18 (CK-18). It is released in response to hepatocyte apoptosis and is significantly increased in individuals with NASH but not simple steatosis. Whilst values correlate with histological improvement over time, optimal cut-offs remain uncertain. A meta-analysis of CK-18 in individuals with or without NASH reported a pooled sensitivity of 66% and specificity of 82%, suggesting inadequate accuracy for clinical use as a stand-alone test[85].

Other potential biomarkers that have been investigated also reflect the underlying pathophysiology of the disease. These include markers of inflammation, such as c-reactive protein (CRP) and tumour necrosis factor (TNF); oxidative stress, such as lipid oxidation products; and adipocytokines and hormones, such as adiponectin, leptin, fibroblast growth factor 21 (FGF21)[84], DPP4 enzyme activity and level[86], and fibroblast activation protein (FAP)[87]. However, none of these have been independently validated for clinical use.

The dose-dependent relationship between liver fibrosis and all-cause mortality suggests that focussing on fibrosis would be of most clinical use. Individual and panels

of biomarkers that specifically measure fibrogenesis and/or fibrinolysis are summarised in *Table 1.5*.

Table 1.5: Specific fibrosis markers and panels[84].

	Description	Accuracy
Individual Fibrosis Marker		
HA	Major component of ECM	AUROC 0.87 for F2 fibrosis and 0.92 for F4 fibrosis
PIIINP	Measurement of synthesis and degradation of type III collagen	
Pro-C3	Measures true formation of type III collagen	
TIMP1	Reflects tissue matrix remodelling	AUROC 0.97 for NASH
Laminin	Non-collagen glycoprotein in basement membranes	AUROC 0.87 for NAFLD with fibrosis
Fibrosis Panel		
ELF Test	PIIINP, HA, TIMP1	AUROC 0.92 for F1 fibrosis, 0.98 for F2 fibrosis, 0.99 for F3 fibrosis
FibroTest	GGT, bilirubin, α_2-macroglobulin, apolipoprotein AI, haptoglobin	AUROC 0.88 for any fibrosis
FibroMeter NAFLD	Body weight, prothrombin index, ALT, AST, ferritin, fasting glucose	AUROC 0.76 for F2 fibrosis, 0.77 for F3 fibrosis
Hepascore	Age, sex, bilirubin, GGT, HA, α_2-macroglobulin	AUROC 0.82 for F3 - F4 fibrosis

ALT, alanine aminotransferase; AST, aspartate aminotransferase; AUROC, area under the receiver operating characteristic curve; ECM, extracellular matrix; ELF, Enhanced Liver Fibrosis; GGT, gamma-glutamyl transferase; HA, hyaluronic acid; NAFLD, non-alcoholic fatty liver disease; PIIINP, procollagen III amino-terminal peptide; Pro-C3, neo-epitope-specific competitive enzyme-linked immunosorbent assay for PIIINP; TIMP1, tissue inhibitor of metalloproteinase 1.

The general pitfalls of the individual tests are that they are not accurate enough to use alone in the populations studied, hence the development of the panels. The panels have mildly superior accuracy, although perform less well at earlier stages of fibrosis, are expensive due to the use of proprietary formulae, and are not currently available in Australia.

1.4.3.2.2 Radiological assessment

a) Ultrasound

On ultrasound, the liver appears hyperechoic with steatosis[88]. It has a sensitivity of 85% and specificity of 94% for detection of steatosis when compared with liver biopsy[89], although it performs less well in individuals with high BMI[90]. The degree of steatosis cannot be quantified, but the lowest detection threshold for steatosis is 30% fat infiltration, and therefore this modality will underdiagnose individuals with steatosis between 5 and 30%. Other relevant features that can be detected using ultrasound include ascites, splenomegaly, and portal hypertension, which are indicators of cirrhosis and decompensated liver failure, and liver lesions (used in routine HCC screening).

b) Transient elastography

The Fibroscan® utilises transient elastography to measure hepatic fat (controlled attenuation parameter (CAP) score) and liver stiffness as a surrogate for fibrosis (liver stiffness measurement (LSM)). Studies have shown a high degree of correlation between Fibroscan® readings and fibrosis stage confirmed on liver biopsy in the NAFLD population[91-93]. However, transient elastography has not been widely implemented due to concerns with equipment cost, limited availability, sub-optimal performance in the morbidly obese population, and a lack of consensus on appropriate cut-off values.

c) Computed tomography, magnetic resonance imaging and proton magnetic resonance spectroscopy

Computed tomography (CT) performs similarly to ultrasound in detecting steatosis[94] but ionising radiation exposure is a major limitation. The sensitivities of magnetic resonance imaging (MRI) and proton magnetic resonance spectroscopy (MRS) are superior to CT[95], but cost and availability limit their use[69]. Both MRI and MRS allow for quantification of steatosis and can accurately detect small amounts of hepatic lipid accumulation[96].

d) Magnetic resonance elastography

Magnetic resonance elastography (MRE) has the benefit of detecting fibrosis with a high level of accuracy across all stages of fibrosis (area under the receiver operating

characteristic curve (AUROC) ≥ 0.86)[97]. Unlike Fibroscan®, it is not affected by high BMI. It is the most expensive and least widely available of all imaging modalities, and therefore is unlikely to be adopted into routine screening practices.

1.4.3.2.3 Clinical risk scores

Other non-invasive methods of assessing liver fibrosis include use of scoring systems based on readily accessible clinical and laboratory parameters. They are summarised in *Table 1.6*.

Table 1.6: Validated clinical risk scores for advanced fibrosis[84].

Test	Clinical/Biochemical Parameters	Accuracy	Derivation Population
APRI	AST, platelet count	AUROC 0.74 for F3 fibrosis	Hepatitis C
BARD Score	AST, ALT, BMI, diabetes	AUROC 0.69 - 0.81 for F3 fibrosis	NAFLD
FIB-4	Age, AST, ALT, platelet count	AUROC 0.83 for F3 fibrosis	Hepatitis C/HIV
NFS	Age, BMI, IFG/diabetes, AST, ALT, platelet count, albumin	AUROC 0.75 - 0.82 for F3 fibrosis	NAFLD (biopsy-proven)

ALT, alanine aminotransferase; APRI, AST to platelet ratio index; AST, aspartate aminotransferase; AUROC, area under the receiver operating characteristic curve; BARD, calculated from BMI, AST:ALT and diabetes presence; BMI, body mass index; FIB-4, fibrosis-4 index; HIV, human immunodeficiency virus; IFG, impaired fasting glucose; NAFLD, non-alcoholic fatty liver disease; NFS, NAFLD fibrosis score.

These clinical risk scores are generally less accurate than the blood fibrosis markers and panels listed in *Table 1.5*, however they have high applicability as they do not require expensive or special tests to calculate. They also have high negative predictive value (NPV; > 90%) in excluding advanced fibrosis and may be used as a screening tool to exclude individuals who are at low risk and do not require further investigation or referral. Of note, however, none of these scores were derived specifically in a population of concomitant NAFLD and T2DM, limiting their utility in this cohort (performance of these clinical risk scores in validation studies of individuals with T2DM will be discussed in *Section 1.5.2*).

1.4.4 Pathogenesis of NASH

The pathogenesis of NAFLD and its progression to NASH with fibrosis has not yet been fully elucidated. There appear to be multiple pathogenic pathways leading to structural and functional damage in the liver, which will be discussed below.

1.4.4.1 Mechanisms involved in hepatic steatosis

Steatosis is the accumulation of lipids in the liver, including triglycerides, free fatty acids (FFA), ceramides, and free cholesterol[98]. This is a result of excess delivery and synthesis of fat in combination with reduced hepatic export and impaired β-oxidation (*Figure 1.6*). In individuals with NAFLD, FFA influx from adipose tissue accounts for approximately 60% of liver triglyceride, *de novo* lipogenesis (DNL) for approximately 25%, and the remainder is sourced from the diet[99]. In comparison, DNL accounts for less than 5% of hepatic triglyceride formation in healthy individuals[100,101].

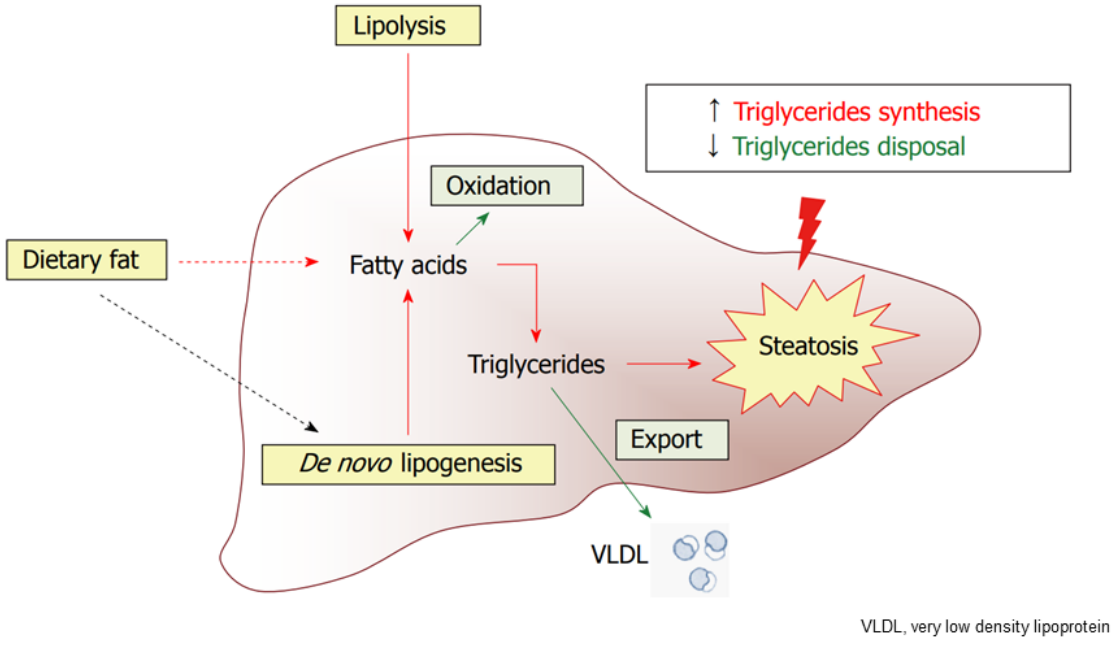

Figure 1.6: Schematic of sources of excess hepatic lipid accumulation due to increased delivery and synthesis of fatty acids and reduced export and oxidation. Image from Ferramosca and Zara, 2014[102].

1.4.4.1.1 Dietary intake contributing to hepatic steatosis

The role of dietary intake in the pathogenesis of NASH has been extensively researched in both clinical and pre-clinical settings. In general, overnutrition leads to excessive conversion of carbohydrates and proteins to triglycerides, and a high fat diet

can lead to NAFLD. However, the fatty acid composition of the diet can affect hepatic lipid metabolism to both encourage pathogenesis of liver disease, but also prevent or reverse disease[102]. For example, whilst high dietary saturated fatty acids are associated with insulin resistance, NAFLD and cardiovascular disease, polyunsaturated fatty acids are potent inhibitors of hepatic lipogenesis.

1.4.4.1.2 Insulin resistance and increased free fatty acids from lipolysis

Although controversies exist regarding the potential protective effects of insulin resistance in T2DM[103], there are clear links between insulin resistance and development and progression of NAFLD. Insulin signalling pathways are affected by hyperinsulinemia, hyperglycaemia, FFA, ceramides, oxidative stress, and inflammation, which lead to and exacerbate insulin resistance[104]. Insulin resistance causes impaired suppression of lipolysis of adipose tissue by insulin, and thus an increase in FFA delivery to the liver, contributing to the accumulation of liver triglycerides.

1.4.4.1.3 De novo lipogenesis

DNL is a process that converts excessive carbohydrates into triglycerides, which can later be used as an energy source via β-oxidation[105]. It is highly sensitive to the diet: for example, hepatic DNL is induced by a high carbohydrate diet[106]. Dysregulation in DNL is observed in individuals with insulin resistance and NAFLD. Hyperinsulinemia inhibits lipolysis in adipose tissue and lowers serum FFA. Insulin resistance prevents the effectiveness of insulin to do this. In the chronic setting, this leads to up-regulation of lipogenic transcription factors[105]. The transcription factors sterol regulatory element-binding protein-1c (SREBP-1c) and carbohydrate response element binding protein (ChREBP), are major regulators of DNL. SREBP-1c expression is increased in response to hyperinsulinaemia whilst ChREBP is a glucose-dependent transcription factor, and both are capable of independently activating genes required for lipogenesis.

1.4.4.1.4 Impairment of β-oxidation

Mitochondrial β-oxidation is the major oxidative pathway for the disposal of fatty acids. The oxidative capacity in the liver can become overwhelmed by the increased influx of fatty acids in NAFLD and thus become a major source of oxidative stress and production of reactive oxygen species (ROS). Efficiency of β-oxidation can be affected

by nutritional status, for example, impairment is seen in vitamin B5 deficiency, excessive alcohol consumption and coenzyme A deficiency. Hyperinsulinemia from insulin resistance may also impair β-oxidation[107]. Activation of peroxisome proliferator-activated receptor α (PPAR-α) stimulates β-oxidation to improve hepatic lipid turnover and prevent development of NASH in mice[108]. Adiponectin has also been implicated, as it has been shown to improve fatty acid oxidation and reduce fatty acid synthesis, with reduction in steatosis and inflammation[109].

1.4.4.1.5 Impaired synthesis and secretion of very-low-density lipoprotein

Impairment in very-low-density lipoprotein (VLDL) synthesis and secretion can contribute to excess fatty acid accumulation and steatosis. A Japanese study reported that VLDL synthesis and removal of lipids from the liver were impaired in individuals with NASH[110]. Another study showed that individuals with NASH may have a defect in postprandial secretion of apolipoprotein B, an important structural component of VLDL, thus leading to impaired synthesis of VLDL and accumulation of triglycerides in the liver[111]. Defects in VLDL can also occur because of dietary deficiencies, such as in protein malnutrition or choline deficiency.

1.4.4.2 Mechanisms involved in hepatic inflammation

Hepatic inflammation is major trigger for the transition of simple steatosis to NASH. The activation of inflammatory pathways results in the release of chemokines, cytokines, and other pro-inflammatory molecules, enabling recruitment of inflammatory cells to the liver to enable coordinated cellular defence and tissue repair. The origin of hepatic inflammation stems from both within the liver (e.g. lipotoxicity, innate immune response and cell death pathways) and from extra-hepatic tissues such as adipose tissue and the gut[112]. *Figure 1.7* depicts some of the major components implicated in hepatic inflammation in NASH.

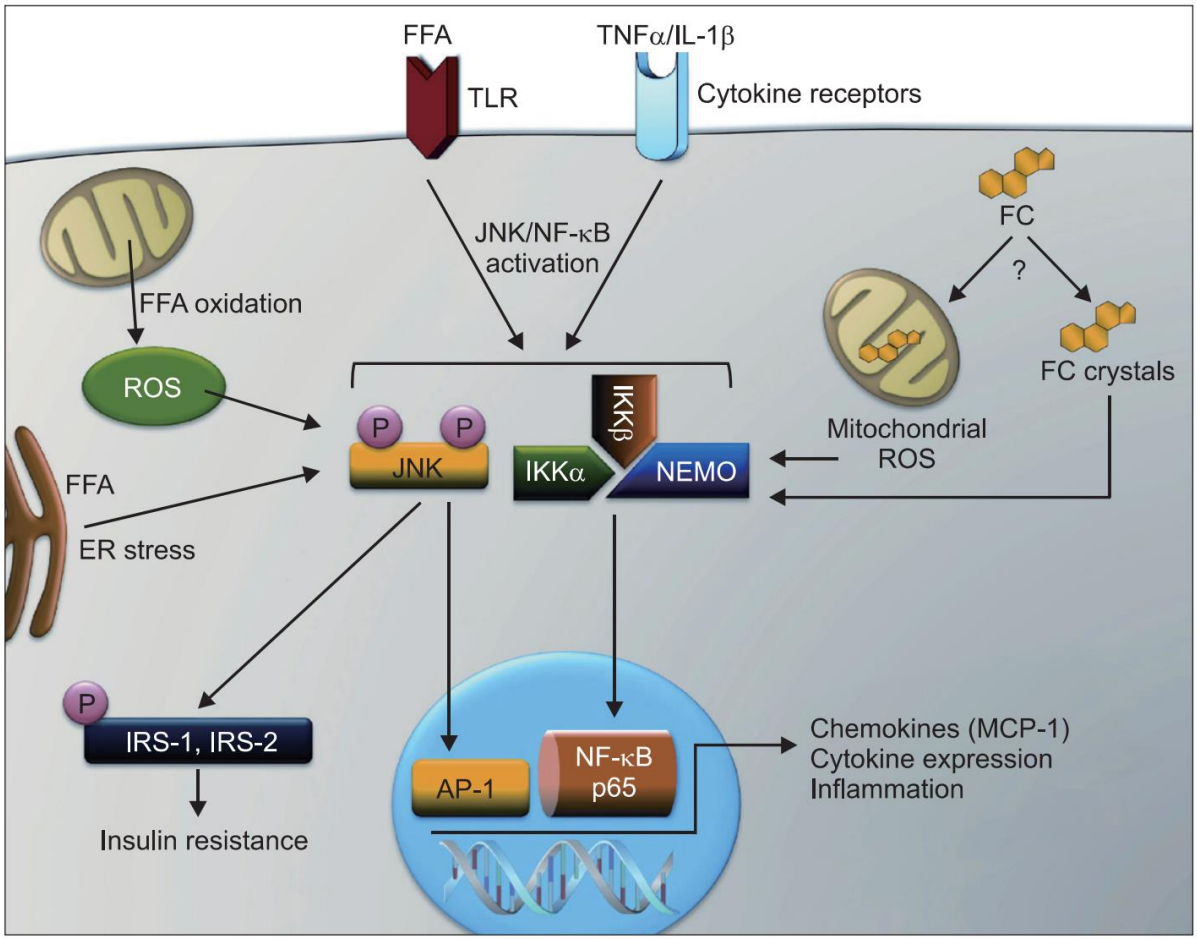

Figure 1.7: Schematic depicting contributors implicated in hepatic inflammation in NASH. Excess lipid accumulation activates signalling pathways to increase pro-inflammatory chemokine and cytokine expression. Image from Farrell et al., 2012[113].

1.4.4.2.1 Innate immunity in the liver

The innate immune system can recognise immunogenic signals released from damaged or dead tissue through pattern recognition receptors (PRRs) that bind to damage-associated molecular patterns (DAMPs). Families of PRRs, including Toll-like receptors (TLRs) and NOD-like receptors (NLRs), are implicated in the pathogenesis and inflammation in NASH[112]. TLR signalling activates transcription factors involved in cytokine and chemokine production. In particular, TLR-2, -4 and -9 are overexpressed in NASH livers and are associated with disease progression[114,115]. The NLRP3 inflammasome is also activated by DAMPs, as well as ROS and FFAs, amongst other factors[112]. NLRP3 activation promotes cell death and expression is increased in humans with NASH[116].

Activation of resident Kupffer cells results in release of cytokines and chemokines and recruitment of other immune cells. Animal studies have shown that the depletion of Kupffer cells in NASH can prevent liver steatosis, inflammation, and fibrosis, and reduce infiltration of other immune cells[117]. Kupffer cells also express TLRs which further contributes to inflammation.

1.4.4.2.2 Hepatocellular stress

a) Lipotoxicity

Lipotoxicity is a major cause of hepatocyte dysfunction that leads to the pathogenesis of NASH[118]. Triglycerides are not thought to be the major determinant of lipotoxicity, whereas other lipid species have been implicated. The accumulation of FFAs in the liver leads to formation of lipotoxic metabolites, including ceramides, diacylglycerols and lysophosphatidylcholine[113,119]. These lipids contribute to activation of signalling cascades and death receptors, endoplasmic reticulum stress, mitochondrial dysfunction, and oxidative stress, ultimately leading to hepatocyte damage and death[98].

b) Oxidative stress

Oxidative stress is important in the progression of NASH[120] and markers of oxidative stress correlate with the severity of liver damage in humans with NASH[121]. Sources of ROS include Kupffer cells and mitochondrial dysfunction in β-oxidation. The formation of lipid peroxidation products can activate HSCs[122], which in turn can produce even more ROS through the expression of nicotinamide adenine dinucleotide phosphate (NADPH) oxidase[123].

c) Endoplasmic reticulum stress

A major source of endoplasmic reticulum (ER) stress is the incomplete folding of proteins. Diabetes increases impaired protein synthesis and amino acid metabolism thereby contributing further to ER stress. ER stress activates the of nuclear factor κB (NF-κB), c-jun N-Terminal kinase (JNK) and CCAAT/enhancer binding protein (C/EBP) pathways, to enhance inflammatory recruitment, worsen insulin resistance, stimulate lipogenesis, and promote oxidative stress[113]. Its role in human NASH has not been fully elucidated, with activation of some pathways but not others[124].

1.4.4.2.3 Pro-inflammatory signalling pathways

Cellular stress leads to the activation of intracellular pro-inflammatory pathways. Major signalling pathways include transcription factor activation of NF-κB and JNK. In the liver, NF-κB regulates the transcription of many pro-inflammatory molecules, including cytokines, chemokines, adhesion molecules, nitric oxide, and cyclo-oxygenase 2. Activation of NF-κB has been identified in human NASH and in animal models of NASH and is thought to play a key role in recruitment of inflammatory molecules[125].

JNK is a member of the mitogen-activated protein kinase (MAPK) family, and is activated by oxidative stress, lipotoxic molecules, or binding to growth factors, TNF receptors or TLRs[113]. JNK activates the mitochondrial apoptosis pathway and induces NF-κB. JNK has also been shown to be activated in humans with NASH and in animal models[126].

1.4.4.2.4 Pro-inflammatory cytokines and chemokines

Pro-inflammatory cytokines are implicated as a major pathogenic component in progression of NASH, leading to cause impaired insulin signalling, cell damage, neutrophil chemotaxis, HSC activation and apoptosis[127]. Activation of the NF-κB pathway leads to release of many cytokines, including TNFα, interleukin-6 (IL-6) and interleukin-8 (IL-8). The Kupffer cells are another source of cytokines from the liver, releasing large amounts of TNFα and IL-6[128]. Other cytokines and chemokines, such as interferon γ (IFN-γ), interleukin-1β (IL1B) and C-C motif chemokine ligand 2 (CCL2) are also thought to play an important role in NASH progression.

1.4.4.2.5 Extra-hepatic factors

a) Adipocytokines

Adiponectin has favourable effects on DNL and β-oxidation. It is hypothesised to activate PPAR-α and AMP-kinase, resulting in increased β-oxidation and decreased synthesis of triglycerides[129]. It also decreases hepatic TNFα production and thus has a direct anti-inflammatory effect[109]. Adiponectin has been shown to inhibit the fibrogenic effects of leptin[130].

b) Intestinal microbes

The gut microbiome may play a role in the pathogenesis of NAFLD, as a source of hepatotoxic oxidative injury. Changes in the gut microbiota can lead to increased gut permeability, translocation of bacteria and movement of microbiota through the portal circulation[131]. This can activate the innate immune system to produce an inflammatory response.

1.4.4.3 Mechanisms involved in hepatic fibrosis

Fibrosis is a part of the wound-healing response characterised by deposition of ECM. Along with necroinflammation, it is a key feature that distinguishes NAFLD from NASH[80]. The severity of liver fibrosis is tightly linked to clinical outcomes, including liver dysfunction and all-cause mortality[67]. The hepatic stellate cell (HSC) has been identified as the key driver of hepatic fibrogenesis: firstly, through increased synthesis and deposition of ECM, and secondly, via cellular proliferation to increase the total number of activated HSCs. However, the development of fibrosis is a balance between deposition and degradation of ECM, and the inhibition of degradation of ECM also contributes to the overall degree of fibrosis.

1.4.4.3.1 Activation of the hepatic stellate cell

Under normal conditions, the HSCs remain quiescent in the space of Disse. Activation occurs in response to a range of chronic insults to the liver, such as occurs in NASH. There are two main phases of activation: initiation and perpetuation, but these may be followed by a resolution phase if the insult is removed[132]. During the initiation phase, hepatocyte apoptosis from the initial injury generates apoptotic bodies, ROS, and paracrine stimulation of HSCs. During the perpetuation phase, these stimuli promote maintenance of the activated phenotype, leading to ongoing generation of fibrosis (*Figure 1.8*). A resolution phase may occur through apoptosis, senescence or quiescence of HSCs[133].

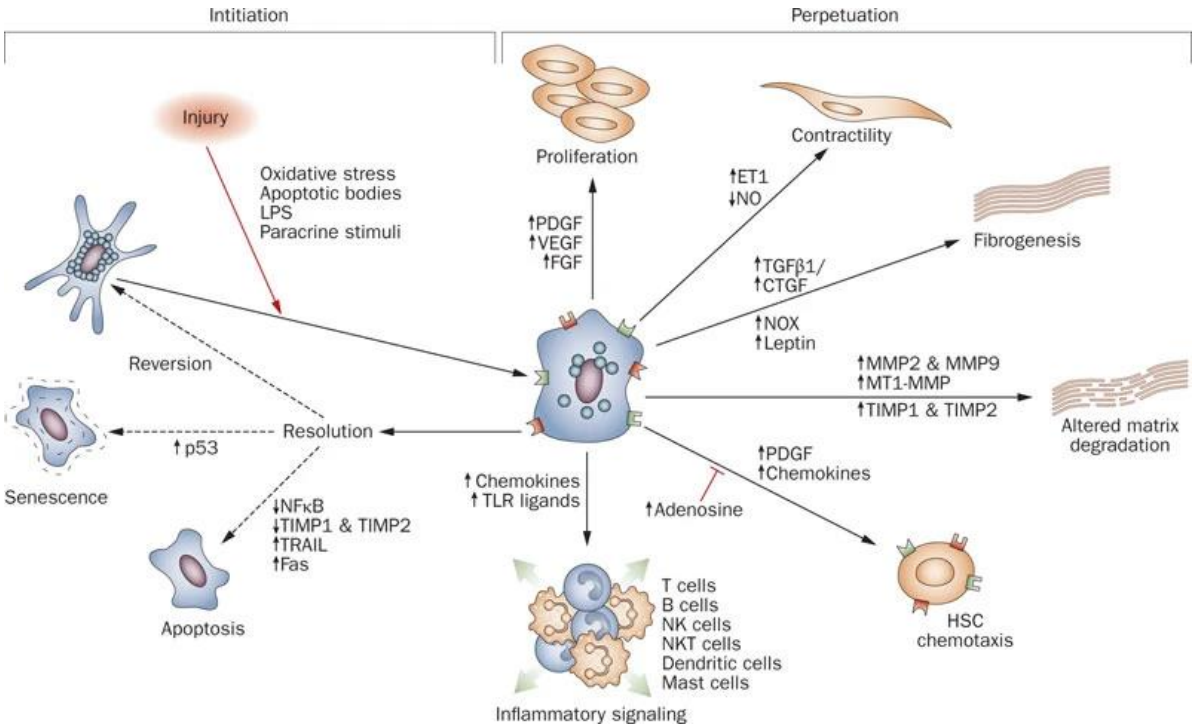

Figure 1.8: Activation of hepatic stellate cells. Initiation phase is stimulated by tissue injury, leading to the perpetuation phase of proliferation, contractility, fibrogenesis, altered matrix degradation, chemotaxis, and inflammatory signalling. Image taken from Friedman, 2010[134].

1.4.4.3.2 Intracellular signalling in the hepatic stellate cell

a) TGFβ1/Smad signalling

The most potent fibrogenic cytokine in the liver is transforming growth factor β1 (TGFβ1), which is mainly derived from HSCs, but also from Kupffer cells, hepatocytes and platelets[135]. TGFβ1 stimulates the synthesis and deposition of many ECM components[136] via Smad protein signalling[137] and HSC activation. However, TGFβ1 also has important roles in hepatocyte regeneration[138] and maintenance of normal liver homeostasis, which makes it a very challenging therapeutic target[139].

Cellular communication network 2 (CCN2), formerly known as connective tissue growth factor (CTGF) is a cysteine-rich matricellular protein, that regulates ECM proteins, and cellular adhesion, migration, proliferation, survival, and differentiation[140,141]. CCN2 is not only up-regulated by TGFβ1, but it also feeds forward to up-regulate the TGFβ1 profibrotic signalling pathway[142,143]. CCN2 has been implicated in development of fibrosis in NASH, clinically and in pre-clinical models[144,145]. The potential role of CCN2 in NASH with fibrosis will be discussed in detail in *Section 1.7.7*.

b) Proliferative signalling

Platelet-derived growth factor (PDGF) signalling leads to HSC activation and proliferation[146]. Binding of PDGF to its receptor leads to activation of several downstream signalling pathways, including the Ras-MAPK and PI3K-AKT pathways. Whilst all isoforms have fibrogenic effects, PDGF-B is the most potent PDGF isoform that mediates HSC proliferation and is regulated by TGFβ1[147-149].

c) MAPK signalling

The MAPK cascades are key intracellular signalling pathways that regulate many cellular responses including proliferation, differentiation, and apoptosis. The MAPK family consists of three members: extracellular signal-regulated kinase (ERK), JNK and p38 MAPK.

As mentioned above, the activation of Ras is an early step in PDGF-stimulated HSCs[150]. There is subsequent activation of Raf-1, MAPK kinase-1/-2 (MEK 1/2), ERK-1 and ERK-2[151]. Activated ERK then phosphorylates transcription factors involved in HSC proliferation[152]. Inhibition of the ERK pathway can suppress PDGF-stimulated mitogenesis and partially decrease PDGF-stimulated chemotaxis, which provides evidence for the key role of ERK signalling in PDGF-driven HSC proliferation and migration[153].

JNK also regulates proliferation of HSCs. JNK can be induced by multiple stressors, including cytokines, UV- and γ-irradiation, cytotoxic drugs and ROS[154]. Upstream signalling kinases, MAPK kinase-4 (MKK3) and MKK7 can regulate JNK activity, and then activate several transcription factors, including the c-Jun and activating transcription factor-2 (ATF-2)[155,156]. Inhibition of JNK in cultured HSCs can reduce cellular proliferation[157].

Finally, p38 MAPK is activated by growth factors, heat shock and ischaemia/reperfusion injury[158]. Phosphorylation of p38 by MKK6 and MKK3 leads to activation of transcription factors, including ATF-2[159]. In contrast to ERK and JNK signalling, p38 inhibits HSC proliferation[157,160].

d) Chemokine pathways

Chemokines induce fibrogenic cell migration to the injury site, thus promoting fibrogenesis and amplifying inflammation. Multiple cells in the liver can both be potential sources or targets of chemokines, depending on the different receptors or ligands that they express. For example, C-C chemokine receptor type 5 (CCR5) is induced by NF-κB signalling and it stimulates HSC migration and proliferation[161]. However, not all chemokines promote fibrogenesis: other chemokines, such as C-X-C motif chemokine ligand 9 (CXCL9) and interleukin-10 (IL-10), can have antifibrotic properties[162].

e) Adipokine pathways

Adipokines have been recognised as another class of mediators of fibrogenesis[163]. Leptin, a circulating hormone, promotes both HSC activation through suppression of PPAR-γ, and tissue inhibitor of metalloproteinase 1 (TIMP1) expression, to promote fibrogenesis and prevent degradation of ECM[164,165]. A reduction in the counter-regulatory hormone adiponectin has been reported in liver fibrosis, and this may contribute to the fibrogenic activity of leptin[166].

1.4.4.3.3 Hepatocyte contribution to fibrogenesis

Hepatocytes are the most abundant cell type in the liver and can also contribute to fibrogenesis. The release of hepatocyte-derived apoptotic bodies after hepatocyte injury promotes HSC activation and differentiation, and thus are potential inducers of liver fibrosis[123,167]. Apoptotic hepatocytes also generate adenosine, which is a mediator of the fibrogenic cascade[168]. Activation of NF-κB in hepatocytes also mediates hepatic fibrosis[169]. Hepatocytes can also produce profibrotic factors, such as CCN2, in response to tissue insult[145].

1.4.4.3.4 Matrix remodelling in liver fibrosis

The normal homeostasis of ECM is regulated by a balance between matrix metalloproteinases (MMPs) and their specific inhibitors, the TIMPs[170]. In fibrosis, there is disruption to the balance of MMPs and TIMPs. Activated HSCs have up-regulated expression of TIMP1, leading to inhibition of MMPs and accumulation of ECM proteins[171]. In particular, there is increased type I, -III and -IV collagen deposition[172]. In addition to preventing fibrinolysis, TIMP1 can also inhibit the apoptosis of activated

HSCs, allowing further promotion of fibrogenesis[173,174]. Matrix metalloproteinase 2 (MMP-2), which suppresses type I collagen expression, is increased in human liver fibrosis, and its absence has been reported to promote fibrogenesis[171].

1.4.5 Management of NAFLD

1.4.5.1 Body weight reduction

1.4.5.1.1 Lifestyle modification

In the absence of any approved medications for the treatment of NAFLD or its subtypes, current recommendations focus on lifestyle modifications to induce weight loss. Weight loss of ≥ 5% has been shown to improve hepatic steatosis, whilst weight loss of ≥ 7% can improve histological disease activity as assessed by the NAS (*Table 1.4*)[175]. Importantly, greater weight loss was associated with greater reduction in liver fat and higher likelihood of NASH resolution and fibrosis regression[176].

1.4.5.1.2 Bariatric surgery

In those unable to achieve or maintain weight loss through lifestyle modification, bariatric surgery may be an option. Some observational studies of bariatric surgery resulting in substantial and sustained body weight reduction (> 15%), have been shown to be associated with less severe, or even resolution of, NASH fibrosis[177-179]. However other studies have reported a persistence of fibrosis despite resolution of NASH[180] or even worsening of fibrosis, at least in the short term follow-up[179,181]. Good quality RCTs with adequate duration follow-up are required to further elucidate the role of bariatric surgery in individuals with NASH fibrosis.

1.4.5.2 Liver-directed pharmacotherapy

Vitamin E has been investigated as an antioxidant treatment for NASH (without diabetes) in multiple clinical trials with mixed results. A large RCT of high-dose Vitamin E versus pioglitazone (PPAR-γ agonist) versus placebo for almost two years reported that individuals on Vitamin E were more likely to have improved histology and ALT[182]. However, the results of a meta-analysis, which included this positive RCT, concluded no benefit from Vitamin E[183]. In fact, Vitamin E has been associated with increased all-cause mortality and risk of prostate cancer, and thus is not routinely prescribed[184].

Thiazolidinediones, a class of diabetes medications (*Section 1.1.5*), have been shown to improve the histological features of ballooning, inflammation and steatosis (odds ratio (OR) 2.11, 2.58 and 3.39, respectively), but not fibrosis, in individuals with NASH[185]. However, results of a sub-analysis suggested that pioglitazone, but not rosiglitazone may improve fibrosis[185], although the safety and side effect profile of these medications significantly limit their use.

There are numerous other drugs in the development pipeline (phase 2 or 3) for the treatment of NASH and fibrosis, targeting metabolic pathways, oxidative stress, inflammation and/or fibrosis. These have been summarised in a review by Albhaisi and Sanyal in 2021[186]. The evidence for GLP-1RAs will be discussed in *Section 1.5.4.1*.

1.4.5.3 Cardiovascular risk factors

Although the development and progression of NAFLD is not thought to be predominantly glucose-mediated, optimising glycaemic control in individuals with concomitant NAFLD and T2DM aims to reduce cardiovascular risk. Options for glycaemic control in T2DM were discussed in *Section 1.1.5* and will be further discussed in relation to NAFLD and NASH with fibrosis in *Section 1.5.4*. Dyslipidaemia and hypertension frequently co-exist in individuals with NAFLD and should be aggressively managed to further reduce the risk of cardiovascular disease.

1.4.5.4 Alcohol intake

Individuals with NAFLD are advised to refrain from heavy alcohol intake, and in particular binge drinking, as this has been linked to disease progression, including worsening steatosis, hepatic injury, and fibrosis[187]. The effects of light or moderate alcohol intake are less clear, but in general, individuals are advised to abstain from drinking alcohol.

1.5 Non-alcoholic Fatty Liver Disease in Type 2 Diabetes Mellitus

The pathogenic relationship between NAFLD and T2DM has been well established[67]. Presence of one disease is a risk factor for development of the other. Approximately 25% of the general population has NAFLD, but this rises to greater than 70% in adults

with T2DM[68,188]. The presence of T2DM is an independent risk factor for progressing to each of the more severe stages of NAFLD, including NASH with fibrosis and cirrhosis[67,189,190]. The growing rates of these concomitant metabolic diseases have significant implications for not only long-term health outcomes at both an individual and public health level, but also impacts on healthcare systems and health economics, related to screening, diagnosis, and management. A greater understanding of the complex and overlapping pathogenic pathways is needed.

1.5.1 Pathogenesis of NASH in T2DM

The pathogenesis and progression of NAFLD from simple steatosis to NASH with fibrosis and beyond in T2DM has not been fully elucidated, and but is likely to arise from a combination of genetic predisposition, environmental exposures, and metabolic derangements. Research has long debunked the simplistic "two-hit hypothesis", where steatosis was thought to be the first "hit", and then exposure to another pathogenic insult, such as oxidative stress, was the second "hit", led to the inflammation and fibrosis observed in NASH[191].

Instead, the progression of NAFLD is hypothesised to be a culmination of a relative insulin deficiency from T2DM causing increasing lipolysis of adipose tissue and fatty acid delivery to the liver, portal hyperinsulinaemia and selective hepatic insulin resistance of pathways controlling glucose but not fat[67]. It is proposed that this differential signalling results in up-regulation of MAPK-related pro-fibrogenic pathways and also SREBP-1 gene expression, which can also be induced by both high fat diets and insulin, and this leads to increased DNL (discussed in *Section 1.4.4.1.3*)[192,193]. Ongoing exposure to toxic lipid species and inflammation can induce hepatic profibrotic pathways via activation of HSCs. Hyperglycaemia, and production of advanced glycation end products, is thought to have only a minor contributing role in stimulating inflammatory and fibrotic pathways. This is summarised in *Figure 1.9*.

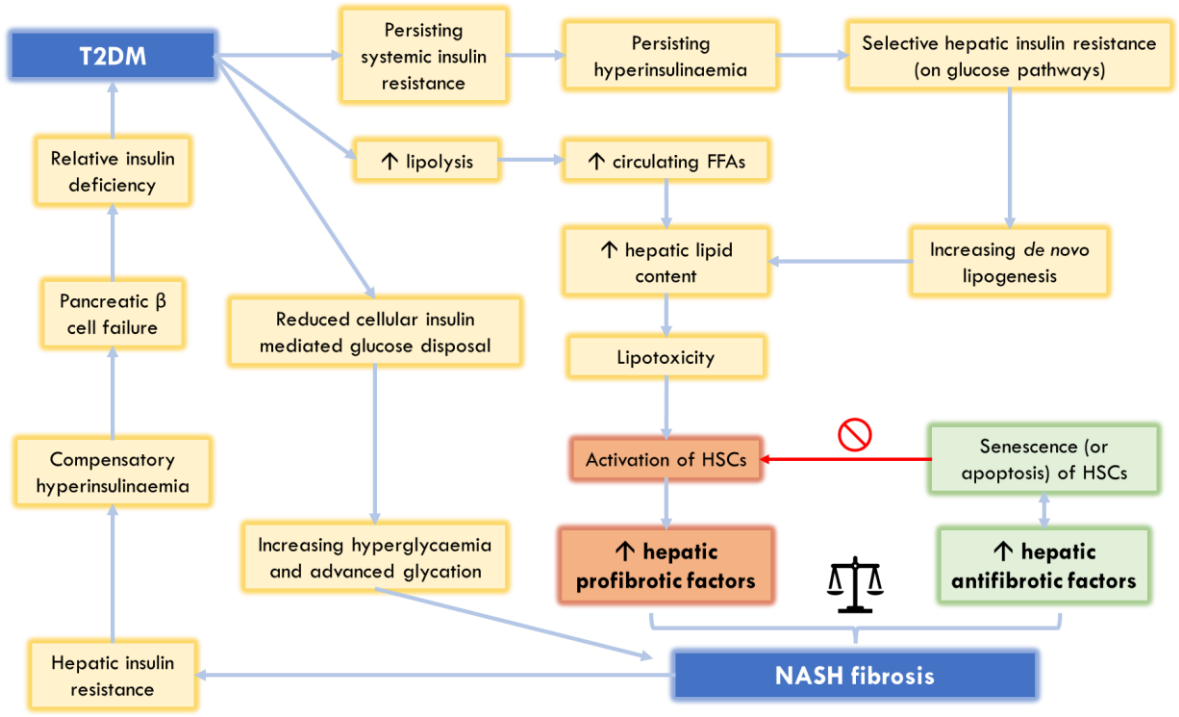

Figure 1.9: Schematic of proposed pathogenic processes by which T2DM promotes development of NASH fibrosis. Image adapted from Williams et al., 2013[67].

1.5.2 Utility of fibrosis markers and clinical risk scores in T2DM

Blood biomarkers and clinical risk scores for advanced liver fibrosis were discussed in *Section 1.4.3.2*. These tests were not developed specifically in a cohort of individuals with concomitant NAFLD and T2DM, although are frequently used. A recent cross-sectional study evaluated a range of clinical risk scores in a cohort of individuals with NAFLD (determined by MRS +/- liver biopsy) and T2DM[194]. Performance of the NAFLD fibrosis score (NFS), fibrosis-4 index (FIB-4), CK-18, BARD (calculated from BMI, AST:ALT and diabetes presence), AST to platelet ratio index (APRI), and neo-epitope-specific competitive ELISA for PIIINP (Pro-C3), were all suboptimal (AUROC < 0.80), and no one test performed better than the others, although they all had good NPV greater than 90%. The FIB-4 performed the best in terms of positive predictive value (PPV) and NPV (80% and 94%, respectively), but the large proportion of indeterminate results when using this score remains a problem. Concern has also been raised about the use of NFS in a diabetes population, as the algorithm includes the presence of diabetes, leading to an elevated score for all pateints[195], yet it tends to misclassify more the prevalence of fibrosis[194,196]. Although several international practice guidelines recommend use of the FIB-4, one group has suggested that accuracy is too low to identify individuals at risk in a T2DM population that has a

moderate prevalence of advanced fibrosis[195,197] and using a higher cut-off in individuals with T2DM may improve the performance[194].

More recently, another risk score has been proposed, call fibrotic NASH index (FNI). It was derived from a cohort of morbidly obese individuals undergoing bariatric surgery, at which point a liver biopsy was obtained. The risk score used a combination of AST, HbA1c, and HDL-c, and had an AUROC of 0.78. The FNI was then validated in a T2DM population, where it had superior performance to the FIB-4[198].

Potential blood biomarkers that have previously been researched by this group include fibroblast activation protein (FAP) and dipeptidyl-peptidase 4 (DPP4). When combining FAP levels and NFS in a screening algorithm, ~40% of patients could be reclassified from "indeterminate risk" to "low risk" category[87]. Low FAP was found to have a good NPV in excluding advanced fibrosis. In addition, circulating DPP4 activity levels and CK-18 levels were associated with liver fibrosis in a cohort of individuals with NAFLD and T2DM[86].

1.5.3 Screening for NAFLD and NASH in T2DM

A joint Clinical Practice Guideline from the European Association for the Study of Liver (EASL), Diabetes (EASD) and Obesity (EASO) on the management of NAFLD was published in 2016[199]. It made a level A2 recommendation (high quality evidence, weaker recommendation) to assess for the presence of NAFLD in all individuals with T2DM, irrespective of their liver enzyme levels. Assessment included a minimum of a liver ultrasound and liver enzymes. However, the authors acknowledged that the availability of resources, the added burden on healthcare systems, and the limited effective treatments, would be important considerations in widespread screening. The American Diabetes Association (ADA) included screening for NAFLD, for the first time, in their 2019 Standards of Medical Care in Diabetes[200]. They recommended that all individuals with T2DM who have biochemical or radiological evidence of NAFLD should receive assessment for NASH and liver fibrosis. They suggest the use of non-invasive tests, such as elastography or fibrosis biomarkers, however the recommendation was based on low level (Level C) evidence. More recently, the American Association of Clinical Endocrinology (AACE) and the American Association for the Study of Liver Diseases (AASLD) published a clinical practice guideline[201].

They have recommended screening of all individuals with T2DM, firstly with the FIB-4, and then further testing with either the Enhanced Liver Fibrosis (ELF) test (*Table 1.5*) or transient elastography (*Section 1.4.3.2.2*) in the event of an indeterminate or high risk score. These were generally Grade B recommendations based on intermediate strength of evidence. There are currently no clinical practice guidelines in Australia for the screening of NAFLD in the T2DM population.

1.5.4 Management of NAFLD and NASH fibrosis in T2DM

The general principles of NAFLD and NASH management were discussed in *Section 1.4.5*, however additional considerations should be made in individuals with T2DM, particularly if they have NASH with ≥ F2 fibrosis[40].

1.5.4.1 Glucagon-like peptide-1 receptor agonists

In an RCT of individuals with NASH and T2DM, liraglutide for 48 weeks resulted in higher rate of NASH resolution and less progression of fibrosis on liver biopsy[202]. A 24-week study of dulaglutide reported improvements in liver fat, but not liver stiffness[203]. More recently, there has been much interest in semaglutide due to its superior weight loss and HbA1c effects. A phase 2 study over 72 weeks showed histological improvements in NASH with semaglutide, but there was no significant improvement in fibrosis stage[204]. The phase 3 trial (ESSENCE) is currently recruiting and the results are keenly awaited[205].

1.5.4.2 Sodium-glucose co-transporter-2 inhibitors

Dapagliflozin has been shown to improve liver steatosis and liver fibrosis (by transient elastography) in an RCT of individuals with NAFLD and T2DM over 24 weeks[206]. The fibrosis benefits were mild, and only found in individuals with significant liver fibrosis. An RCT of empagliflozin showed improvements in liver steatosis but did not evaluate effects on fibrosis[207]. In a small, single-arm pilot study of empagliflozin in individuals with biopsy-proven NASH and T2DM, there were significant improvements in steatosis, ballooning, and fibrosis on a serial liver biopsy after 48 weeks of treatment[208]. Again, it is unclear if these improvements are due to weight reduction induced by SGLT2 inhibitors, or whether there are direct effects on the liver. These preliminary studies show promise, although effects on liver fibrosis in NASH appear mild at best. Larger and longer-term studies are required.

1.5.4.3 Dual glucose-dependent insulinotropic polypeptide and glucagon-like peptide-1 receptor agonists

The co-administration of a dual glucose-dependent insulinotropic polypeptide (GIP) and GLP-1RA has synergistic effects on insulin and glucagon responses in individuals with T2DM. In the SURPASS series of clinical trials, tirzepatide has been shown to have superior effects in weight loss reduction and HbA1c when compared to, or used in combination with, other classes of diabetes medications, and is therefore a potential agent for treatment of NASH. A *post-hoc* exploratory analysis showed promising results in relation to improvements in blood biomarkers of NASH[209]. A phase 2 clinical trial of tirzepatide (SYNERGY-NASH) is currently in progress[210].

1.6 Animal Models of NASH Fibrosis

For over twenty years, researchers have used animal models to improve the understanding of the pathogenesis of NASH and to identify and test potential therapeutic targets[211]. Yet there are still no approved pharmacotherapies for the prevention or treatment of NASH; one of the major barriers to this is the lack of animal models that faithfully mimic the human condition whilst still exhibiting the full spectrum of disease. Some pre-clinical models do not reflect the disease aetiology as it occurs in humans, whilst other models do not always exhibit all the characteristic histological features of human NASH as set out in the Brunt and Kleiner criteria[80] (discussed in *Section 1.4.3.1*).

Recently, Farrell and colleagues proposed a minimum set of requirements for murine models of NASH to maximise the translational value of the research[212]. The main priorities included models that simulated metabolic dysregulation, with weight gain, abnormal lipid distribution, insulin resistance, hyperinsulinaemia and hyperglycaemia, whilst models that featured weight loss, insulin sensitivity or use of toxins were not recommended. Ideally, the liver tissue would be reviewed by a qualified pathologist with experience in human NASH who could apply the relevant scoring systems, but this data should be complemented with further laboratory analysis to confirm and quantify the results in the animal model. For example, using specialised staining to quantify the amount of fibrosis rather than rely solely on the F0 - F4 scale, or to confirm the presence of hepatocyte ballooning using immunohistochemistry.

Another major limitation of many existing animal models is the lack of emphasis on diabetes. As discussed in this literature review earlier (*Section 1.5*), not only is NAFLD and NASH much more prevalent in the diabetes population compared with the general population[68,188], but diabetes is also an independent risk factor for the progression to each of the more severe stages[67,189,190]. A review on mouse models of NASH found that only 25% of studies included features of insulin resistance or diabetes in their model, whilst the other 75% either did not include these features or did not report on them at all[211]. Added to this, there is no consensus on the diagnostic criteria for diabetes in animals, and thus there is heterogeneity in the definitions used.

Pre-clinical models can broadly be categorised into the following groups: diet-induced, deficiency-induced, toxin-induced, genetic, or a combination of these[213]. These will be discussed below, with a focus on development of liver fibrosis in the context of hyperglycaemia and diabetes.

1.6.1 Diet-induced models of NASH fibrosis

A high fat diet is a simple method for inducing obesity and insulin resistance in animals. Diets containing up to 70% of calories from fat result in hepatic steatosis and mild inflammation without significant fibrosis even after prolonged feeding[212]. In the absence of 'force feeding' by gavage, the mild phenotype is a major limitation of these models, as is the variability in inducing mild hyperglycaemia.

Excessive cholesterol has been shown to cause progression of steatosis to NASH[214], and hence cholesterol has been added to a high fat diet in many studies to enhance the disease severity[215]. However, there are concerns that the amount of added cholesterol is not translatable to the human diet. For example, a 2% cholesterol diet for a mouse is equivalent to 2000 mg/day in a human diet, which is almost seven times the average daily intake of cholesterol[216]. In addition, added cholesterol (1.25%) was shown to result in discordant changes in lipid and glucose metabolism, whereby mice had decreased hepatic triglyceride concentrations and cholesterol synthesis, but improvement in insulin and glucose tolerance[217]. Ideally, added cholesterol in animal models should be kept to < 0.5% to maintain some relevance to human disease.

A so-called “Western” diet attempts to emulate unhealthy human intake by combining a mix of excessive fat, sugar, and cholesterol[213]. The compositions can vary quite markedly between studies, making comparisons challenging. In a study of mice fed a Western diet with corn syrup added to drinking water to increase fructose intake, obesity, insulin resistance, mild hyperglycaemia and mild to moderate fibrosis were noted at 24 weeks[218]. Lesser effects were observed in other species, including rats and hamsters, albeit in shorter duration studies[213].

The diet-induced animal model of non-alcoholic fatty liver disease (DIAMOND) mice are an inbred strain (C57BL/6J (B6) and 129S1/SvImJ (S129) mice) which combine genetic effects with an *ad libitum* Western diet (42% fat, 34% sucrose, 0.1% cholesterol, and 4.2% fructose/glucose solution) to induce NASH with significant fibrosis over 52 weeks[219]. These mice display many of the hallmark metabolic and histological features of human NASH, but do not display hyperglycaemia or diabetes.

1.6.2 Deficiency-induced models of NASH fibrosis

The methionine- and choline-deficient (MCD) diet is another frequently used animal model that induces NASH with fibrosis by impairing β-oxidation and VLDL production and secretion, leading to accumulation of FFAs in the liver[213]. Fibrosis occurs within five weeks, but by eight weeks, mice have lost a significant amount of weight due to the hypermetabolic state and display enhanced peripheral insulin sensitivity[212]. In attempts to achieve a more clinically relevant model, some studies have combined the MCD diet (or choline-only-deficient diet) with either a high fat diet or genetically obese strain, such as *db/db* mice[212]. The choline-deficient, L-amino acid-defined (CDAA) diet is also deficient in choline, but has some proteins replaced with L-amino acids[220,221]. Fibrosis takes 20 weeks to develop[222]. Unlike the MCD diet, mice fed a CDAA diet do not lose weight, but nor do they gain weight, compared to controls[222], and they still do not exhibit any of the metabolic disturbances in human NASH. The CDAA diet has also been combined with a high fat diet, however these mice still have decreased weight gain with lower circulating glucose, insulin and lipid concentrations compared with control mice[223,224]. Whilst each of these animal models can robustly induce liver fibrosis, the severe nutritional deficiency required to achieve this and the lack of metabolic disturbances, significantly reduce the utility of these models in studying human NASH.

1.6.3 Toxin-induced models of NASH fibrosis

Models of liver fibrosis that use toxins have arguably the least relevance to human NASH, however the main advantage is the rapid and robust induction of advanced fibrosis, including cirrhosis and even development of HCC. Carbon tetrachloride (CCl_4) has been used in mouse and rat studies, where it generates the trichloromethyl free radical to induce zone 3 (central) fibrosis[225], like human NASH, although the underlying pathogenesis is very different. Cirrhosis can be induced within as little as nine weeks in this model[226]. Thioacetamide (TAA) has also been used in rodents and develop early periportal fibrosis by week six, and cirrhosis by week 16[227]. But early periportal fibrosis is generally a hallmark of NASH in children and not adults[213]. To overcome the lack of metabolic dysfunction in these toxicity models, one study combined low dose CCl_4 with a Western diet[228]. This model induced histological and transcriptomic changes similar to human NASH, but development of cirrhosis by 24 weeks was inconsistent. In addition, the use of CCl_4 mitigated some of the metabolic effects of the Western diet, with reductions in food intake, lesser weight gain, and lower insulin level. Dimethylnitrosamine (DMN) and diethylnitrosamine (DEN) are highly hepatotoxic agents to humans and animals, and whilst models that utilise these agents can induce fibrosis and cirrhosis, they are more suited to studies of liver carcinogenesis[229].

1.6.3.1 Combined streptozotocin and high fat diet-induced models of NASH fibrosis

A major disadvantage of the above-mentioned toxicity models is the absence of metabolic abnormalities, and particularly relevant to this thesis, the absence of diabetes. Streptozotocin (STZ) is frequently used in animal models of diabetes, whereby it destroys pancreatic β cells[230]. Administration of high (cumulative) doses can cause liver toxicity[231] as well as induce an absolute insulin deficiency synonymous with type 1 diabetes mellitus[232,233].

1.6.3.1.1 The Stelic Animal Model

The Stelic Animal Model (STAM™) is a commercially available model that aims to recapitulate human NASH by combining STZ with a high fat diet[234]. Mice are given a single dose (200 µg) of STZ on day two of life, before being commenced on a 32% fat diet from the age of four weeks. The mice progress quickly through each stage of

NASH and have developed HCC by 20 weeks. However, this model is also not a faithful replication of human NASH, as mice are given STZ in the neonatal period and do not display insulin resistance or hyperinsulinaemia[212].

1.6.3.1.2 The Fat and Diabetes model

Our laboratory has established a mouse model that more accurately reflects human NASH. Our Fat and Diabetes (FaD) model induces obesity, insulin resistance and hyperinsulinaemia with a high fat diet (45% kcal fat) commenced at ~five weeks of age and continued for 15 weeks, before subsequent induction of diabetes with two low doses of STZ (65 mg/kg/day)[144,145]. These mice reliably develop significant fibrosis by 20 weeks, and cirrhosis by 40 weeks. In addition, mice exhibited a relative but not absolute insulin deficiency, and the hepatoxic effects of STZ were excluded by demonstrating inhibition of fibrosis with insulin treatment[145].

1.6.5 Genetic models of NASH fibrosis

There are several animal models derived from genetic manipulation that result in hyperphagic-driven obesity. A mutation in the leptin gene (*ob/ob* mice) or leptin receptor (*db/db* mice or *fa/fa* rats) produces animals that exhibit the correct metabolic phenotype of obesity, insulin resistance, dyslipidaemia, and diabetes-range hyperglycaemia[235]. However, whilst they display hepatic steatosis and inflammation, they do not develop fibrosis[235,236]. Addition of a high fat diet or nutrient deficient diet to these models can induce a mild periportal fibrosis[213], but the underlying genetic abnormality is extremely rare in humans, and thus not representative of human NASH.

The *foz/foz* mouse has a spontaneous mutation in the Alström gene (*Alms1*) that also results in hyperphagia, obesity and hyperglycaemia. When fed a high fat diet (43% fat with 0.2% cholesterol), these mice display the histological features of human NASH by 24 weeks, including mild to moderate fibrosis[213,235]. The KK-ay mice have a heterozygous mutation in the Agouti gene, and like the other mice with genetic mutations, display metabolic dysregulation, including hyperglycaemia, but do not develop liver fibrosis alone[237]. They have been used in combination with nutrient deficient diets (+/- high fat diet) to induce fibrosis, however this has been mild at best, and the metabolic phenotype is diminished by the nutrient deficiency[213,224].

Melanocortin 4 receptor deficiency has been identified as the most common monogenic form of obesity in humans, characterised by early-onset severe obesity, hyperphagia and severe hyperinsulinaemia with euglycaemia[238]. Melanocortin 4 receptor-deficient (*Mc4r*$^{-/-}$) mice exhibit a similar metabolic phenotype to humans[239]. When fed a high fat diet, they develop the spectrum of histological features of NASH by 20 weeks, including a moderate degree of fibrosis[239]. Studies of longer duration might elicit more severe fibrotic disease. The absence of diabetes in this model renders it less useful to the context of this thesis.

The above-mentioned genetic models of NASH with fibrosis focus on overnutrition as a key feature. Many other models exist that target specific pathways (e.g., lysophospholipid receptor knockout, apolipoprotein E knockout, phosphatase and tensin homolog knockout, SREBP-1c knockout, microsomal triglyceride transfer protein knockout[212]), but in general, they either do not capture the metabolic disturbances, or do not produce significant liver fibrosis, and thus will not be discussed here.

1.7 The CCN Family

1.7.1 The history of CCN nomenclature

The cellular communication network (CCNs) are a family of six homologous cysteine-rich matricellular proteins with key roles in normal cellular function and tissue pathology[240]. The term CCN was first coined by Bork in 1993, referring to the first letter of each of the first three members: cysteine-rich 6 (CYR61), connective tissue growth factor (CTGF), and nephroblastoma overexpressed (NOV)[241]. Subsequently, three more members, designated Wnt induced secreted proteins (WISP), were identified[242]. The nomenclature of the CCNs were officially changed by the HUGO Gene Nomenclature Committee in 2018, with the aim to eliminate confusion in the literature caused by members being given multiple names, and to acknowledge the interrelated structure and function of the family members[243]. The official names, with their previous names, are listed in *Table 1.7*.

Table 1.7: The official CCN nomenclature. Adapted from Perbal et al., 2018[243]

Current gene symbol	Current gene name	Previous gene symbol	Previous gene name	Alias gene symbols
CCN1	Cellular communication network factor 1	CYR61 IGFBP10	Cysteine rich angiogenic inducer 61	GIG1
CCN2	Cellular communication network factor 2	CTGF	Connective tissue growth factor	IGFBP8
CCN3	Cellular communication network factor 3	NOV	Nephroblastoma overexpressed	IGFBP9
CCN4	Cellular communication network factor 4	WISP1 WISP1-OT1 WISP1 UT1	Wnt1 inducible signalling pathway protein 1	WISP-1
CCN5	Cellular communication network factor 5	WISP2	Wnt1 inducible signalling pathway protein 2	WISP-2 CT58 CTGF-L
CCN6	Cellular communication network factor 6	WISP3	Wnt1 inducible signalling pathway protein 3	WISP-3

1.7.2 Modular structure of the CCN proteins

The CCN proteins have a highly conserved, modular structure, as depicted in *Figure 1.10*[244]. Each protein has five exons interspersed with four introns (except for CCN5 which lacks exon 5). The N-terminus is encoded by exons 1-3 and the C-terminus is encoded by exons 4 and 5. The first exon encodes the signal peptide sequence, followed by four exons that encode four domains: insulin-like growth factor (IGF) binding protein (IGFBP; Module I) domain, von Willebrand Factor C (vWC; Module II) domain, thrombospondin 1 (TSP1; Module III) domain and C-terminal (CT; Module IV) domain. Whilst there is a central hinge between the N- and C-terminus, the regions between each module are also sensitive to proteolysis, allowing production of truncated proteins and individual modules that may express distinct biological properties[245]. The central hinge is not conserved between the CCN proteins, thus allowing binding to different receptors to produce different functions[246].

The CCN proteins are 30 - 40 kDa in size. They share 40 - 60% similarity in their amino acid sequences, including 38 cysteine residues and 17 disulphide bonds (except for CCN5 and CCN6 which have less cysteine residues)[244]. Each protein has an unique

3-dimensional conformation that is dictated by the surface electrostatic charge, which in turn dictates their interaction with other molecules and overall biological function[244]. The structural heterogeneity of the modules is likely to contribute to the functional diversity of CCN proteins[240].

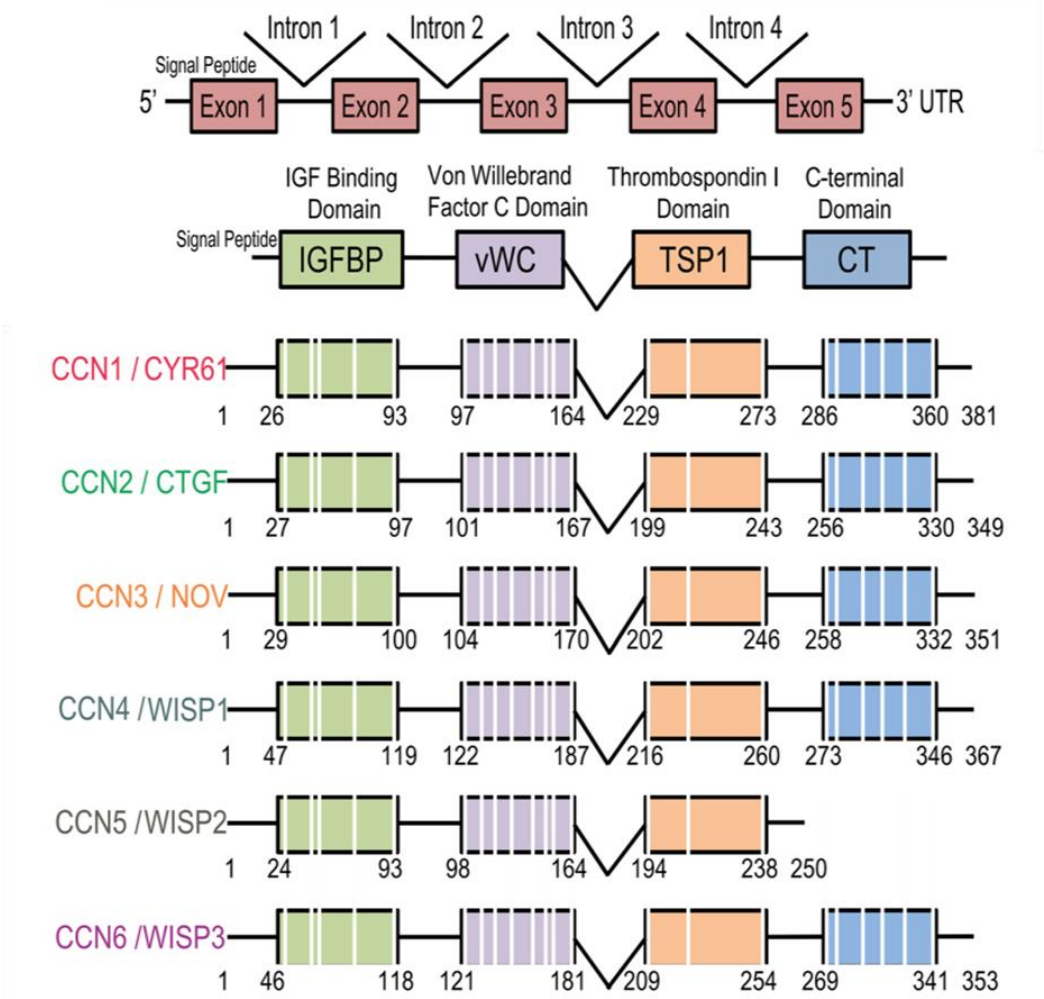

Figure 1.10: Modular structure of CCN proteins. Image from Krupska et al., 2015[244].

The sequence of the IGFBP domain of CCN proteins is very similar to that of traditional IGFBPs, and hence it was initially hypothesised that CCN proteins exerted their actions via binding to IGFs[241]. However, despite the similarity, IGFs have a very poor affinity and sequence homology with CCN proteins that is approximately 100 times lower than within the traditional IGFBPs[247]. The vWC domain is found in over 500 ECM proteins[248]. Its main functions are to regulate bone morphogenic proteins (BMPs) and TGFβ signalling[142]. The TSP domain is also found in many ECM proteins[249]. It has four main functions: cell attachment sites in signalling and adhesion, inhibiting angiogenesis, binding sites for many growth factors and ECM proteins (e.g.,

fibronectin, TGFβ, collagens, integrins, MMPs) and glycosaminoglycan binding sites[250]. Finally, the CT domain contains a cysteine knot motif and can mediate many biological functions including cell adhesion and ECM composition.

1.7.3 Biological roles of the CCN proteins

The CCN proteins regulate a range of biological functions including: mitosis, adhesion, apoptosis, mitogenesis, growth arrest, migration, differentiation and survival [240]. They also have important roles in ECM regulation, embryonic development, skeletal development, inflammation, tumorigenesis, angiogenesis and wound healing[251]. The CCNs are widely expressed in many tissues and organs during embryogenesis, whereas in adulthood expression is down-regulated in most tissues and only up-regulated at sites of inflammation, tissue repair and wound healing[252].

1.7.4 Regulation of the CCN proteins

The CCN proteins are tightly regulated at the transcriptional, post-transcriptional and translational levels in response to cell signals and environmental stimuli, such as growth factors, cytokines, steroid hormones, hypoxia, irradiation or mechanical forces[252].

The CCN proteins do not have a unique receptor. Instead, they can bind to a range of different integrins on different target cell types, thereby eliciting different biological responses[253]. In addition, they can bind to heparin sulphate proteoglycans (HSPGs) through a heparin-binding domain within the CT domain. HSPGs can act as co-receptors for many signalling receptors. The integrins and HSPGs are crucial for the mitogenic and adhesive functions of the CCNs. One example of the multiple biological activities that can be stimulated through binding of discrete domains to different cell surface receptors involves CCN2: it can bind to the low-density lipoprotein (LDL) receptor-related protein 1 (LRP1) via module III[254,255], it can bind to the Wnt co-receptor LDL-receptor-related protein 6 (LRP6) via module IV [256], and it can bind to the tyrosine kinase receptor TrkA[257].

In addition to binding to integrins and HSPGs, CCNs can bind to growth factors and cytokines. For example, CCN2 can bind to TGFβ through module II, thereby enhancing the activity of TGFβ[142]. It can also bind to fibronectin through module IV and to vascular

endothelial growth factor (VEGF) through module III and IV[258], which affects adhesion and angiogenesis. The interaction of CCNs with TNFα significantly alters TNFα activity, converting it from pro-proliferation to a pro-apoptotic cytokine in fibroblasts[259].

1.7.5 The CCNs in inflammation

The CCN proteins can modulate the inflammatory response through regulation of the activity and expression of chemokines and cytokines[260]. In return, some CCN proteins, including CCN1 and CCN2, are induced by inflammatory cytokines[252]. There is activation of the pro-inflammatory NF-κB pathway, as depicted in *Figure 1.11*. The CCN proteins also contribute to inflammatory cell (e.g. immune and vascular cells) adhesion, migration, proliferation and apoptosis[260]. Furthermore, they have been implicated in the pathogenesis of many inflammatory diseases, such as atherosclerosis, rheumatoid arthritis, inflammatory kidney disease, and neuroinflammatory diseases[260]. The role of CCN proteins in inflammation of NASH development has not been fully elucidated.

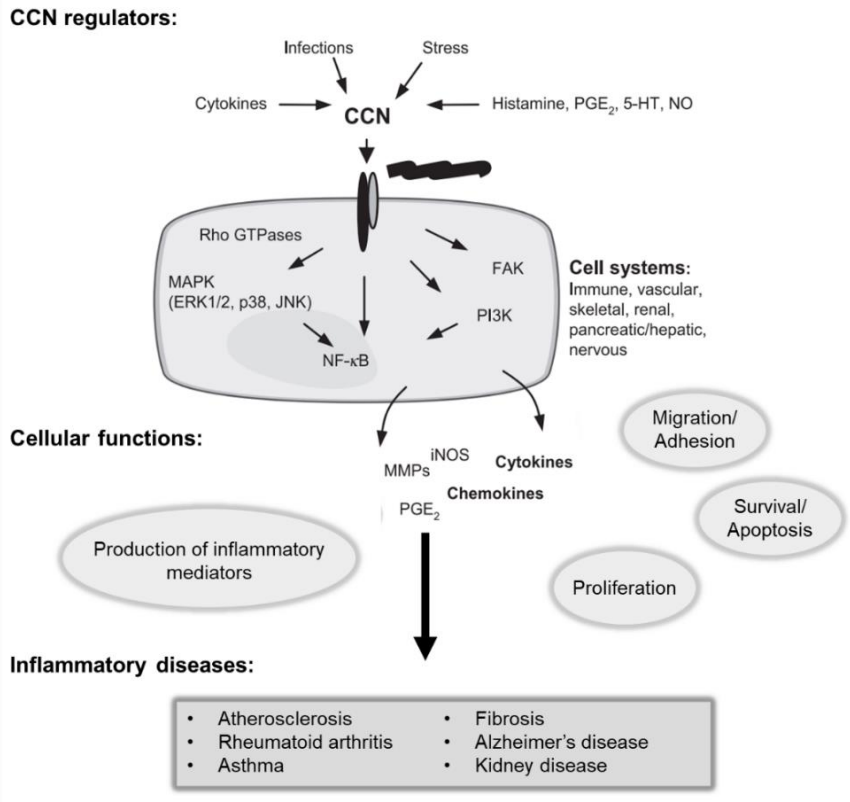

Figure 1.11: Schematic diagram depicting the role of CCN proteins in inflammation. There is activation of multiple intracellular signalling pathways, leading to initiation of diverse cellular functions that may result in inflammatory diseases. Image from Kular et al., 2010[260].

1.7.6 The CCNs in fibrosis

The CCN proteins have been implicated in the pathogenesis of fibrosis, although the exact mechanisms have not been determined. As shown in *Figure 1.12*, the general process is thought to involve tissue injury leading to abnormal expression of CCN proteins; the CCNs then regulate cell functions through interactions with integrins, HSPGs, cytokines and chemokines, altering biological functions and leading to activation of downstream signalling pathways, such as Wnts, TGFβ, and Notch[261]. The biological response of matrix remodelling then depends on whether ECM synthesis or ECM degradation is the dominant process and also potentially quantitative changes in ECM protein ratios. *Table 1.8* outlines the pro- or anti-fibrotic properties of each member of the CCN family, and in which tissues there is evidence of activity.

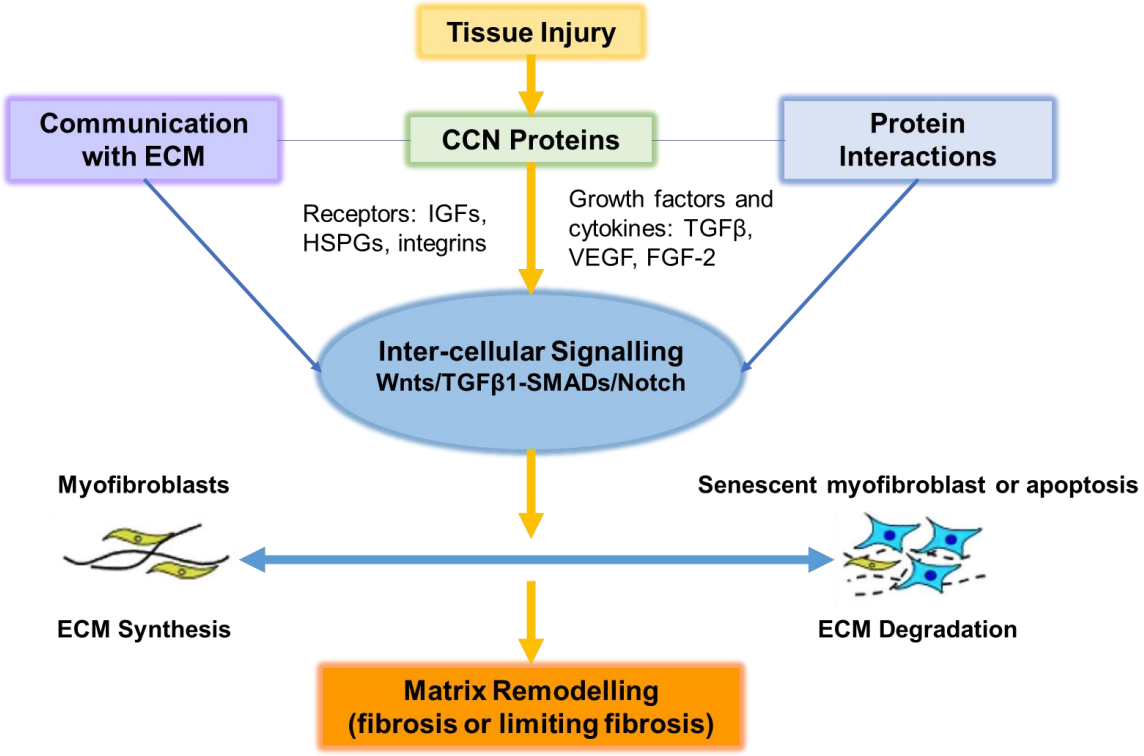

Figure 1.12: Schematic of the role of CCNs in fibrosis. Image from Sun et al., 2020[261].

Table 1.8: Summary of pro- or anti-fibrotic properties of each CCN protein. Adapted from Sun et al., 2020[261].

CCN Protein	Function	Proposed Mechanism	Tissues
CCN1	Anti-fibrotic	Induction of senescence of myofibroblasts[262-266]	Cardiac, liver, lung, kidney, skin
CCN2	Pro-fibrotic	Activation of fibroblasts and HSCs[267-269]	Cardiac, kidney, liver, lung, ocular and neural disorders, systemic sclerosis
CCN3	Anti-fibrotic	Suppression of CCN2[270]	Kidney, liver
CCN4	Pro-fibrotic		Cardiac, liver, lung, skin, submandibular
CCN5	Anti-fibrotic	Inhibition of TGFβ signalling[271]	Cardiac, lung, retinal pigment epithelium, skin
CCN6	Unclear		Lung

1.7.7 The CCNs in diabetes-related complications

The CCN proteins have also been implicated in the development of diabetes-related macro- and micro-vascular complications[272]. Clinical and pre-clinical studies have identified a role of both CCN1 and CCN2 in development of diabetic retinopathy, through pro-angiogenic properties and thickening of the retinal capillary basal lamina[272]. Strong evidence exists for the role of CCN2 in development of diabetic kidney disease, where it may inhibit MMP activity and up-regulate TIMP1 to promote ECM deposition in the kidneys[273]. This is counterbalanced to some degree by up-regulation of CCN3, an inhibitor of CCN2[270]. CCN2 levels are also elevated in atherosclerosis related to cardiovascular and cerebrovascular disease, as well as fibrotic diabetic cardiomyopathy[240,272]. The role of the CCNs in NASH fibrosis, as a non-classical complication of diabetes, will be discussed in *Section 1.7.8* and *1.7.9*.

1.7.8 CCN2 and NASH fibrosis

There has been much research into the role of CCN2 in many different fibrotic liver diseases, with relatively fewer clinical or pre-clinical studies performed specifically in NASH[274]. Liver biopsy studies of individuals with chronic liver diseases (not NASH) have demonstrated increased CCN2 expression, which in general, positively correlated with the degree of fibrosis regardless of the underlying aetiology[267-269]. In a study of sixteen individuals with NASH exclusively, CCN2 overexpression was

observed in 100% of the liver biopsies, and again, the amount of immunostaining was proportional to the fibrosis severity[275].

Early pre-clinical liver fibrosis models (CCl_4 and bile duct ligation) have been used to demonstrate increased liver CCN2 gene expression[267]. Using a translatable mouse model of NASH fibrosis induced by high fat feeding and diabetes (FaD model; *Section 1.6.3.1.2*), our laboratory has shown similar results where there was a trend for increased CCN2 mRNA levels and up-regulated CCN2 protein[145]. Although *in vitro* studies cannot replicate the setting of NASH, they are still important to understanding the relationship between activated HSCs and CCN2. Cultured HSCs were found to be a major source of CCN2 in the liver, with increased mRNA and protein levels, and confirmed with *in situ* hybridisation[267]. CCN2 is produced by many liver cells, including activated HSCs in response to stimuli such as TGFβ, lipid peroxidation products, VEGF, acetaldehyde, or PDGF-BB (summarised in *Figure 1.13*)[269,276]. It is likely that CCN2 has both autocrine and paracrine actions within the liver[274].

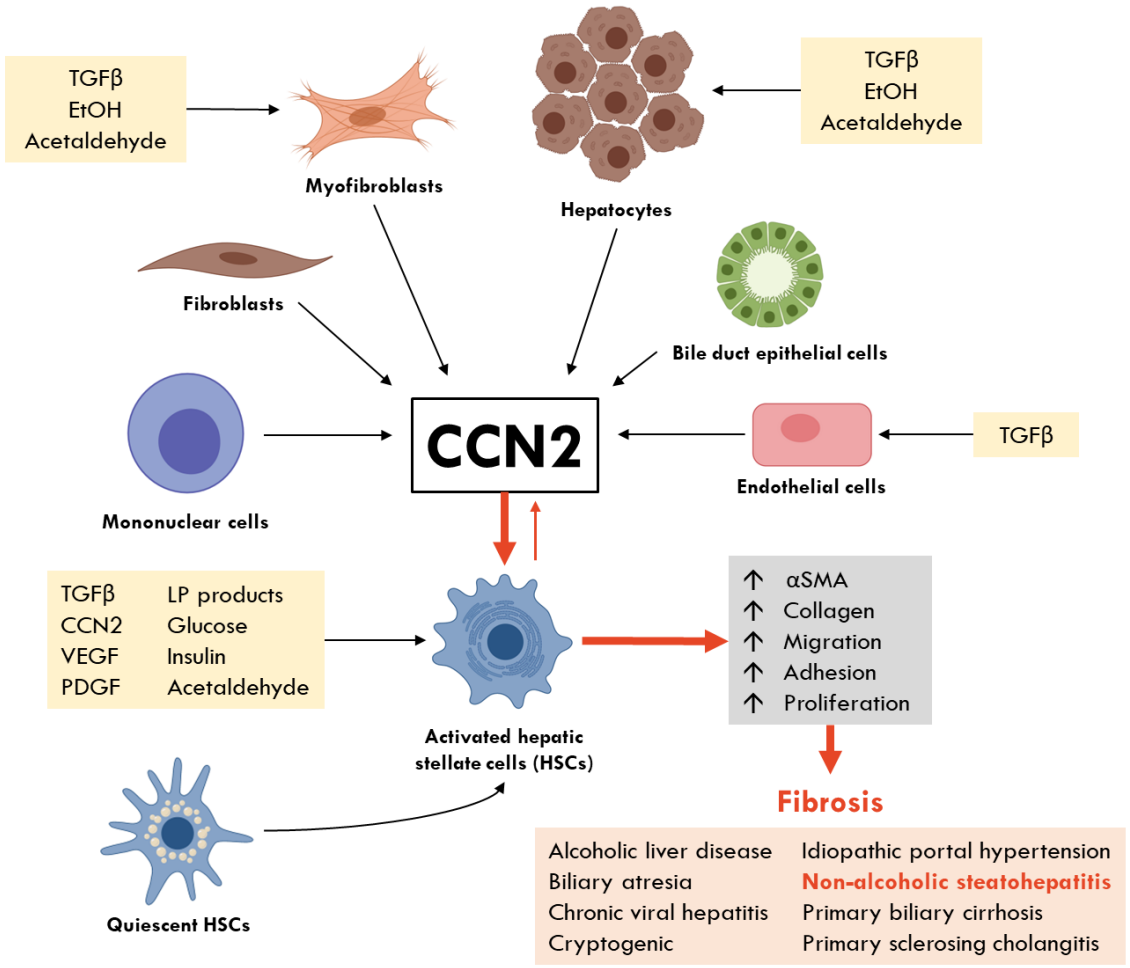

Figure 1.13: The role of CCN2 in fibrotic liver diseases. Most cell types within the liver can be stimulated to produce CCN2 which contributes to activation of the hepatic stellate cells and the fibrotic response. Image from Rachfal et al., 2003[274].

Together, this data suggests that the up-regulation of CCN2 plays a critical role in the pathogenesis of liver fibrosis and may be a target for therapeutic intervention. Our laboratory has demonstrated that systemic administration of a neutralising polyclonal antibody against CCN2 provided some protective effect against the development of NASH fibrosis[144]. Involvement of the MAPK signalling pathways, specifically reduction in phosphorylation of ERK, was identified as a possible mechanism for fibrosis development[144]. In addition, inhibition of CCN2, by anti-CCN2 oligonucleotides[277] and small interfering RNA (siRNA)[278] in non-NASH pre-clinical models has led to decreased liver fibrosis.

Systemic CCN2 may also have clinical utility as a non-invasive biomarker for prediction of fibrosis. Serum CCN2 positively correlates with severity skin, lung, and kidney fibrosis[279-281]. Similar evidence also exists in non-NASH-mediated liver fibrosis[282-285]. Collectively, this data provides support to the hypothesis that CCN2 may be a possible mediator, and pathophysiological biomarker, of liver fibrosis.

1.7.9 CCN1 and NASH fibrosis

There are some clinical and pre-clinical studies reporting on CCN1 in the context of liver fibrosis, but fewer that specifically examine CCN1 in NASH fibrosis. CCN1 protein was found to be highly accumulated in the cytoplasm of hepatocytes of humans with cirrhosis (aetiology unknown), whereas the levels were relatively lower in biopsies from people without liver disease[286]. Similar results were found in a more recent study comparing humans with biopsy-proven NASH versus healthy controls: hepatic CCN1 levels were increased at both the mRNA and protein level in the NASH group[287], however, a limitation of this study was that there was no reported assessment of fibrosis and thus the links between CCN1 and fibrosis were not explored.

Pre-clinical animal models using CCl_4 and bile duct ligation have demonstrated that CCN1 levels are up-regulated in response to liver injury, and that CCN1 functions to inhibit liver fibrosis through induction of senescence of activated HSCs[286,288]. The effects of CCN1 were mediated through the binding of integrin $\alpha_6\beta_1$ to activate the RAC1-NOX1 pathway (*Figure 1.14*)[246]. Subsequently it was shown that in response to CCl_4, mice with hepatocyte-specific deletion of CCN1 exhibited more liver fibrosis and less HSC senescence, whereas overexpression of CCN1 led to reductions in liver fibrosis with more HSC senescence[286]. A study of adenoviral overexpression of CCN1 in primary portal myofibroblasts, cells which also produce ECM, resulted in increased ROS production and cellular senescence, and reduced fibrosis markers[288]. In mice, the systemic delivery of purified CCN1 was able to enhance the regression of established liver fibrosis[286]. These studies support the important antifibrotic role of CCN1 in liver fibrogenesis and provide a rationale for its potential as a therapeutic target.

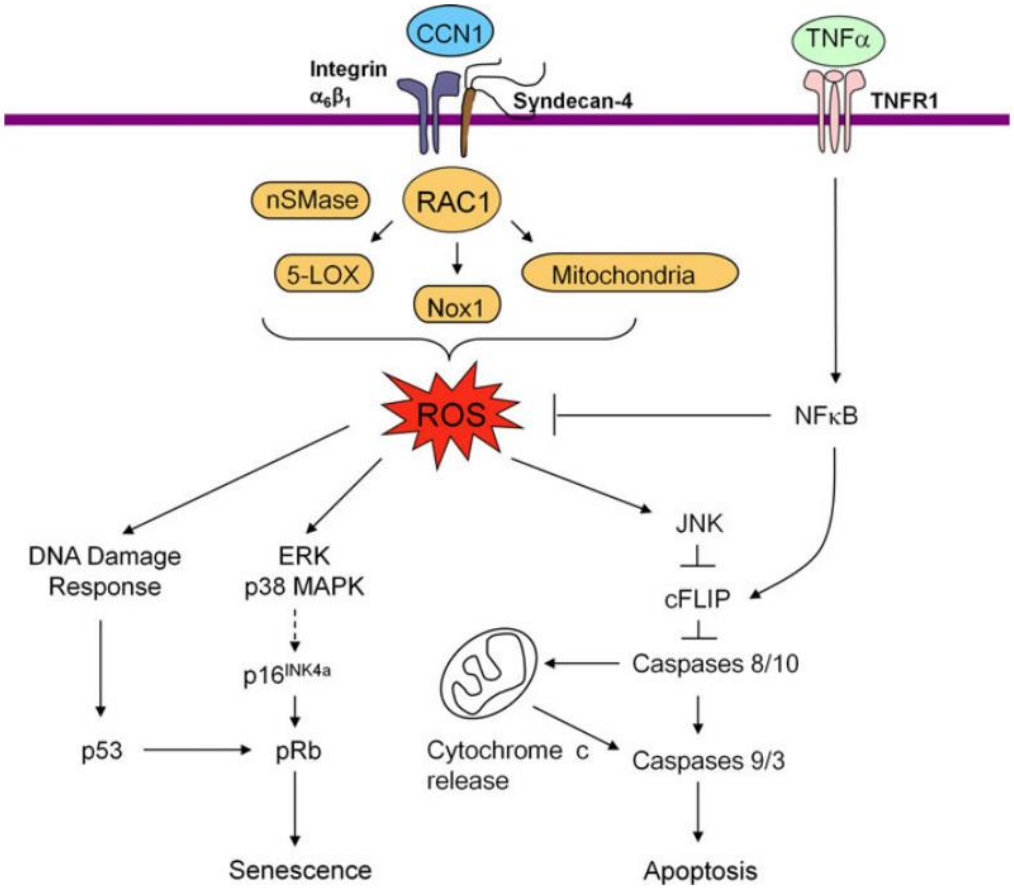

Figure 1.14: Schematic of CCN1-induced senescence and apoptosis through activation of the RAC1-Nox1 pathway. Image from Lau, 2013[246].

However, one study has proposed that CCN1 may promote steatosis and inflammation and identified CCN1 as positive regulator in NASH[287]. Using mouse models of an MCD diet or a 60% high fat diet with added cholesterol, overexpression of CCN1 worsened the severity of steatosis and conversely, down-regulation of CCN1 decreased the severity of steatosis. CCN1 overexpression was also shown to promote macrophage infiltration and pro-inflammatory cytokine production. A major confounder in this study is the lack of fibrosis assessment, which is a key liver endpoint in studies of NASH. Indeed, the degree of fibrosis can affect steatosis, particularly in “burnt out” NASH where there is frequently reduced steatosis observed with severe fibrosis. Therefore, it is difficult to make conclusions about steatosis when there is no report on fibrosis severity. Nevertheless, the effects on inflammation, which may be independent of fibrosis, cannot be ignored. The pro-inflammatory response may be a result of CCN1’s diverse and sometimes discordant functions that are influenced by the cell and environment context[246]. Further studies in this area are needed.

1.8 Thesis Hypotheses and Aims

Given the background described in the literature review, the hypotheses of this thesis were:

1) A dedicated multidisciplinary diabetes and liver clinic can enhance the assessment for NASH fibrosis;
2) Members of the CCN family are implicated in the progression of liver fibrosis in NASH and T2DM:
    a. Hepatocyte-specific CCN2 gene deletion in a pre-clinical model of NASH fibrosis induced by high fat feeding and diabetes, will protect against NASH fibrosis, compared with control mice;
    b. Hepatocyte-specific CCN1 gene deletion in a pre-clinical model of NASH fibrosis induced by high fat feeding and diabetes, will worsen NASH fibrosis, compared with control mice;
3) Circulating CCNs are potential biomarkers of diabetes-related complications, including NASH fibrosis.

The aims of this thesis, respectively, were:

1) To profile the patients seen in a multidisciplinary diabetes and liver clinic in a tertiary hospital:
    a. To determine the prevalence of advanced liver fibrosis in this cohort of patients;
    b. To identify clinical and/or biochemical factors that are associated with advanced liver fibrosis;
2)
    a. To examine whether homozygous gene deletion of hepatocyte-specific CCN2 leads to a less severe NASH fibrosis phenotype compared to control mice exposed to high fat feeding and diabetes;
    b. To examine whether homozygous gene deletion of hepatocyte-specific CCN1 leads to a more severe NASH fibrosis phenotype compared to control mice exposed to high fat feeding and diabetes;
3) To determine if circulating levels of CCN1, CCN2 and CCN3 can be used as potential biomarkers of diabetes-related complications, including NASH fibrosis, in clinical and pre-clinical studies.

This thesis firstly highlights the scope of the problem, that is, the high and under-recognised prevalence of NASH fibrosis in a selected T2DM cohort, observed in a dedicated multidisciplinary diabetes and liver disease clinic. It then uses an established pre-clinical model of NASH fibrosis in combination with novel tissue-specific gene knockouts to explore the role of hepatocyte CCN2 and CCN1 in the development and progression of NASH fibrosis in T2DM. Finally, the work in this thesis examines the utility of circulating CCNs as biomarkers of diabetes complications in a T2DM cohort, as well as their utility as biomarkers for NASH fibrosis in our pre-clinical studies. Collectively, the studies in this thesis reflect translational research in this emerging field of diabetes and NASH, helping to point the way to novel interventions, and exploring markers of disease and potential clinical solutions.

Chapter 2: Materials and Methods

2.1 Reagents

Table 2.1: List of reagents.

Reagent	Manufacturer
Acid casein	NZMP, Richmond, VIC, Australia
AIN-76 Mineral mixture	MP Biomedicals LLC, Solon, OH, USA
AIN Vitamin mixture 76	MP Biomedicals LLC, Solon, OH, USA
Anti-CTGF/CCN2 antibody	GeneTex, Irvine, CA, USA
β-mercaptoethanol	Sigma-Aldrich, St Louis, MO, USA
Bran	Woolworths, Bella Vista, NSW, Australia
Chloroform	Ajax Finechem, Scoresby, VIC, Australia
Cholesterol	Sigma-Aldrich, St Louis, MO, USA
Choline bitartrate	Sigma-Aldrich, St Louis, MO, USA
Citrasol	Labtech Service and Supplies, South Windsor, NSW, Australia
Citric acid	Sigma-Aldrich, St Louis, MO, USA
Clarity™ Western ECL	Bio-Rad, Hercules, CA, USA
DC Protein Assay	Bio-Rad, Hercules, CA, USA
Dibutyl-Phthalate in Xylene	Sigma-Aldrich, St Louis, MO, USA
Dimethyl sulfoxide	Ajax Chemicals, Auburn, NSW, Australia
dNTP	Meridian Bioscience, Memphis, TN, USA
DTT	Invitrogen, Carlsbad, CA, USA
DuoSet® Ancillary Reagent Kit 2	R&D Systems Inc, Minneapolis, MN, USA
Enzyme-linked Immunosorbent Assay Kit for Connective Tissue Growth Factor	Cloud-Clone Corp, Houston, TX, USA
Eosin, alcoholic with phloxine	POCD Scientific, North Rocks, NSW, Australia
Formalin solution, neutral buffered, 10%	Sigma-Aldrich, St Louis, MO, USA
Gelatine powder	Ward McKenzie Pty Ltd, Altona, VIC, Australia
GelRed® nucleic acid stain	Sigma-Aldrich, St Louis, MO, USA
Glucagon	Novo Nordisk Pharmaceuticals Pty Ltd, North Sydney, NSW, Australia
Glucose	Phebra, Lane Cove West, NSW, Australia
Harris' haematoxylin	POCD Scientific, North Rocks, NSW, Australia
Homogenizer spin cartridge	Invitrogen, Carlsbad, CA, USA
Human CTGF/CCN2 DuoSet® ELISA Development System	R&D Systems Inc, Minneapolis, MN, USA
Human NOV/CCN3 DuoSet® ELISA Development System	R&D Systems Inc, Minneapolis, MN, USA

Infinity™ Triglycerides reagent	Thermo Fisher Scientific Inc, Waltham, MA, USA
Insulin glargine	Sanofi, Macquarie Park, NSW, Australia
Insulin neutral	Novo Nordisk Pharmaceuticals Pty Ltd, North Sydney, NSW, Australia
Irradiated Rat and Mouse Diet	Specialty Feeds, Glen Forrest, WA, Australia
Lard	York Foods, Goulburn, NSW, Australia
L-methionine	Sigma-Aldrich, St Louis, MO, USA
Lysing Matrix Tubes, size D	MP Biomedicals Germany, Eschwege, Germany
Methanol	POCD Healthcare, Artarmon, NSW, Australia
MicroAmp™ Optical 384-well Reaction Plate	Applied Biosystems, Waltham, MA, USA
MicroAmp™ Optical Adhesive Film	Applied Biosystems, Waltham, MA, USA
Micro sample tube K3 EDTA	Sarstedt, Numbrecht, Germany
Mouse C-Peptide ELISA Kit	Crystal Chem, Elk Grove Village, IL, USA
Mouse CTGF/CCN2 ELISA Kit	Novus Biologicals, Centennial, CO, USA
Mouse CYR61 SimpleStep ELISA® Kit	Abcam, Cambridge, UK
Mouse Cytokeratin 18 SimpleStep ELISA® Kit	Abcam, Cambridge, UK
Normal saline	Pfizer, West Ryde, NSW, Australia
NOV (CCN3) Mouse SimpleStep ELISA® Kit	Abcam, Cambridge, UK
O.C.T. Compound	Sakura Finetek Inc, Torrance, CA, USA
$Oligo(dT)_{12-18}$ Primer	Invitrogen, Carlsbad, CA, USA
Picric acid	Sigma-Aldrich, St Louis, MO, USA
Polypropylene plastic tubes	Sarstedt, Numbrecht, Germany
Precimat glycerol	Roche, Basel, Switzerland
Protease inhibitor cocktail	Roche, Basel, Switzerland
PureLink™ DNase Set	Invitrogen, Carlsbad, CA, USA
PureLink™ RNA Mini Kit	Invitrogen, Carlsbad, CA, USA
Quantikine® ELISA Human Cyr61/CCN1 Immunoassay	R&D Systems Inc, Minneapolis, MN, USA
Random Hexamer	Invitrogen, Carlsbad, CA, USA
REDExtract-N-Amp Tissue PCR Kit	Sigma-Aldrich, St Louis, MO, USA
Rice starch	MP Biomedicals LLC, Solon, OH, USA
SDS-PAGE gel	Bio-Rad, Hercules, CA, USA
SensiMix™ SYBR® Hi-ROX	Meridian Bioscience, Cincinnati, OH, USA
Sodium chloride	Sigma-Aldrich, St Louis, MO, USA
Strand Buffer, 5x	Invitrogen, Carlsbad, CA, USA
Streptozotocin	Sigma-Aldrich, St Louis, MO, USA
Sucrose	Ajax Finechem, Scoresby, VIC, Australia

Sunflower oil	Woolworths, Bella Vista, NSW, Australia
Superfrost® Plus microscope slides	Lomb Scientific Pty Ltd, Taren Point, NSW, Australia
SuperScript® III Reverse Transcriptase	Invitrogen, Carlsbad, CA, USA
Sweetened condensed milk	Nestlé, Rhodes, NSW, Australia
Tissue-Tek® Cryomold®	Sakura Finetek Inc, Torrance, CA, USA
Ultra Sensitive Mouse Insulin ELISA Kit	Crystal Chem, Downers Grove, IL, USA
Veet Hair Removal Cream	Reckitt Benckiser (Australia) Pty Ltd, Sydney, NSW, Australia

2.2 The Diabetes and Liver Clinic Audit

The Diabetes and Liver Clinic (DLC) Audit has been presented in the format of an unpublished manuscript (Can a Dedicated Diabetes and Liver Clinic Enhance the Assessment for NASH Fibrosis?). The methods are included within the manuscript in *Chapter 3*. The study was approved by the Sydney Local Health District RPA Ethics Committee (Ethics reference number X19-0117 and 2019/ETH02727).

2.3 The CCN2 Study and The CCN1 Study

2.3.1 Animal studies

2.3.1.1 Animal ethics approval

The animal studies undertaken in this thesis were approved by the University of Sydney Animal Ethics Committee (AEC, Project number 2015/874). All mice were housed in the Laboratory Animal Services facility within the Charles Perkins Centre at the University of Sydney.

2.3.1.2 Mouse sub-strains and nomenclature

The two animal studies presented in this thesis are:

1) The CCN2 Study: hepatocyte-specific CCN2 gene knockout (CCN2-KO) mice compared with control sub-strains (AlbCre and $CCN2^{fl/fl}$);

2) The CCN1 Study: hepatocyte-specific CCN1 gene knockout (CCN1-KO) mice compared with control sub-strains (AlbCre and $CCN1^{fl/fl}$).

The nomenclature assigned to each mouse sub-strain is listed in *Table 2.2*.

Table 2.2: Mouse sub-strains used in The CCN2 Study and The CCN1 Study.

Assigned Scientific Name	Abbreviation	Type	Source
B6.Cg-Tg(AlbCre)21Mgn/J	AlbCre	Control	Purchased from The Jackson Laboratory and bred in house
Homozygous $CCN2^{fl/fl}$	$CCN2^{fl/fl}$	Control	Generated and bred in house
$CCN2^{fl}$ x B6.Cg-Tg(AlbCre)21Mgn/J	CCN2-KO	Experimental	Generated and bred in house
Homozygous $CCN1^{fl/fl}$	$CCN1^{fl/fl}$	Control	Generated and bred in house
$CCN1^{fl}$ x B6.Cg-Tg(AlbCre)21Mgn/J	CCN1-KO	Experimental	Generated and bred in house

2.3.1.3 Generation of hepatocyte-specific CCN2 and CCN1 gene knockout mice

The CreLoxP system is a site-specific recombination system widely used for generation of conditional knockout mice. The protein Cre recombinase recognises specific 34 base pair (bp) deoxyribonucleic acid (DNA) sequences, called LoxP sites and excises any DNA sequences between two LoxP sites oriented in the same direction. It allows deletion of the target gene (flanked by LoxP or "floxed") in the specific cell or tissue type. This overcomes challenges associated with whole body gene deletions, which may have undesired systemic effects, including premature lethality.

Hepatocyte-specific AlbuminCre transgenic mice ((B6.Cg-Tg(Alb-Cre)21Mgn/J (AlbCre); The Jackson Laboratory, Bar Harbor, ME, USA) and homozygous CCN2 floxed ($CCN2^{fl/fl}$) mice and homozygous CCN1 floxed ($CCN1^{fl/fl}$) mice were used to generate the hepatocyte-specific CCN2 gene knockout (CCN2-KO) and CCN1 gene knockout (CCN1-KO) mice. Breeding pair mice with double $CCN1^{fl/fl}CCN2^{fl/fl}$ mice were donated by Professor Andrew Leask (School of Dentistry, University of Saskatchewan, Saskatoon, SK Canada) and separated into single $CCN1^{fl/fl}$ and single $CCN2^{fl/fl}$ mice in our laboratory according to the breeding steps shown in *Figure 2.1A*. All mice used in this thesis were bred on a C57BL/6J background. The "6J" and "6N" sub-strains are the most frequently used lines, with the "6J" being preferred for metabolic studies due to its susceptibility to diabetes and obesity. The two sub-strain colonies were separated in the 1950s and have developed significant genetic variation resulting in phenotypic differences related to metabolic and non-metabolic features. This has been summarised by Fontaine and Davis[289].

Dr Xiaoyu Wang (associate supervisor) used the CreLoxP system to generate and breed the hepatocyte-specific CCN2-KO and hepatocyte-specific CCN1-KO mice which were used in the two animal studies presented in this thesis. The breeding steps are shown in *Figure 2.1*. For the generation of the CCN2-KO mice, firstly AlbCre mice were crossed with homozygous $CCN2^{fl/fl}$ mice to produce hemizygous for AlbCre and heterozygous for the LoxP-flanked CCN2 mice. The second cross with $CCN2^{fl/fl}$ mice produced hemizygous for AlbCre and homozygous CCN2-KO mice, followed by a third cross to generate both homozygous for AlbCre and CCN2-KO mice. The same process (with homozygous $CCN1^{fl/fl}$ mice) was used to generate the hepatocyte-specific CCN1-KO mice.

Polymerase chain reaction (PCR) genotyping was performed between each breeding step on DNA extracted from mouse earlobe and liver tissue using REDExtract-N-Amp Tissue PCR Kit (Sigma-Aldrich, St Louis, MO, USA). The PCR products were visualised by GelRed® nucleic acid stain (Sigma-Aldrich, St Louis, MO, USA) on agarose gel. The mice with desired genotypes were selected and used for the next breeding step.

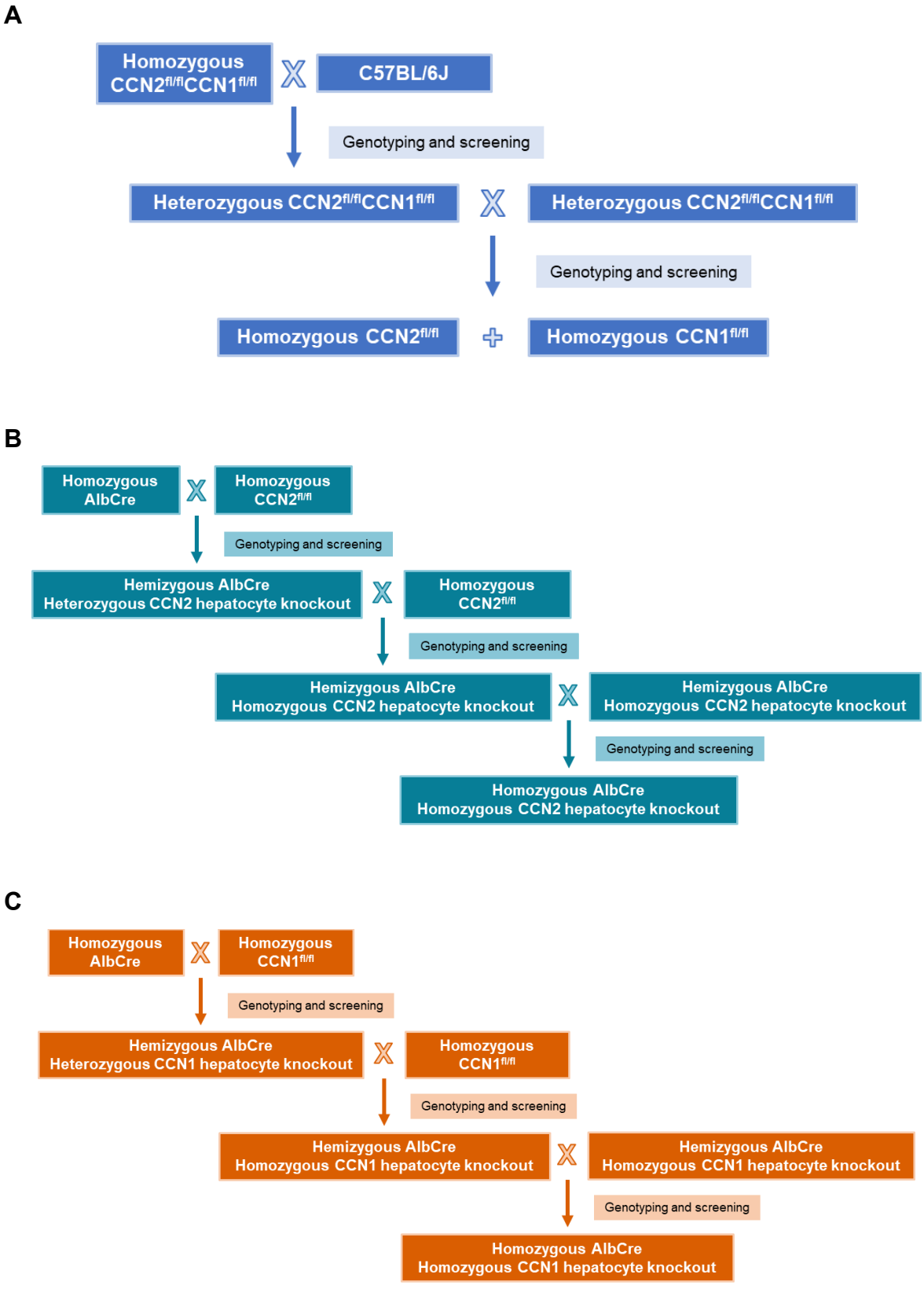

Figure 2.1: Generation of homozygous CCN2$^{fl/fl}$ and CCN1$^{fl/fl}$ mice (A), hepatocyte-specific CCN2-KO mice (B) and hepatocyte-specific CCN1-KO mice (C).

2.3.1.4 Confirmation of hepatocyte CCN2 and CCN1 deletion

All experiments related to the confirmation of hepatocyte CCN2 and CCN1 deletion that are presented in this Methods section were performed by Dr Xiaoyu Wang. Successful deletions of CCN2 and CCN1 DNA from the liver were firstly confirmed by sanger sequencing (data not shown). A 483 bp DNA fragment was deleted from exon 4 of liver CCN2 in the CCN2-KO mice and a 672 bp DNA fragment was deleted from exon 2 of liver CCN1 in the CCN1-KO mice. PCR to measure CCN2 was performed on DNA extracted from ear, kidney, and liver tissue from hepatocyte CCN2-KO mice, and from liver tissue from $CCN2^{fl/fl}$ and wild-type mice. PCR products were electrophoresed on a 1% agarose gel with DNA ladder for sizing (1 Kb Plus DNA Ladder, Invitrogen, Carlsbad, CA, USA). The same was performed for CCN1 in the CCN1-KO mice.

In the CCN2-KO mice (*Figure 2.2A*), there was detection of a shortened CCN2 product (520 bp) in the liver tissue, while full-sized products (1003 bp) were identified in non-liver tissue (ear and kidney) from the CCN2-KO mice and liver tissue from $CCN2^{fl/fl}$ and wild-type mice. Similar findings were observed in the CCN1-KO mice (*Figure 2.2B*), where there was detection of a shortened CCN1 product (709 bp) in the liver tissue, and full-sized products (1381 bp) were identified in non-liver tissue (ear and kidney) from the CCN1-KO mice and liver tissue from the $CCN1^{fl/fl}$ and wild-type mice. These results confirmed that the DNA deletion of CCN2 and CCN1 were specific to the liver, as there was no DNA excision identified in other tissues.

A **B**

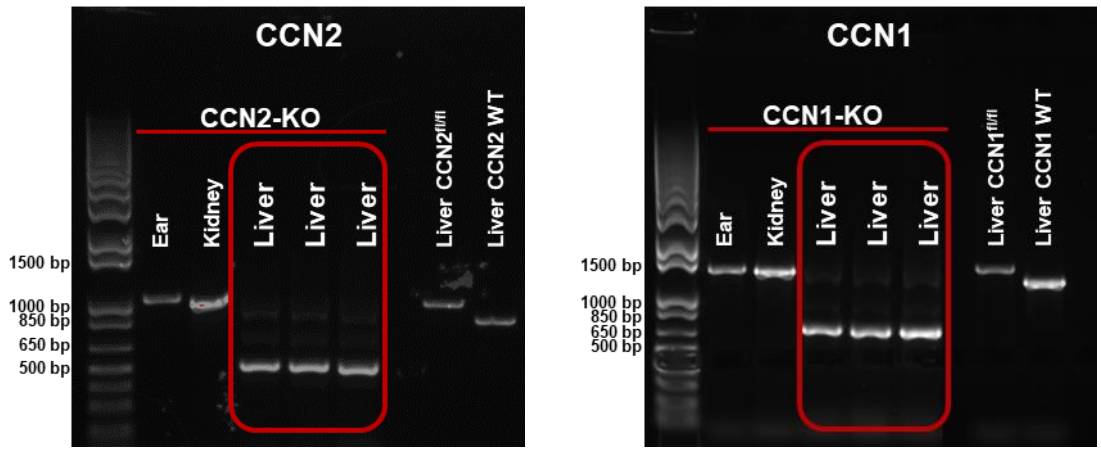

Figure 2.2: DNA deletion of liver CCN2 in CCN2-KO mice (A) and liver CCN1 in CCN1-KO mice (B). Courtesy of Dr Xiaoyu Wang.

Next, the mRNA and protein levels of liver CCN2 in the CCN2-KO mice (*Figure 2.3*) and liver CCN1 in the CCN1-KO mice (*Figure 2.4*) were examined. The mRNA levels were measured using real-time quantitative PCR (qPCR) and the protein levels were detected by Western immunoblot (representative images shown). The CCN2-KO mice had an ~70% reduction in CCN2 mRNA level compared with the control groups. The CCN2 protein also showed low intensity bands in CCN2-KO liver tissue compared with the control group (40 - 60% reduction from repeated immunoblots). The CCN1-KO mice had an ~90% reduction in CCN1 mRNA level compared to the control groups. A reduced CCN1 protein level was also detected. The residual amount of CCN2 and CCN1 mRNA and protein detected in the knockout mouse liver tissue is probably due to production from other liver cell types. The CCN2-KO and CCN1-KO mice exhibited normal viability, fertility, and fecundity.

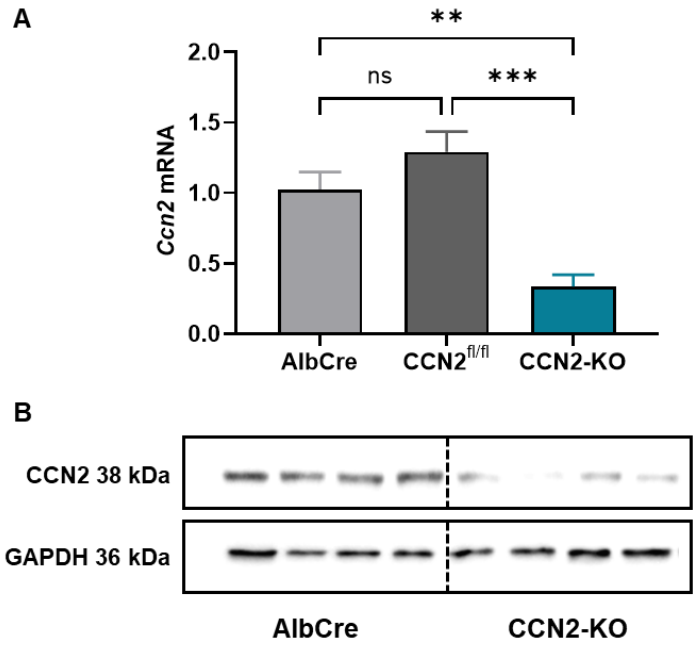

*Figure 2.3: Reduction of CCN2 mRNA (A) and protein (B) level in whole liver tissue from CCN2-KO mice. Data shown as mean ± SEM; n = 3 - 5. ** p-value ≤ 0.01 or ***p-value ≤ 0.001 for comparison with CCN2-KO group using one-way ANOVA with Tukey's correction for multiple comparisons. Courtesy of Dr Xiaoyu Wang.*

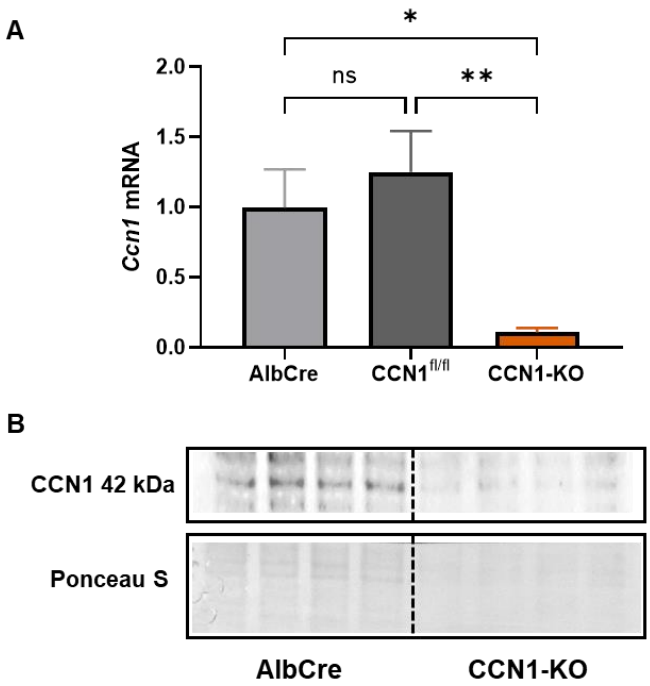

*Figure 2.4: Reduction of CCN1 mRNA (A) and protein (B) level in whole liver tissue from CCN1-KO mice. Data shown as mean ± SEM; n = 4. * p-value ≤ 0.05 or ** p-value ≤ 0.01 for comparison with CCN1-KO group using one-way ANOVA with Tukey's correction for multiple comparisons. Courtesy of Dr Xiaoyu Wang.*

2.3.1.5 Animal numbers

The number of mice used in each group of The CCN2 Study (*Table 2.3*) and The CCN1 Study (*Table 2.4*) are shown below. Two control sub-strains of mice were used for each study, AlbCre mice and the relevant homozygous floxed mice, as our hepatocyte-specific gene knockout mice were genetically derived from both sub-strains. Both sub-strains were recommended by the Jackson Laboratory as suitable controls[290].

Table 2.3: Final number of mice used in The CCN2 Study per group.

	Chow	HFD	HFD+DM	Total
AlbCre	8	8	10	26
CCN2$^{fl/fl}$	10	9	12	31
CCN2-KO	8	9	13	30
Total	26	26	35	87

Table 2.4: Final number of mice used in The CCN1 Study per group.

	Chow	HFD	HFD+DM	Total
AlbCre	8	9	12	29
CCN1$^{fl/fl}$	9	12	11	32
CCN1-KO	10	12	14	36
Total	27	33	37	97

2.3.1.6 Routine animal care

Male mice aged four to seven weeks were acclimatised for one week before entering the study protocol. They were housed two to six per cage with a 12-hour light/dark cycle. Mice were ear notched and had tails marked with permanent marker for identification purposes. Food and water were provided *ad libitum* for the duration of the study. Cages contained non-edible bedding to avoid other potential sources of caloric intake and standard environmental enrichment material.

2.3.1.7 The Fat and Diabetes model

The Fat and Diabetes (FaD) model used for this thesis was based on studies previously published by our laboratory and is summarised in *Figure 2.5*[144,145]. Utilising *ad libitum* high fat feeding to induce insulin resistance, followed by low dose streptozotocin (STZ; Sigma-Aldrich, St Louis, MO, USA) to induce relative insulin deficiency, it reliably produces a phenotype of obesity and hyperglycaemia with development of liver fibrosis within the time course of the protocol. Mice from each sub-strain were randomly allocated to chow, high fat diet (HFD) alone or high fat diet with diabetes (HFD+DM) groups. The chow group was fed a normal diet comprising of standard laboratory chow with 12% kcal fat, 23% kcal protein and 65% kcal carbohydrate (Irradiated Rat and Mouse Diet, Specialty Feeds, Glen Forrest, WA, Australia) that was placed in the cage hopper. The HFD was prepared in-house based on rodent diet D12451 with 45% kcal fat, 20% kcal protein and 35% kcal carbohydrate (D12451, Research Diets Inc, New Brunswick, NJ, USA) as published by others[291,292]. The HFD was placed in a petri dish on the floor of the cage and provided fresh three times per week. The in-house HFD formulation is listed in *Table 2.5*.

Table 2.5: In-house high fat diet formulation.

	Weight (grams)	**% Weight**	**kcal**	**% kcal**	**Manufacturer**
Acid casein	261.0	22.5	986.6	17.8	NZMP, Richmond, VIC, Australia
Lard	250.0	21.6	2212.5	40.0	York Foods, Goulburn, NSW, Australia
Sucrose	224.0	19.3	873.6	15.8	Ajax Finechem, Scoresby, VIC, Australia
Rice starch	215.0	18.6	752.5	13.6	MP Biomedicals LLC, Solon, OH, USA
Bran	57.0	4.9	209.0	3.8	Woolworths, Bella Vista, NSW, Australia
AIN-76 Mineral mixture	51.0	4.4	23.5	0.4	MP Biomedicals LLC, Solon, OH, USA
Gelatine powder	23.0	2.0	79.6	1.4	Ward McKenzie Pty Ltd, Altona, VIC, Australia
AIN Vitamin mixture 76	15.0	1.3	56.9	1.0	MP Biomedicals LLC, Solon, OH, USA
Choline bitartrate	4.6	0.4	0.0	0.0	Sigma-Aldrich, St Louis, MO, USA
L-methionine	3.4	0.3	0.0	0.0	Sigma-Aldrich, St Louis, MO, USA
Cholesterol	3.0	0.3	0.0	0.0	Sigma-Aldrich, St Louis, MO, USA
Sunflower oil	34 mL (31.3 g)	2.7	276.5	5.0	Woolworths, Bella Vista, NSW, Australia
Sweetened condensed milk	15 mL (19.4 g)	1.7	62.9	1.1	Nestle, Rhodes, NSW, Australia
Total	1157.7 g	100.0	5533.6	100.00	

During week 16 approximately half of the HFD mice were rendered diabetic with low dose STZ by intraperitoneal injection. Mice were fasted for four hours prior to injection of freshly prepared STZ (65 mg/kg body weight) diluted in 0.1 M sodium citrate buffer at pH 4.5 (citric acid, Sigma-Aldrich, St Louis, MO, USA; 20% sodium hydroxide). Two injections on consecutive days were administered. On day seven, a random blood glucose level (BGL) was measured using a glucometer (Accu-Chek® Guide, Roche Diabetes Care, North Ryde, NSW, Australia). Whole blood was obtained via a tail vein

nick and a standard blood volume was applied to the glucometer strip as per the manufacturer's instructions. Diabetes was confirmed if the random BGL was greater than 15.0 mmol/L, and if not, a third injection of STZ was administered. The approach of using multiple injections of low dose STZ has previously been shown to resemble a model of T2DM and relative insulin deficiency and does not cause an absolute insulin deficiency as seen when STZ is administered at much higher doses[293]. Non-diabetic mice were injected with vehicle control. All mice were maintained for a further ten weeks, before termination.

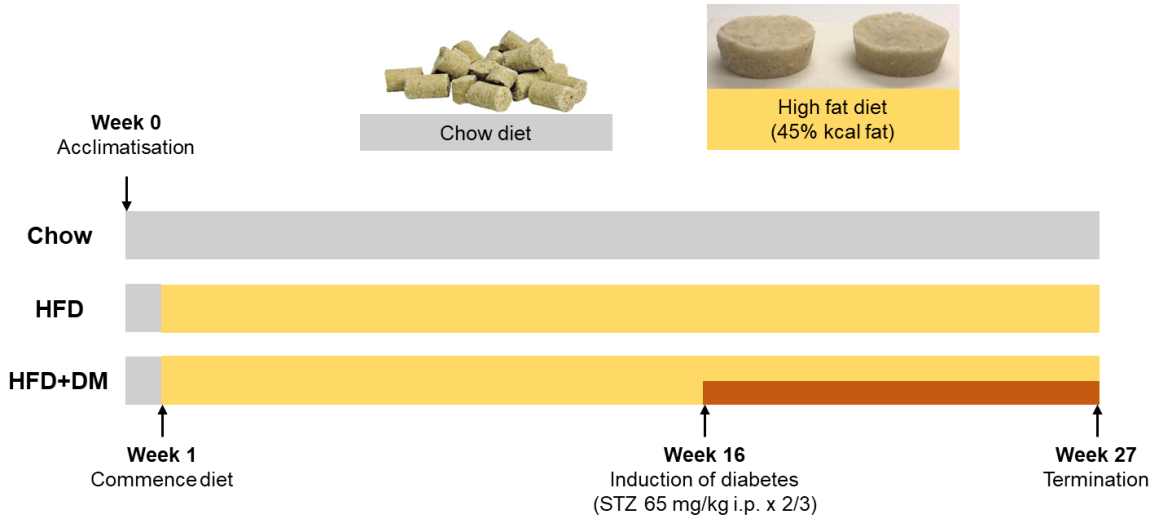

Figure 2.5: Timeline of the FaD model with representative images of chow diet (grey) and high fat diet (yellow).

Mice were weighed weekly until week 15, and then twice-weekly thereafter. A random BGL was measured weekly from week 16 onwards. If a mouse became unwell from severe hyperglycaemia with signs of catabolism (> 15% body weight reduction), then long-acting insulin glargine (1 - 2 units Lantus® 100 Units/mL, Sanofi, Macquarie Park, NSW, Australia) was administered intraperitoneally every second day.

2.3.1.8 Mouse termination and harvest

Mice were euthanised in accordance with the AEC approval. On the morning of termination, mice were fasted for four hours, anaesthetised with isoflurane gas followed by exsanguination via cardiac puncture, and finally had the cervical spinal cord severed. The fresh blood from the cardiac puncture was collected into EDTA tubes (Micro sample tube K3 EDTA; Sarstedt, Numbrecht, Germany) and kept on ice.

In order, the liver, spleen, kidneys, heart, epididymal fat pad, subcutaneous fat pad and gastrocnemius muscle were harvested and weighed. Each organ was then divided into three: one part was snap frozen in liquid nitrogen, one part was fixed in 10% Formalin (neutral buffered; Sigma-Aldrich, St Louis, MO, USA) and one part was placed in Tissue-Tek® Cryomold® (Sakura Finetek Inc, Torrance, CA, USA) molds with O.C.T. Compound (Sakura Finetek Inc, Torrance, CA, USA) and snap frozen in liquid nitrogen. Tissue from all lobes of the liver were harvested and stored, but the right lobe was consistently used in the studies presented in this thesis. All frozen samples were stored long-term at -80°C. The whole blood was centrifuged at 3,000 rpm for 5 min and the plasma was collected and stored at -80°C.

2.3.2 Measures of glucose and insulin resistance

2.3.2.1 Fasting blood glucose level

In addition to the weekly random BGL, the fasting BGL was measured at two timepoints: at week 16 (baseline measure prior to administration of the first STZ or vehicle control injection), and at the time of termination. Both measures were performed after a four hour fast, commenced in the early morning, and using the Accu-Chek® Guide glucometer.

2.3.2.2 Fasting whole blood/plasma insulin level

The fasting insulin level was measured on two occasions using a commercial enzyme-linked immunosorbent assay (ELISA) kit (Ultra Sensitive Mouse Insulin ELISA Kit; Crystal Chem, Downers Grove, IL, USA) according to the manufacturer's instructions. Fasting whole blood insulin level was measured at week 16, prior to administration of the first STZ or vehicle control injection. Fasting plasma insulin level was measured from plasma collected after termination.

In brief, working mouse insulin standards were prepared as per the wide range assay (0 - 12.8 ng/mL). Standards or samples (5 µL) plus 95 µL of sample diluent were added to each well of a guinea pig anti-insulin antibody coated microplate and incubated at 4°C overnight. The following morning, the plate was washed five times, and then 100 µL of horse radish peroxidase-conjugated anti-insulin antibody was added and incubated for 30 min at room temperature. The plate was washed a further seven times, and then 100 µL of 3,3',5,5'-tetramethylbenzidine (TMB) substrate solution was

added and incubated for 40 min at room temperature in the dark. After addition of stop solution, the optical density at 450 nm (reference 630 nm) was measured using a microplate reader (Tecan Infinite® M 1000 Pro) with inbuilt software i-Control™ v1.10 (Tecan, Mannedorf, Switzerland). Mouse insulin concentrations of the samples were interpolated using the standard curve (4-parameter logistic (4PL)) and converted from ng/mL to pM using a factor of 6.

2.3.2.3 Fasting plasma c-peptide level

The fasting plasma c-peptide level was measured using a commercial ELISA kit (Mouse C-Peptide ELISA Kit; Crystal Chem, Elk Grove Village, IL, USA) according to the manufacturer's instructions. In brief, working mouse c-peptide standards were prepared (0 - 6.4 ng/mL). Standards or samples (5 µL) plus 95 µL of sample diluent were added to each well of a rabbit anti-c-peptide antibody coated microplate and incubated for 1 h at room temperature. The plate was washed six times, and then 100 µL horse radish peroxidase-conjugated anti-c-peptide antibody was added and incubated for 1 h at room temperature. The plate was washed another six times, and then 100 µL of TMB substrate solution was added and incubated for 30 min at room temperature in the dark. After addition of stop solution, the optical density at 450 nm (reference 630 nm) was measured using a microplate reader (Tecan Infinite® M 1000 Pro) with inbuilt software i-Control™ v1.10 (Tecan, Mannedorf, Switzerland). Mouse c-peptide concentrations of the samples were interpolated using the standard curve (linear). The unit of measure was converted from ng/mL to pM by multiplying the obtained concentration in ng/mL by 320.3.

2.3.2.4 Insulin tolerance test

An insulin tolerance test (ITT) was performed one to two weeks prior to termination as a measure of whole-body insulin sensitivity. Mice were fasted for two hours from the early morning before intraperitoneal injection of 0.75 IU/kg of body weight of short acting insulin neutral (Actrapid® 100 Units/mL; Novo Nordisk Pharmaceuticals Pty Ltd, North Sydney, NSW, Australia) diluted in normal saline (0.9% sodium chloride injection BP, Pfizer, West Ryde, NSW, Australia). The BGL was measured at time 0, 15-, 30-, 60- and 90-min post-injection using whole blood from a tail vein nick and an Accu-Chek® Guide glucometer. Hypoglycaemia was diagnosed if the BGL was less than 3.0 mmol/L and was managed with intraperitoneal injection of 2 g/kg of 20% glucose

solution (Glucose 50% w/v 50 mL, Phebra, Lane Cove West, NSW, Australia). Glucagon (5 µg/kg intraperitoneal injection; GlucaGen® HypoKit 1 mg/mL, Novo Nordisk Pharmaceuticals Pty Ltd, North Sydney, NSW, Australia) was available, but was not required at any stage. Blood glucose excursion and thus insulin sensitivity was calculated as the area under the curve (AUC), normalised as a percentage to the time 0 BGL. A greater AUC after insulin administration demonstrates resistance to the action of insulin shown by the lower ability to reduce the BGL. This method has been used by others to assess insulin sensitivity[294].

2.3.2.5 Surrogate markers of insulin resistance

The gold standard for assessing insulin resistance in both humans and rodents is the hyperinsulinaemic euglycaemic clamp[295]. However, it is a time consuming procedure and requires skilled technicians to perform, a limitation that has resulted in surrogate measures of insulin resistance to be developed[295-297] that have been used frequently in rodent studies[298,299]. Several different calculations for the surrogate measures of insulin resistance were made and are summarised below in *Table 2.6*.

Table 2.6: Formulae for calculated surrogate markers of insulin resistance.

	Formula
Homeostatic model assessment for insulin resistance (HOMA-IR)[296]	(fasting insulin x fasting glucose)/405
Homeostatic model assessment for β-cell function (HOMA-β)[296]	(360 x fasting insulin) / (fasting glucose – 63)
Quantitative insulin check index of insulin sensitivity (QUICKI)[297]	1 / (log(fasting insulin) + log(fasting glucose))
Glucose to insulin ratio	fasting glucose / fasting insulin

Note: insulin was measured in mIU/L and glucose was measured in mg/dL.

2.3.3 Pre-clinical *in vivo* mouse imaging

All imaging was performed at the Pre-clinical Imaging Core Research Facility in the Charles Perkins Centre at the University of Sydney in accordance with AEC's approved standard operating procedures. Modalities performed at different timepoints are shown in *Table 2.7*.

Table 2.7: In vivo mouse imaging.

	Number of mice	Purpose	The CCN2 Study		The CCN1 Study	
			Week 15	Week 25	Week 15	Week 25
EchoMRI™	All	Body composition	✓	✓	✓	✓
DXA	All	Body composition Bone density	✓	✓	b	b
Ultrasound	n = 3 from each group	Liver steatosis/fibrosis	✓	✓	✓	✓
MRI	n = 3 from each group	Liver steatosis/fibrosis	✓	a	b	b

a: not performed as mice exceeded maximum size for machine. b: not performed due to limited access to facility due to COVID-19 pandemic. DXA, dual energy x-ray absorptiometry; MRI, magnetic resonance imaging.

2.3.3.1 EchoMRI™

Body composition was measured using an EchoMRI™-900-A130 Body Composition Analyzer (EchoMRI™ LLC, Houston, TX, USA), which employs magnetic resonance relaxation analysis for measuring fat tissue, lean tissue, and free and total water mass[300]. The machine was calibrated against a Canola oil standard before each use. Each mouse was weighed prior to being placed inside a red animal tube holder of appropriate size (determined by rounding up the mouse weight in 20 g increments). A smaller cylindrical plastic insert was used to hold the mouse in place, allowing enough room for free access to air through the vents, but not allowing lateral movement which might lead to measurement error. The whole animal tube was placed into the bore of the instrument and scanned in under two minutes. Once completed, each mouse was returned to its cage for recovery. Data was exported as a Microsoft® 365 Excel® file (Microsoft Corporation, Redmond, WA, USA) spreadsheet from the instrument software (v190125; EchoMRI™ LLC, Houston, TX, USA).

2.3.3.2 Faxitron® Ultrafocus 100 dual energy x-ray absorptiometry

Body composition and bone density were measured using Faxitron® Ultrafocus 100 Dual Energy X-ray Absorptiometry (DXA; Hologic, Tucson, AZ, USA). Mice were anaesthetised with isofluorane (3 - 4%) mixed with oxygen (1.5 L/min) in an induction chamber. Mice were transferred to the imaging chamber and placed in the prone

position with limbs outstretched at 90° to the straightened spine to minimise overlap of bones. Standard settings for DXA mode were used: 40 kV; 2.4 sec; 0.2 mA; 4 image averages. Physiological monitoring of the mice occurred throughout the duration of anaesthesia (~7 min). Mice were returned to a warmed cage for recovery after the scan was completed.

The region of interest (entire mouse minus the head and tail) was manually selected from each mouse image, and total weight (g), lean weight (g), fat weight (g), bone area (BA; cm^2), bone mineral content (BMC; g) and bone mineral density (BMD; mg/cm^2) were calculated using Vision DXA v2.4.2U software (Hologic, Tucson, AZ, USA).

2.3.3.3 Liver ultrasound

Liver ultrasound was performed using Vevo 2100 with Vevo LAB v5.5.1.1070 software, and an MS550D (22 - 55 mHz) transducer (FUJIFILM VisualSonics Inc, Toronto, ON, Canada). Anaesthetised mice were transferred to the Vevo 2100 cabinet, placed in the supine position, and had abdominal hair removed with Veet Hair Removal Cream (Reckitt Benckiser (Australia) Pty Ltd, Sydney, NSW, Australia) to avoid image artefact. Ultrasound gel was liberally applied to the abdomen and five B-mode images were acquired from each mouse in standard transverse and sagittal imaging planes of the right and left lobes of the liver and the right liver-kidney interface (see *Figure 2.6*)[301]. The same settings were used for all mice:

- Transmit:
  - frequency 40 MHz
  - power 100%
- Acquisition:
  - frame rate: 21
  - gain: 20.0 dB
  - depth: 13.00 mm, width: 14.08 mm
  - high line density
  - high sensitivity
  - focal zone: 3 - 7 mm
- Display:
  - dynamic range: 65 dB

Physiological monitoring of the mice occurred throughout the duration of anaesthesia (~15 min). Mice were returned to a warmed cage for recovery after the scan was completed.

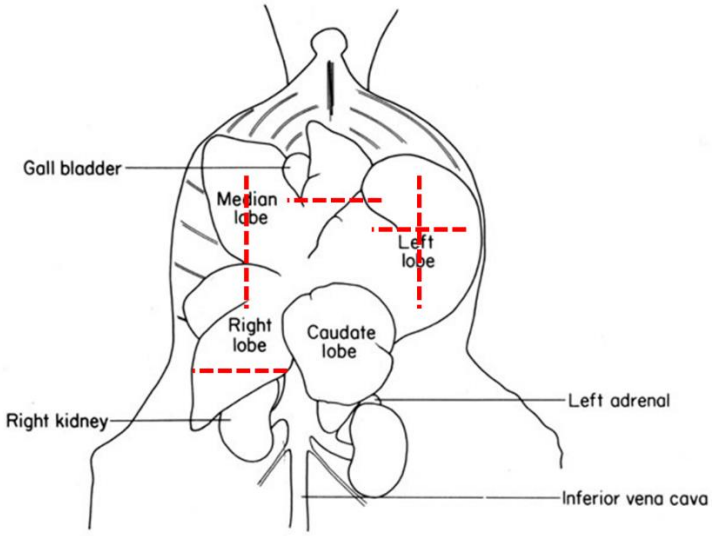

Figure 2.6: Location of sonographic liver images obtained from each mouse. Image adapted from Cook, 1965[302].

Six regions of interest (ROIs) from each liver image were manually selected, to ensure there was comprehensive inclusion of multiple representative sections of the liver. The ROIs were analysed using MaZda v4.6 software (Technical University of Lodz, Lodz, Poland) for echo-intensity (brightness), heterogeneity (local variance within ROI), anisotropy (regional variance between ROIs), and hepatorenal index (HRI; brightness normalised to renal cortex) as described by D'Souza and colleagues[301,303]. Analysis of mouse liver ultrasound images using these parameters has previously been reported to be highly correlated with the degree of liver fibrosis, and provided a novel and non-invasive method to assess liver fibrosis without the need for a tissue sample[301].

2.3.3.4 Liver magnetic resonance imaging

A pre-clinical 7 tesla (7T) magnetic resonance imaging (MRI) machine with mouse body coil (MRS*DRYMAG 7.0TMRI) and inbuilt Preclinical Scan™ v4.0.2.32 software (MR Solutions Ltd, Guildford, Surrey, UK) was used to image the liver, with the aim to explore novel methods to assess for liver fibrosis. The scans were performed with the assistance of Dr Sofie Trajanovska and Dr Binh Pham from the Pre-clinical Imaging Core Research Facility. Mice remained anaesthetised with a mixture of isoflurane and oxygen and underwent strict physiological monitoring for core (rectal) temperature (thermistor temperature probe), respiratory rate (pneumatic pillow sensor) and heart rate (electrocardiogram; ECG) throughout the scan. Mouse body temperature was maintained at 38°C with a heating pad and respiratory rate was maintained between

30 - 50 breaths per minute by adjusting the isoflurane. T2-weighted images were taken with and without fat suppression. Magnetic resonance relaxometry was performed as described before[304]. Data for determining relaxation time T1 of liver tissue was acquired using a rapid acquisition with relaxation enhancement (RARE) approach with repetition times TR = 600 ms, 800 ms, 1200 ms and 1600 ms, and TE = 11 ms with a slice thickness = 0.5 mm, field of view = 32.0 x 32.0 mm, in plane resolution = 125 x 125 x 500 µm and two averages. Data for determining relaxation time T2* were generated with a multigradient echo (MGE) sequence, with TR = 1100 ms, and TE = 3.456 ms, 7.986 ms, 12.426 ms, 16.866 ms, 21.306 ms, 25.746 ms, 30.186 ms, 34.626 ms, slice thickness = 0.5 mm, flip angle = 20, bandwidth = 67 kHz and two averages. Once the MRI scans were completed, mice were returned to a warmed cage with food and water for recovery.

2.3.4 Plasma studies

The following tests were performed on mouse plasma using the AU480 Chemistry Analyzer (Beckman Coulter Australia Pty Ltd, Lane Cove, NSW, Australia) owned by Sydney University's Glycaemic Index Research Service (SUGiRS): alkaline phosphatase (ALP; U/L); alanine aminotransferase (ALT; U/L); aspartate aminotransferase (AST; U/L); total protein (g/L); albumin (g/L); total bilirubin (µmol/L); total cholesterol (mmol/L); triglycerides (mmol/L); high-density lipoprotein cholesterol (HDL-c; mmol/L); low-density lipoprotein cholesterol (LDL-c; mmol/L); and high sensitivity c-reactive protein (hsCRP; mg/L). A total of ~100 µL plasma was required for these tests.

2.3.5 Histological staining

Liver tissue was fixed in 10% Formalin (neutral buffered; Sigma-Aldrich, St Louis, MO, USA) for 24 h before being transferred to 70% ethanol until it was processed, and paraffin embedded. For histological staining, paraffin embedded tissue was sectioned by cutting at 5 µm thickness and placed onto Superfrost® Plus microscope slides (Lomb Scientific Pty Ltd, Taren Point, NSW, Australia) and left to completely dry prior to staining. Sections were deparaffinised in two changes of xylene and rehydrated to water through a series of graded ethanol washes comprising two washes in absolute ethanol, two washes in 95% ethanol, and one wash in 70% ethanol, before rinsing in tap water.

2.3.5.1 Picro Sirius Red staining

2.3.5.1.1 Picro Sirius Red staining protocol

Picro Sirius Red (PSR) staining is commonly used for the staining of collagen fibres, which stain red on a yellow/brown background[305]. Deparaffinised and rehydrated slides were counterstained with Harris' haematoxylin (POCD Scientific, North Rocks, NSW, Australia) for 10 min and washed in running tap water. Slides were then stained in PSR (0.1% Sirius Red in 1.3% saturated aqueous solution of picric acid; Sigma-Aldrich, St Louis, MO, USA) for 60 min, quickly dipped twice in 0.1% acidified water, blotted on filter paper, dehydrated in absolute ethanol, and left to dry. Slides were cleared in Citrasol (Labtech Service and Supplies, South Windsor, NSW, Australia) and coverslipped with Dibutylphthalate Polystyrene Xylene (DPX; Sigma-Aldrich, St Louis, MO, USA). To aid image analysis, a second set of liver sections were stained without the haematoxylin step, because the computer software could not accurately differentiate counterstained cell nuclei could from PSR-positive tissue as they were too similar in colour. Representative images of liver sections with nuclei counterstaining were captured using a light microscope (Olympus BX60 microscope with Olympus DP72 digital camera and cellSens Standard software v2.3; Olympus Australia Pty Ltd, Notting Hill, VIC, Australia).

2.3.5.1.2 Picro Sirius Red staining analysis

Quantitative analysis was performed on non-counterstained PSR-stained sections. Brightfield images were captured with a Leica Aperio ScanScope® XT slide scanner (Leica Microsystems Pty Ltd, Mt Waverly, VIC, Australia) for the CCN2 Study and a light microscope (Olympus BX60 microscope with Olympus DP72 digital camera and cellSens Standard software v2.3; Olympus Australia Pty Ltd, Notting Hill, VIC, Australia) for the CCN1 Study. The slide scanner was used for the CCN2 Study to enable ongoing remote image analysis during the COVID-19 pandemic lockdown. It was located at the Sydney Microscopy and Microanalysis Core Research Facility in the Brain and Mind Centre at the University of Sydney.

QuPath v0.2.3 (open-source software) was used to select representative images of the scanned slides[306], at the same size and magnification as representative images from the Olympus light microscope. The details of the representative captured images from each liver are as follows: four images at 100x magnification, four images at 200x

magnification, six images of central veins at 400x magnification, and six images of portal tracts at 400x magnification. ImageJ 1.53a (open-source software) was used to calculate the % area of red pixels[307]. Noise from artefact was removed using the "remove outliers" function set to radius = 30, threshold = 60, dark outliers. Each image was converted to a grayscale image by splitting it into red, green, and blue channels. The green channel was selected due to the best separation. A threshold was manually chosen that best corresponded to the area of PSR-positive stained tissue. The same threshold was used for all the images in that study (CCN2 Study = 170; CCN1 Study = 195). Data was expressed as % area of PSR-positive stained tissue.

2.3.5.2 Haematoxylin and eosin staining

2.3.5.2.1 Haematoxylin and eosin staining protocol

Haematoxylin and eosin (H&E) staining was used for morphological study of liver tissue. Haematoxylin stains nuclei whilst eosin stains the cytoplasm[308]. Deparaffinised and rehydrated slides were stained with Harris' haematoxylin (POCD Scientific, North Rocks, NSW, Australia) for 2 min, washed in running tap water and dipped 10 times in acid alcohol. After another tap water wash, the slides were dipped 20 times in Scott's Bluing solution (14 g sodium hydrogen carbonate + 80 g magnesium sulphate + 4 L dH_2O) and then washed in tap water again. The slides were then thoroughly washed in 70% ethanol before being stained in two changes of eosin (POCD Scientific, North Rocks, NSW, Australia) for 40 sec each. Slides were dehydrated through graded ethanol, starting at 70% and ending at absolute ethanol. Once dry, slides were cleared, and then coverslipped with DPX (Sigma-Aldrich, St Louis, MO, USA). Representative images from each group were captured using a light microscope (Olympus BX60 microscope with Olympus DP72 digital camera and cellSens Standard software v2.3; Olympus Australia Pty Ltd, Notting Hill, VIC, Australia).

2.3.5.2.2 Haematoxylin and eosin staining analysis

The H&E slides were reviewed by Dr Min Li Huang, a trained anatomical pathologist who was blinded to the study groups. Each slide was scored according to the Brunt criteria for NAFLD[80] and the NAS, which are commonly used in clinical practice[309]. The criteria for each are listed in *Table 2.8* and *Table 2.9*.

Table 2.8: Brunt criteria for NAFLD[80].

	Grade	Definition
Steatosis	0	< 5%
	1	5 - 33%
	2	34 - 66%
	3	> 66%
Fibrosis	0	Absent
	1	Perisinusoidal/pericellular
	2	Periportal
	3	Bridging
	4	Cirrhosis
Necroinflammation	0	Absent
	1	Occasional ballooned hepatocytes and no or very mild inflammation
	2	Ballooning of hepatocytes and mild to moderate portal inflammation
	3	Intra-acinar inflammation and portal inflammation

Table 2.9: NAFLD activity score criteria[309].

	Score	Definition
Steatosis	0	< 5%
	1	5 - 33%
	2	34 - 66%
	3	> 66%
Lobular inflammation	0	Absent
	1	1 focus per 200x field
	2	2 - 4 foci per 200x field
	3	> 4 foci per 200x field
Hepatocellular ballooning	0	Absent
	1	Few ballooned cells
	2	Many cells/prominent ballooning

2.3.6 mRNA levels from whole liver tissue

2.3.6.1 RNA extraction with DNase treatment

Total RNA was isolated from ~30 mg snap frozen liver tissue using the PureLink™ RNA Mini Kit (Invitrogen, Carlsbad, CA, USA) as per the manufacturer's instructions. Lysis buffer (600 µL) containing 1% β-mercaptoethanol (Sigma-Aldrich, St Louis, MO, USA) was added to the liver tissue and thoroughly ground using an RNase-free pestle. The lysate was then transferred to a Homogenizer spin cartridge (Invitrogen, Carlsbad, CA, USA) for 2 min centrifugation at 12,000 g. An equal volume of analytic grade 70%

ethanol was added to the homogenised lysate and mixed by pipette. The tissue homogenate was transferred to a white spin cartridge, centrifuged at 12,000 g for 30 sec and the flow-through was discarded. The same step was repeated until all the tissue homogenate was processed.

The remaining RNA on membrane of the spin cartridge was washed with 350 µL of wash buffer I and centrifuged at 12,000 g for 30 sec and the flow-through was discarded. Then 80 µL of PureLink™ DNase mixture (8 µL reaction buffer, 10 µL DNase and 62 µL RNase-free water; PureLink™ DNase Set; Invitrogen, Carlsbad, CA, USA) was added directly onto the membrane of the spin cartridge and incubated for 15 min at room temperature. This was followed by second wash in 350 µL wash buffer I. After centrifugation, the flow-through was discarded again and the spin cartridge was placed into a new collection tube. Next, 500 µL of wash buffer II was added to the spin cartridge, centrifuged at 12,000 g for 30 sec and the flow-through discarded. This wash step was repeated. The spin cartridge was spun at 12,000 g for 90 sec to remove excess wash buffer and then inserted into a recovery tube. Finally, 100 µL of RNase-free water was added directly onto the centre of the spin cartridge membrane and centrifuged at 12,000 g for 2 min to elute the RNA. The RNA samples were stored at -80°C until further analysis.

2.3.6.2 RNA quantification

The concentration of each RNA sample was determined using a NanoDrop™ 2000c spectrophotometer with inbuilt software NanoDrop™ 2000c v1.3.198 (Thermo Scientific, Waltham, MA, USA), according to the formula: [RNA] = A260 x 40 x dilution factor. The RNA purity was assessed by measuring the A260/A280 and A260/A230 ratios, with acceptable ratios of ~2.0[310].

2.3.6.3 Reverse transcription

Reverse transcription was used to transcribe the total RNA into complementary DNA (cDNA) using the RNA dependent polymerase, reverse transcriptase.[310] The following incubation conditions were used: 65°C for 5 min: 2 µg RNA, 0.5 µg Oligo(dT)$_{12\text{-}18}$ Primer (Invitrogen, Carlsbad, CA, USA), 100 ng Random Hexamer (Invitrogen, Carlsbad, CA, USA) and nuclease-free water to total 26 µL. After brief (> 1 min) cooling at 4°C, 8 µL of 5 x Strand Buffer (250 mM Tris-HCl, 375 mM KCl, 15 mM $MgCl_2$;

Invitrogen, Carlsbad, CA, USA), 2 µL of 0.1 M DTT (Invitrogen, Carlsbad, CA, USA), 2 µL of 200 U/µL SuperScript® III Reverse Transcriptase (Invitrogen, Carlsbad, CA, USA) and 2 µL of 10 mM dNTP mix (Meridian Biosciences, Memphis, TN, USA) were added, with a final volume of 40 µL. Samples were incubated at 25°C for 10 min and 50°C for 60 min followed by heating at 70°C for 15 min to inactivate superscriptase activity. Heating and cooling steps were performed in an Eppendorf® Mastercycler® Nexus Gradient PCR thermal cycler (Eppendorf South Pacific Pty Ltd, Macquarie Park, NSW, Australia). The transcribed cDNA was stored at -30°C.

2.3.6.4 Real-time quantitative polymerase chain reaction

Real-time quantitative polymerase chain reaction (qPCR) was performed using a QuantStudio™ 7 Flex Real-Time PCR System with inbuilt software v1.7.1 (Applied Biosystems, Waltham, MA, USA) with 384-well plates (MicroAmp™ Optical 384-well Reaction Plate with MicroAmp™ Optical Adhesive Film; Applied Biosystems, Waltham, MA, USA). Each reaction contained 1 - 4.5 µL of cDNA, 5 µL of 2 x SensiMix™ SYBR® Hi-ROX (Meridian Bioscience, Cincinnati, OH, USA), 0.25 µL of 10 µM primers (forward and reverse) and made up to 10 µL final volume with nuclease-free water. Thermal cycling conditions were as follows: activation at 95°C for 10 min, followed by 40 cycles of denaturation at 95°C for 10 sec, annealing at 60°C for 15 sec, and elongation at 72°C for 20 sec, followed then by a melt curve. A no-template control was included as a negative control for each primer pair.

A five-point standard curve for each of the genes of interest including the housekeeper gene was constructed by using 1:5 serial dilution of pooled cDNA (1:10 for 18S; 1:2 for CCN3 and FAP). The qPCR efficiencies ranged between 88 and 112%, with an average efficiency of 97%. The R^2 for each standard curve was > 0.97. The cDNA for sample analysis was diluted 1 in 10 in nuclease-free water to achieve cycle thresholds between ~20 - 30 cycles. In general, standards and samples were run in duplicate or triplicate. Data was analysed according to the Pfaffl method[311], thereby accounting for differences in reaction efficiency of the gene of interest and housekeeper gene.

2.3.6.5 Primer sequences

The primer pair sequences used for qPCR were derived from published studies or generated from BLAST searches and are specific to mouse species (*Table 2.10*).

Table 2.10: Primer sequences.

Gene	Forward Primer	Reverse Primer	Source
Acta2	AGAGCAAGAGA GGGATCCTGA	GTCGTCCCAGT TGGTGATGAT	Self-designed using Primer-BLAST
Ccl2	AGGTCCCTGTC ATGCTTCTG	GCTGCTGGTGA TCCTCTTGT	Self-designed using Primer-BLAST
Ccn1	ATGAAGACAGC ATTAAGGACTC	TGCAGAGGGTT GAAAAGAAC	Kawaki et al., 2011[312]
Ccn1 (knockout)*	TGACCAGACTG GCGCTCTC	CTGAGCTCTGC AGATCCCTTTC	Self-designed using Primer-BLAST
Ccn2	AGAGTGGAGCG CCTGTTCTA	GACAGGCTTGG CGATTTTAG	Self-designed using Primer-BLAST
Ccn2 (knockout)*	AGCGGTGAGTC CTTCCAAAG	GGCTCGCATCA TAGTTGGGT	Self-designed using Primer-BLAST
Ccn3	TGAAGTCTCTG ACTCCAGCATT	TGGCTTTCAGG GATTTCTTG	Kawaki et al., 2011[312]
Col1	CCCCGGGACTC CTGGACTT	GCTCCGACACG CCCTCTCTC	Self-designed using Primer-BLAST
Col3	CAAGTCTGGAG TGGGAGGAA	ACCAGCTTGAC CAGGTTCAC	Self-designed using Primer-BLAST
Col4a1	ATCCGGCCCTT CATTAGC	ACTGCGGAATC TGAATGGTC	Adriaenssens et al., 2009[313]
Col4a2	TAGCTCCTCCG GGATCTACC	GCTCTCCAAGG TGGGTGTTA	Adriaenssens et al., 2009[313]
Col6	GAACTTCCCTG CCAAACAGA	CACCTTGTGGA AGTTCTGCTC	Adriaenssens et al., 2009[313]
Dpp4	CTTGCTGCTCC ATGCTGAAC	TGGTGACCATG TGATCCACT	Self-designed using Primer-BLAST
Fap	ACACCACCTAC CCTCACCAC	ACATGCTCCTG GTTCTTTGG	Self-designed using Primer-BLAST
Fn1	GGGTTTTAACT GCGAGAGCA	TGTAGGACTGA CCCCCTTCA	Self-designed using Primer-BLAST
Il1b	GACCTTCCAGG ATGAGGACA	AGCTCATATGG GTCCGACAG	Self-designed using Primer-BLAST
Tgfb1	TGGAGCAACAT GTGGAACTC	GTCAGCAGCCG GTTACCA	Adriaenssens et al., 2009[313]
Timp1	GCATCTGGCAT CCTCTTGTT	CTCGTTGATTTC TGGGGAAC	Self-designed using Primer-BLAST

Tnf	CCCCAAAGGGA TGAGAAGTT	CACTTGGTGGT TTGCTACGA	Self-designed using Primer-BLAST
Rn18s	CGGCTACCACA TACCAAGGAA	GCTGGAATTAA CCGCGGCT	Self-designed using Primer-BLAST
Rplp0	GGCCCTGCACT CTCGCTTT	TGCCAGGACGC GCTTGT	Casellas et al., 2006[314]

Acta2, α smooth muscle actin; *Ccl2*, C-C motif chemokine ligand 2; *Ccn1*, cellular communication network 1; *Ccn2*, cellular communication network 2; *Ccn3*, cellular communication network 3; *Col1*, collagen-I; *Col3*, collagen-III; *Col4a1*, collagen-IVα1; *Col4a2*, collagen-IVα2; *Col6*, collagen-VI; *Dpp4*, dipeptidyl-peptidase 4; *Fap*, fibroblast activation protein; *Il1b*, interleukin-1β; *Tgfb1*, transforming growth factor β1; *Timp1*, tissue inhibitor of metalloproteinase 1; *Tnf*, tumour necrosis factor α; *Rn18s*, 18S ribosomal RNA; *Rplp0*, ribosomal protein, large, P0. * Primer sequences designed to cross the deleted DNA sequence, and thus reduced mRNA level in the knockout mice would be confirmatory of the gene deletion model.

2.3.7 Western immunoblot from whole liver tissue

Frozen liver tissue was homogenised in cold radioimmunoprecipitation assay (RIPA) buffer containing protease inhibitor cocktail (Roche, Basel, Switzerland) and 50 mM NaF. The crude impurities were removed by centrifugation at 10,000 g for 20 min at 4°C. Total protein concentration was measured using the DC Protein Assay (Bio-Rad, Hercules, CA, USA). Samples containing 50 µg of total protein were loaded into each lane and separated by a 4 - 15% gradient sodium dodecyl-sulphate polyacrylamide gel electrophoresis (SDS-PAGE) gel (Bio-Rad, Hercules, CA, USA). Proteins were electro-transferred onto nitrocellulose membrane and membranes were blocked with 5% skim milk/TBS with 0.1% (vol/vol) Tween 20 for 1 hr, followed by incubation with anti-CTGF/CCN2 Antibody (1:10,000 titre; GTX124232, GeneTex, Irvine, CA, USA), in TBST containing 5% skim milk overnight at 4°C. After washing, the membranes were incubated with horseradish peroxidase-conjugated secondary antibody (1:5,000 titre) for 2 h at room temperature. The bands were visualised using Clarity™ Western ECL (Bio-Rad, Hercules, CA, USA) and imaged with ChemiDoc MP Imaging System (Bio-Rad, Hercules, CA, USA). The intensity of each band was quantitated using ImageLab software (Bio-rad, Hercules, CA, USA) and normalised to total protein from Ponceau S staining (multiple housekeeper proteins were affected by the model and not suitable for protein normalisation). Final data of the band intensity for each group was calculated from four immunoblots performed as independent experiments. Western immunoblots were performed by Dr Xiaoyu Wang.

2.3.8 Liver triglyceride quantification

Intrahepatic cell triglycerides were extracted with methanol:chloroform. A 20 - 30 mg piece of liver tissue was weighed before being placed in size D Lysing Matrix Tubes (MP Biomedicals Germany, Eschwege, Germany). The tissue was homogenised with 1 mL of a 1:2 mixture of methanol (POCD Healthcare, Artarmon, NSW, Australia) and chloroform (Ajax Finechem, Scoresby, VIC, Australia) in a FastPrep®-24 machine (6 m/s, 2 x 40 sec; MP Bio, Eschwege, Germany). The homogenate was transferred to polypropylene plastic tubes (Sarstedt, Numbrecht, Germany) and a further 3 mL of methanol:chloroform was added. Tubes were agitated on a rocker overnight at room temperature. The next day, 2 mL of 0.6% sodium chloride (Sigma-Aldrich, St Louis, MO, USA) was added to each sample and vortexed. Tubes were centrifuged at 2,000 rpm for 10 min at room temperature. The bottom layer was transferred to a glass tube with a glass pipette and the sample was dried under nitrogen gas for 45 min at 40°C. Each sample was then dissolved in 500 µL absolute ethanol. Glycerol standards (Precimat Glycerol; Roche, Basel, Switzerland) were prepared ranging from 0.716 to 45.8 nmoles. Standards and samples (5 µL) were added to a 96-well plate and incubated for 20 min at 37°C. Then, 300 µL of warmed Infinity™ Triglycerides reagent (Thermo Fisher Scientific Inc, Waltham, MA, USA) was added to each well and incubated for 30 min at 37°C. The optical density was measured at 490 nm using a plate reader. The amount of triglycerides was calculated from the standard curve, normalised to the starting tissue weight, and expressed as µmoles/g of liver.

The principles behind the Infinity™ Triglycerides reagent are as follows[315,316]: triglycerides are hydrolysed by lipase to free fatty acids and glycerol. Glycerol is phosphorylated by adenosine triphosphate (ATP) by glycerol kinase to produce glycerol-3-phosphate and adenosine diphosphate (ADP). Glycerol-3-phosphate is oxidised by glycerolphosphate oxidase to produce dihydroxyacetone phosphate (DAP) and hydrogen peroxide (H_2O_2). The H_2O_2 reacts with 4-aminoantipyrine (4-AAP) and 3,5-dichloro-2-hydroxybenzene sulfonate (DHBS) to produce a red-coloured dye. The absorbance of the dye is proportional to the concentration of triglycerides present in the sample.

2.3.9 Plasma cytokeratin-18 quantification

The measurement of mouse plasma CK-18 concentration was performed using the Mouse Cytokeratin 18 SimpleStep ELISA® Kit (Abcam, Cambridge, UK) by Dr Xiaoyu Wang. Mouse CK-18 Lyophilized Recombinant Protein standards (0.313 - 20 ng/mL) were prepared as per kit instructions. Standards and samples (50 µL) were added to the pre-coated (proprietary antibody) microplate. Samples were diluted 1 in 3. Antibody cocktail (50 µL) consisting of 10X Mouse CK-18 Capture Antibody, 10X Mouse CK-18 Detector Antibody and Antibody Diluent 4BR were added to each well. The microplate was incubated for 1 h at room temperature on a plate shaker set at 400 rpm. After three washes in Wash Buffer, 100 µL of TMB Development Substrate was added to the microplate and incubated for 10 min at room temperature in the dark on the plate shaker (400 rpm). After addition of Stop Solution, the optical density at 450 nm was measured using a microplate reader (Tecan Infinite® M 1000 Pro) with inbuilt software i-Control™ v1.10 (Tecan, Mannedorf, Switzerland). Mouse plasma CK-18 concentrations of the samples were interpolated using the standard curve (linear) and multiplied by the dilution factor.

2.3.10 Statistical analysis

All results are shown as mean ± SEM (standard error of the mean). Unless otherwise indicated, all data were compared using two-way ANOVA followed by Tukey's correction for multiple comparisons. A p-value ≤ 0.05 was considered statistically significant. All statistical analyses were performed using GraphPad Prism v9.1.1 for Windows (GraphPad Software, San Diego, CA, USA) unless otherwise stated.

2.4 Circulating CCNs

2.4.1 The Diabetes and Steatohepatitis Study

The Diabetes and Steatohepatitis (DaSH) Study was performed by Dr Kathryn H. Williams as part of her PhD, titled *The Clinical Relevance of Non-Invasive Measures of Liver Health and Non-Alcoholic Fatty Liver Disease (NAFLD) in Diabetes Mellitus* and awarded by the University of Sydney in 2016. The prospective, cross-sectional study was described in detail in her PhD thesis, referred to as "Cohort 3", and data from this study was published previously[86,87,317].

In brief, randomly recruited patients attending the Royal Prince Alfred Hospital (RPAH) Diabetes Centre between April 2011 until June 2012 underwent a detailed clinical assessment. Fasting morning blood samples were obtained, and routine tests performed (general biochemistry, liver enzymes, HbA1c, glucose, lipid profile and full blood count). Other, non-NAFLD causes of liver disease were excluded. All subjects underwent a liver ultrasound to assess for steatosis and transient elastography with Fibroscan® to screen for liver fibrosis. Serum and plasma were stored at -80°C for later use. All subjects provided written informed consent prior to undertaking any study procedures. All procedures were approved by the relevant NSW Health Human Research Ethics Committee (HREC) and the University of Sydney HREC and were in accordance with the Declaration of Helsinki (Sydney Local Health Network Protocol No X11-0105 & HREC/11/RPAH/144).

Access to the de-identified database of The DaSH Study and stored serum and plasma samples were made available for further analysis in this thesis.

2.4.1.1 Quantification of circulating CCN concentrations in The DaSH Study

Serum and plasma concentrations of CCN1, CCN2 and CCN3 were measured with commercial ELISA kits (*Table 2.11*). This research was commenced by Mr Kyle WW Lloyd (KL), a student of The Talented Student Program (TSP, The University of Sydney) in the Greg Brown Diabetes and Endocrinology Laboratory, however at the time, there was limited availability of good quality commercial kits. Newer kits with potentially better quality antibodies have since been developed, and these were performed according to the manufacturer's instructions by the author (SP) of this thesis.

Table 2.11: Commercial kits used to measure circulating CCN1, CCN2, and CCN3.

	CCN1		**CCN2**			**CCN3**	
Manufacturer	R&D		Cloud Clone	R&D		R&D	
Catalogue No.	DCYR10		SEA010Hu	DY9190-05		DY1640	
Sample	Serum	-	Serum	Serum	Plasma	Serum	Plasma
Performed by	KL	-	KL	SP	SP	SP	SP

2.4.1.1.1 Human circulating CCN1 concentration

The measurement of human serum CCN1 concentration was performed by Mr Kyle Lloyd using the Quantikine® ELISA Human Cyr61/CCN1 Immunoassay (R&D Systems Inc, Minneapolis, MN, USA). Human CCN1 standards (39.1 - 2 500 pg/mL) were prepared as per kit instructions. Standards and undiluted samples (50 µL) were added in duplicate to a 96-well microplate pre-coated with a monoclonal antibody specific for human CCN1, along with 100 µL of Assay Diluent RD1-36. The microplate was incubated for 2 h at room temperature on an orbital shaker, and then washed four times to remove unbound substances. Human CCN1 Conjugate (200 µL; polyclonal antibody for human CCN1 conjugated to horseradish peroxidase) was added to each well and incubated for 2 h at room temperature on an orbital shaker. The microplate was washed four times, before addition of 200 µL Substrate Solution (TMB plus H_2O_2) and incubated for 30 min at room temperature in the dark. After addition of stop solution, the optical density at 450 nm (reference 540 nm) was measured using a microplate reader (Tecan Infinite® M 1000 Pro) with inbuilt software i-Control™ v1.10 (Tecan, Mannedorf, Switzerland). Human serum CCN1 concentrations of the samples were interpolated using the standard curve (log/log).

2.4.1.1.2 Human circulating CCN2 concentration

The measurement of human serum CCN2 concentration was performed by Mr Kyle Lloyd using the Enzyme-linked Immunosorbent Assay Kit for Connective Tissue Growth Factor (CTGF/CCN2; Cloud-Clone Corp, Houston, TX, USA). Standards (0.47 - 30 ng/mL) were prepared as per kit instructions. Standards and undiluted samples (100 µL) were added in duplicate to the pre-coated microplate (biotin-conjugated antibody specific to CTGF/CCN2) and incubated for 1 h at 37°C. The liquid was removed, and Detection Reagent A (100 µL; avidin conjugated to horseradish peroxidase (HRP)) was added before further incubation for 1 h at 37°C. The microplate was washed three times and then 100 µL of Detection Reagent B (TMB) was added and incubated for 30 min at 37°C. The microplate was washed five times. Substrate solution (90 µL) was added to each well and incubated for 20 min at 37°C in the dark. After addition of stop solution, the optical density at 450 nm was measured using a microplate reader (Tecan Infinite® M 1000 Pro) with inbuilt software i-Control™ v1.10 (Tecan, Mannedorf, Switzerland). Human serum CCN2 concentrations of the samples were interpolated using the standard curve (log/log).

The measurement of human serum and plasma CCN2 concentration was performed by the author using the Human CTGF/CCN2 DuoSet® ELISA Development System with DuoSet® Ancillary Reagent Kit 2 (R&D Systems Inc, Minneapolis, MN, USA). A 96-well microplate was coated overnight at room temperature with goat anti-human CTGF/CCN2 Capture Antibody (100 µL). The following morning, the microplate was washed three times and then blocked with 300 µL of Reagent Diluent and incubated for 1 h at room temperature. Recombinant Human CTGF/CCN2 Standards (31.3 - 2,000 pg/mL) were prepared as per kit instructions. Standards and samples (100 µL) were added to the microplate in duplicate and incubated for 2 h at room temperature. After three more washes, Biotinylated Goat Anti-Human CTGF/CCN2 Detection Antibody (100 µL) was added to the microplate and incubated for 2 h at room temperature. The microplate was washed three times and then Streptavidin-HRP B (100 µL) was added to each well and incubated for 20 min at room temperature in the dark. Following another three washes, Substrate Solution (100 µL; TMB plus H_2O_2) was added and incubated for 20 min at room temperature in the dark. After addition of stop solution, the optical density at 450 nm (reference 540 nm) was measured using a microplate reader (Tecan Infinite® M 1000 Pro) with inbuilt software i-Control™ v1.10 (Tecan, Mannedorf, Switzerland). Human serum and plasma CCN2 concentrations of the samples were interpolated using the standard curve (4PL) and multiplied by the dilution factor.

2.4.1.1.3 Human circulating CCN3 concentration

The measurement of human serum and plasma CCN3 concentration was performed by the author using the Human NOV/CCN3 DuoSet® ELISA Development System with DuoSet® Ancillary Reagent Kit 2 (R&D Systems Inc, Minneapolis, MN, USA). A 96-well microplate was coated overnight at room temperature with goat anti-human NOV Capture Antibody (100 µL). The following morning, the microplate was washed three times and then blocked with 300 µL of Reagent Diluent and incubated for 1 h at room temperature. Recombinant Human NOV Standards (31.3 - 2,000 pg/mL) were prepared as per kit instructions. Standards and samples (100 µL) were added to the microplate in duplicate and incubated for 2 h at room temperature. After three more washes, Biotinylated Goat Anti-Human NOV Detection Antibody (100 µL) was added to the microplate and incubated for 2 h at room temperature. The microplate was washed three times and then Streptavidin-HRP A (100 µL) was added to each well

and incubated for 20 min at room temperature in the dark. Following another three washes, Substrate Solution (100 µL; TMB plus H_2O_2) was added and incubated for 20 min at room temperature in the dark. After addition of stop solution, the optical density at 450 nm (reference 540 nm) was measured using a microplate reader (Tecan Infinite® M 1000 Pro) with inbuilt software i-Control™ v1.10 (Tecan, Mannedorf, Switzerland). Human serum and plasma CCN3 concentrations of the samples were interpolated using the standard curve (4PL) and multiplied by the dilution factor.

2.4.1.1.4 Other biomarkers used in correlative analyses

Measurements of other novel markers were reported in Dr Williams' thesis including HA (Hyaluronan ELISA; R&D Systems, Minneapolis, Minnesota, USA), TIMP1 (TIMP1 ELISA; R&D Systems, Minneapolis, Minnesota, USA), PIIINP (PIIINP RIA; Orion Diagnostica, Espoo, Finland), CK-18 (M30 Apoptosense® ELISA; Peviva, Nacka, Sweden) and brain natriuretic peptide (BNP; BNP EIA Kit, Sigma-Aldrich, St Louis, MO, USA). DPP4 enzyme activity was measured as previously described[318,319]. FAP was measured using a validated in-house enzyme activity assay[319]. The results of these assays were used in the correlative analyses performed by the author of this thesis.

2.4.1.2 Statistical analysis

Standard curves for the commercial ELISA kits were produced with Microsoft Excel for Microsoft 365 (log/log curves) or GraphPad Prism v9.1.1 for Windows (4PL curves; GraphPad Software, San Diego, CA, USA). Results are shown as median [IQR].

Univariate (Spearman's test) and multivariate stepwise linear and logistic regression analyses were used to determined correlations between human circulating CCN concentrations and NASH fibrosis, as well as other clinical, biochemical, or radiological characteristics obtained from The DaSH Study database. Correlative statistics were performed using SPSS version 26.0 (IBM, Armonk, NY, USA). Variables with a p-value ≤ 0.1 were included in the multivariate regression analysis and variables with multicollinearity were excluded. Statistical significance was determined by a p-value ≤ 0.05.

2.4.2 The CCN2 Study and The CCN1 Study

2.4.2.1 Quantification of circulating CCN concentrations in The CCN2 Study and The CCN1 Study

Plasma CCN1, CCN2 and CCN3 concentrations were measured in mice from The CCN2 Study and The CCN1 Study (described in detail in *Section 2.3*) using commercial kits as per the manufacturer's instructions.

2.4.2.1.1 Mouse plasma CCN1 concentration

The measurement of mouse plasma CCN1 concentration was performed using the Mouse CYR61 SimpleStep ELISA® Kit (Abcam, Cambridge, UK). Mouse CYR61 Lyophilized Recombinant Protein standards (62.5 - 4,000 pg/mL) were prepared as per kit instructions. Standards and samples (50 µL) were added to the pre-coated (monoclonal proprietary antibody) microplate**.** Antibody Cocktail (50 µL; 10x Capture Antibody, 10x Detector Antibody and Antibody Diluent 5BI) was added to each well and the microplate was incubated for 1 h at room temperature on a plate shaker. The microplate was washed three times, followed by addition of 100 µL TMB Development Solution with further incubation for 10 min at room temperature on a plate shaker in the dark. After addition of stop solution, the optical density at 450 nm was measured using a microplate reader (Tecan Infinite® M 1000 Pro) with inbuilt software i-Control™ v1.10 (Tecan, Mannedorf, Switzerland). Mouse plasma CCN1 concentrations of the samples were interpolated using the standard curve (4PL) and multiplied by the dilution factor.

2.4.2.1.2 Mouse plasma CCN2 concentration

The measurement of mouse plasma CCN2 concentration was performed using the Mouse CTGF/CCN2 ELISA Kit (Novus Biologicals, Centennial, CO, USA). Reference standards (0.16 - 5 ng/mL) were prepared as per kit instructions. Standards and samples (100 µL) were added to the pre-coated microplate and incubated for 90 min at 37°C. The liquid was removed and 100 µL of Biotinylated Detection Antibody was added to each well and incubated for 1 h at 37°C. The microplate was washed three times, before 100 µL of HRP Conjugate was added and the microplate incubated for 30 min at 37°C. The microplate was washed five times and then 90 µL of Substrate Reagent was added to each well, then incubated for 15 min at 37°C in the dark. After addition of stop solution, the optical density at 450 nm was measured using a

microplate reader (Tecan Infinite® M 1000 Pro) with inbuilt software i-Control™ v1.10 (Tecan, Mannedorf, Switzerland). Mouse plasma CCN2 concentrations of the samples were interpolated using the standard curve (4PL) and multiplied by the dilution factor.

2.4.2.1.3 Mouse plasma CCN3 concentration

The measurement of mouse plasma CCN3 concentration was performed using the NOV (CCN3) Mouse SimpleStep ELISA® Kit (Abcam, Cambridge, UK). Mouse NOV Lyophilized Recombinant Protein standards (0.13 - 8 ng/mL) were prepared as per kit instructions. Standards and samples (50 µL) were added to the pre-coated (proprietary antibody) microplate. Antibody cocktail (50 µL) consisting of 10X Mouse NOV Capture Antibody, 10X Mouse NOV Detector Antibody and Antibody Diluent 4BR was added to each well. The microplate was incubated for 1 h at room temperature on a plate shaker set at 400 rpm. After three washes in Wash Buffer, 100 µL of TMB Development Substrate was added to the microplate and incubated for 20 min at room temperature in the dark on the plate shaker (400 rpm). After addition of stop solution, the optical density at 450 nm was measured using a microplate reader (Tecan Infinite® M 1000 Pro) with inbuilt software i-Control™ v1.10 (Tecan, Mannedorf, Switzerland). Mouse plasma CCN3 concentrations of the samples were interpolated using the standard curve (4PL) and multiplied by the dilution factor.

2.4.2.2 Statistical analysis

Standard curves for the commercial ELISA kits were produced with Microsoft Excel for Microsoft 365 (log/log curves) or GraphPad Prism v9.1.1 for Windows (4PL curves; GraphPad Software, San Diego, CA, USA). Results are shown as mean ± SEM and compared using two-way ANOVA followed by Tukey's correction for multiple comparisons (GraphPad Prism v9.1.1 for Windows, GraphPad Software, San Diego, CA, USA).

Univariate (Pearson's test) analyses were used to determined correlations between mouse plasma CCN concentrations and severity of liver fibrosis, as well as other metabolic, biochemical, or histological characteristics in The CCN2 Study and The CCN1 Study (*Chapters 4* and *5*). Correlative statistics were performed using SPSS version 26.0 (IBM, Armonk, NY, USA). Statistical significance was determined by a p-value ≤ 0.05.

Chapter 3: The Diabetes and Liver Clinic Audit

3.1 Introduction

The first results chapter of this thesis is presented in the format of an unpublished, prepared, manuscript. It is a retrospective audit of the Charles Perkins Centre (CPC) Royal Prince Alfred Hospital (RPAH) Diabetes and Liver Clinic (DLC), which is Australasia's first multidisciplinary clinic dedicated to individuals with diabetes and NAFLD. It highlights the scope of the problem, that is, the high prevalence of NASH fibrosis in individuals with T2DM and offers insight into how this clinic might enhance the assessment for NASH fibrosis.

3.2 Prepared manuscript

Can A Dedicated Diabetes and Liver Clinic Enhance the Assessment for NASH Fibrosis?

Sarah N Parry[1, 3, 4], Amanda Gauld[1], Amelia R Fernandes[1, 2], Kathryn H Williams[1,5,6], Ted Wu[1,3], Avik Majumdar[3, 7], Samantha L Hocking[1, 3, 4, 8], Simone I Strasser[3, 7], and Stephen M Twigg[1, 3, 4]

1. Department of Endocrinology, Royal Prince Alfred Hospital, Sydney, NSW, Australia
2. Faculty of Medicine, University of New South Wales, Sydney, NSW, Australia
3. Central Clinical School, Sydney Medical School, Faculty of Medicine and Health, University of Sydney, Sydney, NSW, Australia
4. Charles Perkins Centre, University of Sydney, Sydney, NSW, Australia
5. Department of Endocrinology, Nepean Hospital, Sydney, NSW, Australia
6. Nepean Clinical School, Sydney Medical School, Faculty of Medicine and Health, University of Sydney, Sydney, NSW, Australia
7. AW Morrow Gastroenterology and Liver Centre, Royal Prince Alfred Hospital, Sydney, NSW, Australia
8. Boden Collaboration, Central Clinical School, Sydney Medical School, Faculty of Medicine and Health, University of Sydney, Sydney, NSW, Australia

Corresponding Author:
Professor Stephen M. Twigg
Email: Stephen.twigg@sydney.edu.au

Funding: This research did not receive any specific grant from funding agencies in the public, commercial or not-for-profit sectors.

Abstract

Aims: To describe the clinical profile of patients attending Australasia's first dedicated Diabetes and Liver Clinic and to identify clinical and/or biochemical predictors of advanced liver fibrosis.

Methods: A retrospective audit of the Charles Perkins Centre Royal Prince Alfred Hospital Diabetes and Liver Clinic was performed. Patients with T2DM were referred if they had abnormal liver enzymes or steatosis on ultrasound. Liver fibrosis severity was determined by transient elastography using Fibroscan®. Clinical risk scores were calculated. Multivariate stepwise regression analysis was used to identify correlates of advanced fibrosis.

Results: Ninety-six patients were included, age 58.6±9.5 yrs, with diabetes duration of 12.6±9.7 yrs, BMI of 33.6±6.4 kg/m^2 and HbA1c of 7.7±1.4%. Overall, 28% had advanced liver fibrosis (LSM ≥ 10.3 kPa), which is ~10% higher than a historic cohort. The NAFLD fibrosis score had good negative predictive value (87%). In this cohort of patients with concomitant diabetes and NAFLD, advanced liver fibrosis was best predicted by a combination of LDL-c, BMI, ALT, and ALP (p-value < 0.005).

Conclusion: A dedicated Diabetes and Liver Clinic has enhanced the assessment for NASH fibrosis, of which the prevalence in this cohort was 28%. The NFS is a useful clinical score for excluding patients with significant liver fibrosis, but other models may perform better in a NAFLD with diabetes population.

Keywords: type 2 diabetes mellitus; non-alcoholic fatty liver disease; non-alcoholic steatohepatitis; liver fibrosis; NAFLD fibrosis score.

Introduction

Non-alcoholic fatty liver disease (NAFLD) has become the leading cause of chronic liver disease worldwide[66]. The increase in prevalence of NAFLD is driven by its epidemiologic and pathophysiologic links to type 2 diabetes mellitus (T2DM) and obesity. Approximately 25% of the general population has NAFLD, but this rises to greater than 70% in adults with obesity or T2DM[68,188]. In addition, the presence of T2DM is an independent risk factor for progressing to each of the more severe stages of NAFLD[67,189,190]. The growing rates of these concomitant metabolic diseases have significant implications not only for long-term health outcomes at both individual and public health levels, but also impacts on healthcare systems and health economics, related to screening, diagnosis, and management.

NAFLD is defined by excessive accumulation of hepatic fat (> 5%), in the absence of secondary causes including excessive alcohol intake. It encompasses a spectrum of disease, from simple steatosis to non-alcoholic steatohepatitis (NASH) and cirrhosis. The later, more severe stages are characterised by hepatic inflammation and fibrosis and are more common in individuals with T2DM compared with the general population[320]. The degree of liver fibrosis is linked to premature mortality from cardiovascular disease and liver-related complications such as hepatocellular carcinoma and end-stage liver failure[67,321-324]. Globally, the rates of liver transplantation with cirrhosis due to NAFLD/NASH as the primary indication are increasing[72]. In the past two decades NASH has overtaken alcoholic liver disease as the second most common indication for transplant in the United States.[73]. In Australia, it remains in third place, behind hepatitis C infection and alcoholic liver disease, but has increased more than five-fold since 2003[74]. The change in trends is partially explained by improved prevention and treatments with vaccination and antiviral therapies for chronic liver disease caused by hepatitis infections[75]. However, the absolute increased prevalence of NAFLD cannot be ignored. In fact, it is expected that by 2030 the prevalence of all stages of NAFLD will have increased by more than 20%, but the prevalence of the most severe stages of fibrosis, that is F3 and F4, will have more than doubled[76].

The gold standard for assessing NAFLD remains liver biopsy, but in most cases, this is unnecessary, highly invasive, and carries inherent risk[82]. Therefore, other methods

of assessing the liver non-invasively have been developed, which can be implemented in the clinical setting[83]. This includes the use of the Fibroscan®, which utilises transient elastography to measure liver stiffness, a surrogate for fibrosis. Studies have shown a high degree of correlation between Fibroscan® readings and fibrosis stage confirmed on liver biopsy in the NAFLD population[91-93]. Local data has reported that the prevalence of NASH fibrosis, defined as a liver stiffness measurement (LSM) of ≥ 10.3 kPa (normal < 5.5 kPa) by Fibroscan®, in unselected patients attending a tertiary diabetes outpatient clinic was 18%[86]. In contrast the general population prevalence rate of NASH fibrosis is less than 5%[83]. This data is in keeping with epidemiological evidence that NAFLD is more likely to progress to more severe stages of liver disease in individuals with T2DM.

In addition to liver imaging, other non-invasive methods of assessing liver fibrosis include use of scoring systems based on readily accessible clinical and laboratory parameters. The NAFLD fibrosis score (NFS) combines data on an individual's age, body mass index (BMI) and presence of diabetes/impaired fasting glucose with biochemical indices of alanine aminotransferase (ALT), aspartate aminotransferase (AST), albumin level, and platelet count[325]. The fibrosis-4 index (FIB-4) combines data on age, ALT, AST, and platelet count, and was first developed for the hepatitis C/HIV co-infection population, but also performs well in the NAFLD population[326]. Both scores have a high negative predictive value when they are below the specified cut-offs[327,328], however neither of these scores were derived from populations with concomitant T2DM and NAFLD exclusively, potentially limiting their utility in this cohort.

A joint Clinical Practice Guideline from the European Association for the Study of Liver (EASL), Diabetes (EASD) and Obesity (EASO) on the management of NAFLD was published in 2016[199]. It made a level A2 recommendation (high quality evidence, weaker recommendation) to assess for the presence of NAFLD in all individuals with T2DM, irrespective of their liver enzyme levels. Assessment included a minimum of a liver ultrasound and liver enzymes. However, the authors acknowledged that the availability of resources, the added burden on healthcare systems, and the limited effective treatments, would be important considerations in widespread screening. The American Diabetes Association (ADA) included screening for NAFLD for the first time

in their 2019 Standards of Medical Care in Diabetes[200]. They recommended that all individuals with T2DM who have biochemical or radiological evidence of NAFLD should receive assessment for NASH and liver fibrosis. They suggest the use of non-invasive tests, such as elastography or fibrosis biomarkers, however the recommendation was based on low level (Level C) evidence. Ultimately, assessment by a liver specialist, with or without a liver biopsy, may still be required to provide a definitive diagnosis. This recommendation contrasts with the Practice Guidance from the American Association for the Study of Liver Diseases, which recommended against routine screening of individuals with diabetes, but to maintain a high index of suspicion for the more severe manifestations of NAFLD, as these are undoubtedly more common in the diabetes population[329].

There are currently no clinical practice guidelines in Australia for the screening of NAFLD in the diabetes population. Latest statistics from the Australian Institute of Health and Welfare indicate that approximately 1.7 million Australian adults have diabetes[330]. Based on this data, over 1 million Australian adults may have NAFLD, and screening and identifying those at highest risk remains a challenge. This is partly due to limited knowledge about the pathogenesis, natural history, and complications of NAFLD/NASH in individuals with T2DM. There are few clinics globally dedicated to diabetes and liver disease and here we report the clinical experience of the first multidisciplinary Diabetes and Liver Clinic (DLC) in Australasia. The aim of this study was to describe the clinical profile of patients attending the DLC and to establish any clinical and/or biochemical parameters that correlate with severe NASH fibrosis in this cohort.

Subjects, Materials and Methods:

Subjects

Data were collected retrospectively from patients who were assessed at the Charles Perkins Centre Royal Prince Alfred Hospital Diabetes and Liver Clinic (CPC RPAH DLC) from its inception in 2016 until 2019. Referral criteria for assessment to this clinic were patients with T2DM who had abnormal blood liver enzyme tests and/or liver steatosis on imaging. Exclusion criteria included individuals without T2DM, those who did not complete the clinical assessment, or those who did not have NAFLD as the primary hepatic abnormality. All patients underwent screening to exclude other

aetiologies of liver disease including autoimmune, infectious, and genetic causes. Alcohol intake was documented, but excessive alcohol intake above the current recommended guidelines of less than 14 standard drinks per week was not an exclusion criterion. Each patient was reviewed by an experienced endocrinologist and hepatologist.

Clinical and biochemical parameters

Information collected from the DLC clinic records included: demographics, past medical history, physical examination findings and pathology results. Detailed history regarding diabetes diagnosis, management and complications was obtained. Biochemical parameters (non-fasting) included: blood electrolytes, liver enzymes, full blood count, international normalised ratio (INR), haemoglobin A1c (HbA1c), fructosamine, glucose, insulin, c-peptide, lipid panel and ferritin, and urine albumin to creatinine ratio (UACr).

Liver assessment

Transient elastography with Fibroscan® (EchoSens, Paris, France) was performed by an experienced hepatologist to measure liver stiffness (liver stiffness measurement; LSM), with either M or XL probe. A minimum of 10 readings with an IQR/median ratio of ≤ 30% was required for a score to be valid[331]. An LSM ≥ 10.3 kPa was deemed to represent advanced liver fibrosis[332]. A secondary analysis was performed using an LSM ≥ 8.5 kPa (supplementary data). The NFS and FIB-4 were calculated as previously described[325,333]. Each patient underwent a dedicated liver ultrasound. A diagnosis of cirrhosis was made by the clinic hepatologist based on clinical, radiological, biochemical and/or histopathological findings. Liver biopsy was not routinely performed, but when undertaken it was reported using the Brunt criteria[80].

Comparison with an unselected T2DM cohort

We compared data from this study with data from a previously reported historic cohort exploring the rates of advanced liver fibrosis in unselected individuals with T2DM from the same tertiary centre[86,87].

Statistical analysis

All statistics were performed using Microsoft Excel or IBM SPSS version 26.0. Two-tailed t-test was used for continuous variables and chi-squared test was used for categorial variables. Univariate (Pearson's test) and multivariate stepwise logistic and linear regression analyses were used to determined correlations between LSM by transient elastography and clinical and biochemical characteristics. Variables with a p-value ≤ 0.1 were included in the multivariate regression analysis. Statistical significance was determined by a p-value ≤ 0.05.

Ethics approval

The study was approved by the Sydney Local Health District RPA Ethics Committee (Ethics reference number X19-0117 and 2019/ETH02727).

Results

Patient characteristics

A total of 119 patients were assessed in the CPC RPAH DLC from 2016 to 2019 (*Supplementary Figure 1*). Eleven patients were excluded who did not have T2DM (no diabetes or type 1 diabetes mellitus (T1DM)) and a further nine patients did not complete the assessment. Three patients were diagnosed with non-NAFLD pathology. In total, 96 patients were included in this study and the clinical characteristics are shown in *Table 1* and the biochemical characteristics are shown in *Table 2*. There were similar numbers of males and females, with a mean age of 58.6 years. Approximately 39% were of Anglo-Saxon descent, with three patients identifying as Aboriginal or Torres Strait Islander. The remainder of the patients were of a mix of Asian, South American, Middle Eastern, European, or from other parts of Oceania. All but one patient had T2DM: one patient was identified as having diabetes secondary to IgG4 pancreatitis; however, he was not excluded as his overall clinical picture was more consistent with insulin resistance and not absolute insulin deficiency. The mean duration of diabetes was 12.6 years, with a range of 0 to 40 years. The mean HbA1c was 7.7% indicating relatively well controlled diabetes. Patients were taking on average two non-insulin diabetes medications. Classes included: biguanides, sulphonylureas, dipeptidyl-peptidase 4 (DPP4) inhibitors, sodium-glucose co-transporter 2 (SGLT2) inhibitors, or glucagon-like peptide-1 (GLP-1) receptor agonists. Almost half were taking either an SGLT2 inhibitor or GLP-1 receptor agonist, classes

of medications which have promising data regarding positive effects for NAFLD in people with diabetes. In addition, 41% of the patients were being treated with insulin (mean total daily dose of insulin = 67 units). Microvascular diabetes-related complications were more frequent than macrovascular complications. Diabetic nephropathy and peripheral neuropathy were the most common complications, present in ~one quarter of all patients.

Over 90% of patients attending the DLC clinic were either overweight or obese, and the mean BMI was 34 kg/m^2. Most patients had hypertension or dyslipidaemia treated with pharmacotherapy. Over 15% of patients also had obstructive sleep apnoea, which whilst not a component of the metabolic syndrome, is strongly associated with the same clinical features. A surprisingly high proportion of the cohort were ex-smokers (38%), whilst almost 10% were active smokers. Levels of alcohol intake above current recommended guidelines were reported in ~15% of patients.

Liver assessment

Fibroscan® readings were obtained on 90 patients. Of these, 25 had advanced fibrosis, as indicated by an LSM ≥ 10.3 kPa (*Figure 1*) which represented 28% of this T2DM cohort. A Fibroscan® reading was not obtained in five patients due to technical challenges with increased body habitus and a further patient did not meet criteria for a valid reading as described in the methods. A clinical diagnosis of liver cirrhosis was made in 16 patients (17%). Rates of liver biopsy were low (11%) in this clinic, but the results were used to confirm the diagnosis in the relevant cases. It should also be noted that a third of the cohort may have had another contributing factor to their degree of liver disease, such as excessive alcohol intake, previous (inactive) hepatitis B infection, or medications associated with liver fibrosis such as methotrexate or tamoxifen use.

The NFS and FIB-4 stratified by degree of liver fibrosis is shown in *Figure 2*. There were 13 out of 64 patients with low LSM that had a low risk NFS, and 9 patients out of 25 with a high LSM that had a high risk NFS. The rate of indeterminate risk NFS was close to 60%. Most patients had a low risk FIB-4, and only 1 patient (out of 16) with cirrhosis had a high risk score. It is notable that for both the NFS and the FIB-4, some, albeit few, advanced fibrosis was present in those with low risk scores, but such cases

were relatively more common with progressively higher risk scores. Overall, the NFS had good negative predictive value (87%, 13 of 15) in those with low risk scores to identify patients unlikely to have advanced fibrosis.

Clinical and biochemical features of individuals with advanced liver fibrosis

Individuals with an LSM ≥ 10.3 kPa were statistically more likely to have peripheral vascular disease or a previous cerebrovascular accident compared with individuals without advanced fibrosis (*Table 1*). However, the number of events in each group were low and the clinical significance is unclear. There was no difference in overall rates of macrovascular complications, nor presence of ischaemic heart disease. Individuals with an LSM ≥ 10.3 kPa were more likely to have a higher HbA1c (8.1 ± 1.4 vs 7.5 ± 1.3 %; p = 0.049) and AST (43.7 ± 21.5 vs 32.1 ± 11.8 U/L; p = 0.016), and lower LDL-C (1.6 ± 0.6 vs 2.1 ± 0.8 mmol/L; p = 0.011) compared with those with an LSM < 10.3 kPa (*Table 2*). Body mass index did not reach statistical significance with a p-value of 0.064 (35.0 ± 5.1 vs 32.6 ± 6.4 kg/m^2).

Correlations between Fibroscan® reading and clinical and biochemical variables

Correlative analysis was performed with LSM by transient elastography as a categorical variable of < or ≥ 10.3 kPa, and separately as a continuous variable (*Supplementary Table 1*). On logistic regression, an LSM of ≥ 10.3 kPa was associated with higher HbA1c, ALP, GGT, and AST, and a lower LDL-c as well as a higher risk FIB-4 (all p ≤ 0.05). Additional variables of BMI, ALT, and systolic blood pressure were included in the multivariate analysis as they had p-values > 0.05 but ≤ 0.1. On multivariate logistic regression, an LSM ≥ 10.3 kPa was best predicted by a combination of lower LDL-C and higher BMI, ALT, and ALP (p < 0.005; *Table 3*). When linear regression was performed, a different set of variables correlated with higher LSM: higher BMI, HbA1c, ALP, GGT, ALT, AST, triglycerides, and systolic blood pressure, as well as insulin therapy and higher risk NFS and FIB-4 (all p ≤ 0.05; *Table 3*). Additional variable of platelet count was included in the multivariate analysis as p-value was > 0.05 but ≤ 0.10. On multivariate analysis, a higher LSM was best predicted by a combination of BMI, platelet count and GGT (p-value < 0.005; *Table 3*). Clinical factors without significant correlation included age, duration of diabetes, presence of diabetes-related complications, c-peptide, ferritin, current or previous smoking, or excessive alcohol intake.

Comparison with a historic type 2 diabetes mellitus cohort.

The demographic and clinical data for this cohort is available in *Supplementary Table 2* and published elsewhere[86,87]. In brief, 106 patients with non-T1DM were recruited and underwent transient elastography. One hundred and two patients had valid Fibroscan® readings, of which 19 readings were ≥ 10.3 kPa (19%). This is almost 10% less than the prevalence reported in the current study.

Discussion

High prevalence of NASH fibrosis in a pre-selected type 2 diabetes mellitus cohort

This study has described the clinical experience of Australasia's first multidisciplinary clinic dedicated to people with diabetes and NAFLD. The prevalence of advanced liver fibrosis in this study, as determined by an LSM ≥ 10.3 kPa was 28%. This was greater than the background population prevalence of ~5% and consistent with previous data that individuals with T2DM are at a greater risk of progressing to more severe phenotypes of NAFLD[67]. The cohort consisted of generally well, community-dwelling outpatients. Although the mean data indicated a middle-aged cohort with long standing diabetes, the ranges identified a diversity of ages, duration of diabetes and ethnicity. Over 90% of the cohort were overweight or obese, with high prevalence of hypertension (> 70%) and/or dyslipidaemia (> 80%), as well as diabetes-related complications (> 50% at least one complication). The prevalence of the metabolic syndrome in this cohort was not formally assessed as waist circumference was not routinely measured. However, it is reasonable to assume that the rate was very high: all patients had diabetes, and there was high prevalence of all other criteria[334].

The prevalence of advanced fibrosis in our current cohort was ~10% higher than our historic cohort of unselected individuals with T2DM. Both studies used an LSM threshold of ≥ 10.3 kPa, which was chosen based on a study by Wong and colleagues[332]. This cut-off had a negative predictive value of 99% for detecting cirrhosis on liver biopsy, with high sensitivity and specificity. It is noted that other studies use different LSM thresholds, many of which were lower than the cut-off used in our study[335]. Therefore, although comparison between studies is challenging, the prevalence reported here may be an underestimate. In fact, when using an LSM threshold of ≥ 8.5 kPa, the prevalence of advanced fibrosis in our cohort was 38% (*Supplementary Table 3*). Nevertheless, the use of lower thresholds has significant

implications for the degree of fibrosis detected, with lower thresholds likely to detect lesser degrees of fibrosis. This reduces the clinical relevance, as highest priority should be given to identifying individuals with more severe fibrosis and therefore at higher risk of morbidity and mortality.

A study of unselected outpatients with T2DM found that an LSM ≥ 7.65 kPa had a 35% overall prevalence and a 75% positive predictive value for identifying biopsy-proven fibrosis of ≥ F2[336]. This early study is one of few studies that utilised liver biopsy, albeit in small numbers, and highlighted that significant liver fibrosis was under-recognised in the T2DM population. In comparison to our study performed in an outpatient population with diabetes, a prospective study screening hospitalised inpatients with diabetes using transient elastography found a lower prevalence of 16% with severe fibrosis (defined as LSM > 8.7 kPa), despite worse glycaemic control with an average HbA1c of 8.7%[337]. However, their cohort had a mean BMI of 25 kg/m^2 and 52% of included patients had T1DM, which may partly explain the lower prevalence, despite using a lower LSM threshold. There have been multiple recent studies that have found similar results, that is, a lower prevalence of advanced fibrosis compared to the data reported in this current study, when recruiting unselected or consecutive patients from regular outpatient diabetes clinics[338-342]. In contrast, one study from a Japanese cohort had a similar prevalence, if not higher, of advanced fibrosis, with 34% of the cohort having an LSM ≥ 9.7 kPa[343]. Overall, this suggests that a dedicated Diabetes and Liver Clinic, where there is pre-selection based on other factors such as deranged liver enzyme tests or radiological evidence of steatosis, may be able to attract a higher referral rate for more severe liver disease than a more general diabetes clinic.

Predicting NASH fibrosis in a diabetes cohort

There was a significant correlation between LSM and BMI on univariate analysis. This supports recommendations to these patients that weight reduction may improve liver health, certainly steatosis and possibly prevent progression of inflammation and fibrosis. Metabolic surgery resulting in substantial and sustained body weight reduction (> 15%) has been shown to be associated with less severe, or even resolution of, NASH fibrosis[177-179]. We also found a univariate correlation for HbA1c, as well as a significantly higher HbA1c in the group with LSM ≥ 10.3 kPa. Unlike macro- and micro-vascular complications of diabetes, liver fibrosis is not thought to be primarily mediated

by hyperglycaemia, and there is a lack of strong data to suggest that improving glycaemic control improves NASH fibrosis. Although this is cross-sectional data, the correlation with HbA1c is difficult to explain. The HbA1c was not statistically significant in the multivariate analysis, nor has it been in other similar studies. It also does not form part of any clinical risk score calculations, although the inclusion of diabetes or impaired glucose tolerance in the NFS may mask the need for a biochemical index such as HbA1c. Our study did not find any correlations between advanced liver fibrosis and traditional hyperglycaemia-driven diabetes-related complications, most likely due to the relatively smaller sample size with low event numbers. There is wider evidence that links the presence of NASH with macro- and micro-vascular complications, most strongly for cardiovascular disease, but also chronic kidney disease (CKD) and peripheral neuropathy[321,344,345]. Concerningly, NASH and CKD may co-exist, and significantly increase cardiovascular risk[346]. In addition, the de Ledinghen study reported that higher LSM by transient elastography was associated with previous cardiovascular event, past history of diabetic foot ulcer, and an absence of diabetic retinopathy[337].

Whilst the relationship between metabolic syndrome, obesity and NAFLD have been established, there is still some uncertainty as to the clinical implications of NAFLD in the diabetes population. Proposed mechanisms for the progression of NAFLD in diabetes relates to increased insulin resistance resulting in relative hyperinsulinaemia[347]. Our study did not find a correlation between liver stiffness and biochemical markers of insulin resistance, such as c-peptide or c-peptide:glucose ratio or insulin level. This analysis was likely confounded by the fact that the blood samples were not performed in the fasting state, and as such, the HOMA-IR could not be calculated either. In addition, patients with T2DM receiving insulin therapy were excluded from the insulin analysis (but not the c-peptide analysis) as their insulin levels would be a measure of both endogenous and exogenous insulin. Statistical analyses without these exclusions yielded similar non-significant results. Further studies in a T2DM population investigating this relationship of insulin resistance, relative insulin deficiency, and hyperinsulinaemia, with NASH fibrosis, are required.

Although both the NFS and FIB-4 had good negative predictive value in our cohort of 87% and 85%, respectively, FIB-4 out-performed the NFS in the univariate analysis.

In fact, when LSM was analysed as a dichotomous variable, it was not significantly associated with NFS. The NFS and FIB-4 (and body weight) were not included in the multivariate analysis due to multicollinearity. Our statistical models showed that advanced liver fibrosis with LSM ≥ 10.3 kPa was best predicted by lower LDL-c and higher BMI, ALT, and ALP. The association of higher ALP is unexpected, and difficult to explain. Other small cross-sectional studies of individual with biopsy-proven NASH have found similar associations on univariate and multivariate analysis, including in a T2DM population[348,349]. Whilst raised ALP is generally seen in cholestatic liver diseases, it may be possible that a ductular reaction associated with liver fibrosis results in bile duct injury and release of ALP into the serum although there is little evidence in the literature to support this[350]. Correlations with ALT and BMI are expected, as both are components of the NFS. We hypothesise that the lower LDL-c may reflect the high rates of medications used for the treatment of dyslipidaemia, as higher LDL-c is usually associated with a worse metabolic state[351]. This is also concordant with the higher rates of peripheral vascular disease and cerebrovascular accidents in individuals with advanced fibrosis, as these patients were more likely to have had more aggressive treatment of their dyslipidaemia. Further analysis of LDL-c subclass may also have been useful in determining atherogenic potential, and therefore cardiovascular risk.

In a separate model where LSM was analysed as a continuous variable, increasing LSM was predicted by higher GGT and BMI, and lower platelet count. Again, the correlation of higher GGT is unusual in liver fibrosis, and may be non-specific, although other studies have shown similar results[338,340,342]. This data may be confounded by alcohol intake, where 15% of this cohort self-reported exceeding 140 g/week of alcohol, which was the national recommendation at the time of data collection but has since been reduced to 100 g/week.

Both combinations of variables from the multivariate analysis differ from those in the NFS and FIB-4, and notably do not include advancing age as an independent variable. This suggests that, at least in our study, relatively young individuals with T2DM remain at risk of advanced liver fibrosis, along with older individuals. In addition, the absence of AST from both models is unusual given the strong relationship between AST levels and NASH, and the significant difference between individuals with and without

advanced fibrosis found in this study. Regardless, the novel combination of variables from our models may have utility in predicting advanced fibrosis in a pre-selected T2DM population and should be further tested in larger cohorts.

Improving patient outcomes with a multidisciplinary Diabetes and Liver Clinic

As aforementioned, this study is unique in that individuals with T2DM have been pre-screened, or pre-selected based on the presence of deranged liver function tests or radiological evidence of steatosis. These patients were then subsequently offered review in our multidisciplinary clinic by a hepatologist and endocrinologist. Most other studies have reported on unselected cohorts of individuals with T2DM[86,336,338-341,343], whereas this study reports on a pre-selected cohort, thereby potentially targeting a higher risk group. This is supported by the higher prevalence of severe disease reported here.

Whilst the data presented in this study represents the first review of each patient at the DLC, each patient was subsequently offered annual follow-up. Unfortunately, the capture of longitudinal data has been significantly affected by the COVID-19 pandemic and is not reported here. Nevertheless, screening in the DLC has identified individuals with serious complications, including ~17% of the cohort with a clinical diagnosis of cirrhosis. This has enabled subsequent systematic screening for the complications of cirrhosis, including hepatocellular carcinoma, hepatic insufficiency, and portal hypertension. It has provided an opportunity to be proactive and offer potentially lifesaving treatment for a disease that was previously undiagnosed. Thus, such a clinic, with specialist review by both endocrinologists and hepatologists in a multidisciplinary setting, has the potential to improve patient outcomes.

Although it is acknowledged that many healthcare sites may not have the capacity or resources to set up such a specialised clinic, there are further benefits to establishing a dedicated Diabetes and Liver Clinic. In the absence of any approved drug treatments for NASH fibrosis, there is intense interest in the development of therapeutics, which may either prevent development, delay progression, and/or reverse NASH fibrosis. At the time of writing, the National Institutes of Health Clinical Trials register currently lists more than 500 clinical trials for NASH, including 150 trials that specifically include a diabetes population[352]. Clinics such as the DLC can be used to identify patients that

may be suitable for enrolment into relevant ethically approved clinical trials, with the aim of developing effective drug treatments.

Challenges of currently available screening tools for NASH

It is only in recent years that the link between NAFLD and diabetes has been recognised and there remains a general low level of awareness amongst health practitioners. Contributing to this is a lack of early warning symptoms, and a longstanding pervasive clinician attitude as to a common benign nature of NAFLD. There are also significant challenges in diagnosis, and the current lack of a simple, widely available biomarker for NASH means that a pragmatic diagnostic and staging approach is needed.

While there is little consensus across international guidelines, screening algorithms commonly utilise combinations of liver enzyme tests, a clinical score(s) and transient elastography. Liver enzyme tests need to be interpreted with caution as results within the reported normal range do not necessarily exclude severe disease. Transient elastography may be unreliable in people with morbid obesity, even with availability of the larger-sized XL probe[353]. Our cohort was predominantly overweight or obese, and there were six patients where even a hepatologist experienced in undertaking transient elastography could not obtain a reliable reading owing to patient body habitus. Due to the difficulties in obtaining a clear diagnosis of NAFLD severity in the absence of routine liver biopsy, as well as the limitations of using other screening tools independently, risk scores were created to assist with predicting the diagnosis based on readily available clinical and biochemical parameters. Both the NFS and FIB-4 have been shown to be better than other scoring systems at predicting overall mortality, but they are not accurate enough to be used alone in the clinical setting[354]. A high NFS score in our series clearly enhanced the likelihood of a high Fibroscan® reading, as did a high FIB-4, although the sensitivity was only 36% and 4%, respectively. The high number of indeterminate scores limits their utility as a stand-alone assessment tool. Nevertheless, these scores may help to exclude people with T2DM who are at the lowest risk of NASH fibrosis and thus who may not need to be further investigated by transient elastography or other methods for severe NASH fibrosis[87]. Indeed, if we used a low NFS to exclude patients needing further assessment, the population with

elevated LSM could have been increased to 31% in this series, however this would be at the expense of excluding two patients with an LSM ≥ 10.3 kPa in the current cohort.

There is much interest in using blood biomarkers to identify persons with advanced liver fibrosis. A comprehensive review was published by Wong and colleagues and such a review would be beyond the scope of this paper[84]. However, whilst several specific fibrosis markers, as well as combination panels have been researched, questions about accuracy and concerns about cost remain. Other potential markers that have been researched by this group include fibroblast activation protein (FAP) and dipeptidyl-peptidase 4 (DPP4) activity. When combining FAP levels and NFS in a screening algorithm, ~40% of patients could be reclassified from "indeterminate risk" to "low risk" category[87]. In addition, circulating DPP4 levels were associated with LSM ≥ 10.3 kPa[86]. Importantly, both studies were performed in cohorts of individuals with concomitant NAFLD and diabetes, exclusively.

Is screening individuals with T2DM for NASH a cost-effective process?

Individuals with T2DM are at significantly higher risk of developing advanced liver fibrosis and dying from cardiovascular disease and liver-related complications. Without consensus on the best approach to screening, and without any approved treatments, it is difficult to assess cost-effectiveness of screening. There is little published data that focusses specifically on a diabetes cohort, with most analysis studies reporting on the primary care setting on hypothetical cohorts or individuals with confirmed NAFLD or risk factors for NAFLD[355-358]. When studying a T2DM cohort exclusively, a model of hypothetical patients found that screening (liver ultrasound +/- liver biopsy), reduced both the number of individuals who developed cirrhosis and liver related deaths, but this was offset by the side effects of treatment, which in this study was pioglitazone[359]. Overall, the screening strategy was found not to be cost-effective. In contrast, a subsequent study using ultrasound with liver enzymes (AST or ALT), followed by transient elastography, with prescribed intensive lifestyle intervention or pioglitazone was found to be cost effective[360]. The authors explained the difference in results compared to the Corey et al study was because of the inclusion of the costs associated with diagnosis of hepatocellular carcinoma and liver transplant into their model. A large, multi-national study also found that using transient elastography was a cost-effective intervention in primary care, and even more effective when applied to

a diabetes cohort[361]. Further cost-analysis studies for different screening algorithms are needed, ideally which can be applied to an Australian population.

Strengths of this study

A major strength of this study is its exclusive use of a T2DM population with concomitant NAFLD. The increased risk of severe liver disease posed by T2DM is under-recognised and under-studied. The use of a pre-selected cohort, versus a more general cohort of all-comers to an outpatient diabetes clinic, has enabled an even higher risk group to be targeted for more intensive investigation.

Limitations of this study

Limitations of this study include the retrospective collection of data. In addition, the rates of liver biopsy were low, and therefore a histological diagnosis was lacking in most patients. However, this is acceptable in routine clinical practice, where liver biopsy, whilst a gold standard, is not common. The majority of patients were referred from a tertiary hospital outpatient diabetes clinic, and it could be argued that these patients may have self-selected and were more likely to be health conscious. This study has not reported on progression of NAFLD, although with time, longitudinal data will be obtained, and this will provide further insight into the natural history of diabetes and NAFLD and NASH.

Conclusion

The prevalence of more severe phenotypes of NAFLD was higher in this cohort compared with other cohorts, including inpatients with diabetes and patients attending a diabetes centre outpatient service. The results contained herein support the establishment of the multidisciplinary Diabetes and Liver Clinic in identifying patients with diabetes who have more severe liver fibrosis due to NASH or cirrhosis. The correlation between higher LSM by transient elastography and higher HbA1c and BMI, whilst cross-sectional, supports a need to focus on improving glycaemic control and body weight to reduce the risks associated with liver fibrosis, particularly in the absence of any proven pharmacological therapy directed at the liver. Further studies are needed to assess the natural history of this condition with diabetes, and identification of other biomarkers of disease severity or progression. With time, it is expected that more accurate and cost-effective screening methods to assess for

NASH fibrosis severity will be developed, and they may be combinations of: clinical risk scores for fibrosis with transient elastography and/or dedicated fibrosis blood biomarker assays, to better determine who should have a liver biopsy. Whether those with NASH fibrosis of, for example, moderate severity should be prioritised for metabolic surgery is also an important topic for future studies. In addition, definitive clinical trial results investigating agents that may specifically prevent, stabilise, and reverse NASH fibrosis in people with diabetes, are keenly awaited.

Figures and Tables

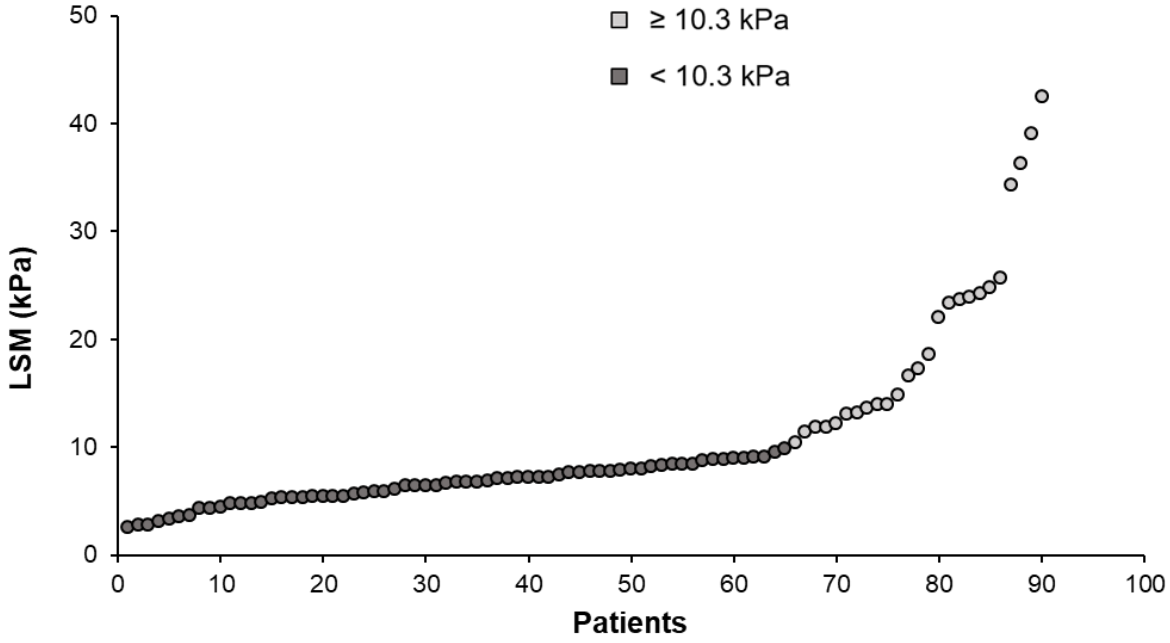

Figure 1: LSM for each patient. LSM, liver stiffness measurement.

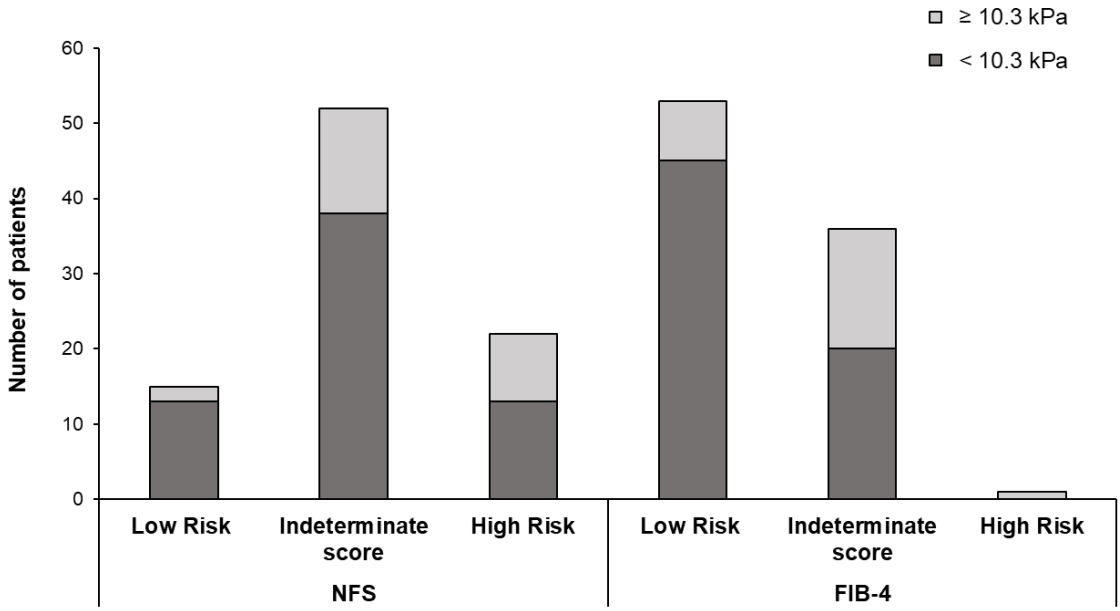

Figure 2: Rates of low, indeterminate, and high risk NFS and FIB-4, stratified by dichotomised LSM. FIB-4, fibrosis-4 index; LSM, liver stiffness measurement; NFS, NAFLD fibrosis score.

Table 1: Clinical characteristics of participants in The DLC Audit.

	All Patients		LSM < 10.3 kPa		LSM ≥ 10.3 kPa		p-value
Gender, % male (n)	52.1 (50)	n = 96	56.9 (37)	n = 65	40.0 (10)	n = 25	0.150
Age, years (range)	58.6 ± 9.5 (33 - 85)	n = 96	57.5 ± 9.3 (36 - 75)	n = 65	61.1 ± 9.1 (47 - 83)	n = 25	0.104
Duration of diabetes, years (range)	12.6 ± 9.7 (0 - 40)	n = 96	11.8 ± 9.3 (0 - 39)	n = 65	13.6 ± 9.7 (0 - 40)	n = 25	0.425
Number of non-insulin diabetes medications	2.0 ± 0.9	n = 96	1.9 ± 1.0	n = 65	2.2 ± 0.9	n = 25	0.295
Insulin therapy, % (n)	40.6 (39)	n = 96	35.4 (23)	n = 65	52.0 (13)	n = 25	0.150
Total daily dose of insulin, units (range)	66.6 ± 43.6 (10 - 178)	n = 39	59.2 ± 35.7 (18 - 150)	n = 23	83.6 ± 53.8 (20 - 178)	n = 13	0.160
≥ one microvascular complication, % (n)	54.2 (52)	n = 96	56.9 (37)	n = 65	44.0 (11)	n = 25	0.271
Peripheral neuropathy	27.1 (26)	n = 96	27.7 (18)	n = 65	28.0 (7)	n = 25	0.977
Diabetic retinopathy	15.8 (15)	n = 95	16.9 (11)	n = 65	16.0 (4)	n = 25	0.916
Diabetic nephropathy	26.0 (25)	n = 96	27.7 (18)	n = 65	12.0 (3)	n = 25	0.115
≥ one macrovascular complication, % (n)	16.7 (16)	n = 96	15.4 (10)	n = 65	24.0 (6)	n = 25	0.338
Ischaemic heart disease	10.4 (10)	n = 96	12.3 (8)	n = 65	8.0 (2)	n = 25	0.560
Peripheral vascular disease	5.2 (5)	n = 96	1.5 (1)	n = 65	16.0 (4)	n = 25	0.007*
Cerebrovascular accident	4.2 (4)	n = 96	1.5 (1)	n = 65	12.0 (3)	n = 25	0.031*
Body weight, kg	94.6 ± 20.7	n = 95	91.4 ± 20.3	n = 64	97.7 ± 19.7	n = 25	0.187
BMI, kg/m^2	33.6 ± 6.4	n = 94	32.6 ± 6.4	n = 64	35.0 ± 5.1	n = 25	0.064
Overweight/obese, % (n)	92.7 (89)	n = 94	90.6 (24)	n = 64	96.0 (58)	n = 25	0.397
History of hypertension, % (n)	71.9 (69)	n = 96	69.2 (19)	n = 65	76.0 (45)	n = 25	0.526
Systolic blood pressure, mmHg	133.0 ± 19.1	n = 90	131.7 ± 18.8	n = 63	139.4 ± 19.1	n = 23	0.101
Diastolic blood pressure, mmHg	78.2 ± 9.5	n = 88	78.8 ± 10.4	n = 62	77.1 ± 6.7	n = 22	0.386
History of dyslipidaemia, % (n)	80.2 (77)	n = 96	80.0 (52)	n = 65	80.0 (20)	n = 25	1.00
LSM, kPa	7.7 [5.7 - 11.7]	n = 96	6.8 [5.3 - 7.9]	n = 65	17.3 [13.2 - 24.2]	n = 25	<0.001*

Data expressed as mean ± SD, % (n) or median [IQR]. * p-value ≤ 0.05 using two-tailed t-test for continuous variables or chi-squared test for categorical variables. BMI, body mass index; LSM, liver stiffness measurement.

Table 2: Biochemical characteristics of participants in The DLC Audit[a].

	All Patients		LSM > 10.3 kPa		LSM ≥ 10.3 kPa		p-value
HbA1c, %	7.7 ± 1.4	n = 95	7.5 ± 1.3	n = 64	8.1 ± 1.4	n = 25	0.049*
Random glucose, mmol/L	9.2 ± 4.0	n = 93	9.0 ± 4.0	n = 64	9.3 ± 3.6	n = 23	0.745
Random insulin, pmol/L	188.3 ± 182.4	n = 52	168.5 ± 152.8	n = 41	307.0 ± 290.3	n = 8	0.226
Random c-peptide, pmol/L	1806.7 ± 1164.1	n = 89	1813.5 ± 1196.4	n = 61	1893.3 ± 1145.6	n = 23	0.780
C-peptide:glucose	212.0 ± 149.7	n = 88	219.0 ± 162.0	n = 61	202.3 ± 110.7	n = 22	0.499
ALP, U/L	88.3 ± 36.8	n = 96	82.4 ± 30.1	n = 65	99.7 ± 48.3	n = 25	0.105
GGT, U/L	122.2 ± 193.1	n = 96	93.0 ± 101.2	n = 65	207.6 ± 329.3	n = 25	0.099
ALT, U/L	48.1 ± 31.1	n = 96	43.9 ± 23.8	n = 65	55.1 ± 38.5	n = 25	0.184
AST, U/L	35.3 ± 15.7	n = 96	32.1 ± 11.8	n = 65	43.7 ± 21.5	n = 25	0.016*
Albumin, g/L	42.6 ± 5.7	n = 96	42.4 ± 6.3	n = 65	43.2 ± 4.5	n = 25	0.489
Platelet count, x 10^9/L	234.8 ± 65.9	n = 96	241.8 ± 67.8	n = 65	216.2 ± 64.6	n = 25	0.104
Ferritin, µg/L	186.1 ± 164.3	n = 94	170.4 ± 139.2	n = 64	200.2 ± 193.4	n = 24	0.494
Total cholesterol, mmol/L	4.1 ± 1.0	n = 95	4.2 ± 1.1	n = 64	3.8 ± 0.9	n = 25	0.102
Triglycerides, mmol/L	2.3 ± 1.2	n = 95	2.2 ± 1.1	n = 64	2.4 ± 1.2	n = 25	0.432
HDL-c, mmol/L	1.2 ± 0.5	n = 96	1.2 ± 0.3	n = 65	1.2 ± 0.5	n = 25	0.850
LDL-c, mmol/L	1.9 ± 0.8	n = 87	2.1 ± 0.8	n = 61	1.6 ± 0.6	n = 22	0.011*
Creatinine, µmol/L	73.8 ± 24.1	n = 96	72.4 ± 21.4	n = 65	73.0 ± 26.9	n = 25	0.926
UACr, mg/mmol Cr	8.4 ± 24.2	n = 87	7.4 ± 18.4	n = 61	3.2 ± 6.7	n = 20	0.140

Data expressed as mean ± SD. [a] non-fasting blood sample. * p-value ≤ 0.05 using two-tailed t-test. ALP, alkaline phosphatase; ALT, alanine aminotransferase; AST, aspartate aminotransferase; GGT, gamma-glutamyl transferase; HbA1c, haemoglobin A1c; HDL-c, high-density lipoprotein cholesterol; LDL-c, low-density lipoprotein cholesterol; LSM, liver stiffness measurement; UACr, urine albumin to creatinine ratio.

Table 3: Multivariate regression analysis.

LSM ≥ 10.3 kPa			**LSM continuous variable**		
Variable	**Beta**	**p-value**	**Variable**	**Beta**	**p-value**
Constant	-6.107	0.004	Constant	3.038	0.525
LDL-c	-1.874	0.004	BMI	0.350	0.002
BMI	0.141	0.011	Platelet count	-0.030	0.007
ALT	0.028	0.028	GGT	0.021	<0.001
ALP	0.026	0.008			
Summary:			**Summary:**		
$\chi^2 = 26.032$			F = 15.493		
$R^2 = 0.396$			$R^2 = 0.354$		
p-value < 0.005			p-value < 0.005		

ALP, alkaline phosphatase; ALT, alanine aminotransferase; BMI, body mass index; GGT, gamma-glutamyl transferase; LDL-c, low-density lipoprotein cholesterol; LSM, liver stiffness measurement.

Supplementary Data

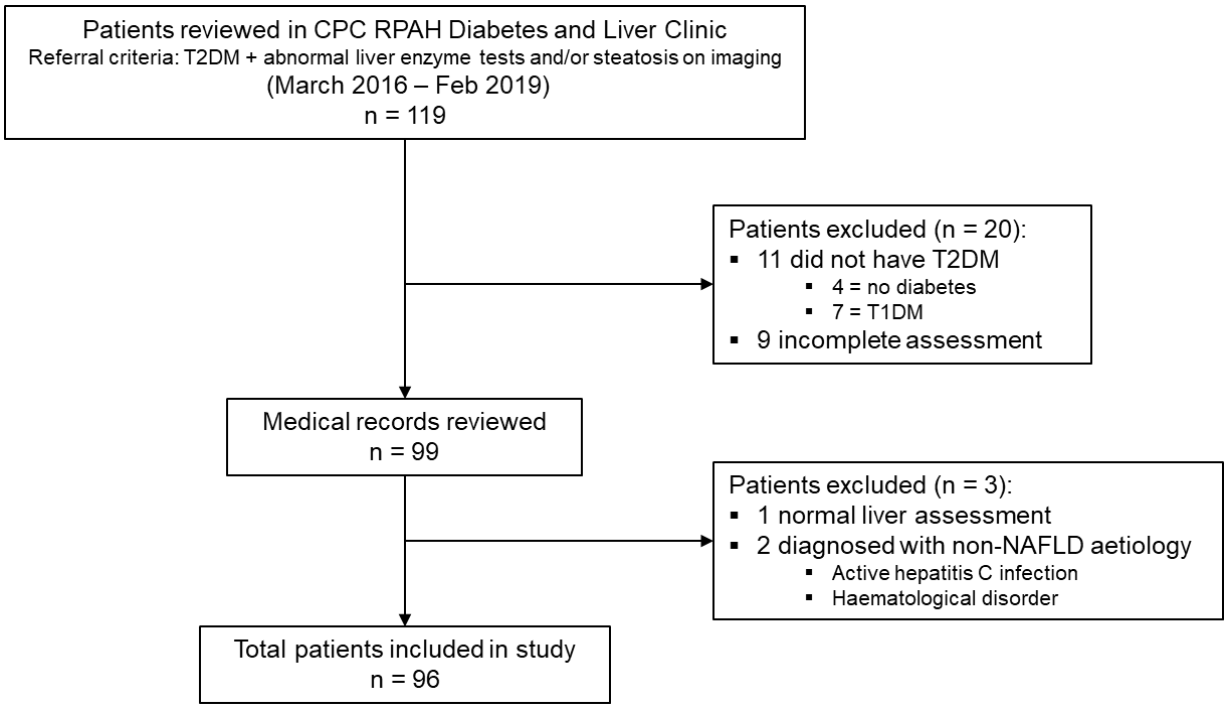

Supplementary Figure 1: Flow chart of patients included and excluded from the study. CPC RPAH, Charles Perkins Centre Royal Prince Alfred Hospital; NAFLD, non-alcoholic fatty liver disease; T1DM, type 1 diabetes mellitus; T2DM, type 2 diabetes mellitus.

Supplementary Table 1: Univariate correlations between LSM and clinical and biochemical variables.

	LSM ≥ 10.3 kPa		LSM continuous variable	
Variable	**Pearson r**	**p-value**	**Pearson r**	**p-value**
Age	0.173	0.102	0.174	0.101
Sex	-0.152	0.153	-0.111	0.296
Body weight	0.140	0.189	0.231	**0.029[a]**
BMI	0.179	**0.093***	0.270	**0.010***
NFS	0.173	0.105	0.228	**0.032[a]**
FIB-4	0.322	**0.002[a]**	0.427	**<0.001[a]**
Random glucose	0.034	0.757	0.030	0.784
HbA1c	0.220	**0.038***	0.246	**0.020***
C-peptide	0.030	0.784	-0.033	0.768
UACr	-0.110	0.327	-0.126	0.262
ALP	0.212	**0.044***	0.368	**<0.001***
GGT	0.260	**0.013***	0.456	**<0.001***
ALT	0.175	**0.099***	0.209	**0.048***
AST	0.329	**0.002***	0.369	**<0.001***
AST:ALT	0.062	0.564	0.038	0.720
Platelet count	-0.171	0.108	-0.206	**0.051***
Albumin	0.064	0.549	0.008	0.939
Ferritin	0.086	0.425	-0.055	0.611
Total cholesterol	-0.167	0.117	-0.051	0.637
Triglycerides	0.087	0.415	0.208	**0.050***
HDL-c	-0.024	0.826	-0.017	0.871
LDL-c	-0.237	**0.031***	-0.113	0.309
Dyslipidaemia	0.000	1.000	0.061	0.569
Systolic blood pressure	0.182	**0.094***	0.286	**0.008***
Diastolic blood pressure	-0.079	0.476	-0.007	0.951
Hypertension	0.067	0.531	0.119	0.263
Duration of diabetes	0.087	0.414	0.086	0.418
Insulin therapy	0.152	0.153	0.253	**0.016***
Any microvascular complication	-0.116	0.276	-0.053	0.618
Peripheral neuropathy	0.003	0.977	0.028	0.793
Diabetic retinopathy	-0.011	0.917	0.081	0.448
Diabetic nephropathy	-0.166	0.117	-0.137	0.198
Any macrovascular complication	0.101	0.344	0.062	0.559
Any diabetic complication	-0.094	0.377	-0.025	0.814
Smoker (current or previous)	-0.033	0.756	-0.006	0.958
Excessive alcohol intake	-0.117	0.275	-0.139	0.195

* p-value ≤ 0.1 for inclusion in multivariate regression analysis. [a] not included in multivariate regression analysis due to multicollinearity. ALP, alkaline phosphatase; ALT, alanine aminotransferase; AST, aspartate aminotransferase; AST:ALT, AST to ALT ratio; BMI, body mass index; FIB-4, fibrosis-4 index; GGT, gamma-glutamyl transferase; HbA1c, haemoglobin A1c; HDL-c, high-density lipoprotein cholesterol; LDL-c, low-density lipoprotein cholesterol; LSM, liver stiffness measurement; NFS, NAFLD fibrosis score; UACr, urine albumin to creatinine ratio.

Supplementary Table 2: Characteristics from historic cohort of patients with T2DM.

	All Patients	
Gender, % male (n)	62.6 (66)	n = 106
Age, years (range)	62.6 ± 9.6 (40 - 82)	n = 106
Duration of diabetes, years (range)	11.2 ± 8.5 (0 - 41)	n = 106
Insulin therapy, % (n)	35.8 (38)	n = 106
HbA1c, %	7.5 ± 1.2	n = 106
Body weight, kg	89.2 ± 22.1	n = 106
BMI, kg/m^2	31.2 ± 6.6	n = 106
LSM, kPa	5.8 [4.4 - 8.3]	n = 102

Data expressed as mean ± SD, % (n) or median [IQR]. BMI, body mass index; HbA1c, haemoglobin A1c; LSM, liver stiffness measurement; T2DM, type 2 diabetes mellitus.

Supplementary Table 3: Comparison of the NFS and FIB-4 using LSM cut-off of 8.5 kPa and 10.3 kPa.

	LSM ≥ 8.5 kPa (38%, 34/90)		**LSM ≥ 10.3 kPa (28%, 25/90)**	
	NFS	**FIB-4**	**NFS**	**FIB-4**
NPV	80% (12/15)	77% (41/53)	87% (13/15)	85% (45/53)
PPV	59% (13/22)	100% (1/1)	41% (9/22)	100% (1/1)
Sensitivity	38% (13/34)	3% (1/34)	36% (9/25)	4% (1/25)
Specificity	22% (12/55)	73% (41/56)	20% (13/64)	69% (45/65)

FIB-4, fibrosis-4 index; LSM, liver stiffness measurement; NFS, NAFLD fibrosis score; NPV, negative predictive value; PPV, positive predictive value.

3.3 Concluding remarks

The DLC audit has highlighted the high prevalence of NASH fibrosis in a cohort of individuals with T2DM, and that without this service, these individuals would remain undiagnosed and unable to access important medical care to monitor progression of disease and prevention and management of related complications. It has also explored variables that may potentially be used to predict advanced fibrosis in a T2DM population. Given the high prevalence and significant potential adverse outcomes, a better understanding of the pathogenesis of NASH fibrosis in the setting of T2DM is required. The upcoming two results chapters explore the role of two members of the CCN family that may be involved in the development of fibrosis in the liver, using a pre-clinical model of NASH fibrosis.

Chapter 4: Effects of hepatocyte-specific CCN2 gene deletion on the development of NASH fibrosis in a mouse model of high fat feeding and diabetes (The CCN2 Study)

4.1 Introduction

Cellular communication network factor 2 (CCN2) is a cysteine-rich matricellular protein involved in the regulation of cellular proliferation, differentiation, survival, adhesion, and ECM production[274]. It has been implicated in the pathogenesis of many fibrotic disease, including in the liver. Clinical and pre-clinical studies have shown increased CCN2 at the mRNA and protein levels in fibrotic livers[267-269,275]. Our laboratory has previously published two key articles in this area. The first reported on the up-regulation of CCN2 in a pre-clinical mouse model of NASH fibrosis induced by high fat feeding and diabetes[145]. The second used systemic administration of a neutralising antibody against CCN2 to demonstrate a protective effect against the development of NASH fibrosis using the same model[144]. Together, these data suggest that CCN2 may not only be a marker, but also a mediator, of progression of fibrosis in NASH.

CCN2 has normal biological functions in many cell types and tissues throughout the body. Systemic inhibition is likely to have a range of adverse effects, especially in normal wound healing. In fact, CCN2-null mice are perinatal lethal due to respiratory failure as a result of defects in ribcage ossification[362]. Embryos also exhibit lung hypoplasia[363] and reduced pancreatic β cell mass[364]. Thus, it is important to elicit the role of liver CCN2 in the development of liver fibrosis and establish whether specifically down-regulating liver CCN2 has a protective effect on the liver.

The study presented in this chapter uses a novel pre-clinical model, whereby the gene and environment interaction can be explored. The aim of this study was to examine whether homozygous gene deletion of hepatocyte-specific CCN2 leads to a less severe NASH fibrosis phenotype compared to control mice exposed to high fat feeding and diabetes.

4.2 Methods

The Methods are described in detail in *Section 2.3* and a summary is provided here. This study used hepatocyte-specific CCN2 gene knockout (CCN2-KO) mice, generated by Dr Xiaoyu Wang using the CreLoxP system, in the FaD model of NASH fibrosis developed previously by this laboratory. In brief, male control mice (AlbCre and $CCN2^{fl/fl}$) and CCN2-KO mice were fed a high fat diet (45% kcal) for 15 weeks

before the induction of diabetes with multiple low dose intraperitoneal injections of STZ (HFD+DM groups). Mice were then maintained for a further 10 weeks before termination. Additional mice from each of the three sub-strains were fed either standard chow (Chow groups) or high fat diet (HFD groups) for the duration of the study. Thus, there were nine groups in this study. Metabolic outcomes were measured, and routine plasma biochemistry analysed. The primary outcome was the development of NASH fibrosis, which was assessed histologically by PSR and H&E staining (see *Section 2.3.5*). The mRNA levels of fibrosis and inflammatory markers were measured using qPCR (see *Section 2.3.6*).

Unless otherwise specified, data is presented as mean ± SEM and analysed using a two-way ANOVA with Tukey's correction for multiple comparison. The statistical analyses presented in this chapter have focussed on the interactions between the three mouse sub-strains for the same "diet" (i.e., AlbCre HFD+DM vs $CCN2^{fl/fl}$ HFD+DM vs CCN2-KO HFD+DM). Interactions between the three "diets" have been tested within the two-way ANOVA (i.e., AlbCre Chow vs AlbCre HFD vs AlbCre HFD+DM), however the statistical results have not been routinely shown. This is because the FaD model has already been validated and published before[144,145], and replication of the model was not the primary focus of this current study. Note that * has been used to denote comparisons between the three mouse sub-strains for the same "diet," $^{\#}$ denotes comparisons between Chow vs HFD or HFD+DM for the same mouse sub-strain, and $^{\$}$ denotes comparisons between HFD vs HFD+DM for the same mouse sub-strain. AlbCre groups are depicted in light grey, $CCN2^{fl/fl}$ groups in dark grey and CCN2-KO groups in green.

4.3 Results

4.3.1 Reduction in whole liver tissue CCN2 in CCN2-KO mice

Successful deletion of the hepatocyte CCN2 gene was confirmed by measuring the mRNA level of CCN2 from whole liver tissue. In the basal state, CCN2-KO mice fed a chow diet had 25% and 43% reduction in CCN2 mRNA level compared to AlbCre and CCN2$^{fl/fl}$ Chow mice, respectively, although this was not statistically significant on a two-way ANOVA (*Figure 4.1*). As expected, CCN2 mRNA level was induced in HFD and HFD+DM groups in the control sub-strains, AlbCre and CCN2$^{fl/fl}$, but to a significantly lesser degree in the CCN2-KO HFD+DM group. There was a 56% reduction in CCN2 mRNA level in the CCN2-KO HFD+DM mice compared with the AlbCre HFD+DM mice (1.87 ± 0.24 vs 4.29 ± 1.48, p = 0.023) and a 65% reduction when compared with the CCN2$^{fl/fl}$ HFD+DM mice (1.87 ± 0.24 vs 5.30 ± 0.98, p = 0.004). The protein levels of CCN2 were numerically reduced in the Chow and HFD+DM groups compared with the control sub-strains of mice (*Figure 4.2*). The persistent, albeit lesser expression of CCN2 in the CCN2-KO mice is hypothesised to be derived from non-hepatocyte liver cells.

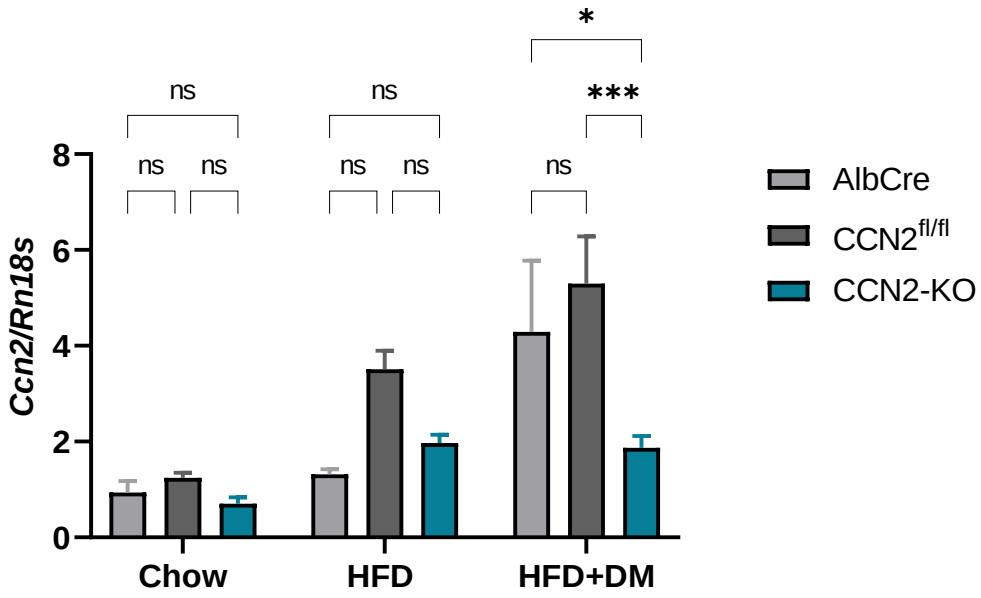

*Figure 4.1: Ccn2 mRNA levels in whole liver tissue measured by qPCR. Data shown as mean ± SEM as relative fold change of AlbCre Chow and CCN2$^{fl/fl}$ Chow groups; n = 8 - 13. * p-value ≤ 0.05 or *** p-value ≤ 0.001 for comparison of mouse sub-strains within the same "diet" subgroup using two-way ANOVA with Tukey's correction for multiple comparisons. ns, not significant.*

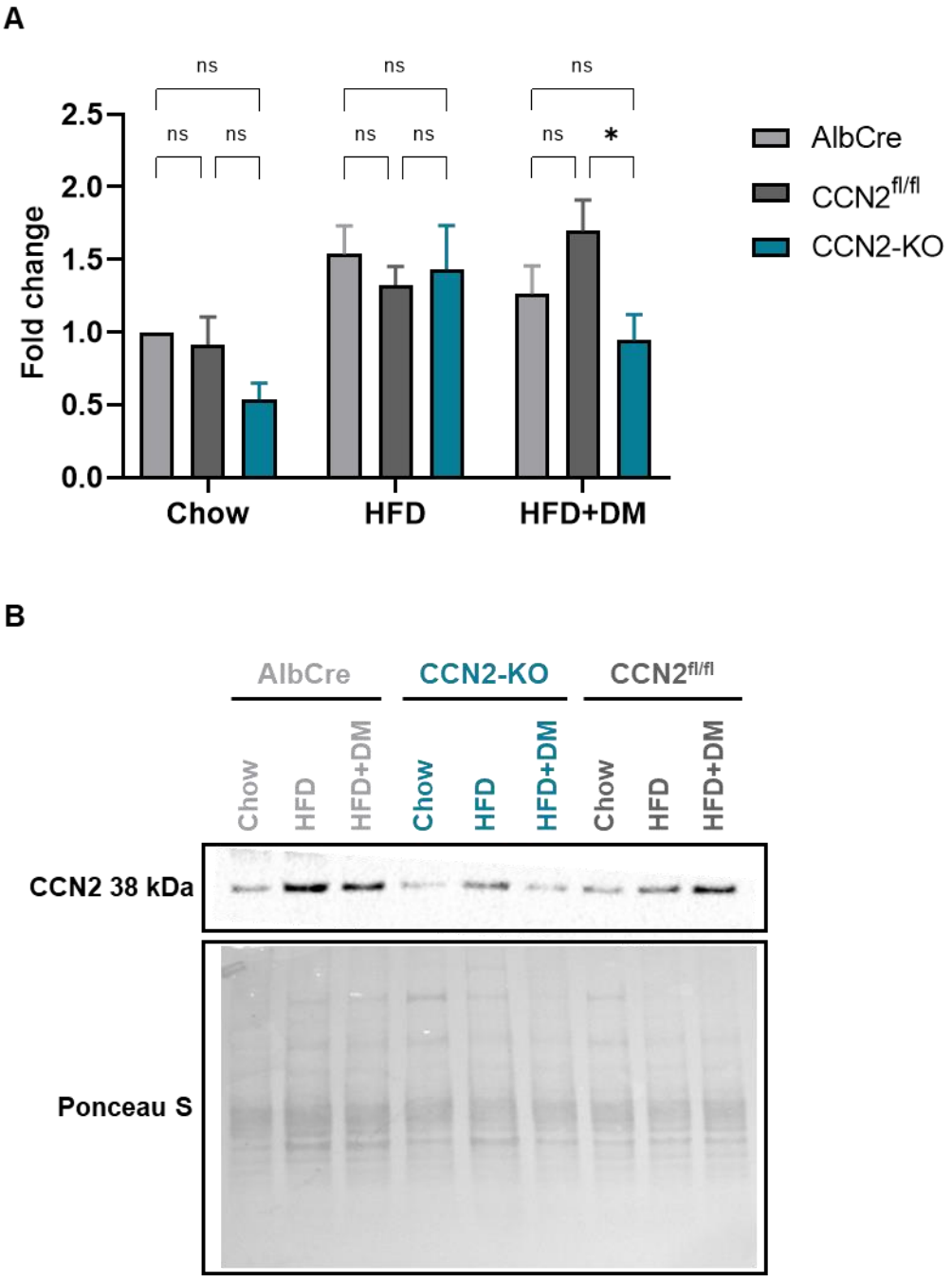

*Figure 4.2: CCN2 protein level in whole liver tissue measured by Western immunoblot (A) with representative image (B). Note that the sample order in (A) and (B) are different. Data shown as mean ± SEM as relative fold change of AlbCre Chow group; n = 4. * p-value ≤ 0.05 for comparison of mouse sub-strains within the same "diet" subgroup using two-way ANOVA with Tukey's correction for multiple comparisons. ns, not significant. Courtesy of Dr Xiaoyu Wang.*

4.3.2 Metabolic outcomes

4.3.2.1 Body weight

Mice were weighed weekly for the duration of the study (*Figure 4.3*). Chow fed mice (triangles) gradually gained weight consistent with normal growth and development. HFD and HFD+DM mice quickly gained excess weight with high fat feeding. At week 16, diabetes was induced in the HFD+DM mice (circles) with 2 - 3 injections of low dose STZ. These mice had an expected and brief reduction in body weight for approximately two weeks before body weight plateaued. HFD mice (squares) continued to gain weight throughout the study.

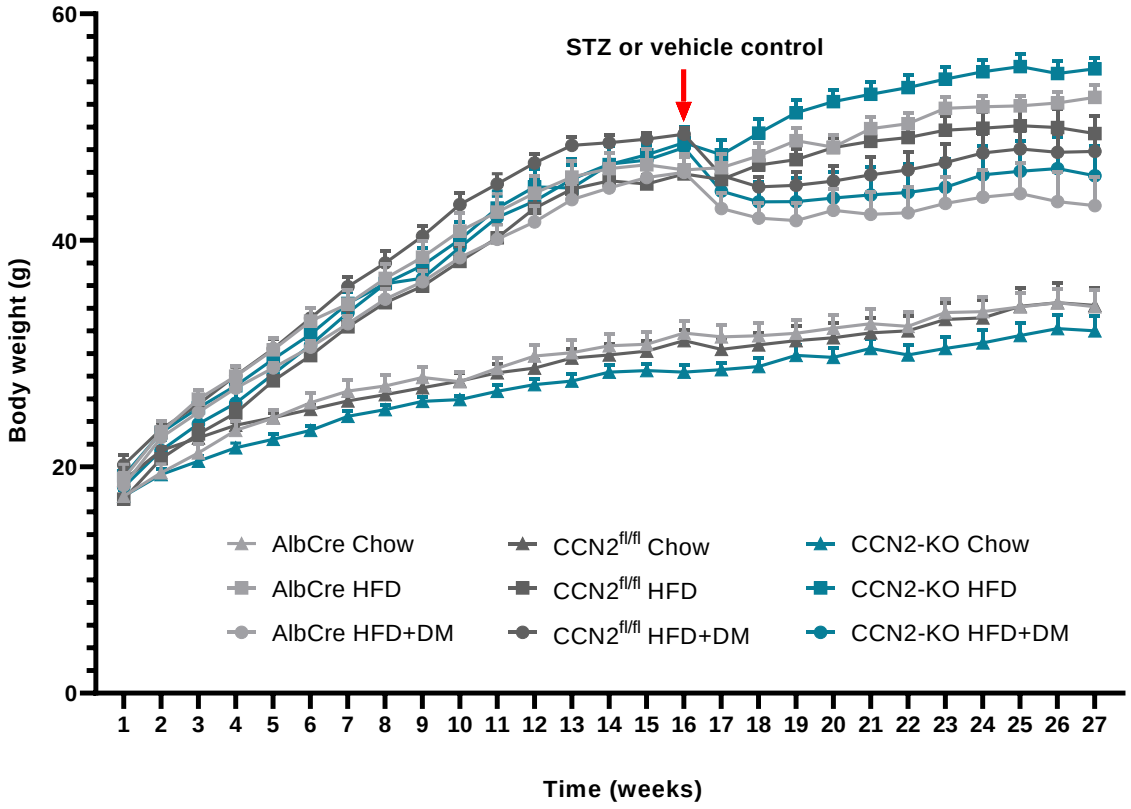

Figure 4.3: Weekly body weight per mouse group. Data shown as mean ± SEM; n = 8 - 13. STZ, streptozotocin.

At the end of the study, total weight gain was similar for each mouse sub-strain within the same "diet" subgroup, with no difference observed in the CCN2-KO mice compared with the AlbCre or $CCN2^{fl/fl}$ mice (*Figure 4.4*). HFD mice gained the most weight (31 - 36 g), followed by HFD+DM mice (24 - 28 g), with Chow mice gaining the least weight (15 - 16 g).

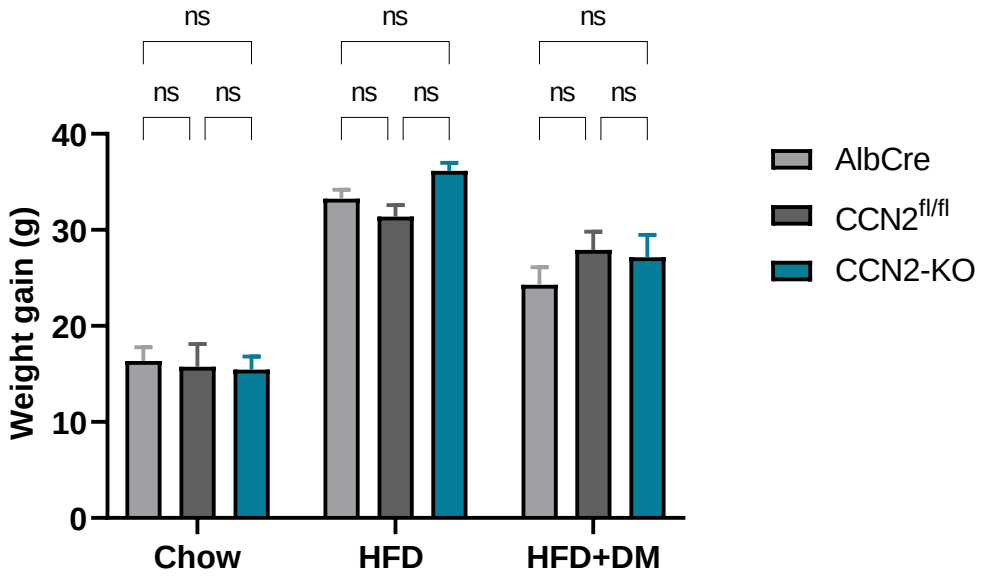

Figure 4.4: Total body weight gain. Data shown as mean ± SEM; n = 8 - 13. ns (not significant), p-value > 0.05 for comparison of mouse sub-strains within the same "diet" subgroup using two-way ANOVA with Tukey's correction for multiple comparisons.

The mean body weights of the mice at termination are shown in *Table 4.1*. All HFD and HFD+DM mice were significantly heavier than Chow mice in the same mouse sub-strain (statistics comparing different "diet" groups not shown). The HFD+DM mice were statistically less heavy than the HFD mice by ~10g, except in the $CCN2^{fl/fl}$ mice, where the mean termination body weights were similar.

Table 4.1: Body weight (grams) at termination.

	Chow	HFD	HFD+DM
AlbCre	33.76 ± 1.48	52.20 ± 1.14	42.61 ± 2.68
$CCN2^{fl/fl}$	34.54 ± 1.75	48.51 ± 1.57	48.06 ± 1.54
CCN2-KO	32.85 ± 1.29	55.33 ± 1.06	45.35 ± 2.83

Data shown as mean ± SEM; n = 8 - 13.

4.3.2.2 Blood glucose levels

BGLs were measured weekly from week 16 to the end of the study. After induction of diabetes with STZ, mice in the HFD+DM groups (circles) developed hyperglycaemia with BGLs ranging between 15 - 25 mmol/L throughout the remainder of the study (*Figure 4.5*). The Chow and HFD mice remained normoglycaemic.

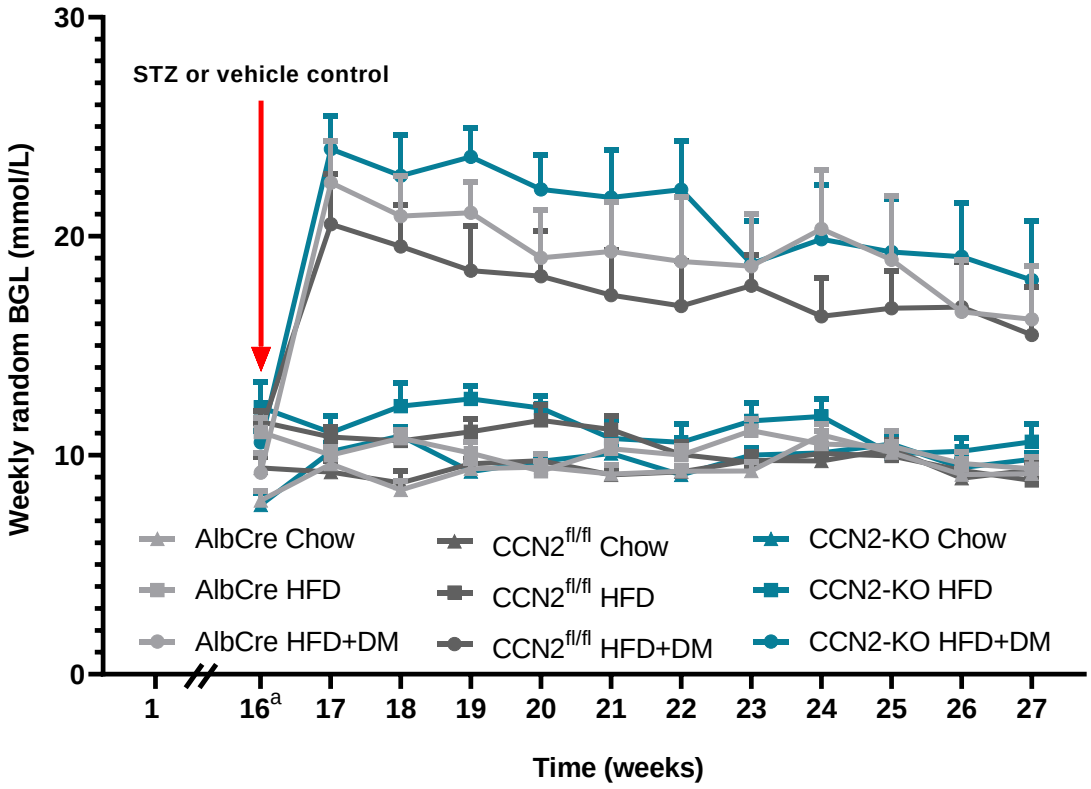

Figure 4.5: Weekly random blood glucose levels. Data shown as mean ± SEM; n = 8 - 13. [a] fasting BGL. BGL, blood glucose level; STZ, streptozotocin.

The mean of the weekly BGLs from week 17 to 27 are shown in *Table 4.2*. The HFD+DM mice had significantly higher mean BGL compared with the respective Chow and HFD mice of the same mouse sub-strain. Mean BGLs in the HFD+DM mice were 17 - 21 mmol/L, representing a moderate degree of hyperglycaemia without induction of severe catabolism. There was no difference in mean BGLs between the Chow mice and the HFD mice which were maintained from 9 - 11 mmol/L. Glucose levels in the CCN2-KO mice were not different to the AlbCre and $CCN2^{fl/fl}$ mice.

Table 4.2: Mean random BGL (mmol/L) from week 17 to 27.

	Chow	HFD	HFD+DM
AlbCre	9.45 ± 0.19	10.14 ± 0.30	19.27 ± 2.07$^{\#\#\#\#\#, \$\$\$\$}$
$CCN2^{fl/fl}$	9.44 ± 0.22	10.30 ± 0.39	17.63 ± 1.85$^{\#\#\#\#, \$\$\$}$
CCN2-KO	9.91 ± 0.12	11.23 ± 0.62	21.03 ± 1.93$^{\#\#\#\#, \$\$\$\$}$

Data shown as mean ± SEM; n = 8 - 13. $^{\#\#\#\#}$ p-value ≤ 0.0001 for Chow vs HFD+DM of the same mouse sub-strain, or $^{\$\$\$}$ p-value ≤ 0.001 or $^{\$\$\$\$}$ p-value ≤ 0.0001 for HFD vs HFD+DM of the same mouse sub-strain, using two-way ANOVA with Tukey's correction for multiple comparisons. BGL, blood glucose level.

4.3.2.3 Evaluation of insulin resistance

4.3.2.3.1 Fasting whole blood insulin level at week 16.

The fasting whole blood insulin level was measured using a commercial ELISA kit at week 16 of the study. This timepoint was prior to induction of diabetes in the HFD+DM mice and therefore *Figure 4.6* only shows chow fed mice (Chow groups) or high fat fed mice (combination of mice allocated to the HFD or HFD+DM groups). Mice that were high fat fed for 15 weeks had already developed marked hyperinsulinaemia compared to standard chow fed mice but did not develop significant hyperglycaemia. There was no effect of the CCN2-KO in these parameters compared with the AlbCre or CCN2$^{fl/fl}$ mice.

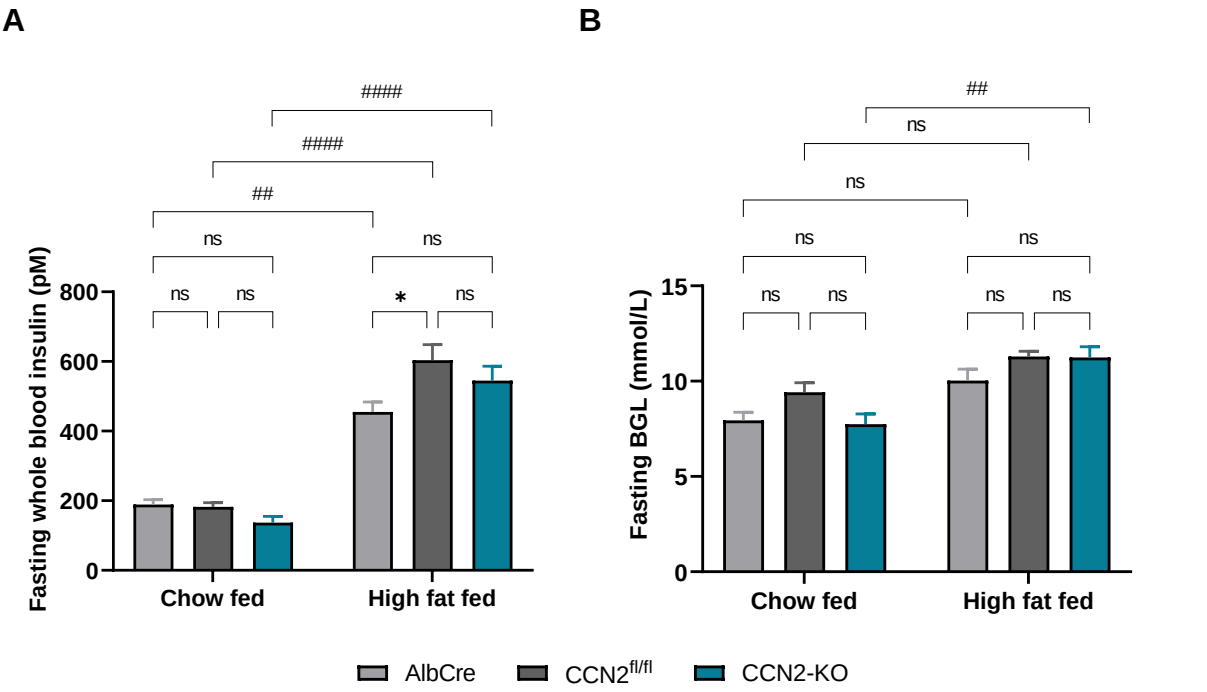

*Figure 4.6: Fasting whole blood insulin levels (A) and BGL (B) obtained at week 16 in mice fed either a chow or high fat diet. Data shown as mean ± SEM; n = 8 - 22. * p-value ≤ 0.05 for comparison of mouse sub-strains within the same "diet" subgroup, or # p-value ≤ 0.05, ## p-value ≤ 0.01, ### p-value ≤ 0.001 or #### p-value ≤ 0.0001 for chow fed vs high fat fed within the same mouse sub-strain, using two-way ANOVA with Tukey's correction for multiple comparisons. BGL, blood glucose level; ns, not significant.*

4.3.2.3.2 Fasting plasma insulin and c-peptide levels at termination

Using commercial ELISA kits, insulin and c-peptide levels were measured from plasma obtained in the fasting state at termination (*Figure 4.7*). As expected, mice from HFD groups exhibited markedly hyperinsulinaemia across all three mouse strains. Mice from the HFD+DM groups had insulin levels that were similar to the Chow groups, and in the context of hyperglycaemia, was indicative of relative insulin deficiency (model of T2DM) rather than absolute insulin deficiency (model of T1DM). A similar pattern was observed in c-peptide levels.

The AlbCre HFD mice had significantly higher insulin and c-peptide levels compared with $CCN2^{fl/fl}$ HFD mice, and higher c-peptide level compared with CCN2-KO HFD mice. However, there was no difference in the concentration of the matched fasting capillary BGL amongst the different sub-strains (*Figure 4.7C*). Differences in the assessment of insulin may be due to the different genetic background of the sub-strains and a variable response to metabolic stress, which was most evident between the two control sub-strains. Importantly, the two control sub-strains generally had similar outcomes in the multiple measures of insulin resistance that were undertaken (*Section 4.3.2.3.3* and *4.3.2.3.4*). Otherwise, there was no effect of the CCN2-KO in insulin or c-peptide levels compared with the AlbCre or $CCN2^{fl/fl}$ mice across the Chow and HFD+DM subgroups.

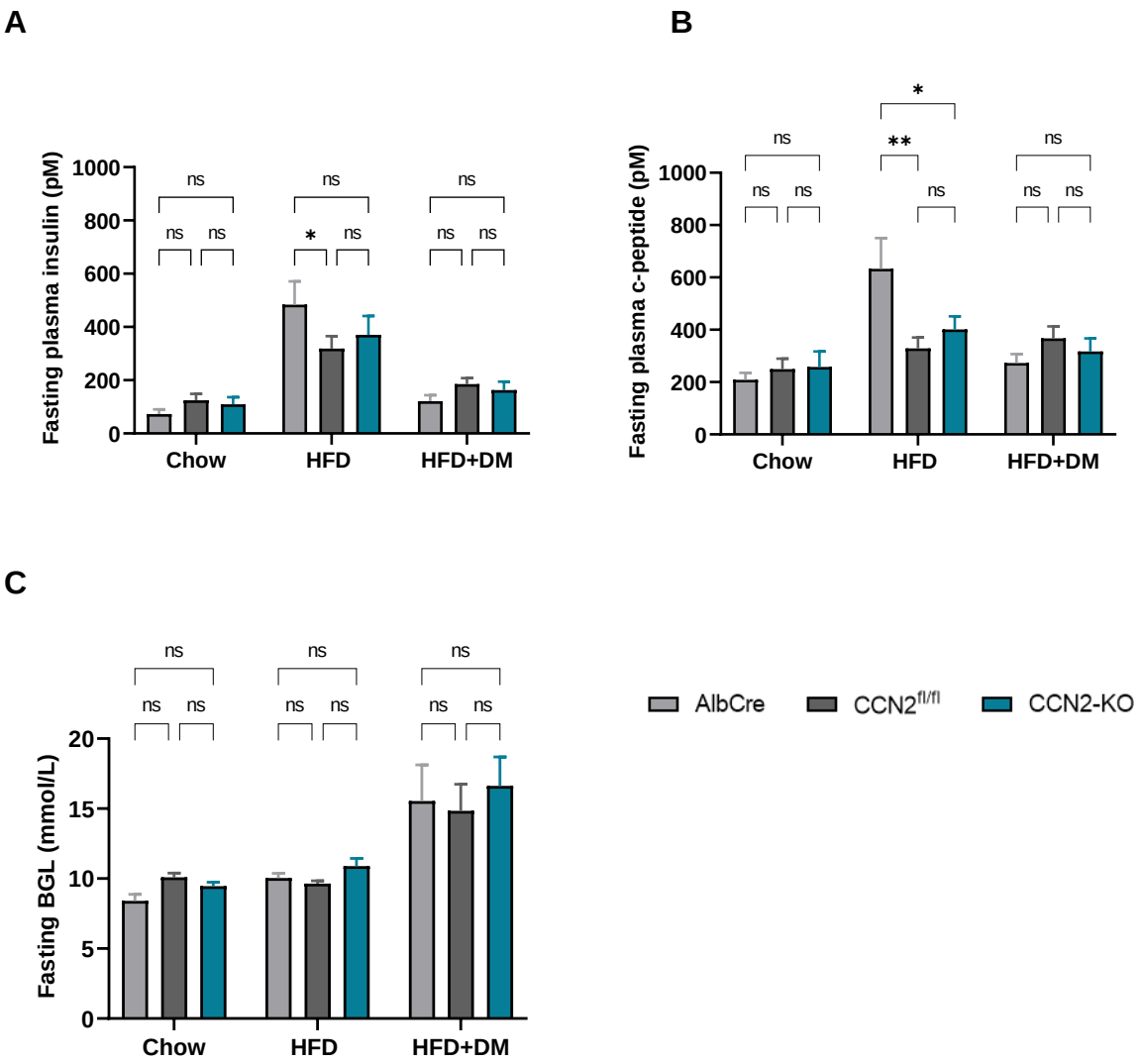

*Figure 4.7: Fasting plasma insulin (A) and c-peptide (B) levels, with matched fasting capillary BGL (C). Data shown as mean ± SEM; n = 8 - 13. * p-value ≤ 0.05 or ** p-value ≤ 0.01 for comparison of mouse sub-strains within the same "diet" subgroup using two-way ANOVA with Tukey's correction for multiple comparisons. BGL, blood glucose level; ns, not significant.*

4.3.2.3.3 Insulin tolerance test

An ITT was performed prior to termination as a measure of whole-body insulin sensitivity, but some caution should be made in interpreting the results due to the wide differences in glucose concentrations between groups. At baseline, the AlbCre Chow group showed statistically significant lower normalised area AUC compared to the $CCN2^{fl/fl}$ Chow and CCN2-KO Chow groups (AlbCre: 4055 ± 1181, $CCN2^{fl/fl}$: 6625 ± 232, and CCN2-KO: 6286 ± 197; *Figure 4.8*). There was no difference in the normalised AUC amongst mouse sub-strains in the HFD or HFD+DM groups. All HFD groups had statistically higher normalised AUC compared with the Chow and HFD+DM groups of the same mouse sub-strain (statistics comparing different "diet" groups not shown), confirming the greatest degree of insulin resistance in these HFD mice. There was no difference in insulin sensitivity between the Chow and HFD+DM groups. The non-normalised data depicting the shape of each curve is also shown in *Figure 4.8*.

Of note, three mice from the AlbCre Chow group and four mice from the CCN2-KO HFD group received a lower dose of insulin (0.65 units/kg) to reduce the risk of hypoglycaemia during the initial attempt at this procedure. Once this was excluded as a major concern, all other mice received the full insulin dose (0.75 units/kg). Five mice from the AlbCre Chow group (full insulin dose) developed hypoglycaemia and received intraperitoneal injections of 20% glucose to normalise their BGLs. For the purpose of data analysis, the last BGL taken before glucose was given was carried forward to all later timepoints. Ultimately, there was no effect of the hepatocyte-specific CCN2-KO on the ITT results, although the data suggests that the AlbCre mice were more insulin sensitive at baseline compared with the other mouse sub-strains.

A

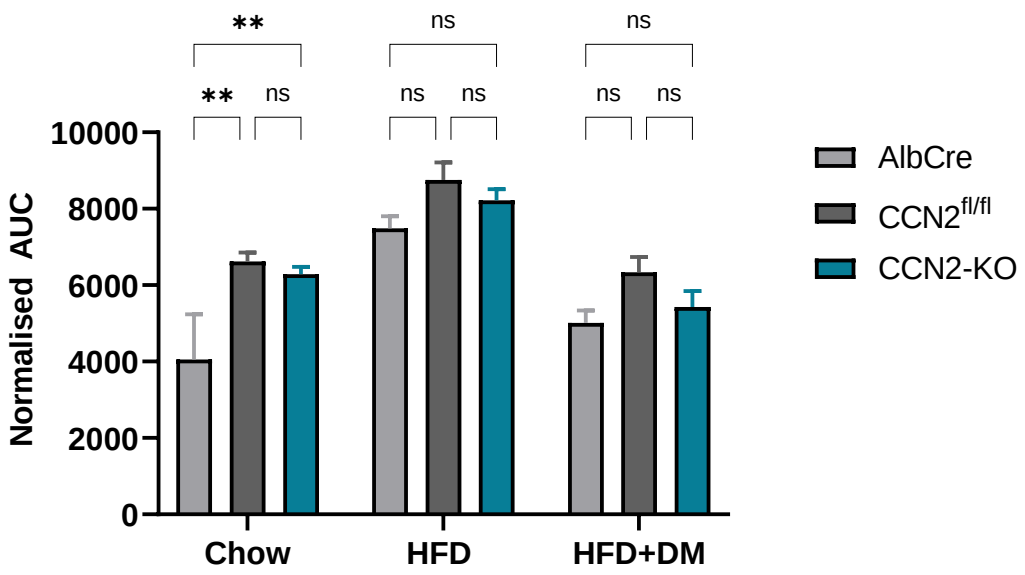

B

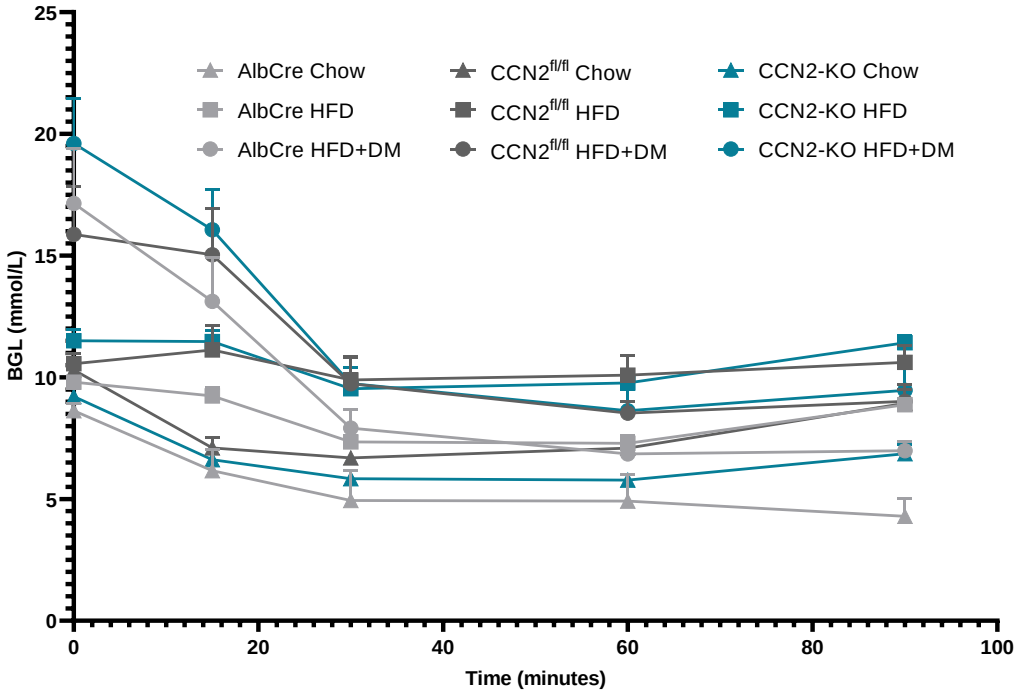

*Figure 4.8: Insulin tolerance test with normalised incremental AUC (A) and non-normalised time course data (B). Data shown as mean ± SEM; n = 8 - 13. ** p-value ≤ 0.01 for comparison of mouse sub-strains within the same "diet" subgroup using two-way ANOVA with Tukey's correction for multiple comparisons. AUC, area under the curve; BGL, blood glucose level; ns, not significant.*

4.3.2.3.4 Calculated measures of insulin resistance

In addition to the ITT, other calculated measures of insulin resistance were performed using the results of the fasting capillary BGL at termination, fasting plasma insulin level and/or fasting plasma c-peptide level (*Figure 4.9*). The trends within each of these measures were similar: highest level of insulin resistance in the HFD groups, and similar levels of insulin resistance amongst Chow and HFD+DM groups. There was no effect of the CCN2-KO on these surrogate markers of insulin resistance.

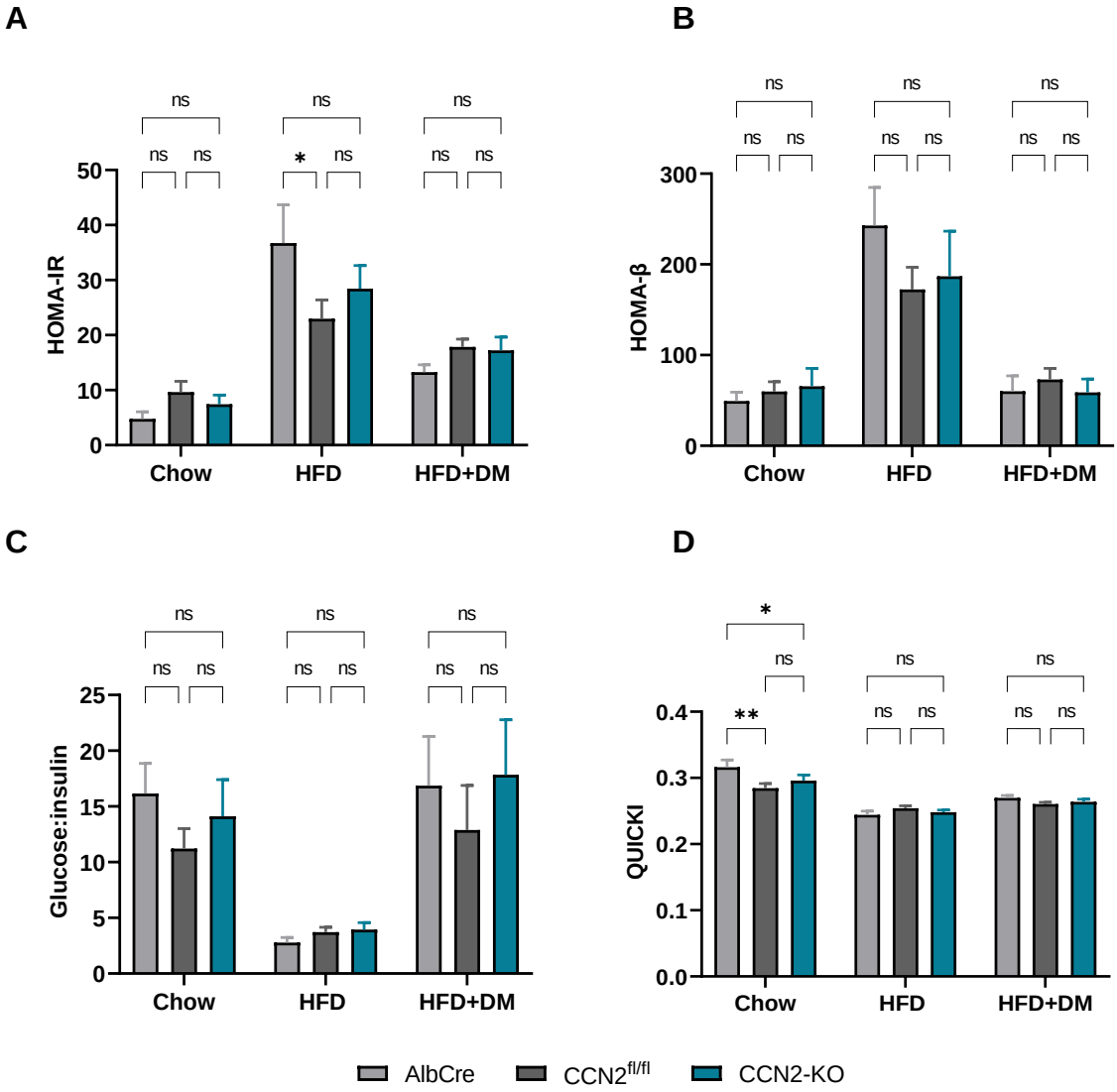

*Figure 4.9: Calculated measures of insulin resistance: HOMA-IR (A), HOMA-β (B), glucose to insulin ratio (C), and QUICKI (D). Data shown as mean ± SEM; n = 8 - 13. * p-value ≤ 0.05, ** p-value ≤ 0.01 or *** p-value ≤ 0.001 for comparison of mouse sub-strains within the same "diet" subgroup using two-way ANOVA with Tukey's correction for multiple comparisons. HOMA-IR, homeostatic model assessment for insulin resistance; HOMA-β, homeostatic model assessment for β-cell function; QUICKI, quantitative insulin check index of insulin sensitivity; ns, not significant.*

4.3.2.4 Assessment of body composition

4.3.2.4.1 EchoMRI™

Fat mass and lean mass of the mice were measured using EchoMRI™. Results expressed as a percentage of total body weight are shown in *Figure 4.10* and absolute mass data is shown in *Table 4.3*. At both week 15 and week 25, HFD and HFD+DM mice had significantly higher fat mass percentage and lower lean mass percentage compared with the Chow group of the same mouse sub-strain (statistics comparing different "diet" groups not shown). There was no significant difference between mouse sub-strains, except in the AlbCre HFD+DM group, which had slightly lower fat mass percentage and higher lean mass percentage than both the $CCN2^{fl/fl}$ HFD+DM and CCN2-KO HFD+DM groups at both timepoints. The CCN2-KO did not affect body composition as measured by EchoMRI™.

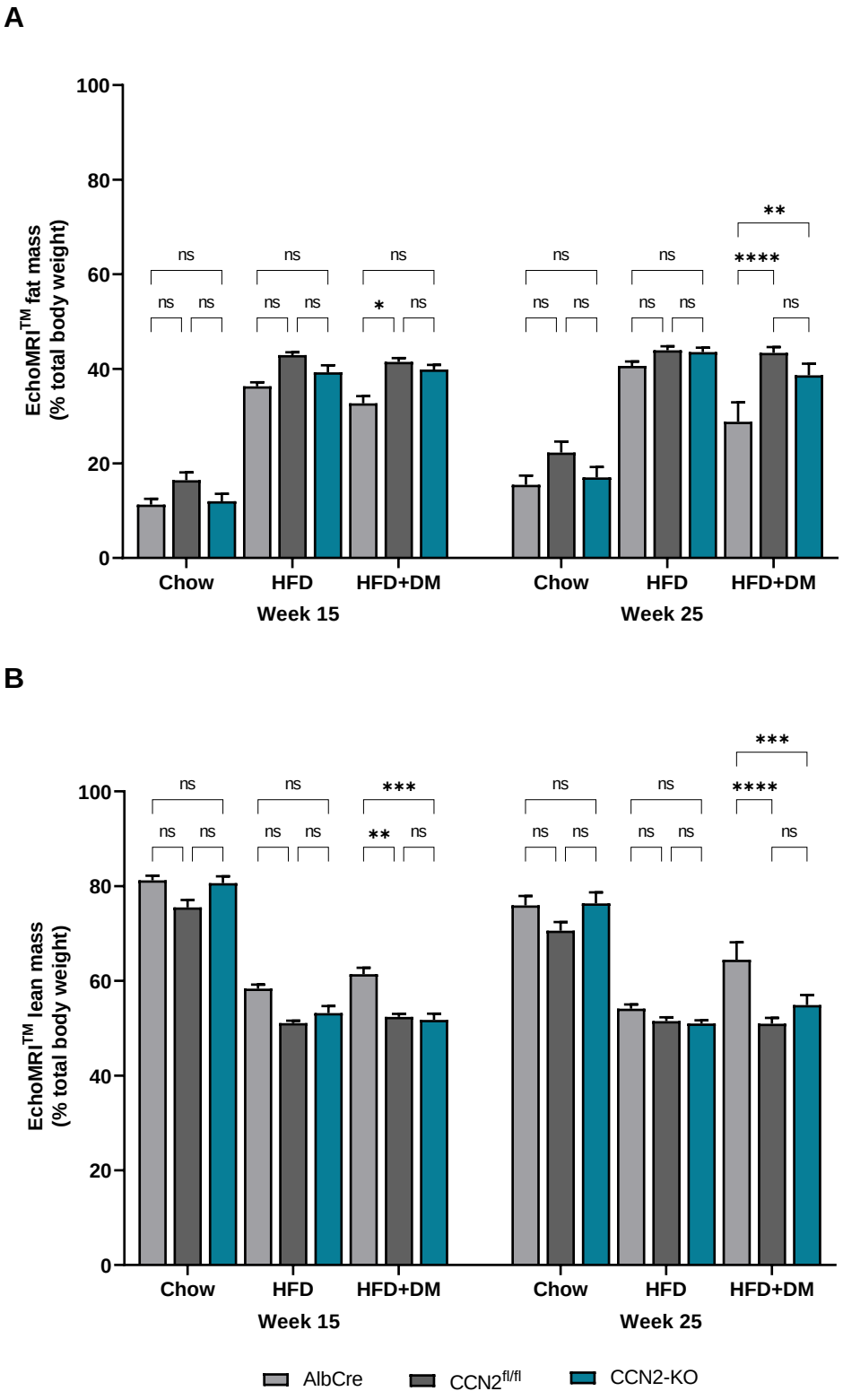

*Figure 4.10: Body composition by EchoMRI™: fat mass expressed as percentage of total body weight (A) and lean mass expressed as percentage of total body weight (B) at week 15 and week 25. Note that at week 15, HFD+DM groups were not yet diabetic. Data shown as mean ± SEM; n = 8 - 13. * p-value ≤ 0.05, ** p-value ≤ 0.01, *** p-value ≤ 0.001 or **** p-value ≤ 0.0001 for comparison of mouse sub-strains within the same "diet" subgroup using mixed-effects analysis with Šidák's correction for multiple comparisons. ns, not significant.*

Table 4.3: Body composition by EchoMRI™ and DXA: absolute fat mass, lean mass, and total body weight at week 15 and week 25.

EchoMRI™	**Chow**			**HFD**			**HFD+DM**		
Week 15	**AlbCre**	**CCN2$^{fl/fl}$**	**CCN2-KO**	**AlbCre**	**CCN2$^{fl/fl}$**	**CCN2-KO**	**AlbCre**	**CCN2$^{fl/fl}$**	**CCN2-KO**
Fat mass (g)	3.56 ± 0.42	5.22 ± 0.70	3.46 ± 0.52	16.69 ± 0.85	19.84 ± 0.55	18.87 ± 1.23	14.89 ± 1.01	20.54 ± 0.53	19.14 ± 0.86
Lean mass (g)	25.45 ± 0.63	23.15 ± 0.45	22.78 ± 0.30	26.66 ± 0.65	23.56 ± 0.30	25.21 ± 0.44	27.58 ± 0.33	25.92 ± 0.37	24.58 ± 0.59
Total body weight (g)	31.39 ± 0.95	30.85 ± 1.09	28.33 ± 0.69	45.80 ± 1.49	46.17 ± 0.78	47.68 ± 1.51	45.12 ± 1.14	49.51 ± 0.59	47.83 ± 1.52
Week 25	**AlbCre**	**CCN2$^{fl/fl}$**	**CCN2-KO**	**AlbCre**	**CCN2$^{fl/fl}$**	**CCN2-KO**	**AlbCre**	**CCN2$^{fl/fl}$**	**CCN2-KO**
Fat mass (g)	5.41 ± 0.80	7.88 ± 1.15	5.45 ± 0.83	21.06 ± 0.74	21.93 ± 1.07	24.01 ± 0.92	13.63 ± 2.49	20.89 ± 1.15	18.68 ± 2.01
Lean mass (g)	25.96 ± 0.81	23.72 ± 0.51	23.51 ± 0.27	28.02 ± 0.52	25.51 ± 0.64	27.99 ± 0.38	27.64 ± 0.37	24.14 ± 0.54	24.85 ± 0.69
Total body weight (g)	34.31 ± 1.26	33.95 ± 1.52	31.01 ± 1.11	51.81 ± 0.98	49.69 ± 1.69	54.99 ± 1.05	44.16 ± 2.53	47.70 ± 1.62	46.44 ± 2.72
DXA	**Chow**			**HFD**			**HFD+DM**		
Week 15	**AlbCre**	**CCN2$^{fl/fl}$**	**CCN2-KO**	**AlbCre**	**CCN2$^{fl/fl}$**	**CCN2-KO**	**AlbCre**	**CCN2$^{fl/fl}$**	**CCN2-KO**
Fat mass (g)	5.94 ± 0.91	9.04 ± 0.91	7.64 ± 0.57	19.62 ± 0.98	20.16 ± 0.89	20.05 ± 0.64	17.90 ± 0.76	20.56 ± 0.56	20.75 ± 0.83
Lean mass (g)	20.33 ± 0.99	17.07 ± 0.37	16.37 ± 0.26	20.73 ± 0.80	20.15 ± 0.95	21.56 ± 0.96	21.68 ± 1.05	22.08 ± 0.56	21.13 ± 1.05
Total body weight (g)	26.27 ± 0.80	26.17 ± 0.99	24.01 ± 0.68	40.35 ± 1.33	40.30 ± 0.67	41.61 ± 1.21	39.58 ± 0.81	42.64 ± 0.47	41.89 ± 1.26
Week 25	**AlbCre**	**CCN2$^{fl/fl}$**	**CCN2-KO**	**AlbCre**	**CCN2$^{fl/fl}$**	**CCN2-KO**	**AlbCre**	**CCN2$^{fl/fl}$**	**CCN2-KO**
Fat mass (g)	10.30 ± 0.84	12.39 ± 1.04	10.81 ± 0.77	24.01 ± 0.61	25.32 ± 1.59	26.38 ± 0.60	17.71 ± 2.11	24.53 ± 1.16	22.07 ± 1.84
Lean mass (g)	19.74 ± 0.69	17.35 ± 0.46	16.41 ± 0.49	22.41 ± 0.43	19.46 ± 0.85	23.16 ± 0.54	21.45 ± 0.43	18.73 ± 0.52	19.13 ± 0.75
Total body weight (g)	30.04 ± 1.16	29.73 ± 1.40	27.21 ± 1.13	46.42 ± 0.94	44.78 ± 1.61	49.54 ± 0.75	39.16 ± 2.36	39.68 ± 3.55	41.21 ± 2.45

Data shown as mean ± SEM; n = 8 - 13. Please note that as per the Methods, relevant p-values have been identified in the relevant Figures, not in the Table.

4.3.2.4.2 Dual X-ray Absorptiometry

Body composition and BMD were measured using DXA. Representative images of a normal weight, chow fed mouse and an obese, high fat fed mouse are shown in *Figure 4.11*. The pattern of results of fat mass and lean mass percentage were similar to those found in body composition analysis using EchoMRI™, although DXA relatively over-estimated the fat mass by approximately 10% (*Figure 4.12* and *Table 4.3*). The systematic discrepancy is likely because DXA performs a 2-dimensional analysis, whereas EchoMRI™ performs a 3-dimensional analysis and is therefore more accurate.

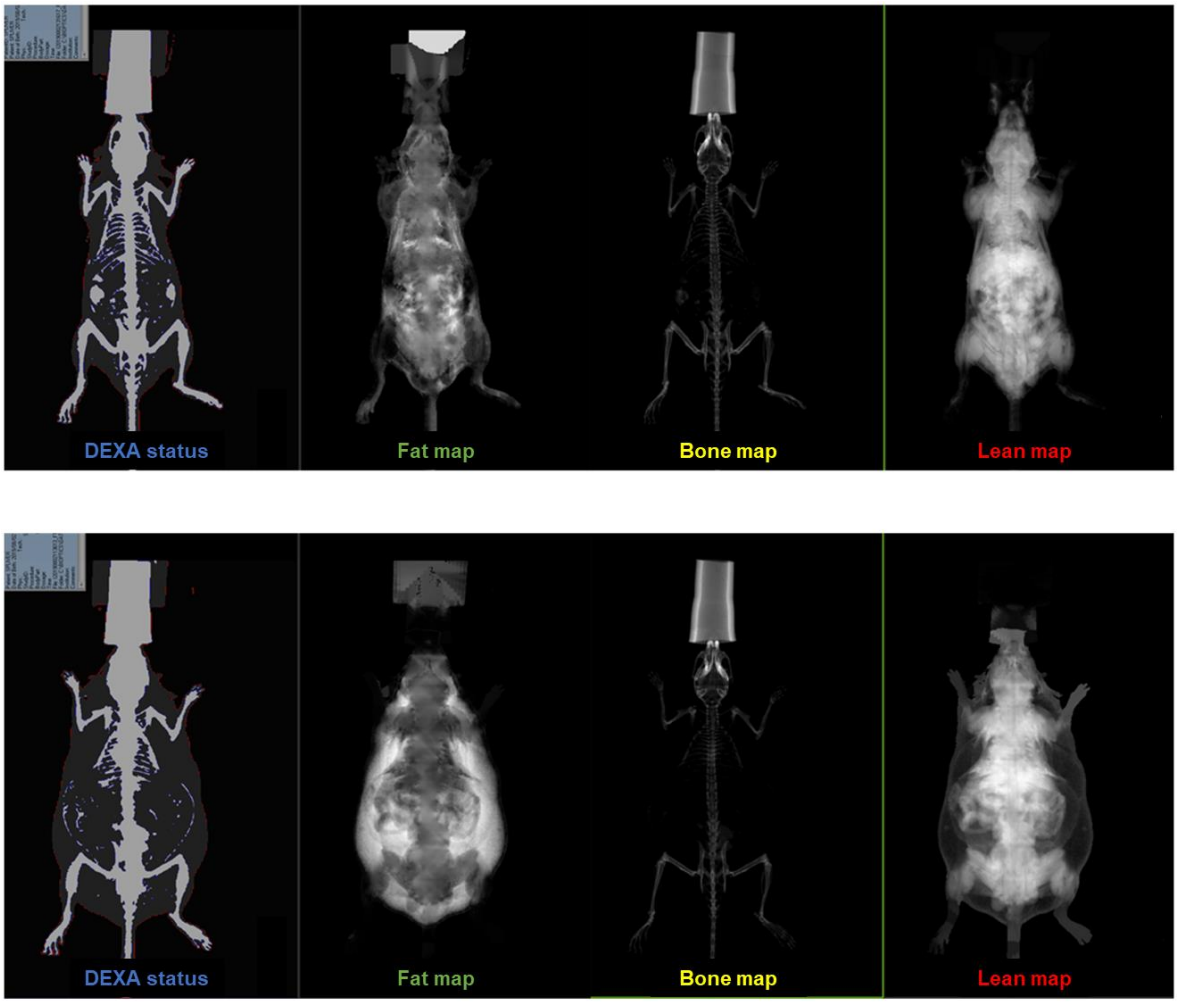

Figure 4.11: Representative images of a normal weight, chow fed mouse (top row) and obese, high fat fed mouse (bottom row) undergoing DXA scan. From left to right: DXA status (green); fat map (blue); bone map (yellow); lean map (red).

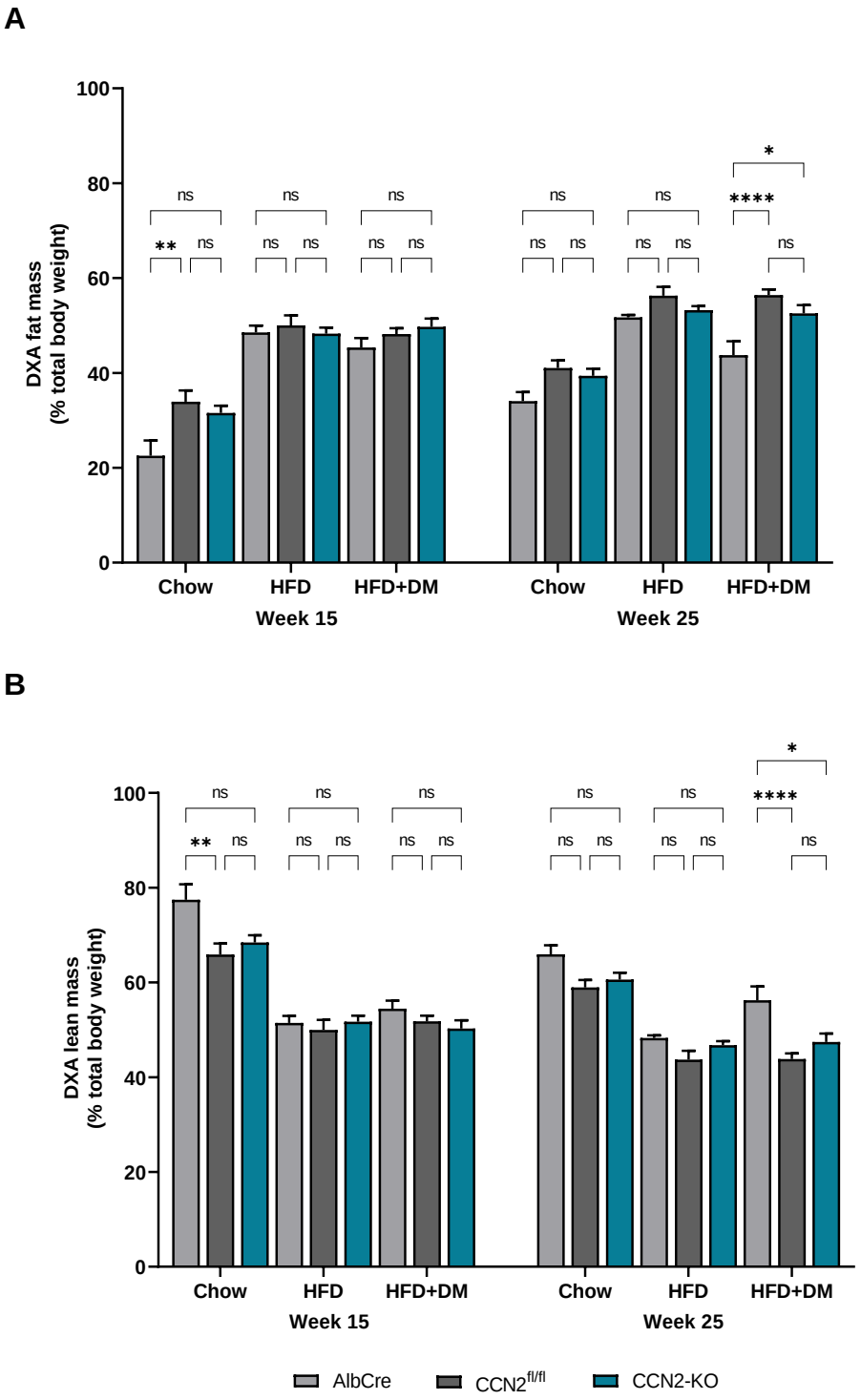

*Figure 4.12: Body composition by DXA: fat mass expressed as percentage of total body weight (A) and lean mass expressed as percentage of total body weight (B) at week 15 and week 25. Note that at week 15, HFD+DM groups were not yet diabetic. Data shown as mean ± SEM; n = 8 - 13. * p-value ≤ 0.05, ** p-value ≤ 0.01 or **** p-value ≤ 0.0001 for comparison of mouse sub-strains within the same "diet" subgroup using mixed-effects analysis with Šidák's correction for multiple comparisons. DXA, dual x-ray absorptiometry; ns, not significant.*

BMD was measured using DXA and the results are shown in *Figure 4.13*. Reductions in BMD occurred as early as 15 weeks in the CCN2$^{fl/fl}$ and CCN2-KO HFD and HFD+DM groups. This was maintained at week 25, where the AlbCre HFD mice, but not the AlbCre HFD+DM, also had reduced BMD. Measurements of bone area and bone mineral content are shown in *Table 4.4*. The CCN2-KO did not affect bone outcomes.

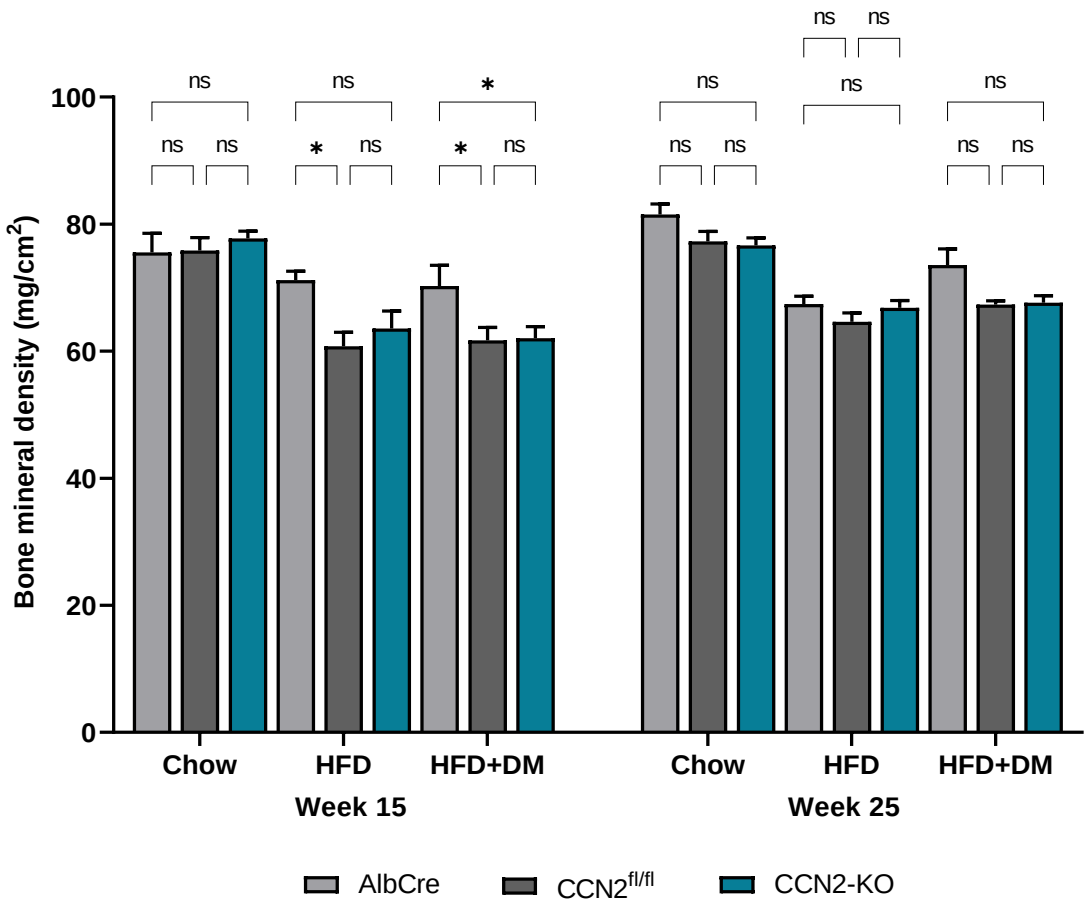

*Figure 4.13: Bone mineral density at week 15 and week 25. Note that at week 15, HFD+DM groups were not yet diabetic. Data shown as mean ± SEM; n = 8 - 13. * p-value ≤ 0.05 for comparison of mouse sub-strains within the same "diet" subgroup using mixed-effects analysis with Šidák's correction for multiple comparisons. ns, not significant.*

Table 4.4: Bone area, bone mineral content, and bone mineral density at week 15 and week 25.

	Chow			HFD			HFD+DM		
Week 15	**AlbCre**	**CCN2$^{fl/fl}$**	**CCN2-KO**	**AlbCre**	**CCN2$^{fl/fl}$**	**CCN2-KO**	**AlbCre**	**CCN2$^{fl/fl}$**	**CCN2-KO**
BA (cm^2)	7.36 ± 0.19	7.72 ± 0.17	7.05 ± 0.11	8.84 ± 0.13	8.84 ± 0.23	9.47 ± 0.37	9.95 ± 0.34	9.34 ± 0.27	9.94 ± 0.30
BMC (g)	0.55 ± 0.01	0.59 ± 0.02	0.55 ± 0.01	0.63 ± 0.02	0.54 ± 0.03	0.59 ± 0.01	0.70 ± 0.05	0.57 ± 0.02	0.62 ± 0.03
BMD (mg/cm^2)	75.53 ± 3.03	75.84 ± 2.06	77.75 ± 1.13	71.17 ± 1.42	60.77 ± 2.21	63.57 ± 2.73	70.25 ± 3.26	61.69 ± 2.06	62.06 ± 1.79
Week 25	**AlbCre**	**CCN2$^{fl/fl}$**	**CCN2-KO**	**AlbCre**	**CCN2$^{fl/fl}$**	**CCN2-KO**	**AlbCre**	**CCN2$^{fl/fl}$**	**CCN2-KO**
BA (cm^2)	7.73 ± 0.22	8.03 ± 0.22	7.98 ± 0.20	9.54 ± 0.09	9.73 ± 0.40	9.65 ± 0.16	8.99 ± 0.35	9.69 ± 0.20	9.41 ± 0.34
BMC (g)	0.63 ± 0.03	0.62 ± 0.01	0.61 ± 0.02	0.64 ± 0.01	0.63 ± 0.04	0.64 ± 0.01	0.65 ± 0.01	0.65 ± 0.02	0.63 ± 0.02
BMD (mg/cm^2)	81.52 ± 1.65	77.27 ± 1.59	76.65 ± 1.21	67.44 ± 1.22	64.63 ± 1.41	66.83 ± 1.13	73.57 ± 2.51	67.33 ± 0.58	67.65 ± 1.10

Data shown as mean ± SEM; n = 8 - 13. BA, bone area; BMC, bone mineral content; BMD, bone mineral density. Please note that as per the Methods, relevant p-values have been identified in relevant Figures, not in the Table.

4.3.2.5 Organ weights at termination

The wet weight of the liver, epididymal fat pads, subcutaneous (dorsolumbar) fat pads, gastrocnemius muscles, spleen, kidneys, and heart were measured at termination and normalised against total body weight (*Figure 4.14*). The absolute data is shown in *Table 4.5*. The livers of the HFD (AlbCre: 7.41 ± 0.28, $CCN2^{fl/fl}$: 7.63 ± 0.49, and CCN2-KO: 8.27 ± 0.30 % TBW) and HFD+DM (AlbCre: 6.95 ± 0.40, $CCN2^{fl/fl}$: 7.09 ± 0.24, and CCN2-KO: 7.86 ± 0.49 % TBW) mice were approximately two-fold heavier than the Chow mice (AlbCre:3.73 ± 0.11, $CCN2^{fl/fl}$: 4.08 ± 0.06, and CCN2-KO: 3.69 ± 0.14 % TBW). There was no difference in normalised liver weight between HFD and HFD+DM mice. There was no effect from CCN2-KO on liver size (*Figure 4.14A*).

Absolute epididymal fat mass, as a marker of visceral fat in mice, was generally higher in the HFD and HFD+DM groups compared with the Chow groups, but after normalisation against their total body weight, there was no statistical difference observed (*Figure 4.14B*). The $CCN2^{fl/fl}$ Chow mice (1.63 ± 0.26 g) had unusually high epididymal fat mass compared to the AlbCre (1.11 ± 0.16 g) and CCN2-KO (1.16 ± 0.18 g) Chow mice. There was no difference in the liver to epididymal fat mass ratio between mouse sub-strains, although the ratio was elevated in HFD and HFD+DM groups compared with Chow groups (*Figure 4.14C*). Subcutaneous fat pads were systematically resected from the dorsolumbar region and were significantly larger in mice that had been high fat fed (*Figure 4.14D*). Conversely, gastrocnemius muscle weight was lower in HFD and HFD+DM mice (*Figure 4.14E*). These results were consistent with the body composition data measured by EchoMRI™ and DXA. Normalised spleen mass was similar across most groups (*Figure 4.14F*). Normalised kidney (*Figure 4.14G*) and heart (*Figure 4.14H*) mass were reduced in the HFD and HFD+DM groups. Across all measured organs, there was no difference in normalised weight between HFD and HFD+DM groups, except in the AlbCre HFD+DM mice. These mice displayed an unusual phenotype of lower subcutaneous fat pad mass and higher gastrocnemius muscle, spleen, kidney, and heart weights, although these results may be due to the slightly lower total body weight in these mice.

Overall, the CCN2-KO did not affect any of the organ weights, indicating a lack of a systemic effect from the hepatocyte-specific gene deletion.

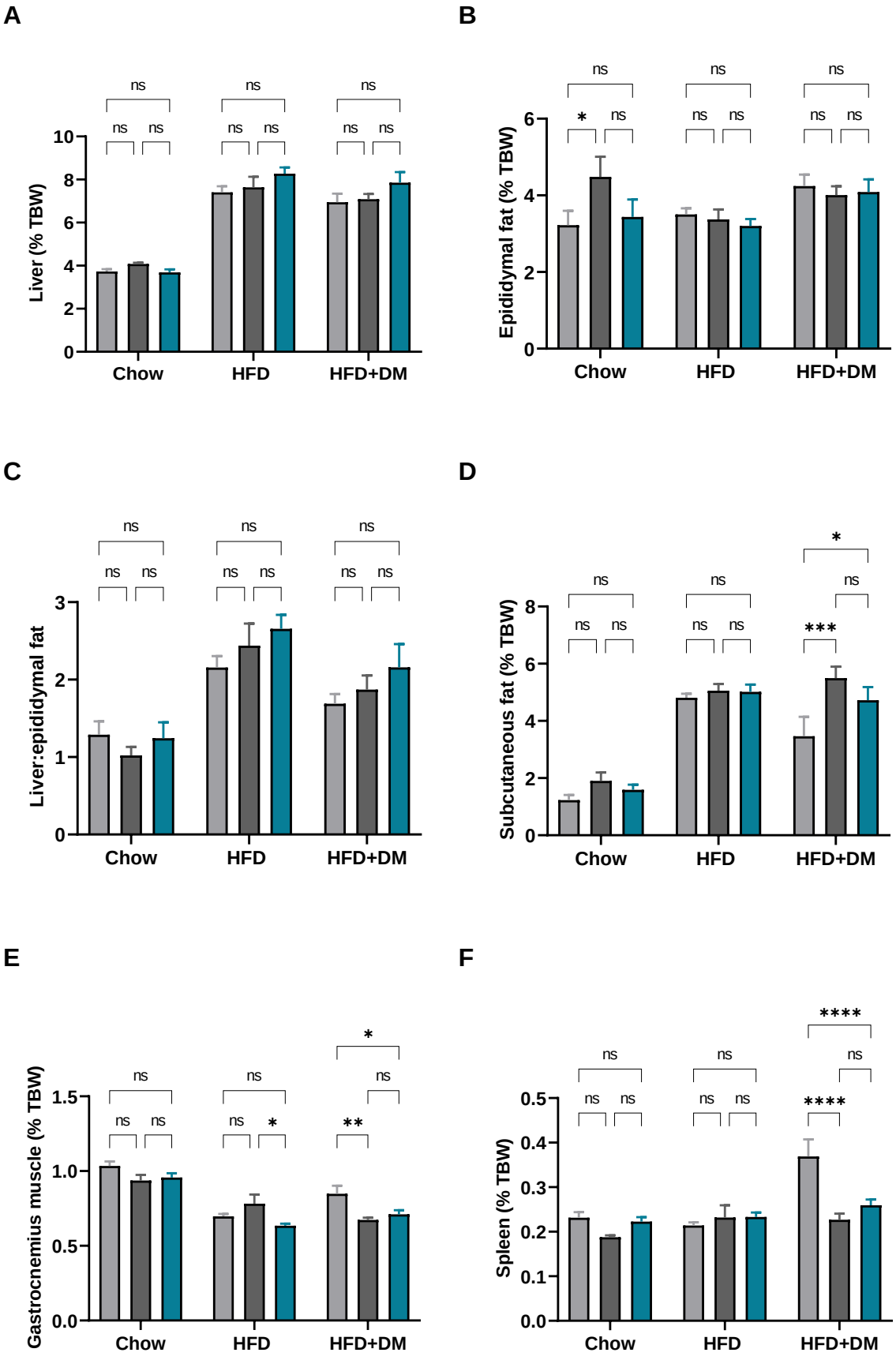
A
Liver (% TBW)
0
2
4
6
8
10
ns
Chow
HFD
HFD+DM
B
Epididymal fat (% TBW)
0
2
4
6
*
ns
C
Liver:epididymal fat
0
1
2
3
D
Subcutaneous fat (% TBW)
0
2
4
6
8
*
***
E
Gastrocnemius muscle (% TBW)
0.0
0.5
1.0
1.5
*
**
F
Spleen (% TBW)
0.0
0.1
0.2
0.3
0.4
0.5
****

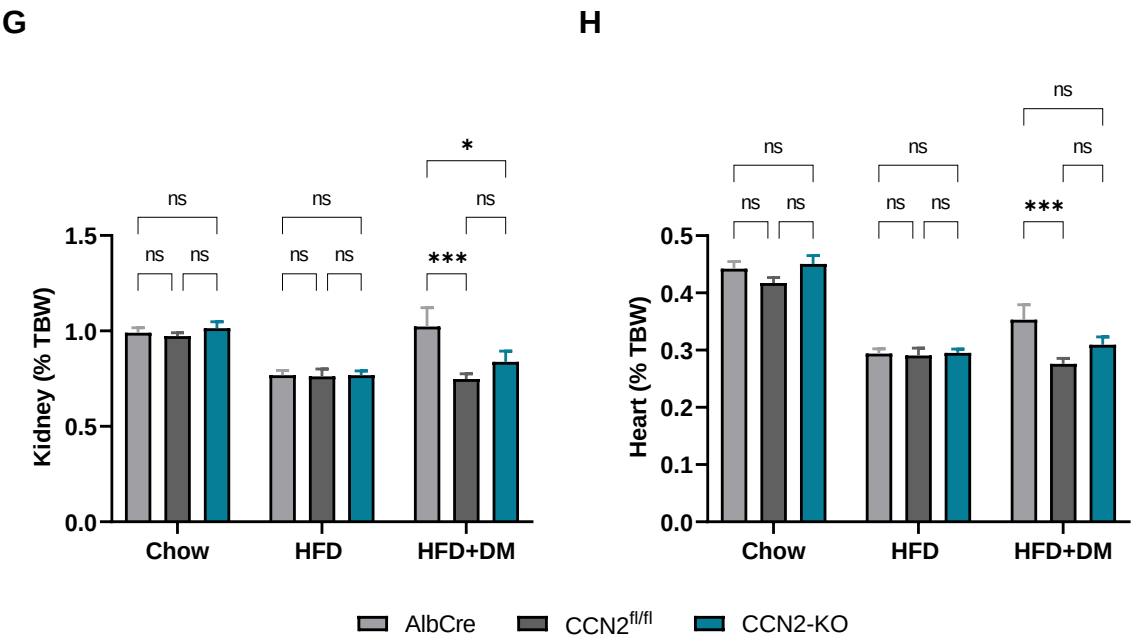

*Figure 4.14: Organ wet weights expressed as percentage of total body weight: liver (A), epididymal fat (B), liver to epididymal fat ratio (C), subcutaneous fat (D), gastrocnemius muscle (E), spleen (F), kidney (G), and heart (H). Data shown as mean ± SEM; n = 8 - 13. * p-value ≤ 0.05, ** p-value ≤ 0.01, *** p-value ≤ 0.001 or **** p-value ≤ 0.0001 for comparison of mouse sub-strains within the same "diet" subgroup using two-way ANOVA with Tukey's correction for multiple comparisons. TBW, total body weight; ns, not significant.*

Table 4.5: Organ wet weights (grams) at termination.

	Chow			HFD			HFD+DM		
	AlbCre	**CCN2$^{fl/fl}$**	**CCN2-KO**	**AlbCre**	**CCN2$^{fl/fl}$**	**CCN2-KO**	**AlbCre**	**CCN2$^{fl/fl}$**	**CCN2-KO**
Liver	1.26 ± 0.07	1.42 ± 0.09	1.21 ± 0.05	3.89 ± 0.24	3.76 ± 0.31	4.59 ± 022	2.96 ± 0.24	3.40 ± 0.16	3.57 ± 0.30
Epididymal fat	1.11 ± 0.16	1.63 ± 0.26	1.16 ± 0.18	1.83 ± 0.09	1.61 ± 0.08	1.77 ± 0.10	1.85 ± 0.21	1.90 ± 0.09	1.81 ± 0.14
Liver:epididymal fat	1.29 ± 0.17	1.02 ± 0.11	1.24 ± 0.20	2.16 ± 0.15	2.44 ± 0.28	2.66 ± 0.18	1.69 ± 0.12	1.87 ± 0.18	2.16 ± 0.30
Subcutaneous fat	0.42 ± 0.07	0.70 ± 0.14	0.53 ± 0.07	2.51 ± 0.08	2.45 ± 0.14	2.78 ± 0.17	1.64 ± 0.39	2.70 ± 0.24	2.28 ± 0.31
Gastrocnemius muscle	0.35 ± 0.008	0.32 ± 0.005	0.31 ± 0.007	0.36 ± 0.007	0.38 ± 0.032	0.35 ± 0.005	0.35 ± 0.006	0.32 ± 0.006	0.31 ± 0.014
Spleen	0.08 ± 0.006	0.06 ± 0.003	0.07 ± 0.004	0.11 ± 0.005	0.11 ± 0.008	0.13 ± 0.004	0.15 ± 0.010	0.11 ± 0.008	0.12 ± 0.010
Kidney	0.33 ± 0.02	0.33 ± 0.01	0.33 ± 0.01	0.40 ± 0.02	0.37 ± 0.01	0.42 ± 0.01	0.41 ± 0.02	0.35 ± 0.004	0.36 ± 0.01
Heart	0.15 ± 0.006	0.14 ± 0.006	0.15 ± 0.006	0.15 ± 0.004	0.14 ± 0.004	0.16 ± 0.004	0.14 ± 0.004	0.13 ± 0.002	0.14 ± 0.005
Total body weight	33.76 ± 1.48	34.54 ± 1.75	32.85 ± 1.29	52.20 ± 1.14	48.51 ± 1.57	55.33 ± 1.06	42.61 ± 2.68	48.06 ± 1.54	45.35 ± 2.83

Data shown as mean ± SEM; n = 8 - 13. Please note that as per the Methods, relevant p-values have been identified in the relevant Figures, not in the Table.

4.3.2.6 Routine fasting plasma biochemistry

4.3.2.6.1 Liver-related tests

The AST and ALT levels were markedly elevated in the HFD and HFD+DM groups compared with the Chow groups (*Figure 4.15* and *Table 4.6*; statistics comparing different "diet" groups not shown). There was a trend to higher AST and ALT level in the AlbCre HFD+DM compared with the $CCN2^{fl/fl}$ HFD+DM and CCN2-KO HFD+DM groups (*Figure 4.15A* and *B*). In contrast, both AST and ALT were significantly lower in the AlbCre HFD mice compared with the CCN2-KO HFD mice but not the $CCN2^{fl/fl}$ HFD mice. The AST to ALT ratio can be used clinically to suggest the aetiology and severity of the abnormal enzyme results. The lower ratio observed in the HFD and HFD+DM mice was due to the relatively higher rise in ALT compared with rise in AST and was consistent with significant hepatocellular injury (*Figure 4.15C*). The ALP levels were also elevated in the HFD and HFD+DM mice compared with Chow mice across all three mouse sub-strains (*Figure 4.15D*). However, in the HFD+DM groups, the CCN2-KO mice had a significantly reduced level of ALP compared with the AlbCre mice but not the $CCN2^{fl/fl}$ mice (AlbCre: 33.46 ± 7.22, $CCN2^{fl/fl}$: 23.31 ± 2.32, and CCN2-KO: 18.41 ± 2.35 U/L). Total protein and albumin levels are measures of liver synthetic function. Total protein was not reduced in HFD+DM groups compared with the respective Chow group of the same sub-strain, however, within the HFD+DM groups, the total protein in the AlbCre mice was significantly lower than the $CCN2^{fl/fl}$ and CCN2-KO groups (AlbCre: 44.82 ± 0.95, $CCN2^{fl/fl}$: 50.44 ± 0.78, and CCN2-KO: 53.05 ± 2.94 g/L; *Table 4.6*). A similar pattern was observed in albumin levels, and AlbCre HFD+DM mice had significantly lower albumin levels compared with AlbCre Chow mice (AlbCre Chow: 29.89 ± 0.27 vs AlbCre HFD+DM: 27.23 ± 0.47 g/L, $p = 0.040$; *Figure 4.15E*). Total bilirubin levels were generally very low, with no clear pattern identified (*Figure 4.15F*). The automated analyser was unable to detect GGT in mouse plasma, and platelet count was not assessed either as it required stored whole blood, which was not available.

In general, this data indicates that hepatocyte CCN2 deletion did not affect plasma markers of liver damage, except for the reduction in ALP under HFD+DM conditions.

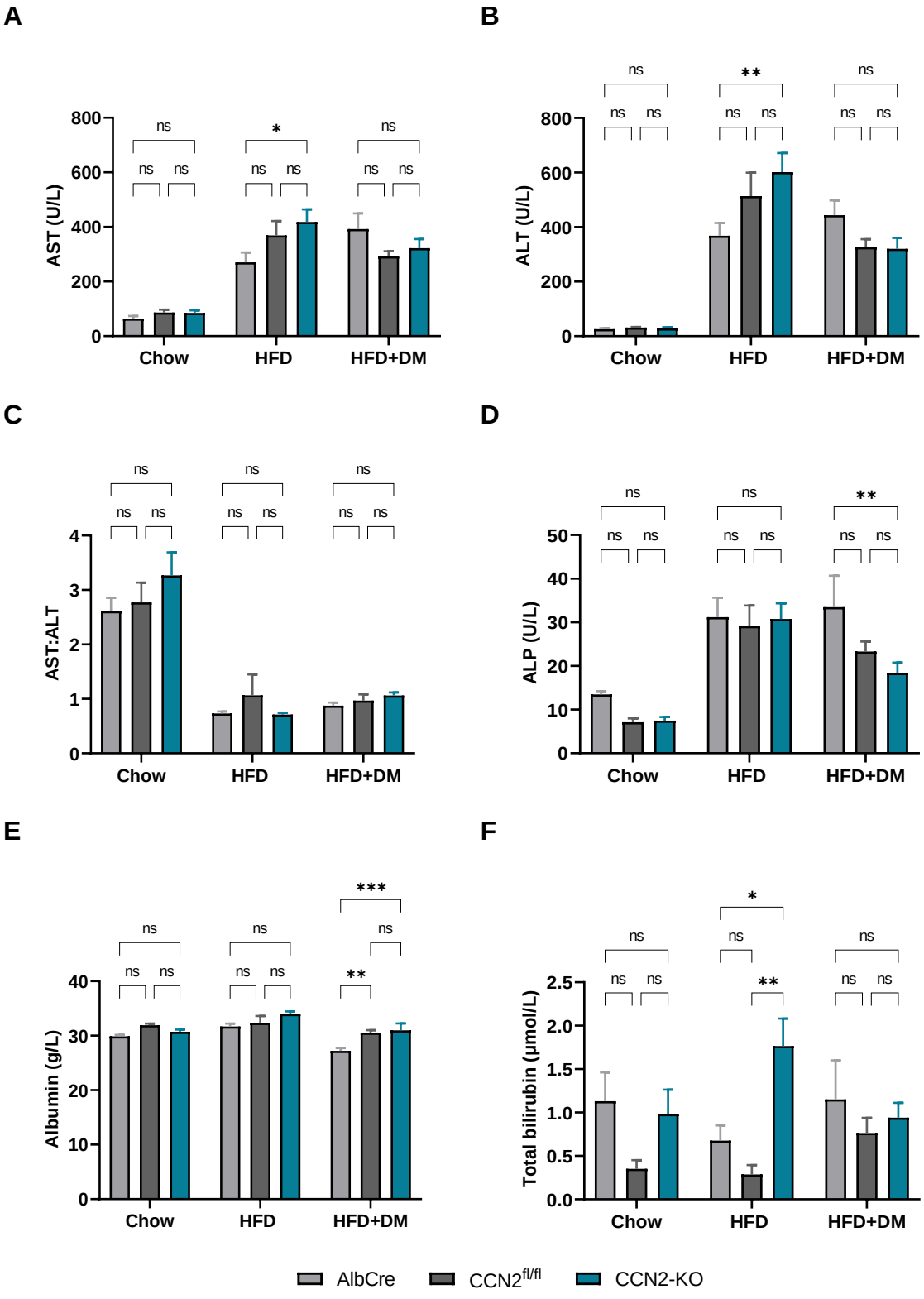

*Figure 4.15: Liver-related plasma tests: AST (A), ALT (B), AST:ALT (C), ALP (D), albumin (E), and total bilirubin (F). Data shown as mean ± SEM; n = 7 - 12. * p-value ≤ 0.05, ** p-value ≤ 0.01 or *** p-value ≤ 0.001 for comparison of mouse sub-strains within the same "diet" subgroup using two-way ANOVA with Tukey's correction for multiple comparisons. ALP, alkaline phosphatase; ALT, alanine aminotransferase; AST, aspartate aminotransferase; AST:ALT, AST to ALT ratio; ns, not significant.*

4.3.2.6.2 Lipid panel

Total cholesterol, HDL-c, and LDL-c were elevated in all groups that were fed a high fat diet, but to a higher degree in the HFD groups compared with the HFD+DM groups (*Figure 4.16* and *Table 4.6*; statistics comparing different "diet" groups not shown). In the HFD+DM groups, total cholesterol, HDL-c, and LDL-c were all significantly lower in the AlbCre mice compared with CCN2$^{fl/fl}$ and CCN2-KO mice. Fasting triglyceride levels were lower in the HFD and HFD+DM groups compared with Chow groups, with no statistical difference between mouse strains.

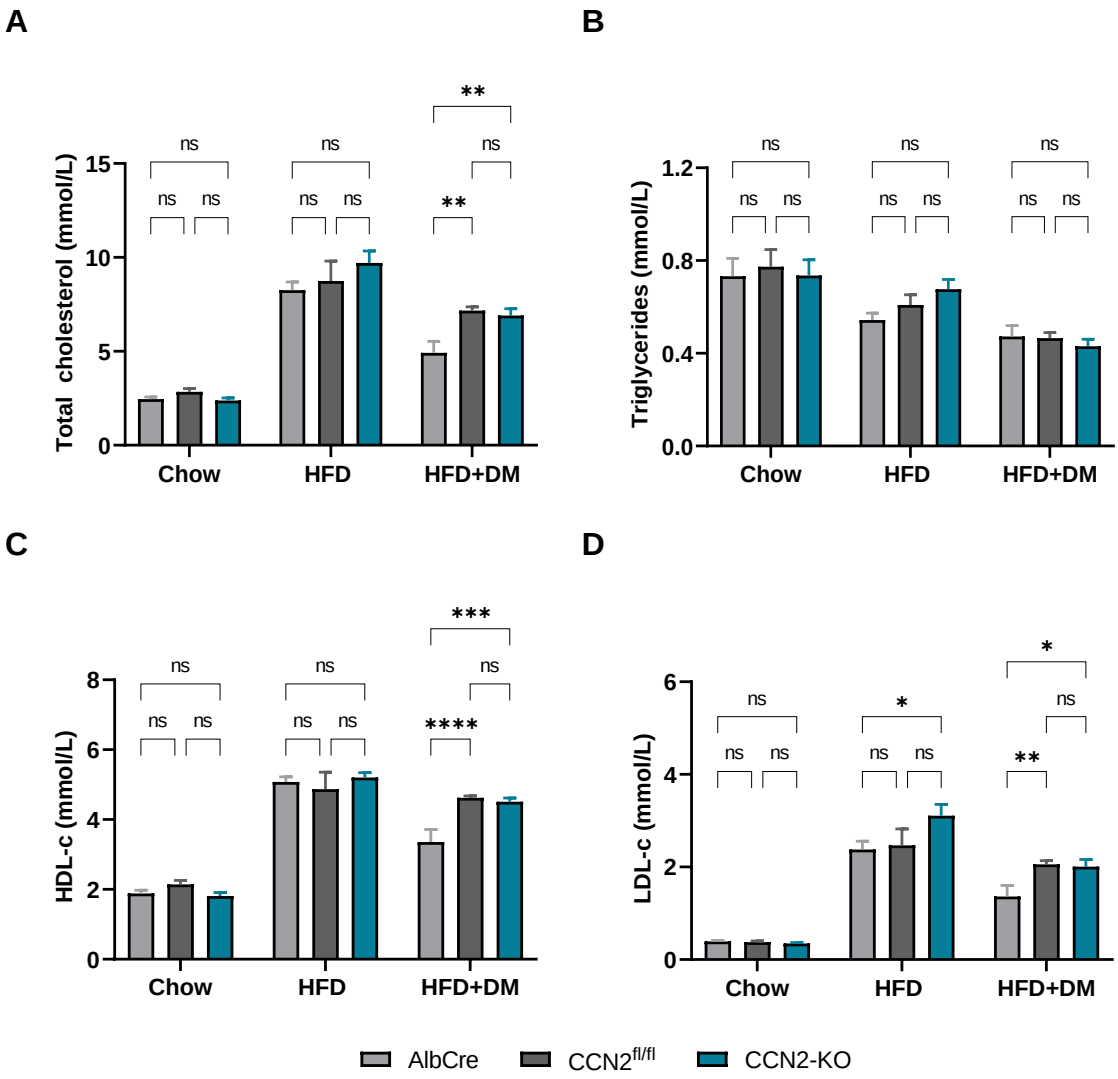

*Figure 4.16: Fasting plasma lipid panel: total cholesterol (A), triglycerides (B), HDL-c (C), and LDL-c (D). Data shown as mean ± SEM; n = 7 - 12. * p-value ≤ 0.05, ** p-value ≤ 0.01, *** p-value ≤ 0.001 or **** p-value ≤ 0.0001 for comparison of mouse sub-strains within the same "diet" subgroup using two-way ANOVA with Tukey's correction for multiple comparisons. HDL-c, high-density lipoprotein cholesterol; LDL-c, low-density lipoprotein cholesterol; ns, not significant.*

Table 4.6: Routine fasting plasma biochemistry.

	Chow			HFD			HFD+DM		
	AlbCre	**CCN2$^{fl/fl}$**	**CCN2-KO**	**AlbCre**	**CCN2$^{fl/fl}$**	**CCN2-KO**	**AlbCre**	**CCN2$^{fl/fl}$**	**CCN2-KO**
AST (U/L)	64.02 ± 9.82	86.33 ± 10.35	84.76 ± 9.83	270.28 ± 36.19	368.93 ± 52.96	418.18 ± 46.48	392.52 ± 56.99	292.53 ± 18.71	322.32 ± 33.50
ALT (U/L)	25.57 ± 3.79	31.77 ± 1.62	28.42 ± 4.27	368.60 ± 46.64	513.81 ± 85.68	601.36 ± 70.28	443.40 ± 54.45	326.36 ± 29.64	320.42 ± 39.96
AST:ALT	2.61 ± 0.25	2.77 ± 0.36	3.27 ± 0.42	0.73 ± 0.04	1.06 ± 0.38	0.71 ± 0.03	0.87 ± 0.06	0.97 ± 0.11	1.06 ± 0.06
ALP (U/L)	13.49 ± 0.76	7.09 ± 0.87	7.49 ± 0.83	31.17 ± 4.47	29.13 ± 4.72	30.79 ± 3.58	33.46 ± 7.22	23.31 ± 2.32	18.41 ± 2.35
Albumin (g/L)	29.89 ± 0.27	31.92 ± 0.31	30.71 ± 0.41	31.68 ± 0.55	32.35 ± 1.26	33.97 ± 0.47	27.23 ± 0.47	30.55 ± 0.45	30.99 ± 1.26
Total protein (g/L)	43.55 ± 0.38	46.96 ± 0.50	45.00 ± 0.47	52.18 ± 1.17	54.13 ± 1.63	58.05 ± 1.49	44.82 ± 0.95	50.44 ± 0.78	53.05 ± 2.94
Total bilirubin (µmol/L)	1.13 ± 0.33	0.35 ± 0.10	0.98 ± 0.28	0.68 ± 0.18	0.29 ± 0.11	1.77 ± 0.32	1.15 ± 0.45	0.76 ± 0.18	0.94 ± 0.17
Total cholesterol (mmol/L)	2.46 ± 0.11	2.85 ± 0.17	2.38 ± 0.14	8.26 ± 0.44	8.74 ± 1.06	9.71 ± 0.63	4.92 ± 0.61	7.17 ± 0.19	6.91 ± 0.36
Triglycerides (mmol/L)	0.73 ± 0.08	0.77 ± 0.07	0.74 ± 0.07	0.54 ± 0.03	0.61 ± 0.04	0.68 ± 0.04	0.47 ± 0.05	0.47 ± 0.02	0.43 ± 0.03
HDL-c (mmol/L)	1.88 ± 0.09	2.15 ± 0.11	1.81 ± 0.10	5.08 ± 0.15	4.87 ± 0.49	5.20 ± 0.14	3.36 ± 0.36	4.62 ± 0.05	4.51 ± 0.10
LDL-c (mmol/L)	0.39 ± 0.02	0.38 ± 0.03	0.35 ± 0.02	2.38 ± 0.18	2.47 ± 0.35	3.11 ± 0.24	1.36 ± 0.24	2.06 ± 0.08	2.01 ± 0.15

Data shown as mean ± SEM; n = 7 - 12. ALP, alkaline phosphatase; ALT, alanine aminotransferase; AST, aspartate aminotransferase; AST:ALT, AST to ALT ratio; HDL-c, high-density lipoprotein cholesterol; LDL-c, low-density lipoprotein cholesterol. Please note that as per the Methods, relevant p-values have been identified in the relevant Figures, not in the Table.

4.3.3 The effects of hepatocyte CCN2 deletion on NASH fibrosis

The gold standard for assessing the development of NASH fibrosis in humans is via a core liver biopsy, and use of standard histological staining such as H&E staining, with or without the use of a dedicated fibrosis stain, such as PSR staining or Masson's Trichrome staining[80]. We elected to use both H&E and PSR staining in assessing the main histological features of NASH: fibrosis, inflammation, hepatocyte ballooning, and steatosis. Each of these features were assessed using multiple approaches as described in the Methods (*Section 2.3.5*). In addition, other techniques, such as measurement of mRNA levels of key fibrosis and inflammation markers, were used to provide additional support to the histological outcomes.

4.3.3.1 The effects of hepatocyte CCN2 deletion on liver fibrosis

4.3.3.1.1 Assessment of liver fibrosis by histology

The primary outcome of this study was to assess the development of liver fibrosis, which, in humans, links strongly to loss of liver function and increased mortality[321-324,365]. Two different methods of assessing fibrosis were used: quantification using image analysis software and grading according to the Brunt criteria by an independent anatomical pathologist. Both methods were applied to PSR-stained liver tissue.

A) Quantification of liver fibrosis using image analysis software

The details of the methods are described in *Section 2.3.5.1*. In brief, 4 - 6 images per stained liver tissue section were taken at three magnifications (100x, 200x, and 400x) and ImageJ software was used to calculate the percent area of the PSR-positive stained tissue. The threshold settings were optimised using the HFD+DM groups, and then the same analysis settings were applied to the Chow and HFD groups.

The percent area of PSR-positive stained tissue at various magnifications is shown in *Figure 4.17*. At all three magnifications, there were very low levels (< 1%) of PSR-positive tissue in all three Chow groups, which was consistent with an absence of liver fibrosis. Some PSR-positive stained tissue was evident due to the staining of collagen fibres that normally line the blood vessel walls. Fibrosis levels in the HFD groups were also relatively low and may be an underestimate as the threshold settings were not optimised specifically for these groups. Regardless, there was no effect of the CCN2-KO in the HFD group and percent of PSR-positive tissue was similar to the AlbCre and

CCN2$^{fl/fl}$ HFD groups. The HFD+DM groups all had greater percent of PSR-positive tissue compared with the Chow and HFD groups (statistics comparing different “diet” groups not shown). The CCN2-KO groups displayed significantly lower percentage of PSR-positive stained tissue across all three magnifications, including at more detailed areas of the central vein and the portal tracts. Although fibrosis was generally most abundant at the level of the portal tract, the relative reduction was greatest at the central vein, where there was approximately 50% reduction in percent area of fibrosis. Representative images are shown in *Figures 4.18 - 4.20*.

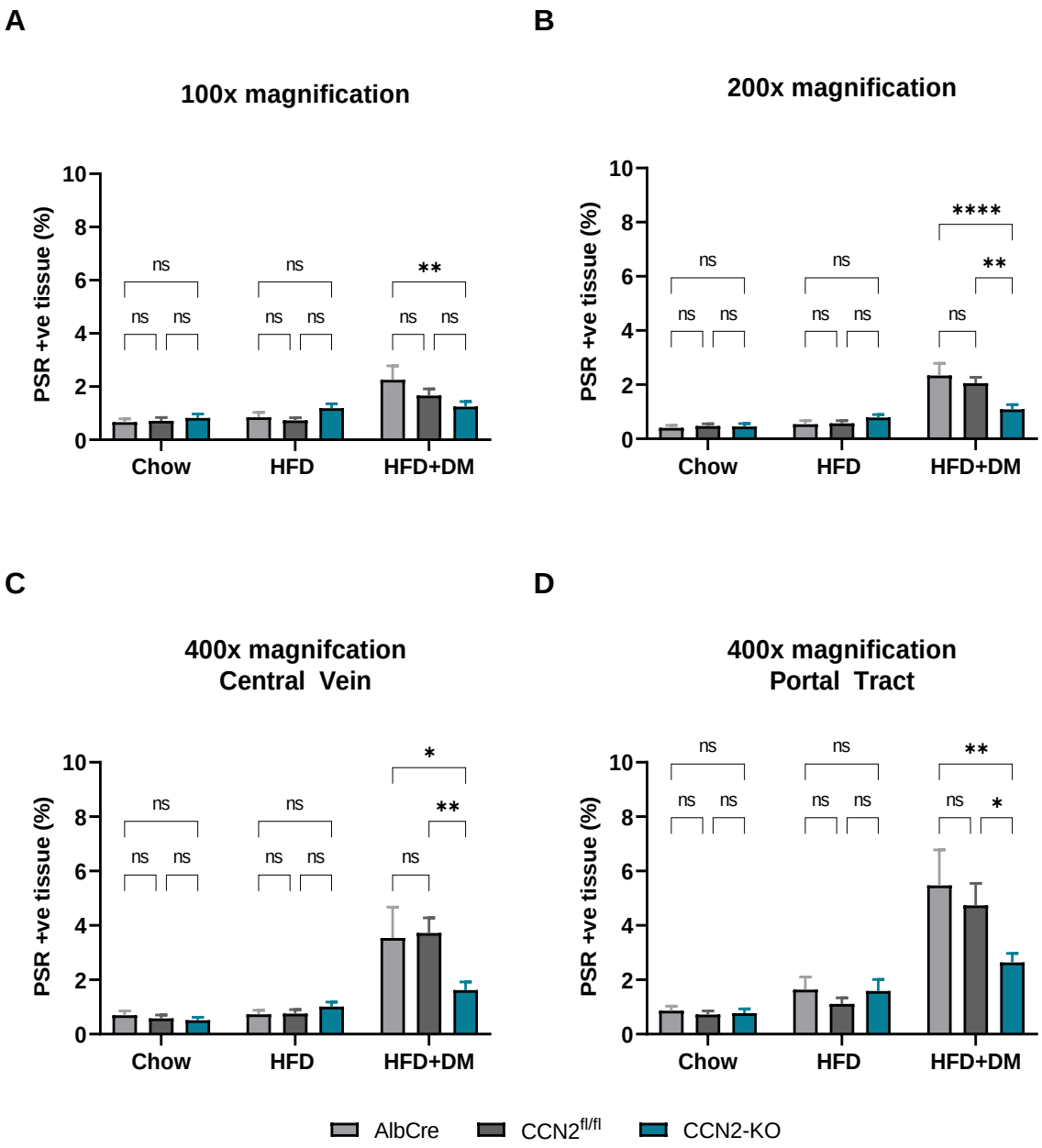

*Figure 4.17: Quantification of fibrosis of PSR-stained liver tissue with images taken at 100x magnification (A), 200x magnification (B), and 400x magnification focussing on central veins (C) and portal tracts (D). Data shown as mean ± SEM; n = 6 - 13. * p-value ≤ 0.05, ** p-value ≤ 0.01 or **** p-value ≤ 0.0001 for comparison of mouse sub-strains within the same "diet" subgroup using two-way ANOVA with Tukey's correction for multiple comparisons. PSR, Picro Sirius Red; ns, not significant.*

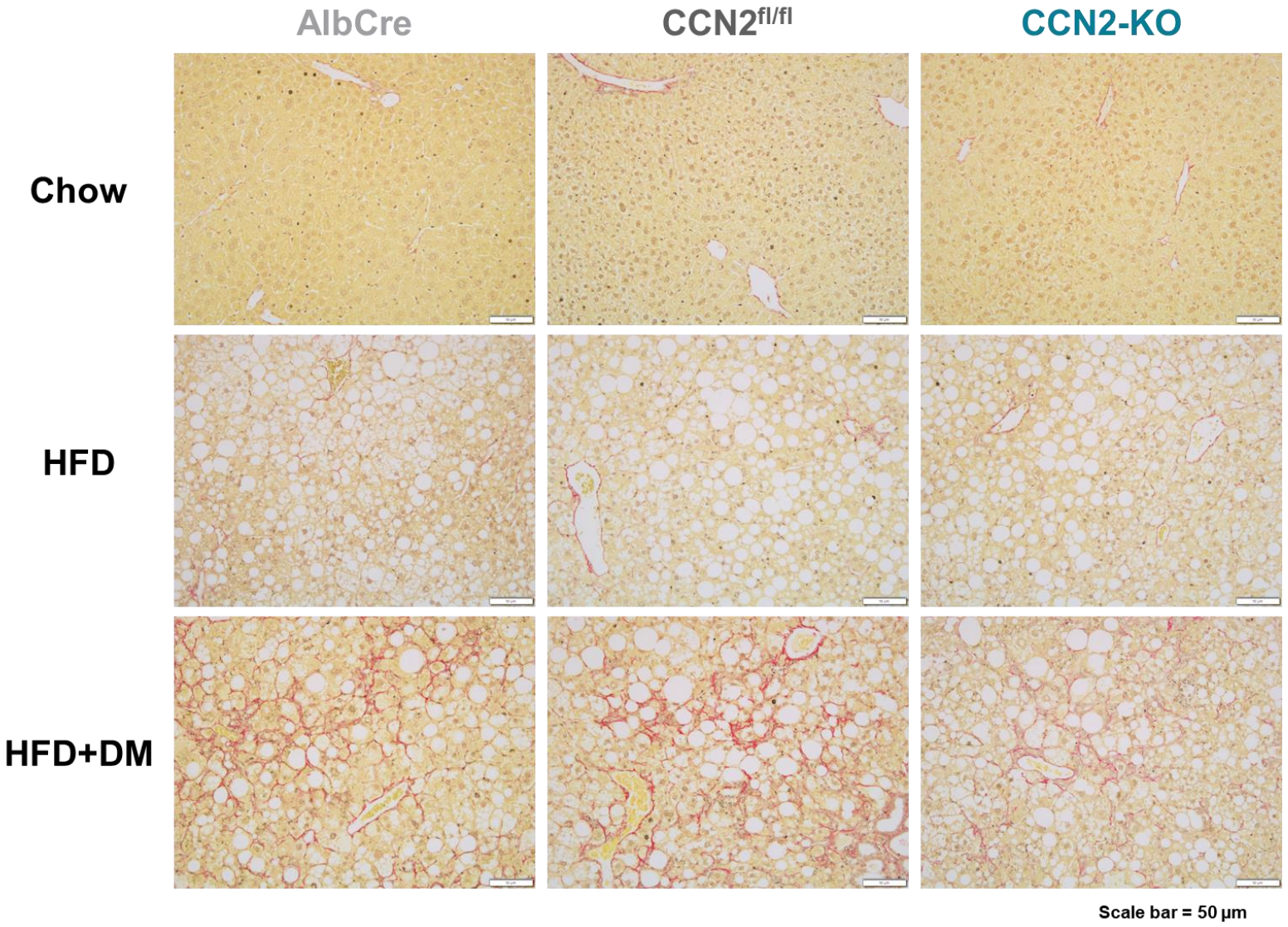

Figure 4.18: Representative histological images of PSR-stained liver tissue (200x magnification).

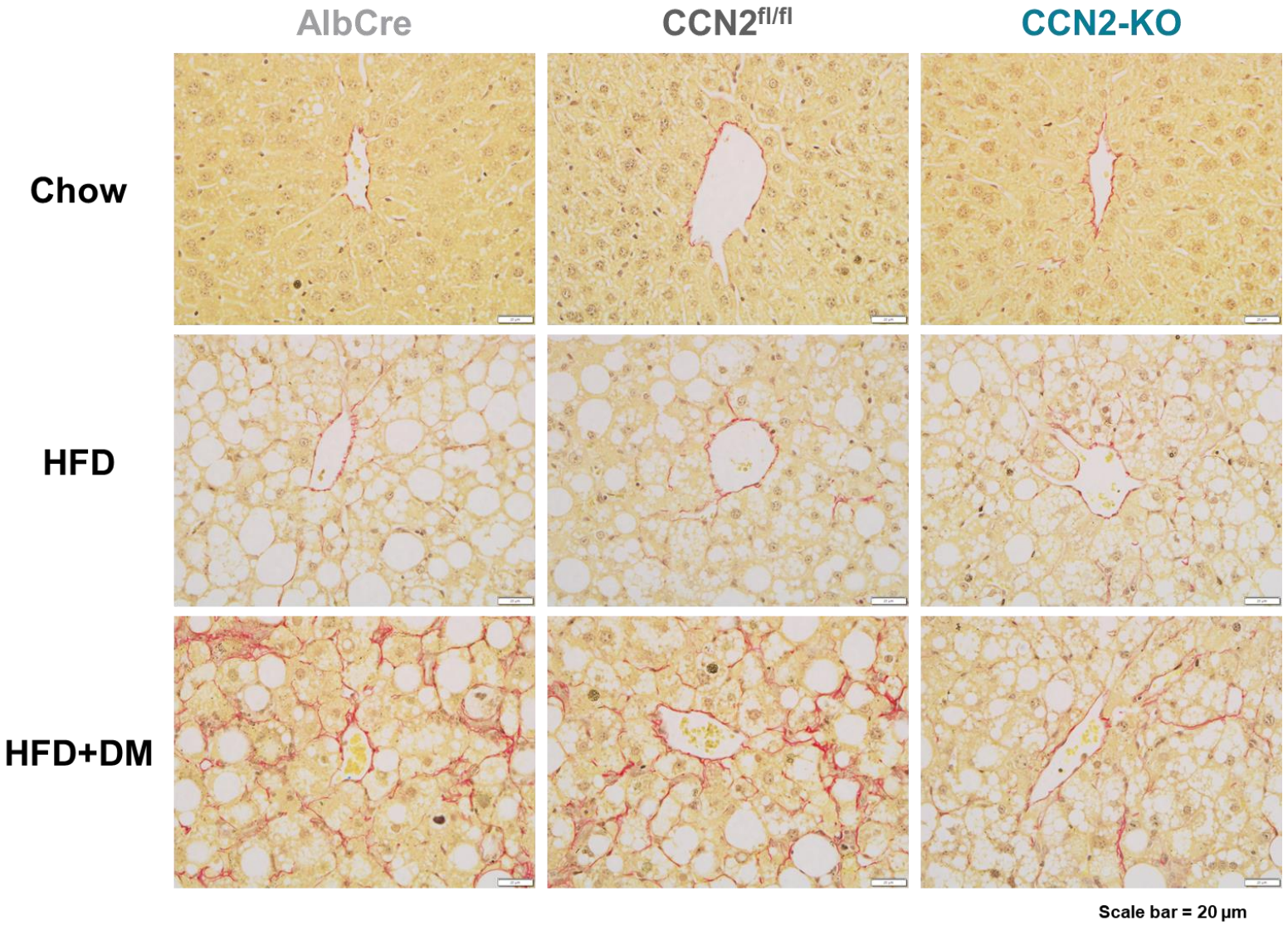

Figure 4.19: Representative histological images of central veins from PSR-stained liver tissue (400x magnification).

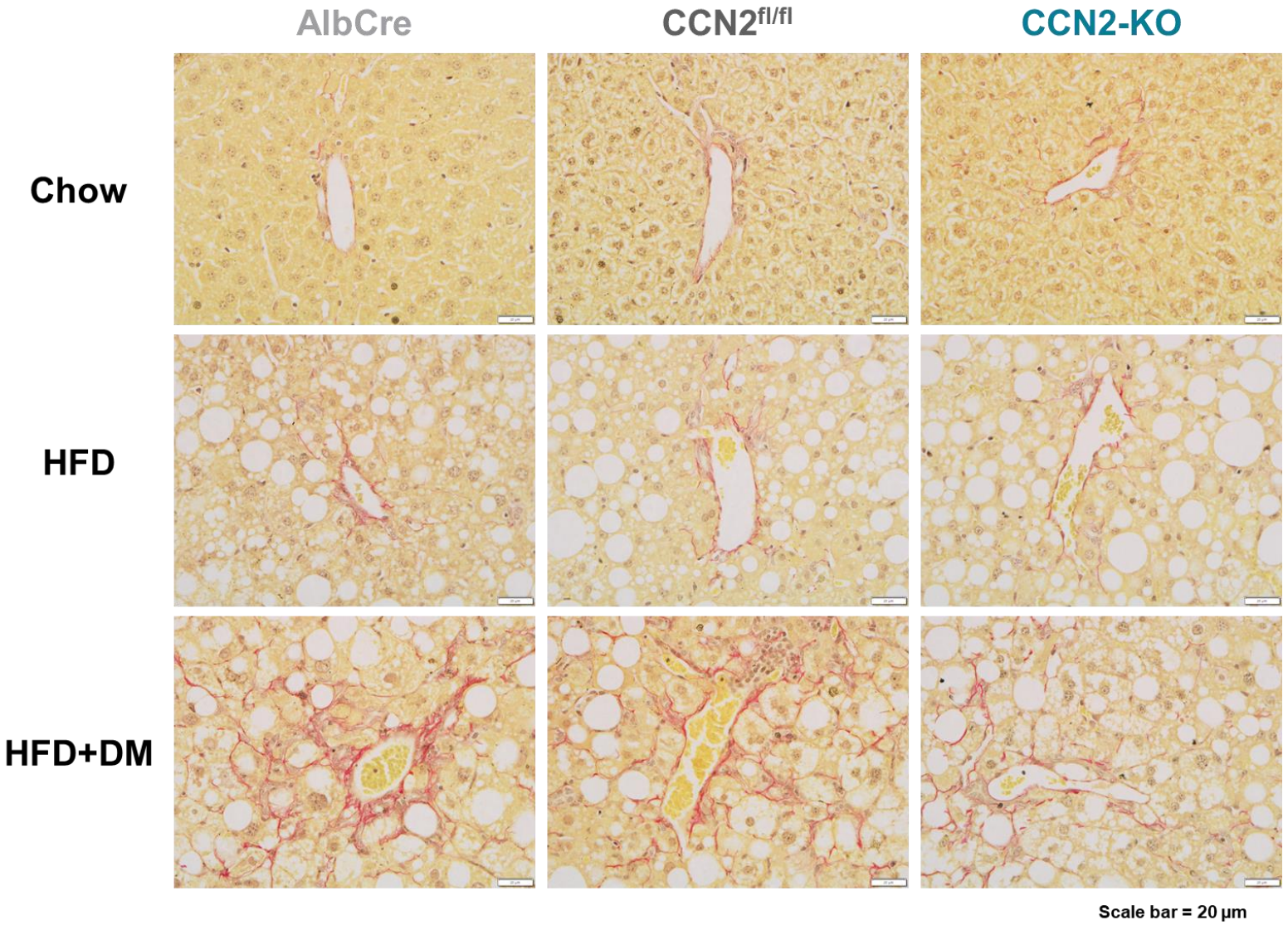

Figure 4.20: Representative histological images of portal tracts from PSR-stained liver tissue (400x magnification).

B) Grading of liver fibrosis according to the Brunt criteria

The Brunt criteria grades liver fibrosis according to its regionality, and unlike the method used in the previous section, is not quantitative. An absence of fibrosis is F0, perisinusoidal fibrosis is F1, periportal fibrosis is F2, bridging fibrosis is F3, and cirrhosis is F4. A higher stage represents more severe disease and worse prognosis. Mice from the HFD+DM groups exhibited the highest fibrosis grade, although there was no difference detected in the CCN2-KO group (AlbCre: 2.8 ± 0.5, $CCN2^{fl/fl}$: 2.6 ± 0.2, and CCN2-KO: 2.8 ± 0.2; *Figure 4.21* and *Table 4.7*). There was no fibrosis (F0) observed in the Chow fed mice, and the HFD mice had an intermediary grade of fibrosis.

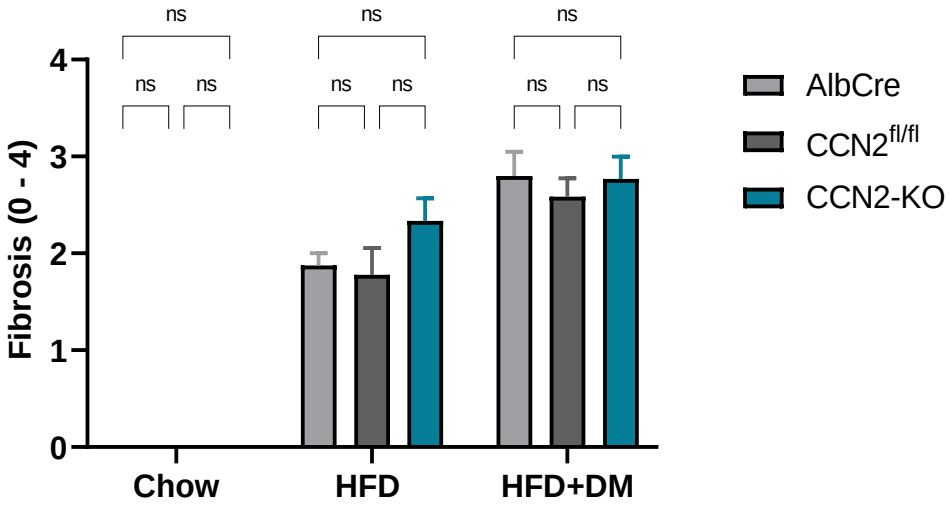

Figure 4.21: Fibrosis grade according to the Brunt criteria. Data shown as mean ± SEM; n = 7 - 13. Ns (not significant), p-value > 0.05 for comparison of mouse sub-strains within the same "diet" subgroup using two-way ANOVA with Tukey's correction for multiple comparisons.

4.3.3.1.2 mRNA levels of fibrosis markers from whole liver tissue

Figure 4.22 and *Table 4.8* show the mRNA levels of fibrosis markers from whole liver tissue. In general, the expression of collagen-I, -III, -IVα1, -IVα2 and -VI, TGFβ1, fibronectin, ACTA2 and TIMP1 were increased in all of the HFD+DM groups compared with the Chow groups, and to a lesser extent, increased in all of the HFD groups (statistics comparing different "diets" not shown). There was no significant difference in the mRNA level of these genes between the AlbCre HFD+DM group and the $CCN2^{fl/fl}$ HFD+DM group, indicating that the two control sub-strains behaved in a similar manner. There was a statistically significant reduction in CCN2-KO HFD+DM

collagen-I mRNA level of 45% compared with the CCN2$^{fl/fl}$ HFD+DM group (CCN2$^{fl/fl}$: 17.4 ± 3.4 vs CCN2-KO: 9.6 ± 1.6, p = 0.049) but not the AlbCre HFD+DM group (AlbCre: 15.1 ± 5.2 vs CCN2-KO: 9.6 ± 1.6, p = 0.248; *Figure 4.22A*). The same pattern was observed in collagen-VI mRNA level, where there was a reduction in the CCN2-KO HFD+DM group of 32% compared with the CCN2$^{fl/fl}$ HFD+DM group (CCN2$^{fl/fl}$: 8.6 ± 1.2 vs CCN2-KO: 5.8 ± 0.9, p = 0.022) but not the AlbCre HFD+DM group (AlbCre: 6.1 ± 1.1 vs CCN2-KO: 5.8 ± 0.9, p = 0.969; *Figure 4.22D*). There was no statistical difference in collagen-III (*Figure 4.22B*), -IVα1 (*Table 4.8*) or -IVα2 (*Figure 4.22C*) mRNA levels between the CCN2-KO HFD+DM group and either of the control sub-strain HFD+DM groups, although the fold changes were numerically smaller in the CCN2-KO HFD+DM group. The mRNA level of TGFβ1, an up- and down-stream regulator of CCN2, was induced by HFD+DM, but to a lesser extent in the CCN2-KO HFD+DM group (AlbCre: 5.2 ± 0.9, CCN2$^{fl/fl}$: 4.5 ± 0.5, and CCN2-KO: 3.2 ± 0.3; *Figure 4.22E*). The interaction was significant between AlbCre HFD+DM and CCN2-KO HFD+DM (p = 0.002) and trending between CCN2$^{fl/fl}$ HFD+DM and CCN2-KO HFD+DM (p = 0.056). There was also a reduction in the mRNA level of fibronectin (*Figure 4.22F*), another component of the ECM, in the CCN2-KO HFD+DM group versus the CCN2$^{fl/fl}$ HFD+DM group (p = 0.015) and a trend for reduction versus the AlbCre HFD+DM group (p = 0.054). There was no significant difference in the mRNA levels of ACTA2 or TIMP1 amongst the different sub-strains of mice for the same “diet” subgroup, although there was a trend to reduced TIMP1 in the CCN2-KO HFD+DM group (*Table 4.8*). In general, there was no statistical differences between mouse sub-strains in the HFD groups, except for unexpected higher mRNA level of TGFβ1 (*Figure 4.22E*) and fibronectin (*Figure 4.22F*) in the CCN2$^{fl/fl}$ HFD group.

In summary, the overall pattern indicated a reduction in fibrosis markers across the board in the CCN2-KO HFD+DM mice compared with the control sub-strains, although this did not always meet statistical significance when using a rigorous test such as a two-way ANOVA with Tukey’s correction for multiple comparisons.

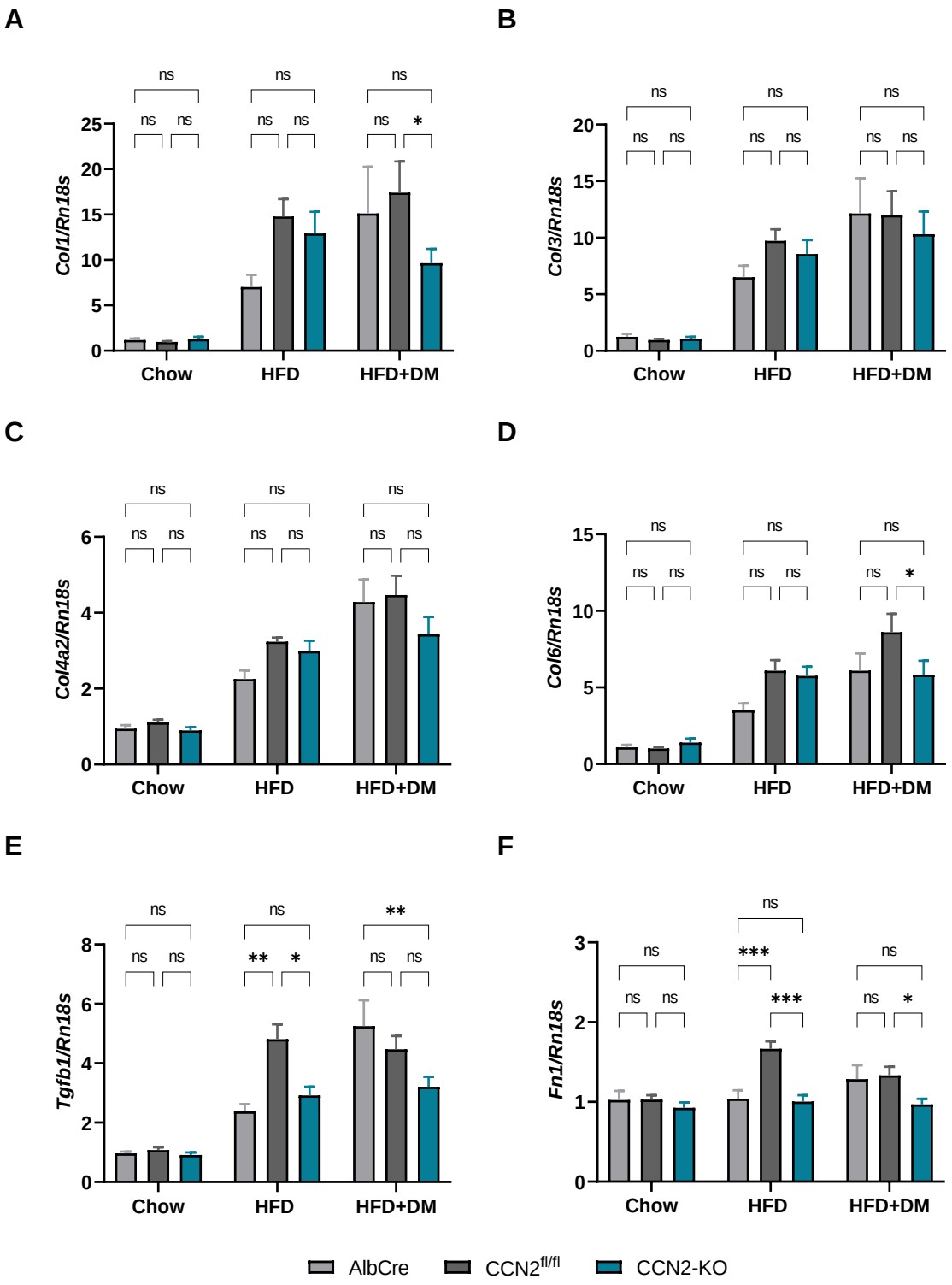

*Figure 4.22: mRNA levels of fibrosis markers Col1 (A), Col3 (B), Col4a2 (C), Col6 (D), Tgfb1 (E), and Fn1 (F). Data shown as mean ± SEM; n = 8 - 13. * p-value ≤ 0.05, ** p-value ≤ 0.01 or *** p-value ≤ 0.001 for comparison of mouse sub-strains within the same "diet" subgroup using two-way ANOVA with Tukey's correction for multiple comparisons. Col1, collagen-I; Col3, collagen-III; Col4a2, collagen-IVα2; Col6, collagen-VI; Fn1, fibronectin; Rn18s, 18S ribosomal RNA; Tgfb1, transforming growth factor β1; ns, not significant.*

4.3.3.2 The effects of hepatocyte CCN2 deletion on liver inflammation

4.3.3.2.1 Assessment of liver inflammation by histology

A) Assessment of lobular inflammation

In addition to fibrosis, a major hallmark of NASH is the development of inflammation[80]. Lobular inflammation was scored on H&E-stained tissue according to the NAS criteria (0 = absent, 1 = 1 focus, 2 = 2 - 4 foci, or 3 = > 4 foci per 200x field) by an independent anatomical pathologist (*Figure 4.23* and *Table 4.7*). The HFD+DM groups had the highest degree of lobular inflammation, with a mean of 2 - 4 foci per 200x field in each mouse sub-strain (AlbCre: 2.3 ± 0.3, CCN2$^{fl/fl}$: 2.4 ± 0.2, and CCN2-KO: 2.4 ± 0.2). The HFD groups had an intermediary level of lobular inflammation, although the CCN2-KO HFD group were scored statistically higher than the AlbCre HFD group, but not the CCN2$^{fl/fl}$ HFD group. The Chow groups all had a mean score of less than 1.

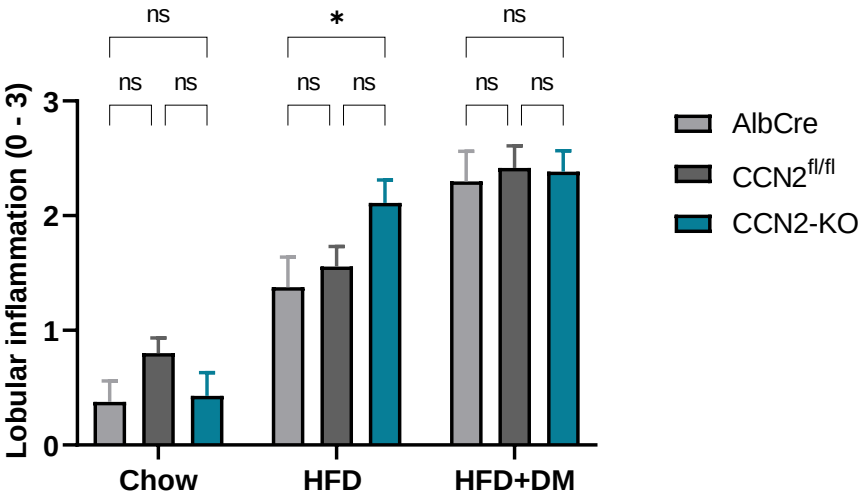

*Figure 4.23: Lobular inflammation scored according to the NAS criteria. Data shown as mean ± SEM; n = 7 - 13. * p-value ≤ 0.05 for comparison of mouse sub-strains within the same "diet" subgroup using two-way ANOVA with Tukey's correction for multiple comparisons. ns, not significant.*

B) Assessment of portal inflammation

Portal inflammation was scored on H&E-stained tissue according to the Brunt criteria (0 = absent, 1 = mild, 2 = moderate, or 3 = severe) by an independent anatomical pathologist (*Figure 4.24* and *Table 4.7*). The HFD+DM groups had the highest degree of portal inflammation, which was graded as moderate (AlbCre: 2.2 ± 0.3, CCN2$^{fl/fl}$: 2.3 ± 0.2, and CCN2-KO: 2.5 ± 0.2). The HFD groups had a mild degree of portal inflammation. The Chow groups all had low levels of portal inflammation. There was no effect from the CCN2-KO on the degree of portal inflammation.

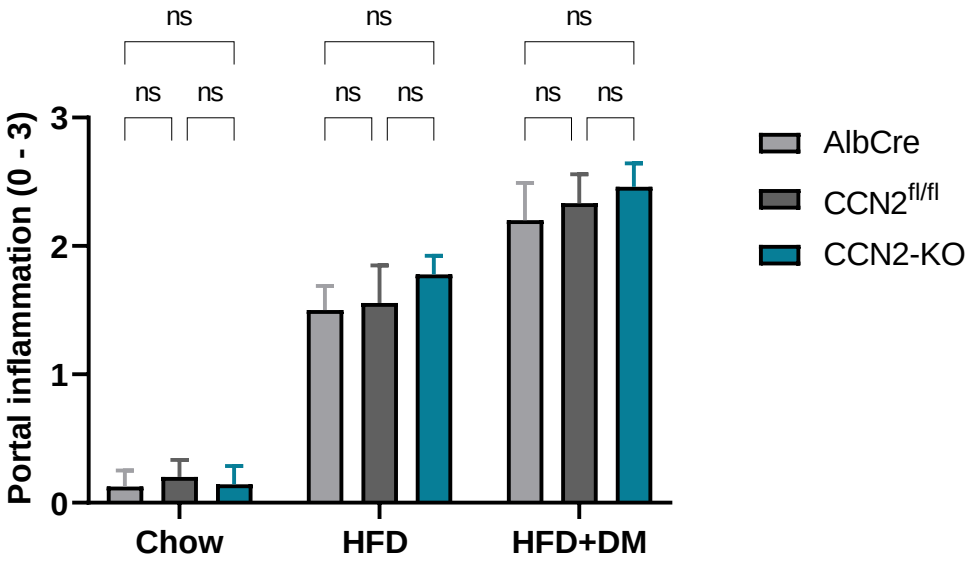

Figure 4.24: Portal inflammation scored according to the Brunt criteria. Data shown as mean ± SEM; n = 7 - 13. ns (not significant), p-value > 0.05 for comparison of mouse sub-strains within the same "diet" subgroup using two-way ANOVA with Tukey's correction for multiple comparisons.

4.3.3.2.2 mRNA levels of inflammation markers from whole liver tissue

The mRNA levels of inflammation markers IL1B, CCL2, and TNF were measured (*Figure 4.25* and *Table 4.8*). Unlike the fibrosis markers, where the two control mouse sub-strains, AlbCre and CCN2$^{fl/fl}$, rendered similar results, there was a clear distinction between the AlbCre HFD+DM and the CCN2$^{fl/fl}$ HFD+DM groups across all three inflammation genes: the AlbCre HFD+DM mice displayed significantly higher mRNA levels of IL1B, CCL2 and TNF compared with the CCN2$^{f/fl}$ HFD+DM mice. The CCN2-KO HFD+DM mice also had significantly lower expression of all three genes compared with the AlbCre HFD+DM mice, and in addition, had reduced expression of CCL2 compared with the CCN2$^{fl/fl}$ HFD+DM mice, but not IL1B or TNF.

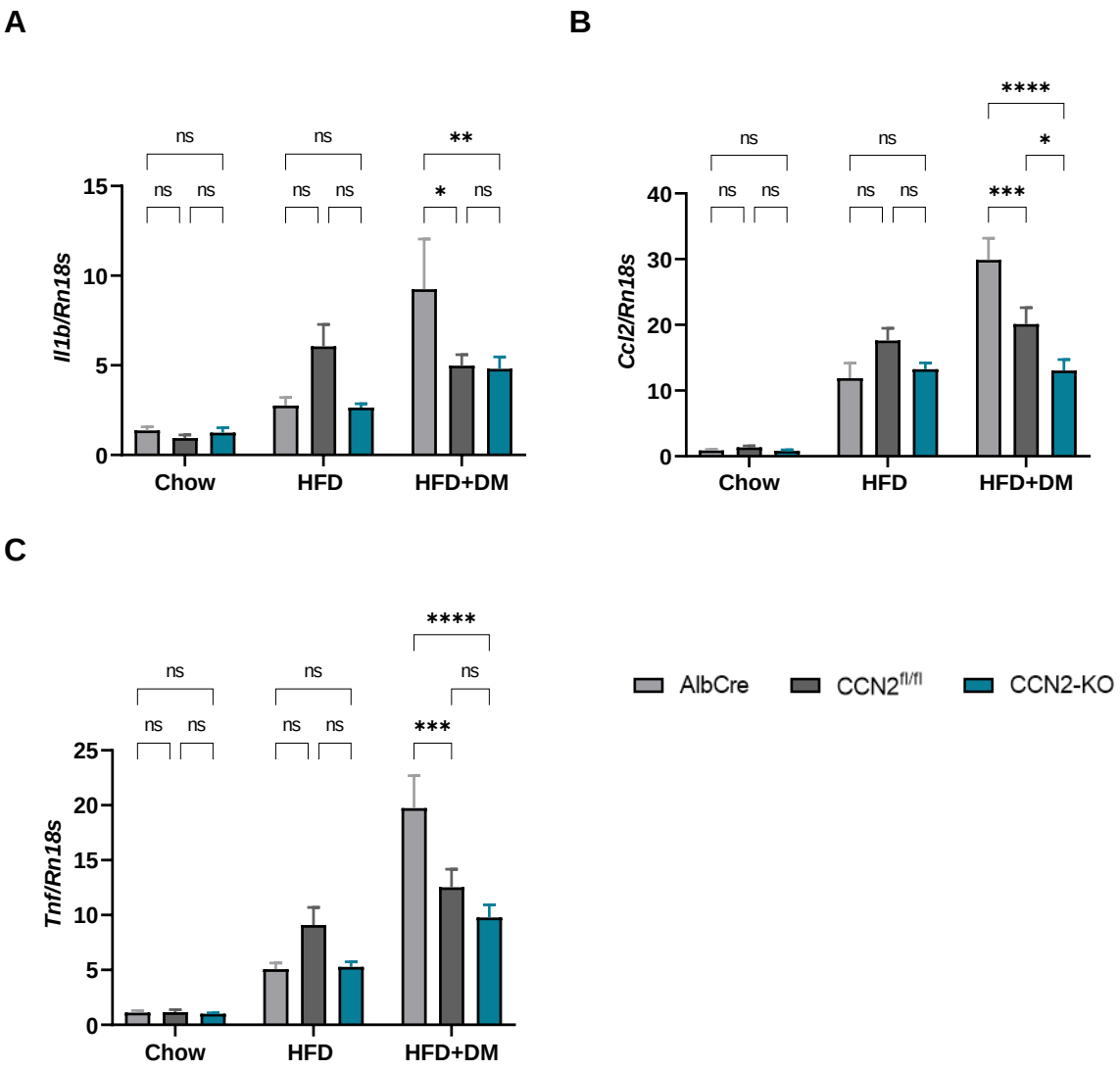

*Figure 4.25: mRNA levels of inflammation markers Il1b (A), Ccl2 (B), and Tnf (C). Data shown as mean ± SEM; n = 8 - 13. * p-value ≤ 0.05, ** p-value ≤ 0.01, *** p-value ≤ 0.001 or **** p-value ≤ 0.0001 for comparison of mouse sub-strains within the same "diet" subgroup using two-way ANOVA with Tukey's correction for multiple comparisons. Ccl2, C-C motif chemokine ligand 2; Il1b, interleukin-1β; Rn18s, 18S ribosomal RNA; Tnf, tumour necrosis factor α; ns, not significant.*

4.3.3.3 The effects of hepatocyte CCN2 deletion on hepatocyte ballooning

4.3.3.3.1 Assessment of hepatocyte ballooning by histology

The development of hepatocyte ballooning is the pathognomonic histological feature of NASH[80]. Ballooning was scored on H&E-stained tissue according to the NAS criteria (0 = absent, 1 = few, or 2 = many) by an independent anatomical pathologist (*Figure 4.26* and *Table 4.7*). The HFD+DM groups had the highest degree of ballooning, the HFD groups had an intermediary level, and the Chow groups had no ballooning present. There was no effect from the CCN2-KO on hepatocyte ballooning.

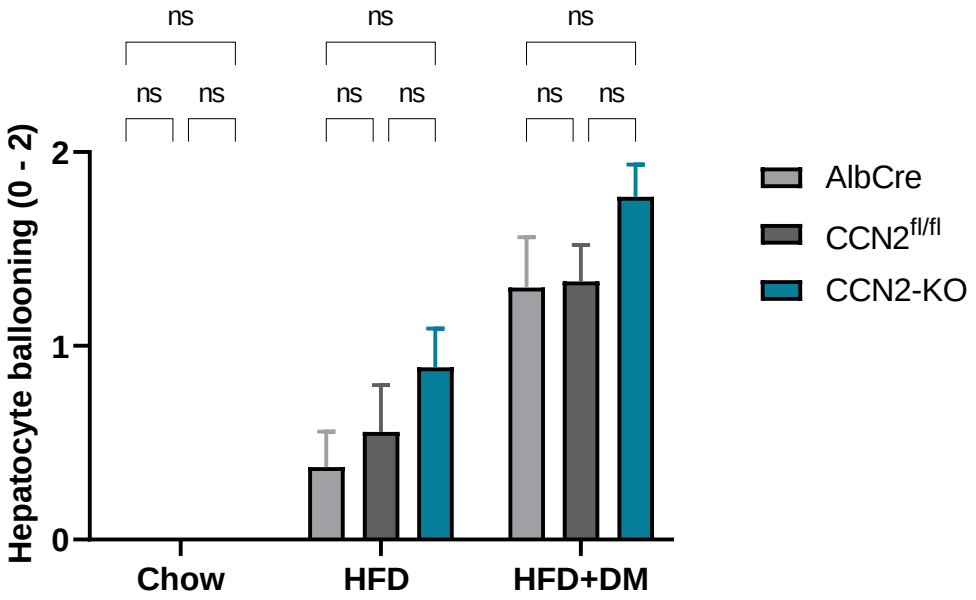

Figure 4.26: Hepatocyte ballooning scored according to the NAS criteria. Data shown as mean ± SEM; n = 7 - 13. ns (not significant), p-value > 0.05 for comparison of mouse sub-strains within the same "diet" subgroup using two-way ANOVA with Tukey's correction for multiple comparisons.

4.3.3.4 The effects of hepatocyte CCN2 deletion on liver steatosis

4.3.3.4.1 Assessment of liver steatosis by histology

Steatosis was scored on H&E-stained tissue according to the NAS criteria (0 = < 5%, 1 = 5 - 33%, 2 = 34 - 66%, or 3 = > 66%) by an independent anatomical pathologist (*Figure 4.27* and *Table 4.7*). All Chow groups had < 5% steatosis, whereas all mice fed a high fat diet (HFD and HFD+DM groups) had very high levels of steatosis. There was no effect from the CCN2-KO on the degree of steatosis.

4.3.3.4.2 Measurement of liver triglycerides

Triglycerides were extracted from whole liver tissue and measured using a colorimetric assay[315,316]. High fat fed mice (HFD and HFD+DM groups) had higher amounts of triglyceride compared with Chow groups (*Figure 4.28*). The CCN2-KO HFD+DM group had approximately one third more triglyceride content compared with the AlbCre HFD+DM and CCN2$^{fl/fl}$ HFD+DM groups (AlbCre: 51.4 ± 2.1, CCN2$^{fl/fl}$: 56.2 ± 1.7, and CCN2-KO: 78.2 ± .5).

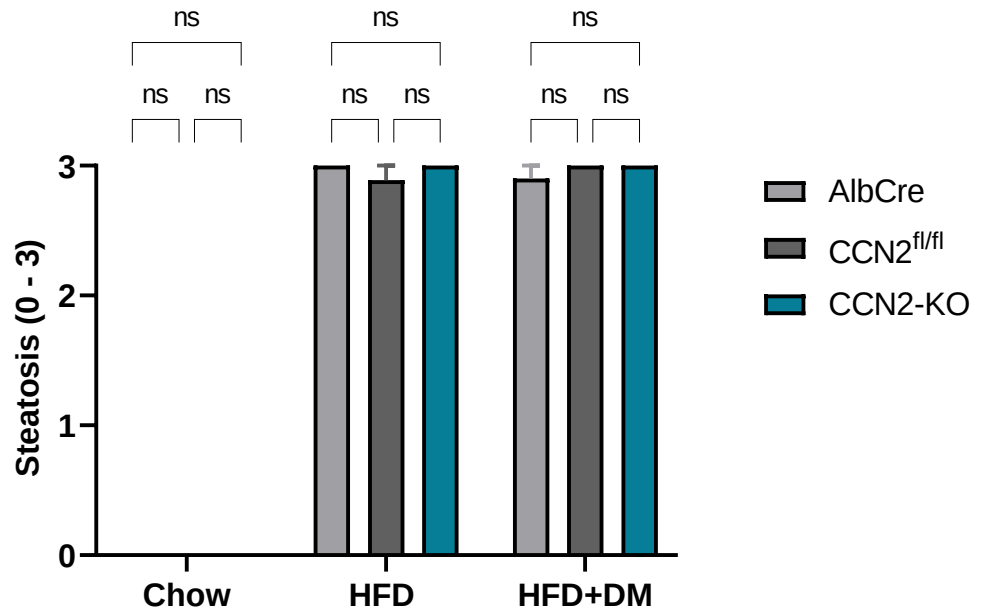

Figure 4.27: Steatosis scored according to the NAS criteria. Data shown as mean ± SEM; n = 7 - 13. ns (not significant), p-value > 0.05 for comparison of mouse sub-strains within the same "diet" subgroup using two-way ANOVA with Tukey's correction for multiple comparisons.

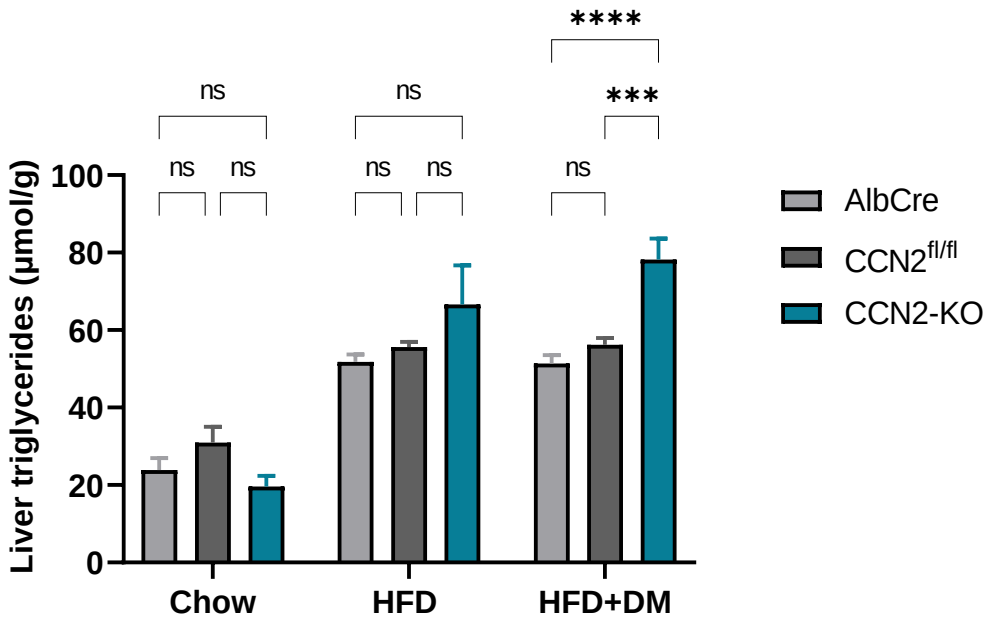

*Figure 4.28: Amount of liver triglycerides. Data shown as mean ± SEM; n = 8 - 13. *** p-value ≤ 0.001 or **** p-value ≤ 0.0001 for comparison of mouse sub-strains within the same "diet" subgroup using two-way ANOVA with Tukey's correction for multiple comparisons. ns, not significant.*

4.3.3.5 The effects of hepatocyte CCN2 deletion on the NAS

The NAS is calculated by the addition of scores for lobular inflammation, hepatocyte ballooning, and steatosis. As expected, the HFD+DM mice had the highest NAS, the HFD mice had an intermediary score, and the Chow mice had the lowest score (*Figure 4.29* and *Table 4.7*). Again, there was no effect observed from the CCN2-KO of this composite outcome, except in the HFD groups where the CCN2-KO HFD mice had a slightly higher NAS compared with the AlbCre HFD group but not the $CCN2^{fl/fl}$ HFD group. Representative images of the H&E-stained tissue from which the NAS was scored are shown in *Figure 4.30*.

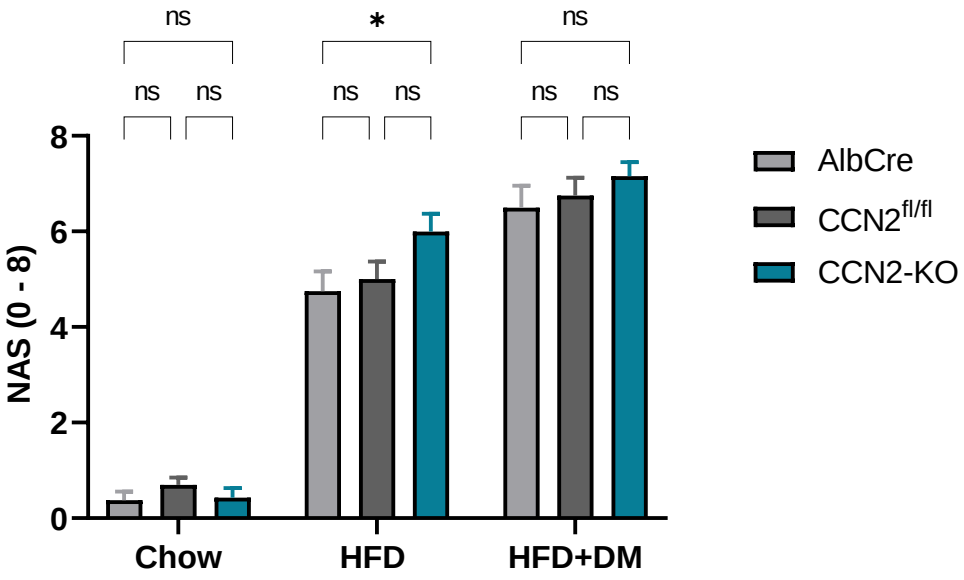

*Figure 4.29: NAS score. Data shown as mean ± SEM; n = 7 - 13. *, p-value ≤ 0.05 for comparison of mouse sub-strains within the same "diet" subgroup using two-way ANOVA with Tukey's correction for multiple comparisons. ns, not significant.*

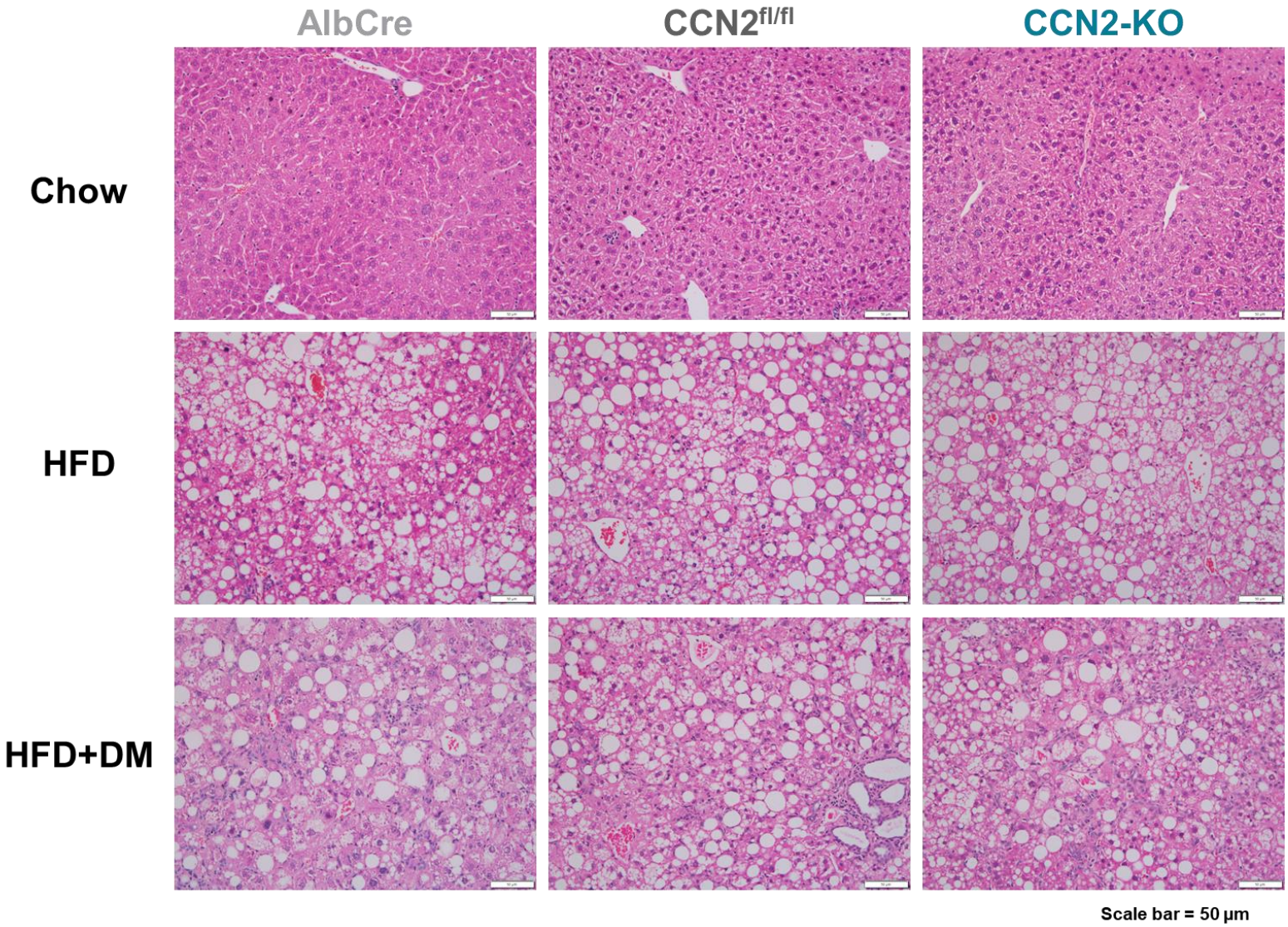

Figure 4.30: Representative histological images of H&E-stained liver tissue (200x magnification).

Table 4.7: Components of the Brunt and NAS criteria.

	Chow			HFD			HFD+DM		
	AlbCre	**CCN2$^{fl/fl}$**	**CCN2-KO**	**AlbCre**	**CCN2$^{fl/fl}$**	**CCN2-KO**	**AlbCre**	**CCN2$^{fl/fl}$**	**CCN2-KO**
Fibrosis (0 - 4)	0.0 ± 0.0	0.0 ± 0.0	0.0 ± 0.0	1.9 ± 1.1	1.8 ± 0.3	2.3 ± 0.2	2.8 ± 0.2	2.6 ± 0.2	2.8 ± 0.2
Lobular Inflammation (0 - 3)	0.4 ± 0.2	0.8 ± 0.1	0.4 ± 0.2	1.4 ± 0.3	1.6 ± 0.2	2.1 ± 0.2	2.3 ± 0.3	2.4 ± 0.2	2.4 ± 0.2
Portal Inflammation (0 - 3)	0.1 ± 0.1	0.2 ± 0.1	0.1 ± 0.1	1.5 ± 0.2	1.6 ± 0.3	1.8 ± 0.1	2.2 ± 0.3	2.3 ± 0.2	2.5 ± 0.2
Hepatocyte Ballooning (0 - 2)	0.0 ± 0.0	0.0 ± 0.0	0.0 ± 0.0	0.4 ± 0.2	0.6 ± 0.2	0.9 ± 0.2	1.3 ± 0.3	1.3 ± 0.2	1.8 ± 0.2
Steatosis (0 - 3)	0.0 ± 0.0	0.0 ± 0.0	0.0 ± 0.0	3.0 ± 0.0	2.9 ± 0.1	3.0 ± 0.0	2.9 ± 0.1	3.0 ± 0.0	3.0 ± 0.0
NAS (0 - 8)	0.4 ± 0.2	0.7 ± 0.2	0.4 ± 0.2	4.8 ± 0.4	5.0 ± 0.4	6.0 ± 0.4	6.5 ± 0.5	6.8 ± 0.4	7.2 ± 0.3

Data shown as mean ± SEM; n = 8 - 13. NAS, NAFLD activity score. Please note that as per the Methods, relevant p-values have been identified in the relevant Figures, not in the Table.

4.3.4 Potential biomarkers of NASH fibrosis in T2DM

4.3.4.1 mRNA levels of potential biomarkers

4.3.4.1.1 Other CCN family members

The mRNA levels of other CCN family members, CCN1 and CCN3 were measured (*Figure 4.31* and *Table 4.8*). CCN1 mRNA level was elevated in the AlbCre HFD+DM group, whilst the CCN2$^{fl/fl}$ and CCN2-KO HFD+DM groups had similar CCN1 levels to the basal state. In contrast, CCN3 mRNA level was highest in the CCN2$^{fl/fl}$ HFD+DM group, although this was not statistically significant.

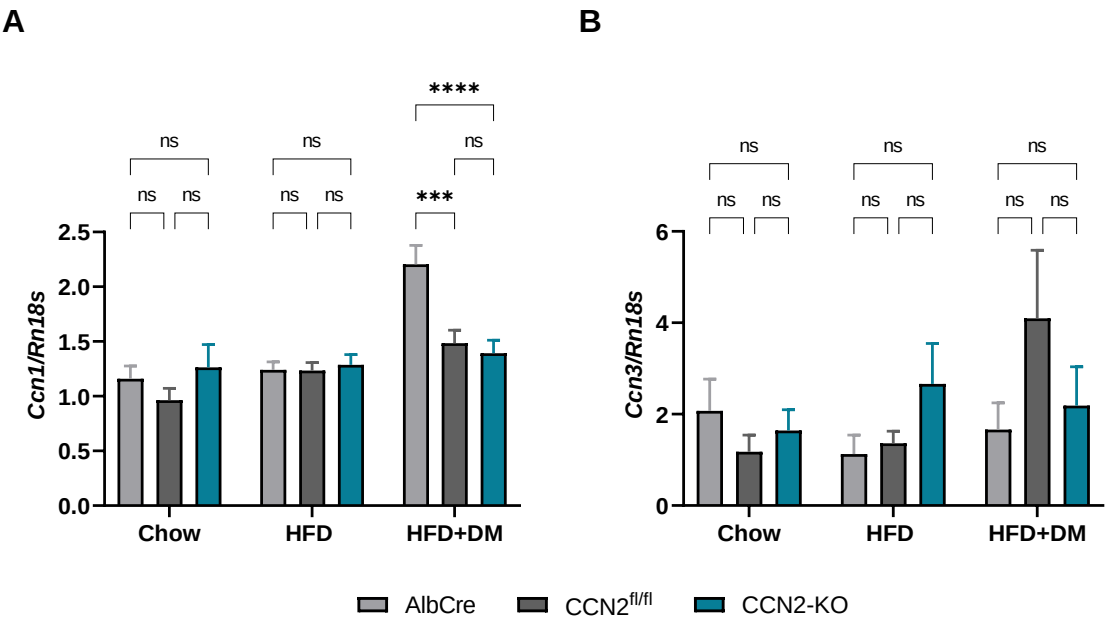

*Figure 4.31: mRNA levels of Ccn1 (A) and Ccn3 (B). Data shown as mean ± SEM; n = 8 - 13. *** p-value ≤ 0.001 or **** p-value ≤ 0.0001 for comparison of mouse sub-strains within the same "diet" subgroup using two-way ANOVA with Tukey's correction for multiple comparisons. Ccn1, cellular communication network 1; Ccn3, cellular communication network 3; Rn18s, 18S ribosomal RNA; ns, not significant.*

4.3.4.1.2 The DPP4 family

FAP is a marker of HSC activation, which are the predominant cells responsible for the deposition of ECM in the liver[67]. FAP is a member of the DPP4 family, and expresses not only DPP4 activity, but also collagenase activity[366]. There is increased mRNA level of DPP4 in liver tissue in the presence of liver disease[367], and circulating DPP4 activity is associated with hepatocyte apoptosis and fibrosis in humans with NASH and diabetes[86]. In this study, the mRNA level of FAP was numerically higher in the HFD groups compared with the Chow groups, with highest expression in the

HFD+DM, and provides further evidence of a fibrotic process in the model. DPP4 mRNA level was statistically lower in the CCN2-KO HFD+DM group compared with both the AlbCre HFD+DM and CCN2$^{fl/fl}$ HFD+DM groups (AlbCre: 1.1 ± 0.2, CCN2$^{fl/fl}$: 1.2 ± 0.1, and CCN2-KO: 0.7 ± 0.0), which may be consistent with lesser liver disease in the experimental group (*Figure 4.32* and *Table 4.8*).

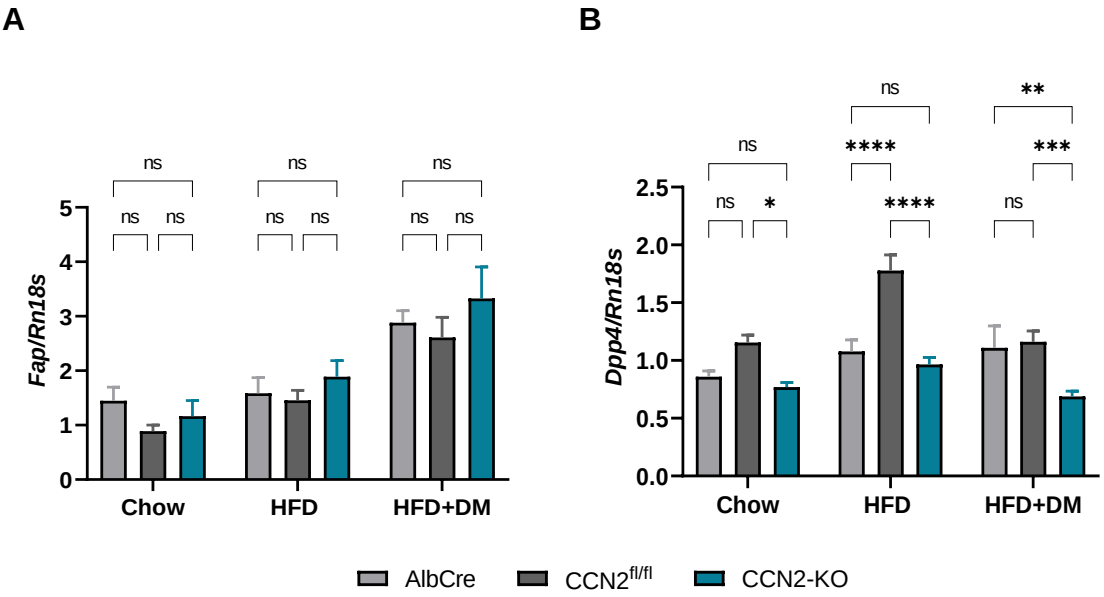

*Figure 4.32: mRNA levels of Fap (A) and Dpp4 (B). Data shown as mean ± SEM; n = 8 - 13. * p-value ≤ 0.05, ** p-value ≤ 0.01, *** p-value ≤ 0.001 or **** p-value ≤ 0.0001 for comparison of mouse sub-strains within the same "diet" subgroup using two-way ANOVA with Tukey's correction for multiple comparisons. Dpp4, dipeptidyl-peptidase 4; Fap, fibroblast activation protein; Rn18s, 18S ribosomal RNA; ns, not significant.*

Table 4.8: mRNA levels normalised to the housekeeper gene and expressed as fold change (reference group = AlbCre Chow + CCN2$^{fl/fl}$ Chow).

	Chow			HFD			HFD+DM		
	AlbCre	**CCN2$^{fl/fl}$**	**CCN2-KO**	**AlbCre**	**CCN2$^{fl/fl}$**	**CCN2-KO**	**AlbCre**	**CCN2$^{fl/fl}$**	**CCN2-KO**
Col1	1.2 ± 0.2	1.0 ± 0.1	1.3 ± 0.3	7.0 ± 1.4	14.8 ± 1.9	12.9 ± 2.4	15.1 ± 5.2	17.4 ± 3.4	9.6 ± 1.6
Col3	1.2 ± 0.2	1.0 ± 0.1	1.1 ± 0.2	6.5 ± 1.0	9.7 ± 1.0	8.6 ± 1.2	12.1 ± 3.1	12.0 ± 2.1	10.3 ± 2.0
Col4a1	1.4 ± 0.4	1.0 ± 0.1	1.0 ± 0.1	2.8 ± 0.4	4.7 ± 0.3	4.5 ± 0.5	6.0 ± 0.9	5.6 ± 0.7	4.6 ± 0.8
Col4a2	0.9 ± 0.1	1.1 ± 0.1	0.9 ± 0.1	2.3 ± 0.2	3.2 ± 0.1	3.0 ± 0.3	4.3 ± 0.6	4.5 ± 0.5	3.4 ± 0.5
Col6	1.1 ± 0.2	1.0 ± 0.1	1.4 ± 0.3	3.5 ± 0.5	6.1 ± 0.7	5.8 ± 0.6	6.1 ± 1.1	8.6 ± 1.2	5.8 ± 0.9
Tgfb1	1.0 ± 0.1	1.1 ± 0.1	0.9 ± 0.1	2.4 ± 0.2	4.8 ± 0.5	2.9 ± 0.3	5.2 ± 0.9	4.5 ± 0.4	3.2 ± 0.3
Fn1	1.0 ± 0.1	1.0 ± 0.1	0.9 ± 0.1	1.0 ± 0.1	1.7 ± 0.1	1.0 ± 0.1	1.3 ± 0.2	1.3 ± 0.1	1.0 ± 0.1
Acta2	1.5 ± 0.3	1.0 ± 0.2	2.0 ± 0.5	1.6 ± 0.4	1.9 ± 0.2	3.0 ± 0.8	2.6 ± 0.3	3.1 ± 0.5	2.6 ± 0.5
Timp1	1.7 ± 0.5	1.2 ± 0.3	0.9 ± 0.2	23.2 ± 4.2	44.6 ± 7.5	46.9 ± 5.3	51.7 ± 9.2	56.6 ± 10.4	41.6 ± 8.9
Il1b	1.4 ± 0.2	0.9 ± 0.2	1.2 ± 0.3	2.8 ± 0.5	6.1 ± 1.2	2.6 ± 0.2	9.2 ± 2.8	5.0 ± 0.6	4.8 ± 0.7
Ccl2	0.9 ± 0.2	1.4 ± 0.2	0.8 ± 0.2	11.9 ± 2.3	17.6 ± 1.8	13.2 ± 1.0	29.9 ± 3.3	20.1 ± 2.5	13.1 ± 1.7
Tnf	1.1 ± 0.2	1.2 ± 0.2	1.0 ± 0.1	5.1 ± 0.6	9.1 ± 1.6	5.3 ± 0.5	19.7 ± 3.0	12.5 ± 1.6	9.8 ± 1.1
Ccn1	1.2 ± 0.1	1.0 ± 0.1	1.3 ± 0.2	1.2 ± 0.1	1.2 ± 0.1	1.3 ± 0.1	2.2 ± 0.2	1.5 ± 0.1	1.4 ± 0.1
Ccn3	2.1 ± 0.7	1.2 ± 0.4	1.6 ± 0.5	1.1 ± 0.4	1.4 ± 0.3	2.7 ± 0.9	1.7 ± 0.6	4.1 ± 1.5	2.2 ± 0.8
Dpp4	0.9 ± 0.0	1.2 ± 0.1	0.8 ± 0.0	1.1 ± 0.1	1.8 ± 0.1	1.0 ± 0.1	1.1 ± 0.2	1.2 ± 0.1	0.7 ± 0.0
Fap	1.4 ± 0.3	0.9 ± 0.1	1.2 ± 0.3	1.6 ± 0.3	1.5 ± 0.2	1.9 ± 0.3	2.9 ± 0.2	2.6 ± 0.4	3.3 ± 0.6

Data shown as mean ± SEM; n = 8 - 13. *Acta2*, α smooth muscle actin; *Ccl2*, C-C motif chemokine ligand 2; *Ccn1*, cellular communication network 1; *Ccn3*, cellular communication network 3; *Col1*, collagen-I; *Col3*, collagen-III; *Col4a1*, collagen-IVα1; *Col4a2*, collagen-IVα2; *Col6*, collagen-VI; *Dpp4*, dipeptidyl-peptidase 4; *Fap*, fibroblast activation protein; *Fn1*, fibronectin; *Il1b*, interleukin-1β; *Tgfb1*, transforming growth factor β1; *Timp1*, tissue inhibitor of metalloproteinase 1; *Tnf*, tumour necrosis factor α. Please note that as per the Methods, relevant p-values have been identified in the relevant Figures, not in the Table.

4.3.4.2 Plasma cytokeratin-18

CK-18 has been proposed as a potential biomarker for NASH fibrosis. Plasma concentrations of CK-18 were highest in the HFD+DM groups and were progressively lower in each of the HFD groups and the Chow groups of the same mouse sub-strain (statistics comparing different "diet" groups not shown; *Figure 4.33*). The CCN2-KO HFD+DM group had significantly lower concentration of CK-18 compared with the AlbCre HFD+DM group but not the $CCN2^{fl/fl}$ HFD+DM group.

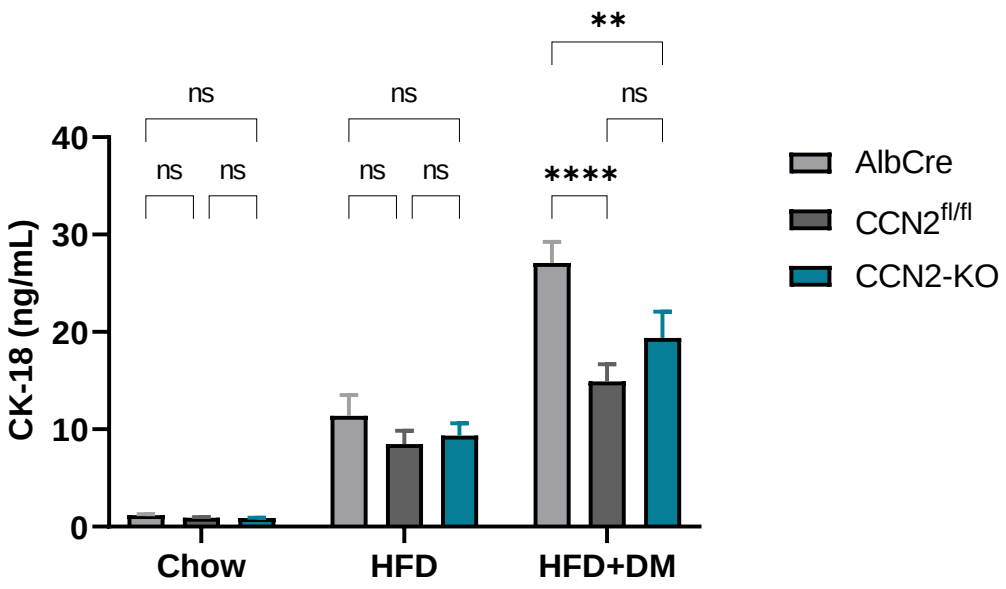

*Figure 4.33: Plasma cytokeratin-18 quantification. Data shown as mean ± SEM; n = 8 - 13. ** p-value ≤ 0001 or **** p-value ≤ 0.0001 for comparison of mouse sub-strains within the same "diet" subgroup using two-way ANOVA with Tukey's correction for multiple comparisons. CK-18, cytokeratin-18; ns, not significant.*

4.3.5 Pre-clinical *in vivo* mouse imaging

4.3.5.1 Liver ultrasound

It has been reported in the literature that liver ultrasound can be used as a novel non-invasive method for assessing liver fibrosis in mice[301,303] but unfortunately attempts to replicate this were unsuccessful. The recommended ultrasound images were captured according to the published methods; however, the analysis of the data is complex and requires specialised software and external assistance. Ultrasound images taken at week 25 of high fat fed mice demonstrated hyperechoic liver tissue and hepatomegaly. Representative images are shown in *Figure 4.34*.

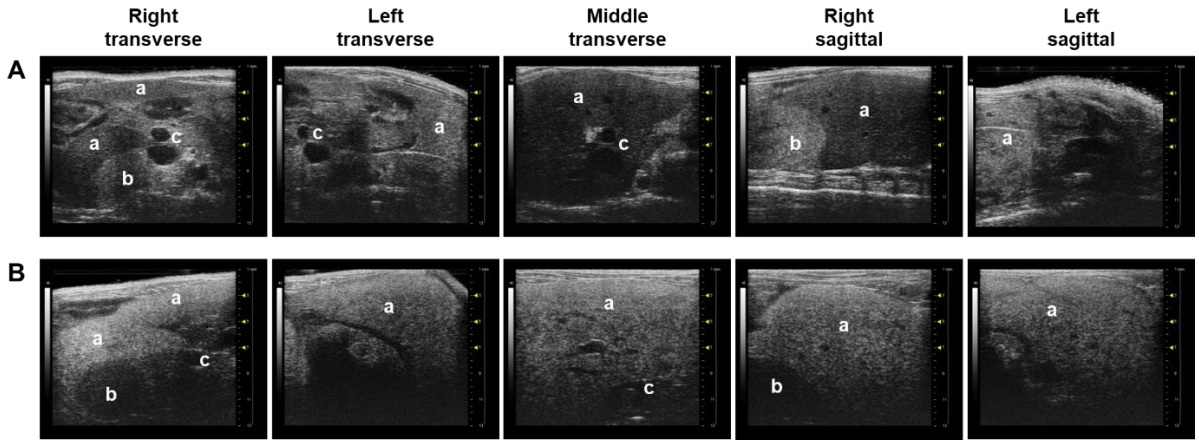

Figure 4.34: Representative liver ultrasound images taken at week 25 of a chow fed mouse (A) and an HFD+DM mouse (B). a, liver tissue; b, right kidney; c, blood vessels.

4.3.5.2 Liver MRI

The initial plan was to perform serial liver MRIs at week 15 and week 25 of the study, to explore novel methods of assessing liver fibrosis. However, at week 15, high fat fed mice were already at the upper end of the weight limit for the MRI chamber, and thus no serial MRIs were performed. T1-weighted MRI images taken at week 15 of high fat fed mice demonstrated hyperintensity of the liver tissue, hepatomegaly and increased subcutaneous fat. Representative images are shown in *Figure 4.35*.

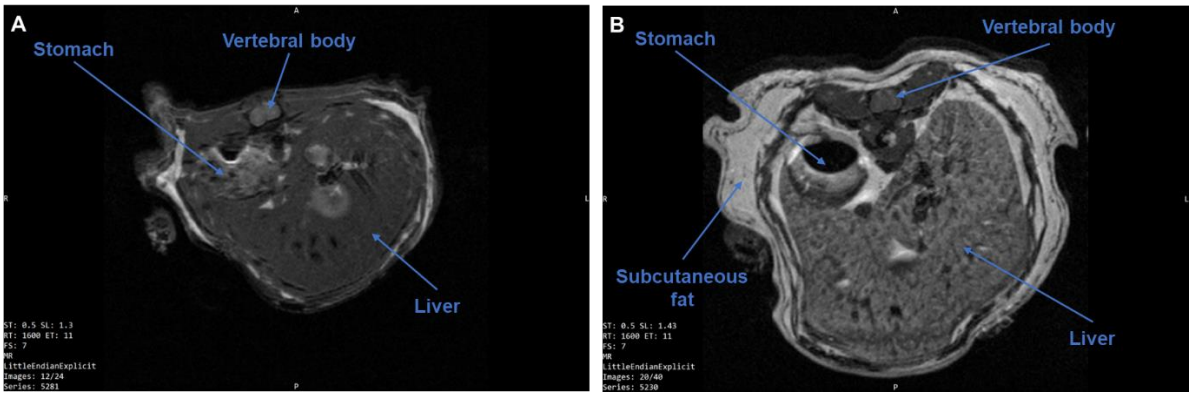

Figure 4.35: Representative T1 axial MRI images taken at week 15 of a chow fed mouse (A) and a high fat fed mouse (B).

4.4 Discussion

4.4.1 Summary of main findings

The CCN2 Study demonstrated that targeting hepatocyte CCN2 provided some protection from the development of NASH fibrosis induced by high fat feeding followed by diabetes. Quantitative histological analysis showed a reduced amount of liver fibrosis in the CCN2-KO HFD+DM mice compared with the control sub-strain mice (AlbCre HFD+DM and $CCN2^{fl/fl}$ HFD+DM groups), with supporting data from decreased mRNA levels of fibrosis markers in liver tissue. There were no differences observed in the CCN2-KO HFD+DM mice in the components of the NAS or Brunt criteria, however these scoring systems have not been validated in mice. There were reduced liver inflammation markers and increased liver fat in the CCN2-KO HFD+DM mice. These findings were in the absence of any observed systemic or metabolic changes in the CCN2-KO mice.

4.4.2 Prevention of hepatic fibrosis with deletion of hepatocyte CCN2

The exact mechanisms by which deletion of hepatocyte CCN2 protects the liver from fibrogenesis in this pre-clinical model is unclear. CCN2 is a well-recognised mediator of the fibrotic process, including in the liver, as it activates HSCs and regulates ECM production[261,274]. Recently published research by this laboratory demonstrated protection from NASH fibrosis using systemic administration of a neutralising polyclonal antibody against CCN2[144]. This current study has now identified a similar finding of attenuated fibrotic change, when targeting hepatocyte CCN2 with genetic manipulation.

There was concomitant inhibition of mRNA levels of key collagen and profibrotic genes. There were significant reductions in collagen-I and -VI in the CCN2-KO HFD+DM mice. Collagen-I and -VI are the main collagens deposited in increased fibrosis. Similar results were identified in the neutralising polyclonal CCN2 antibody study[144]. Collagen-VI production is tightly linked to activated HSCs and has autocrine effects. It is unclear in this study whether CCN2 is inducing changes in collagen-VI via direct effects on hepatocytes or indirect effects on HSCs. Further studies assessing protein levels of the collagens are needed, including by Western immunoblot and/or immunohistochemistry.

It has previously been reported that one potential mechanism by which CCN2 promotes fibrosis is through the inhibition of ECM degradation by increasing expression of TIMP1[273]. This study demonstrated a 20 - 26% reduction in TIMP1 mRNA level in the CCN2-KO HFD+DM group, however this did not reach statistical significance. Nevertheless, changes in TIMP1 regulated by CCN2 may still have a minor effect on development of liver fibrosis and further studies in this area are required.

Whilst this thesis has primarily focussed on describing the phenotype of the CCN2-KO HFD+DM mice, it is important to consider future studies for investigation of potential mechanisms that may explain the findings. The MAPK signalling pathways have been implicated in matrix regulation, and CCN2 is known to activate these cascades[368]. Proliferation of HSCs is promoted by activation of ERK and JNK, whilst p38 is a potent inhibitor[153,157,160]. Investigation of these pathways in the study of the neutralising polyclonal CCN2 antibody showed reduction of ERK phosphorylation in mice with reduced liver fibrosis[144]. Future studies for The CCN2 Study will include investigation of the MAPK pathways through assessment of protein levels of total and phosphorylated ERK, JNK and p38 by Western immunoblot.

It is unknown whether the hepatocyte deletion of CCN2 reduces the signal to HSCs. Activated HSCs are the cell type driving ECM production and fibrosis in the liver and ACTA2 is frequently used as a marker of activated HSCs[369]. In this study, the mRNA level of ACTA2 was not reduced in the CCN2-KO HFD+DM mice, however the protein level was not assessed. It may be that ACTA2 undergoes post-transcriptional modifications and is more heavily regulated at the protein level than the mRNA level. Analysis of ACTA2 by Western immunoblot and/or immunohistochemistry should be assessed to determine whether reductions in fibrosis are related to reduction in the overall number of activated HSCs.

4.4.3 Reduced hepatic inflammation with hepatocyte CCN2 deletion

CCN2 is known to have pro-inflammatory effects and is implicated in multiple inflammatory disorders. CCN2 can both induce and be induced by inflammatory cytokines and chemokines[252,260]. The role of CCN2 in the inflammation of NASH is unclear. This study showed that hepatocyte deletion of CCN2 decreased CCL2 mRNA

level compared with both the AlbCre and CCN2$^{fl/fl}$ groups, and IL1B and TNF were reduced compared with the AlbCre but not CCN2$^{fl/fl}$ groups. This data suggests that CCN2 also contributes to the inflammatory change in this model, and related signalling pathways, such as NF-κB, need to be further investigated.

Assessment of liver tissue histopathology with standard H&E staining did not reveal a difference in lobular or portal inflammatory cell infiltration in the CCN2-KO HFD+DM mice. This was reported as per the NAS and Brunt criteria, respectively, by an independent anatomical pathologist[80,81]. It is likely that this method of assessment is not sensitive enough to detect small changes in inflammation, and further assessment using immunohistochemistry may be required to detect more subtle changes. Evaluation of macrophage involvement, using F4/80 or CD68 staining, is especially relevant, given the changes in CCL2 mRNA level identified in this study. CCL2 is a key chemokine regulating migration and infiltration of monocytes and macrophages[370].

4.4.4 Increased hepatic steatosis with hepatocyte CCN2 deletion

There is no literature to suggest that hepatocyte CCN2 directly affects liver fat. Instead, the increased amount of triglycerides measured in the livers of CCN2-KO HFD+DM mice is hypothesised to be reflective of the lesser severity of liver fibrosis. As liver fibrosis becomes more advanced, there may be resolution of steatosis, in a process called “burnt out” NASH[371,372]. However, a significant amount of fat, usually more than the diagnostic 5%, remains, and thus a difference on a scale of 0 - 3 using the NAS/Brunt criteria may not necessarily be expected.

4.4.5 Liver tissue CCN2 levels with hepatocyte CCN2 deletion

In the mice with hepatocyte CCN2 deletion, the CCN2 mRNA level was non-significantly reduced by 25 - 43% in the basal state, improving to a significant reduction of 56 - 65% in the HFD+DM group. The four-fold increase in CCN2 mRNA level from Chow to HFD+DM in each of the control mouse sub-strains indicates that CCN2 is robustly induced in this model. The hepatocyte deletion of CCN2 partially prevents the induction of CCN2, which increased by only two-fold in these mice. The protein level of CCN2 was reduced by 25 - 45% in the CCN2-KO HFD+DM group compared with the control mouse sub-strains. CCN2 can be produced by all cell types in the liver and the persistent expression of CCN2 in these mice is hypothesised to be derived from

non-hepatocyte liver cells, which account for ~20% of liver volume[60,274]. Despite not achieving a near-complete liver CCN2 deletion, this model has still produced a phenotype of improved liver fibrosis. It may be that achieving a higher reduction in liver CCN2 may more effectively prevent liver fibrosis.

4.4.6 Targeting CCN2 in other liver cells

The hepatocyte source of CCN2 was targeted in this study as hepatocytes are the most abundant cell type in the liver[60]. Another cell type of significant interest is the HSC. The activation and recruitment of an increased number of HSCs are important stages in the development of fibrosis. CCN2 is one of many mediators involved in this process, and is produced by all cell types in the liver, including by HSCs[274]. CCN2 is thought to have autocrine and paracrine effects in the liver, and thus targeting hepatocytes only may not be sufficient to completely prevent development of liver fibrosis. It has been shown here that liver CCN2 can still be induced in mice with a hepatocyte CCN2 deletion, suggesting that other sources may be involved. Targeting CCN2 in HSCs, either in addition to hepatocytes or independently, may offer better outcomes in prevention of liver fibrosis.

4.4.7 Absence of systemic effects of hepatocyte CCN2 gene deletion

The effect on the liver from the hepatocyte CCN2 deletion occurred in the absence of any systemic differences between the mouse sub-strains. The CCN2-KO mice exhibited similar metabolic outcomes compared with the AlbCre and $CCN2^{fl/fl}$ mice, including in weight, glycaemia, insulin resistance, body composition, organ weights, and circulating lipids.

4.4.8 Systemic differences in the two control sub-strain HFD+DM groups

In this study, the AlbCre HFD+DM group was systemically different to the $CCN2^{fl/fl}$ HFD+DM group. The AlbCre HFD+DM group had lower fat mass and higher lean mass, despite no statistical difference in the mean termination weight. These mice also had higher spleen, kidney, and heart mass when normalised to total body weight. Plasma ALP and CK-18 were higher, and albumin was lower, suggesting worse liver damage, but histological analysis did not identify a difference in fibrosis endpoints. The mRNA levels of inflammation markers were also significantly higher in the AlbCre HFD+DM group, compared with the $CCN2^{fl/fl}$ HFD+DM group. This constellation of

differences is challenging to explain. The mice were otherwise systemically well, with no indication of poor well-being to suggest an infective or inflammatory process. Another explanation may be inherent to the use of Cre transgene mice: it has been identified that Cre itself can produce phenotype changes, Cre can be active in undesired sites, and Cre activity can be mosaic[373]. These issues will be discussed in further detail in *Chapter 7*, along with the rationale for using two control sub-strains.

4.4.9 Conclusion

The CCN2 Study has confirmed previous findings that the combination of high fat feeding and diabetes leads to development of NASH with significant fibrosis. Using this model, it has been demonstrated that mice with hepatocyte CCN2 deletion developed less NASH fibrosis and reduced inflammation. These findings were in the absence of any systemic difference at baseline between the CCN2-KO mice and the AlbCre or $CCN2^{fl/fl}$ control mice. This data provides further evidence that CCN2 is increasingly a potential target for limiting progression of NASH fibrosis in the setting of T2DM and this has implications for development of potential therapeutic agents.

Chapter 5: Effects of hepatocyte-specific CCN1 gene knockout on the development of NASH fibrosis in a mouse model of high fat feeding and diabetes (The CCN1 Study)

5.1 Introduction

Cellular communication network factor 1 (CCN1) is a cysteine-rich matricellular protein involved in inflammation and tissue repair. CCN1 has antifibrotic properties and has been implicated in the regression of liver fibrosis through induction of senescence of activated HSCs[246]. This has three main effects: senescent cells can no longer proliferate to create more ECM-producing cells, senescent cells express the senescence-associated secretory phenotype (SASP) to up-regulate MMPs and down-regulate collagens and TGFβ1, and finally, senescent cells can be removed by natural killer cells to accelerate wound repair[246].

Clinical and pre-clinical studies have shown increased CCN1 at the mRNA and protein levels in fibrotic livers disease[286-288]. The hepatocyte-specific CCN1 gene knockout mouse has previously been used to study the role of CCN1, albeit in a model that lacked the metabolic features that are relevant to human NASH. However, the study elegantly showed that mice with hepatocyte-specific deletion of CCN1 exhibited more liver fibrosis and less HSC senescence, whilst overexpression of CCN1 led to reductions in liver fibrosis with more HSC senescence[286]. Confusion has arisen since the more recent publication of a study claiming CCN1 to be a positive regulator of NASH, although this study did not report on any fibrosis endpoints[287]. Further studies on the role of CCN1 in the development of NASH with fibrosis using relevant models are needed.

The study presented in this chapter uses a novel pre-clinical model, whereby the gene and environment interaction can be explored. The aim of the study was to examine whether homozygous gene deletion of hepatocyte CCN1 leads to a more severe NASH fibrosis phenotype compared to control mice exposed to high fat feeding and diabetes.

5.2 Methods

The Methods are described in detail in *Section 2.3* and a summary is provided here. This study used hepatocyte-specific CCN1 gene knockout mice (CCN1-KO), generated by Dr Xiaoyu Wang using the CreLoxP system, in the FaD model of NASH fibrosis developed previously by this laboratory. In brief, male control mice (AlbCre

and CCN1$^{fl/fl}$) and CCN1-KO mice were fed a high fat diet (45% kcal) for 15 weeks before the induction of diabetes with multiple low dose intraperitoneal injections of STZ (HFD+DM groups). Mice were then maintained for a further 10 weeks before termination. Additional mice from each of the three sub-strains were fed either standard chow (Chow groups) or high fat diet (HFD groups) for the duration of the study. Thus, there were nine groups in this study. Metabolic outcomes were measured, and routine plasma biochemistry analysed. The primary outcome was the development of NASH fibrosis, which was assessed histologically by PSR and H&E staining. The mRNA levels of fibrosis and inflammatory markers were measured using qPCR.

Unless otherwise specified, data is presented as mean ± SEM and analysed using a two-way ANOVA with Tukey's correction for multiple comparison. The statistical analyses presented in this chapter have focussed on the interactions between the three mouse sub-strains for the same "diet" (i.e., AlbCre HFD+DM vs CCN1$^{fl/fl}$ HFD+DM vs CCN1-KO HFD+DM). Interactions between the three "diets" have been tested within the two-way ANOVA (i.e., AlbCre Chow vs AlbCre HFD vs AlbCre HFD+DM), however the statistical results have not been routinely shown. This is because the FaD model has already been validated and published before[144,145], and replication of the model was not the primary focus of this current study. For reference, * has been used to denote comparisons between the three mouse sub-strains for the same "diet" and $^{\#}$ denotes comparisons between Chow vs HFD or HFD+DM for the same mouse sub-strain. AlbCre groups are depicted in light grey, CCN1$^{fl/fl}$ groups in dark grey and CCN1-KO groups in orange.

5.3 Results

5.3.1 Reduction in whole liver tissue CCN1 mRNA level in CCN1-KO mice

Successful deletion of the hepatocyte CCN1 gene was confirmed by measuring the mRNA level of CCN1 from whole liver tissue. The CCN1-KO mice fed a chow diet had an ~95% reduction in CCN1 mRNA level compared with the AlbCre and CCN1$^{fl/fl}$ Chow mice (*Figure 5.1*). There was a 93% reduction in the CCN1 mRNA level in the CCN1-KO HFD+DM mice compared with the AlbCre HFD+DM mice (0.13 ± 0.02 vs 1.83 ± 0.22, $p < 0.001$) and an 80% reduction when compared with the CCN1$^{fl/fl}$ HFD+DM mice (0.13 ± 0.02 vs 0.64 ± 0.10, $p = 0.022$). The residual amount of CCN1 detected in the CCN1-KO mice is hypothesised to be derived from non-hepatocyte liver cells.

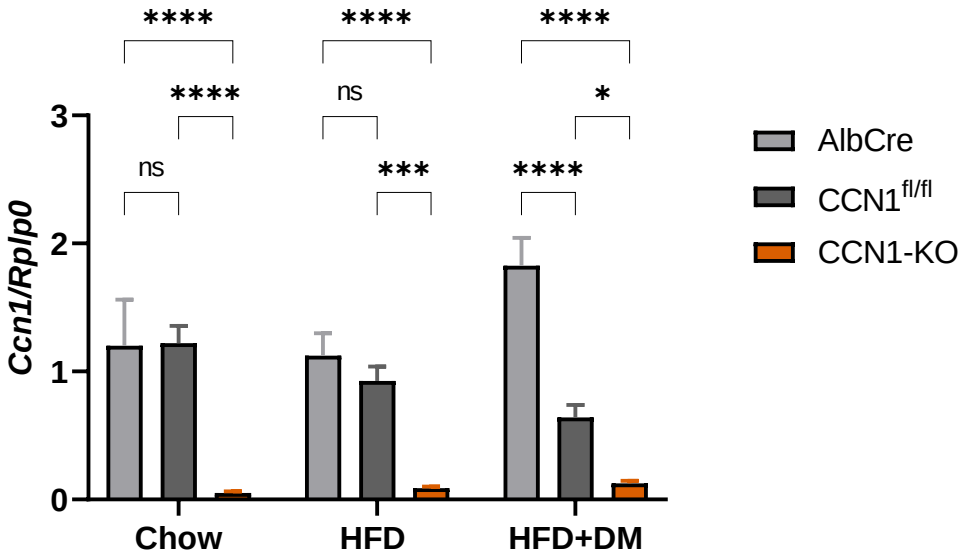

*Figure 5.1: Ccn1 mRNA levels in whole liver tissue measured by qPCR. Data shown as mean ± SEM as relative fold change of AlbCre Chow and CCN1$^{fl/fl}$ Chow groups; n = 8 - 14. * p-value ≤ 0.05, *** p-value ≤ 0.001 or **** p-value ≤ 0.0001 for comparison of mouse sub-strains within the same "diet" subgroup using two-way ANOVA with Tukey's correction for multiple comparisons. ns, not significant.*

5.3.2 Metabolic outcomes

5.3.2.1 Body weight

Mice were weighed weekly for the duration of the study (*Figure 5.2*). Chow fed mice (triangles) gradually gained weight consistent with normal growth and development. The HFD and HFD+DM mice quickly gained excess weight with high fat feeding. At week 16, diabetes was induced in the HFD+DM mice (circles) with 2 - 3 injections of low dose STZ. These mice had an expected and brief reduction in body weight for approximately three weeks before body weight plateaued in the AlbCre HFD+DM and CCN1$^{fl/fl}$ HFD+DM groups, and body weight was re-gained in the CCN1-KO HFD+DM mice. The HFD mice (squares) continued to gain weight throughout the study.

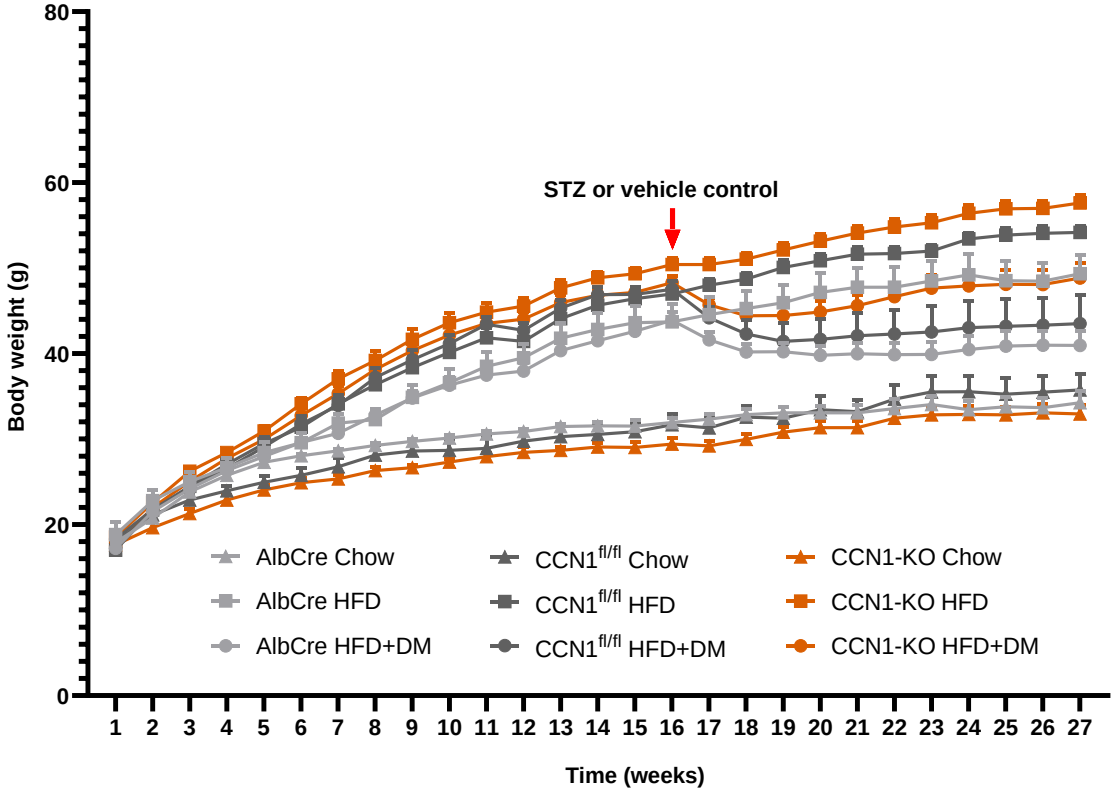

Figure 5.2: Weekly body weight per mouse group. Data shown as mean ± SEM; n = 8 - 14. STZ, streptozotocin.

At the end of the study, total weight gain was similar between all three Chow groups (*Figure 5.3*). However, there was significantly greater mean total weight gain in the CCN1-KO HFD mice compared with the AlbCre HFD mice, and in the CCN1-KO HFD+DM mice (31.25 ± 1.71 g) compared with the AlbCre HFD+DM (24.34 ± 1.76 g) and CCN1$^{fl/fl}$ HFD+DM mice (25.34 ± 3.03 g).

The mean body weights of the mice at termination are shown in *Table 5.1*. All HFD and HFD+DM mice were significantly heavier than Chow mice of the same mouse sub-strain and the HFD mice were also significantly heavier than the HFD+DM mice (statistics comparing different "diet" groups not shown). The CCN1-KO mice were numerically the heaviest of the HFD and HFD+DM subgroups, and this was statistically significant when compared with the corresponding AlbCre mice, but not the CCN1$^{fl/fl}$ mice of the same "diet" subgroup.

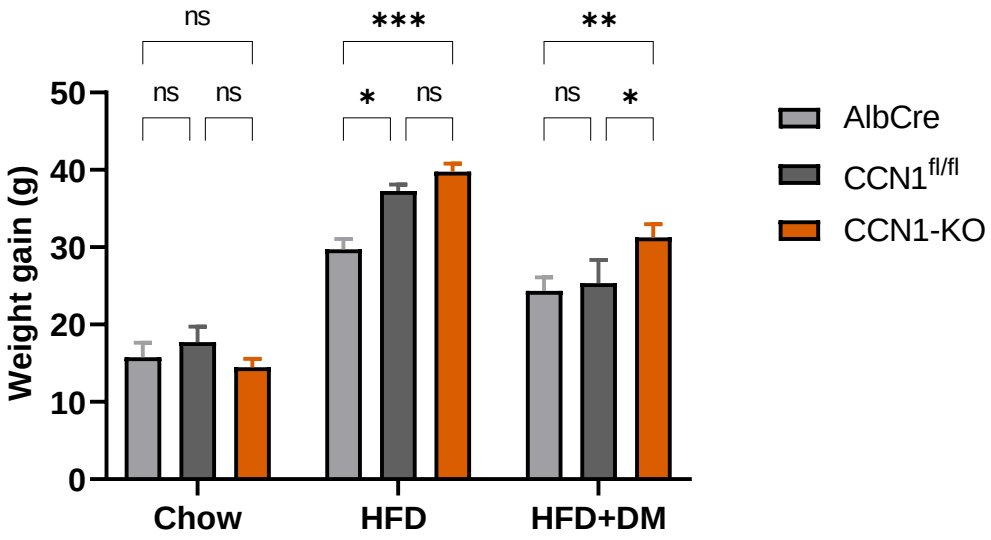

*Figure 5.3: Total body weight gain. Data shown as mean ± SEM; n = 8 - 14. * p-value ≤ 0.05, ** p-value ≤ 0.01 or *** p-value ≤ 0.001 for comparison of mouse sub-strains within the same "diet" subgroup using two-way ANOVA with Tukey's correction for multiple comparisons. ns, not significant.*

Table 5.1: Body weight (grams) at termination.

	Chow	HFD	HFD+DM
AlbCre	33.66 ± 1.57	48.54 ± 2.33	41.57 ± 1.82
CCN1$^{fl/fl}$	35.74 ± 1.76	54.28 ± 0.84	43.64 ± 3.31
CCN1-KO	32.13 ± 1.11	58.31 ± 0.89**	48.71 ± 1.718**

Data shown as mean ± SEM; n = 8 - 14. ** p-value ≤ 0.01 for comparison of AlbCre vs CCN1-KO within the same "diet" subgroup using two-way ANOVA with Tukey's correction for multiple comparisons.

5.3.2.2 Blood glucose levels

BGLs were measured weekly from week 16 to the end of the study. After induction of diabetes with STZ, mice in the HFD+DM groups (circles) developed hyperglycaemia (*Figure 5.4*). Despite starting at a similar baseline glucose level, the CCN1-KO HFD+DM mice (13 - 22 mmol/L) did not achieve the same severity of hyperglycaemia as the AlbCre HFD+DM and CCN1$^{fl/fl}$ HFD+DM mice (17 - 29 mmol/L). The Chow and HFD mice remained normoglycaemic.

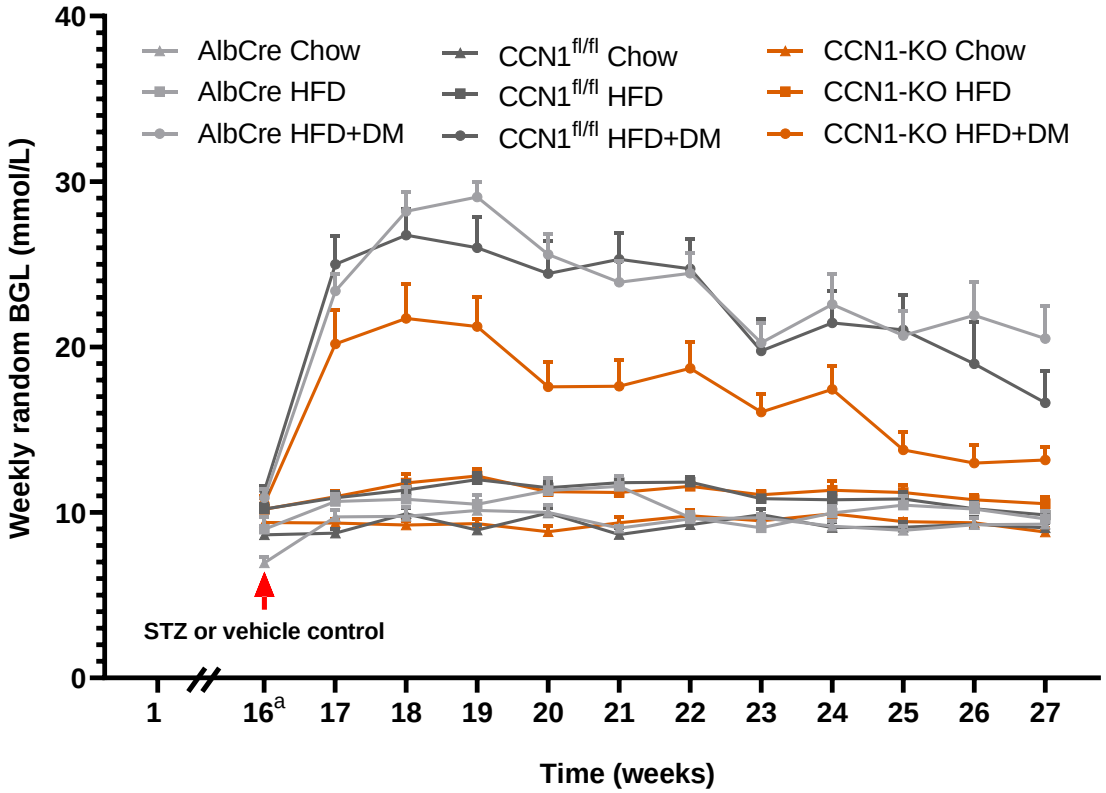

Figure 5.4: Weekly random blood glucose levels. Data shown as mean ± SEM; n = 8 - 14. BGL, blood glucose level; STZ, streptozotocin. [a] fasting BGL.

The mean of the weekly BGLs from week 17 to 27 are shown in *Table 5.2*. All HFD+DM groups had significantly higher mean BGL compared with the respective Chow and HFD groups of the same mouse sub-strain (statistics comparing different "diet" groups not shown). Mean BGLs in the HFD+DM mice ranged from 17 - 24 mmol/L, representing a moderate degree of hyperglycaemia without induction of severe catabolism. Notably, the mean BGL of the CCN1-KO HFD+DM group was significantly lower than both of the other HFD+DM groups but remained higher than the Chow and

HFD groups. There was no difference in mean BGLs between the Chow mice and the HFD mice which were maintained from 9 - 11 mmol/L.

Table 5.2: Mean random BGL (mmol/L) from week 17 to 27.

	Chow	HFD	HFD+DM
AlbCre	9.51 ± 0.17	10.34 ± 0.44	23.70 ± 0.19****
CCN1$^{fl/fl}$	9.28 ± 0.19	11.08 ± 0.23	22.74 ± 1.75***
CCN1-KO	9.38 ± 0.17	11.28 ± 0.26	17.27 ± 1.30

Data shown as mean ± SEM; n = 8 - 14. *** p-value ≤ 0.001 or **** p-value ≤ 0.0001 for comparison of AlbCre or CCN1$^{fl/fl}$ vs CCN1-KO within the same "diet" subgroup using two-way ANOVA with Tukey's correction for multiple comparisons. BGL, blood glucose level.

5.3.2.3 Evaluation of insulin resistance

5.3.2.3.1 Fasting whole blood insulin level at week 16

The fasting whole blood insulin level was measured using a commercial ELISA kit at week 16 of the study. This time-point was prior to induction of diabetes in the HFD+DM mice and therefore *Figure 5.5* shows either chow fed mice (Chow groups) or high fat fed mice (combination of mice allocated to the HFD or HFD+DM groups). Mice that were high fat fed for 15 weeks had already developed marked hyperinsulinaemia compared to standard chow fed mice. By this timepoint, the AlbCre ($p < 0.001$) and CCN1$^{fl/fl}$ ($p = 0.021$) high fat fed mice had a mean fasting BGL 2 - 3 mmol/L higher than their respective chow fed groups, although there was no significant difference in fasting BGL between the high fat fed groups.

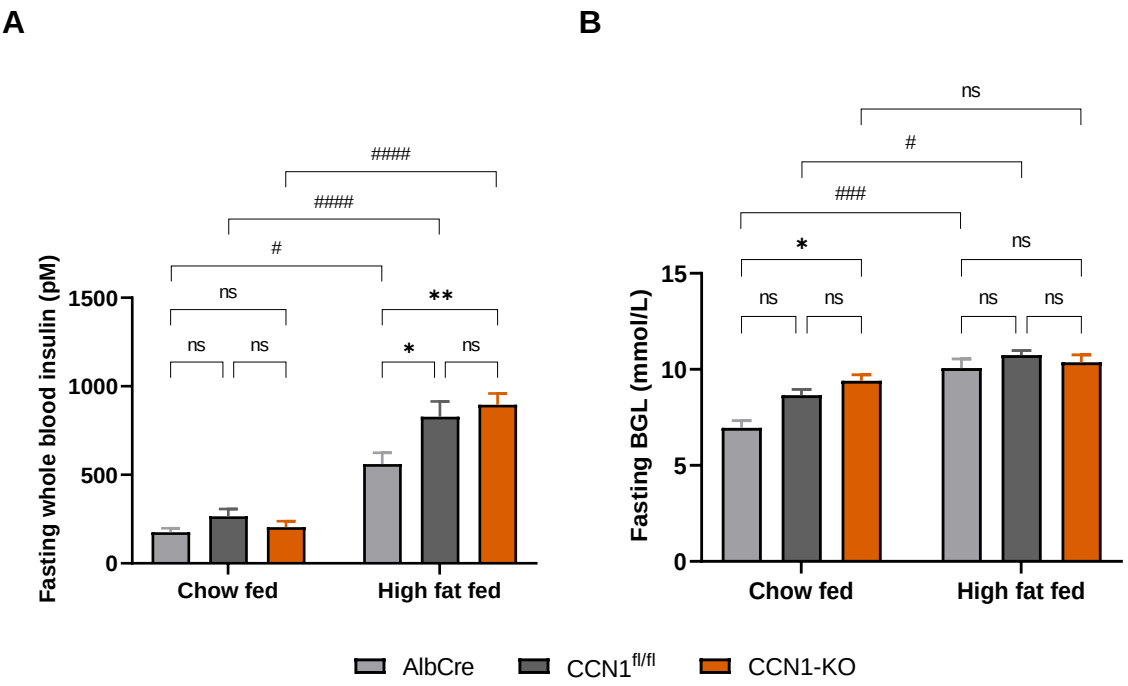

*Figure 5.5: Fasting whole blood insulin levels (A) and BGL (B) obtained at week 16 in mice fed either a chow or high fat diet. Data shown as mean ± SEM; n = 8 - 26. * p-value ≤ 0.05 or ** p-value ≤ 0.01 for comparison of mouse sub-strains within the same "diet" subgroup, or # p-value ≤ 0.05, ### p-value ≤ 0.001 or #### p-value ≤ 0.0001 for chow fed vs high fat fed within the same mouse sub-strain, using two-way ANOVA with Tukey's correction for multiple comparisons. BGL, blood glucose level; ns, not significant.*

5.3.2.3.2 Fasting plasma insulin and c-peptide levels at termination

Using commercial ELISA kits, insulin and c-peptide levels were measured from plasma obtained in the fasting state at termination (*Figure 5.6*). As expected, mice from the HFD groups exhibited marked hyperinsulinaemia across all three mouse sub-strains, with the highest level in the CCN1-KO group (statistically significant vs AlbCre but not $CCN1^{fl/fl}$). Mice from the HFD+DM groups had insulin levels that were similar to the Chow groups, and in the context of hyperglycaemia, was indicative of relative insulin deficiency (model of T2DM) rather than absolute insulin deficiency (model of T1DM). The insulin level in the CCN1-KO HFD+DM group (263 ± 49 pM) was approximately double that of the AlbCre HFD+DM (123 ± 14 pM) and $CCN1^{fl/fl}$ HFD+DM (141 ± 20 pM) groups, but this was not statistically significant. The c-peptide levels followed a similar pattern to the insulin levels, where the CCN1-KO HFD+DM mice had numerically higher c-peptide levels, but also a lesser degree of hyperglycaemia on the matched fasting BGL.

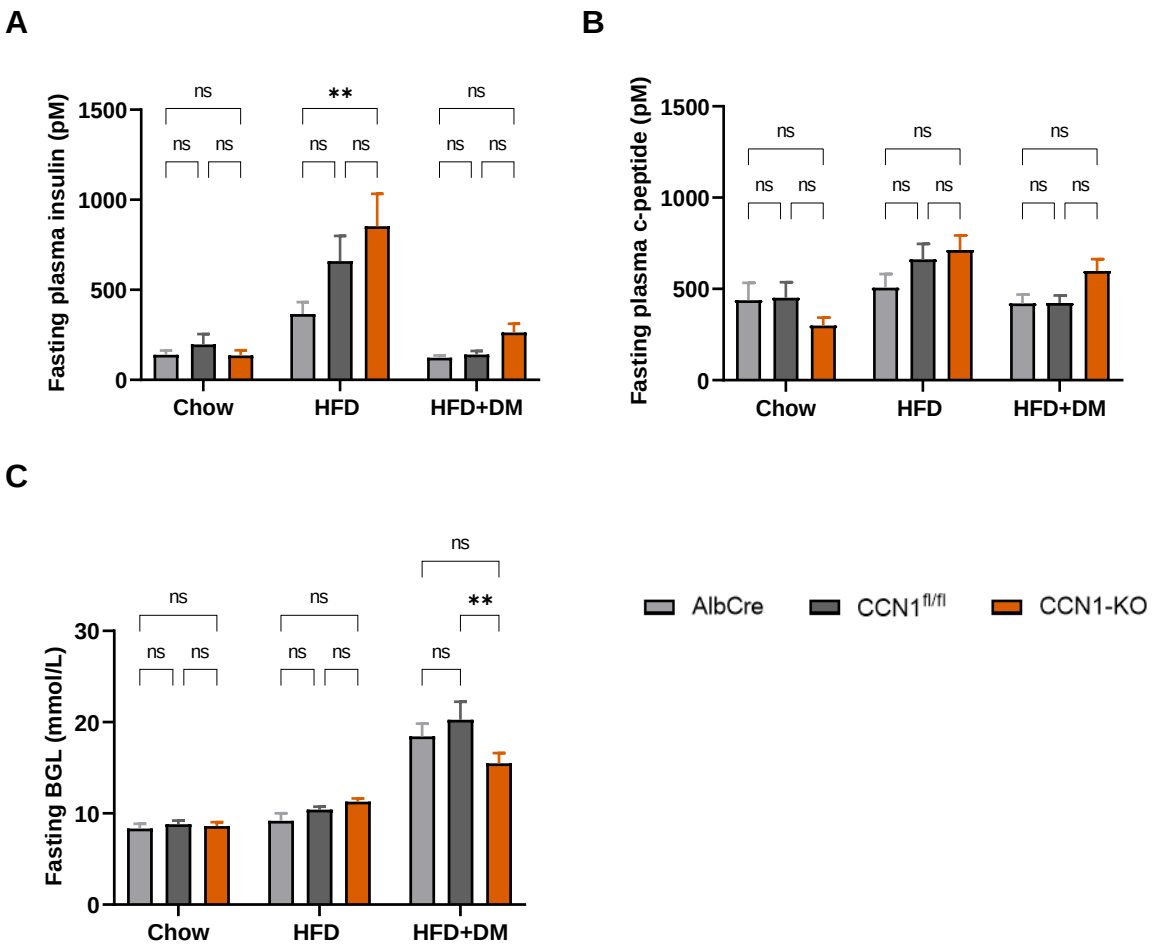

*Figure 5.6: Fasting plasma insulin (A) and c-peptide (B) levels, with matched fasting BGL (C). Data shown as mean ± SEM; n = 8 - 14. ** p-value ≤ 0.01 for comparison of mouse sub-strains within the same "diet" subgroup using two-way ANOVA with Tukey's correction for multiple comparisons. BGL, blood glucose level; ns, not significant.*

5.3.2.3.3 Insulin tolerance test

An ITT was performed prior to termination as a measure of whole-body insulin sensitivity, but some caution should be made in interpreting the results due to the wide differences in glucose concentrations between groups. The normalised AUC was similar at baseline amongst the three mouse sub-strains (*Figure 5.7*). There was no significant increase in AUC in the AlbCre HFD or CCN1$^{fl/fl}$ HFD groups compared with the corresponding Chow groups of the same mouse sub-strain, but there was a small but significant increase in AUC in the CCN1-KO HFD mice compared with the CCN1-KO Chow mice, indicating reduced insulin sensitivity or increased insulin resistance (statistics comparing different "diet" groups not shown). The CCN1-KO HFD+DM group had the highest insulin resistance of the HFD+DM groups, which was

statistically significant compared with the CCN1$^{fl/fl}$ HFD+DM group but not the AlbCre HFD+DM group (AlbCre: 6074 ± 802, CCN1$^{fl/fl}$: 5664 ± 386, and CCN1-KO: 7294 ± 550). The non-normalised data depicting the shape of each curve is also shown in *Figure 5.7*, which further highlights the increased insulin resistance of the CCN1-KO HFD and the CCN1-KO HFD+DM groups.

A

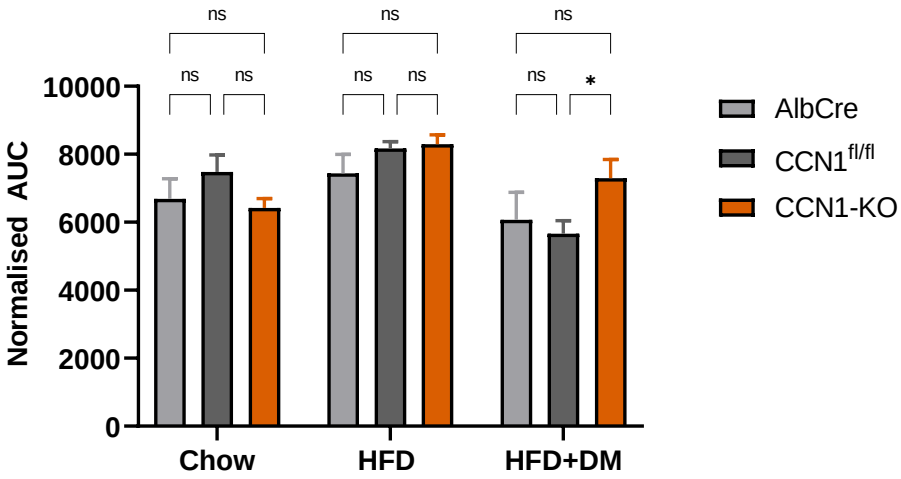

B

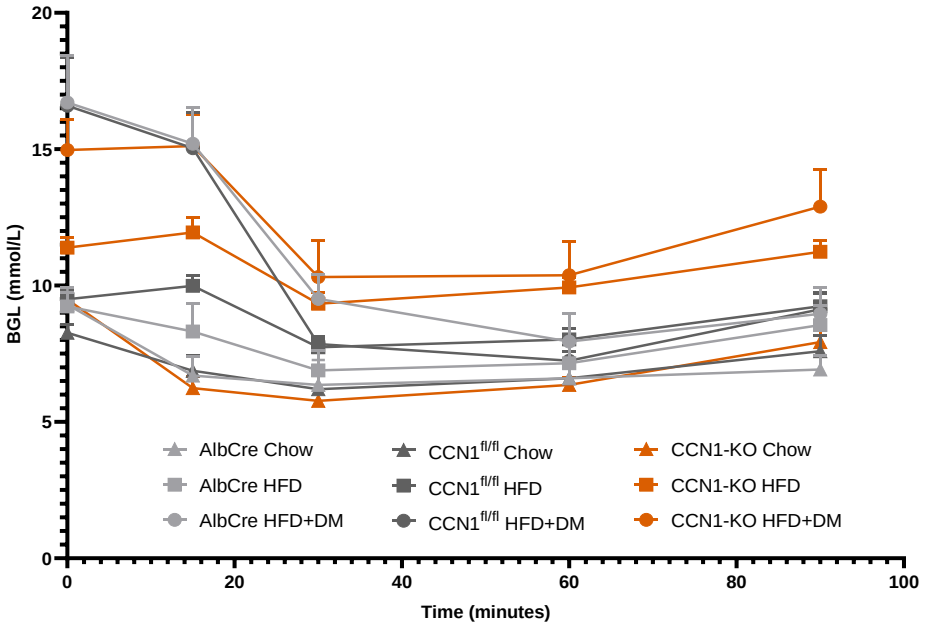

*Figure 5.7: Insulin tolerance test with normalised incremental AUC (A) and non-normalised time course data (B). Data shown as mean ± SEM; n = 5 - 14. * p-value ≤ 0.05 for comparison of mouse sub-strains within the same "diet" subgroup using two-way ANOVA with Tukey's correction for multiple comparisons. AUC, area under the curve; BGL, blood glucose level; ns, not significant. Note: three mice from the AlbCre Chow group and one mouse from the AlbCre HFD group did not undergo the ITT.*

5.3.2.3.4 Calculated measures of insulin resistance

In addition to the ITT, other calculated measures of insulin resistance were performed using the results of the fasting BGL at termination, fasting plasma insulin level and/or fasting plasma c-peptide level (*Figure 5.8*). The HOMA-IR results followed a similar pattern as the ITT, whereby the CCN1-KO HFD and CCN1-KO HFD+DM groups had the highest degree of insulin resistance within their "diet" subgroups, although this did not reach statistical significance when using the rigorous test of a two-way ANOVA with Tukey's correction for multiple comparisons. The HOMA-β results showed a trend to increased insulin secretion in the CCN1-KO HFD and CCN1-KO HFD+DM groups. The glucose to insulin ratio was relatively lower in the CCN1-KO HFD+DM group compared with the AlbCre HFD+DM ($p = 0.033$) and $CCN1^{fl/fl}$ HFD+DM ($p = 0.010$) groups (AlbCre: 18.7 ± 2.3, $CCN1^{fl/fl}$: 19.9 ± 3.6, and CCN1-KO: 10.1 ± 2.3), also consistent with a higher degree of insulin resistance being present.

As these findings are from fasting blood samples and it is mainly the liver that regulates fasting glucose, these results likely reflect predominantly a degree of hepatic insulin resistance being present in the CCN1-KO HFD+DM group, although recognising that the formal assessments for insulin resistance, were statistically negative across the groups. The data for HOMA-β suggest that the CCN1-KO HFD+DM may have some greater pancreatic β cell function. Collectively, these data in the CCN1-KO mice under the HFD+DM conditions of this model suggest that pancreatic β cell function is partially improved and it more than compensates for the insulin resistance in the mice to improve blood glucose levels.

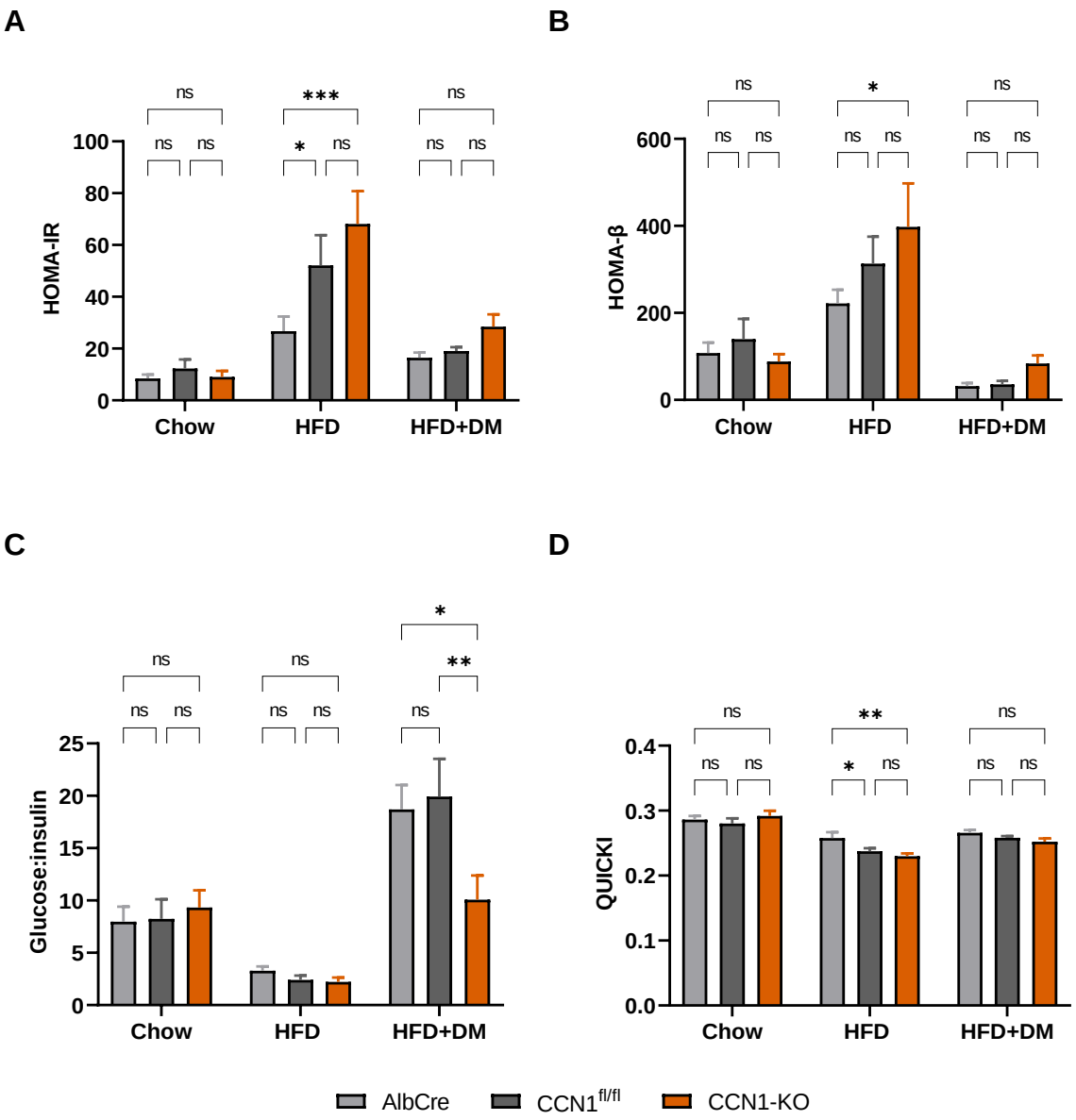

*Figure 5.8: Calculated measures of insulin resistance: HOMA-IR (A), HOMA-β (B), glucose to insulin ratio (C), and QUICKI (D). Data shown as mean ± SEM; n = 8 - 14. * p-value ≤ 0.05, ** p-value ≤ 0.01 or *** p-value ≤ 0.001 for comparison of mouse sub-strains within the same "diet" subgroup using two-way ANOVA with Tukey's correction for multiple comparisons. HOMA-β, homeostatic model assessment for β-cell function; HOMA-IR, homeostatic model assessment for insulin resistance; QUICKI, quantitative insulin check index of insulin sensitivity; ns, not significant.*

5.3.2.4 Assessment of body composition using EchoMRI™

Body composition including fat mass and lean mass were assessed using EchoMRI™ at two timepoints, week 15 and week 25. Results expressed as a percentage of total body weight are shown in *Figure 5.9* and absolute mass data is shown in *Table 5.3*. At both week 15 and week 25, the HFD and HFD+DM mice had significantly higher fat mass percentage and lower lean mass percentage compared with the Chow group of the same mouse sub-strain (statistics comparing different "diet" groups not shown). At week 15, there was no statistical difference in fat mass percentage between mice of the same "diet" subgroup, however there was already a significant reduction in lean mass percentage in the CCN1-KO HFD+DM mice compared with the AlbCre HFD+DM group (56.77 ± 0.65 vs 64.89 ± 2.10 %, p = 0.018). By week 25, the CCN1-KO HFD+DM group had significantly higher fat mass percentage compared with the AlbCre HFD+DM group (41.72 ± 1.22 vs 29.26 ± 2.98 %, p = 0.038) and lower lean mass percentage compared with both the AlbCre HFD+DM (p < 0.001) and CCN1$^{fl/fl}$ HFD+DM (p = 0.003) groups (AlbCre: 66.30 ± 2.74, CCN1$^{fl/fl}$: 64.57 ± 3.84, and CCN1-KO: 54.77 ± 1.08 %). This translated to a significantly higher fat to lean mass ratio in the CCN1-KO HFD+DM group.

A

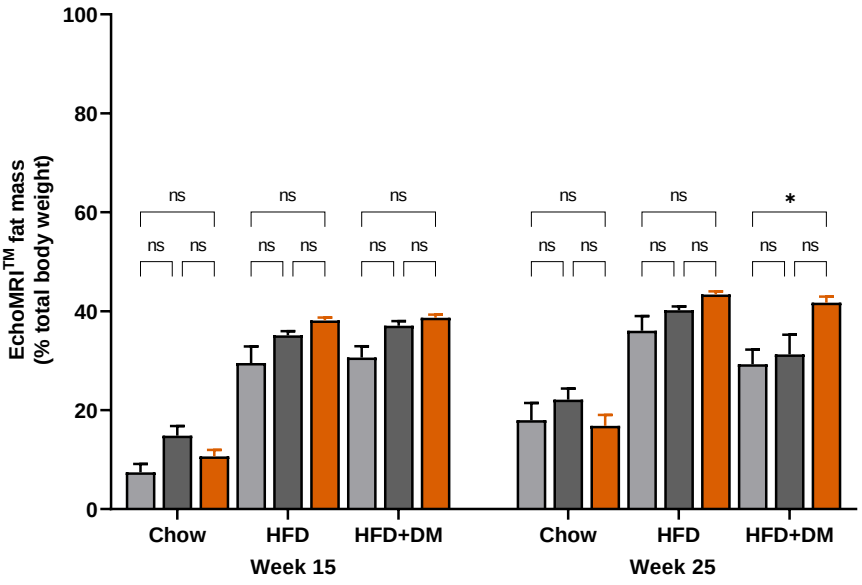

B

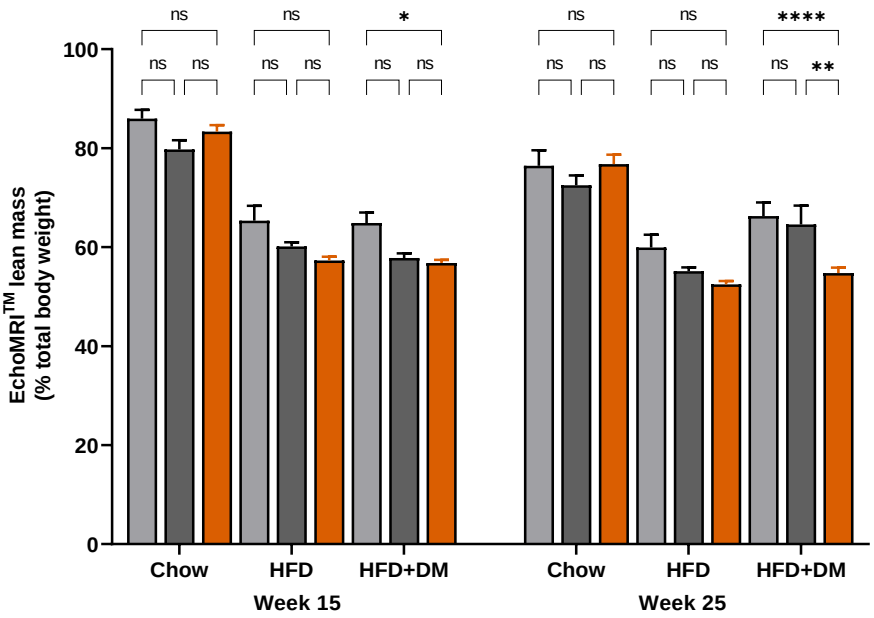

C

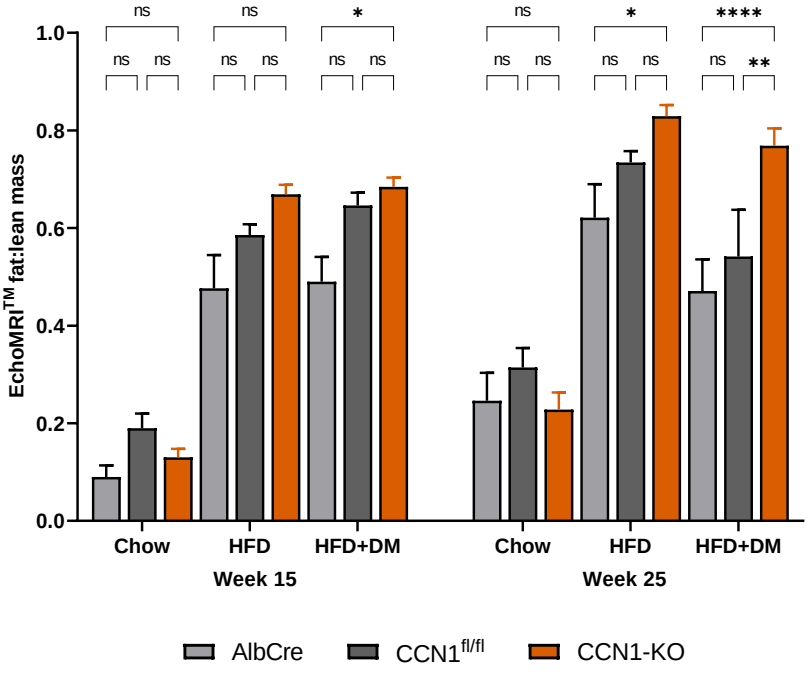

*Figure 5.9: Body composition by EchoMRI™: fat mass expressed as percentage of total body weight (A), lean mass expressed as percentage of total body weight (B), and fat to lean mass ratio (C), at week 15 and week 25. Note that at week 15, HFD+DM groups were not yet diabetic. Data shown as mean ± SEM; n = 5 - 14. * p-value ≤ 0.05, ** p-value ≤ 0.01 or **** p-value ≤ 0.0001 for comparison of mouse sub-strains within the same "diet" subgroup using mixed-effects analysis with Šidák's correction for multiple comparisons. ns, not significant. Note: three mice from the AlbCre Chow group, one mouse from the AlbCre HFD group and one mouse from the CCN1-KO HFD+DM group did not undergo the week 25 body composition analysis.*

Table 5.3: Body composition by EchoMRI™: absolute fat mass, lean mass, and total body weight at week 15 and week 25.

	Chow			HFD			HFD+DM		
Week 15	**AlbCre**	**CCN1$^{fl/fl}$**	**CCN1-KO**	**AlbCre**	**CCN1$^{fl/fl}$**	**CCN1-KO**	**AlbCre**	**CCN1$^{fl/fl}$**	**CCN1-KO**
Fat mass (g)	2.43 ± 0.61	4.69 ± 0.80	3.12 ± 0.41	13.08 ± 1.82	16.06 ± 0.65	18.67 ± 0.54	13.00 ± 1.24	17.42 ± 0.65	18.10 ± 0.41
Lean mass (g)	27.31 ± 0.38	24.21 ± 0.62	24.21 ± 0.43	27.52 ± 0.60	27.33 ± 0.40	27.94 ± 0.27	26.81 ± 0.39	27.05 ± 0.46	26.59 ± 0.51
Total body weight (g)	31.84 ± 0.59	30.54 ± 1.26	29.07 ± 0.49	42.74 ± 1.91	45.56 ± 0.96	48.86 ± 0.74	41.67 ± 1.09	46.90 ± 0.95	46.83 ± 0.74
Week 25	**AlbCre**	**CCN1$^{fl/fl}$**	**CCN1-KO**	**AlbCre**	**CCN1$^{fl/fl}$**	**CCN1-KO**	**AlbCre**	**CCN1$^{fl/fl}$**	**CCN1-KO**
Fat mass (g)	6.60 ± 1.52	8.16 ± 1.20	5.70 ± 0.88	18.03 ± 2.09	21.76 ± 0.61	24.77 ± 0.70	12.48 ± 1.72	14.72 ± 2.80	20.39 ± 1.18
Lean mass (g)	27.18 ± 0.63	25.49 ± 0.87	25.11 ± 0.38	28.77 ± 0.58	29.78 ± 0.45	29.85 ± 0.29	26.69 ± 0.46	26.85 ± 0.77	26.32 ± 0.72
Total body weight (g)	35.78 ± 1.57	35.49 ± 1.85	32.90 ± 0.99	48.71 ± 2.45	54.08 ± 0.81	56.98 ± 0.87	40.95 ± 1.71	43.32 ± 3.24	48.38 ± 1.80

Data shown as mean ± SEM; n = 5 - 14. Please note that as per the Methods, relevant p-values have been identified in the relevant Figures, not in the Table. Note: three mice from the AlbCre Chow group, one mouse from the AlbCre HFD group and one mouse from the CCN1-KO HFD+DM group did not undergo the week 25 body composition analysis.

5.3.2.5 Organ weights at termination

The wet weight of the liver, epididymal fat pads, subcutaneous (dorsolumbar) fat pads, gastrocnemius muscles, spleen, kidneys, and heart were measured at termination and normalised against total body weight (*Figure 5.10*). The absolute data is shown in *Table 5.4*.

The normalised liver weights of the HFD and HFD+DM mice were approximately two-fold heavier than the Chow mice, consistent with hepatomegaly from steatosis (*Figure 5.10A*). The CCN1-KO HFD group had significantly higher liver weight compared with the AlbCre HFD and $CCN1^{fl/fl}$ HFD groups, but this pattern was not evident in the HFD+DM groups, where CCN1-KO HFD+DM mice had lower liver weights compared with the $CCN1^{fl/fl}$ HFD+DM mice but not the AlbCre HFD+DM mice.

Epididymal fat mass, a marker of visceral fat in mice, was generally higher in the HFD and HFD+DM groups compared with the Chow groups (*Figure 5.10B*). The CCN1-KO HFD and CCN1-KO HFD+DM mice had significantly higher absolute epididymal fat mass compared with the AlbCre and $CCN1^{fl/fl}$ mice in the same "diet" subgroup (*Table 5.4*; statistics comparing different "diet" groups not shown), however this was not observed after normalisation to total body weight. Subcutaneous fat pads were systematically resected from the dorsolumbar region and were significantly larger in mice that had been high fat fed (*Figure 5.10D*). The CCN1-KO HFD+DM mice had significantly greater normalised subcutaneous fat mass compared with the AlbCre HFD+DM and $CCN1^{fl/fl}$ HFD+DM mice (AlbCre: 3.02 ± 0.44, $CCN1^{fl/fl}$: 2.94 ± 0.53, and CCN1-KO: 4.04 ± 0.23 % TBW). In contrast, the CCN1-KO HFD+DM mice had significantly reduced normalised gastrocnemius muscle mass compared with the AlbCre HFD+DM and $CCN1^{fl/fl}$ HFD+DM mice (AlbCre: 0.82 ± 0.03, $CCN1^{fl/fl}$: 0.80 ± 0.05, and CCN1-KO: 0.65 ± 0.02 % TBW; *Figure 5.10E*). These findings are consistent with the body composition data (*Section 5.3.2.4*). In addition, the CCN1-KO HFD+DM mice had significantly lower normalised kidney mass (*Figure 5.10G*), but there was no difference observed in normalised spleen (*Figure 5.10F*) or heart (*Figure 5.10H*) mass. These data show overall, greater fat in the subcutaneous and epididymal tissue of the CCN1-KO HFD and the CCN1-KO HFD+DM groups.

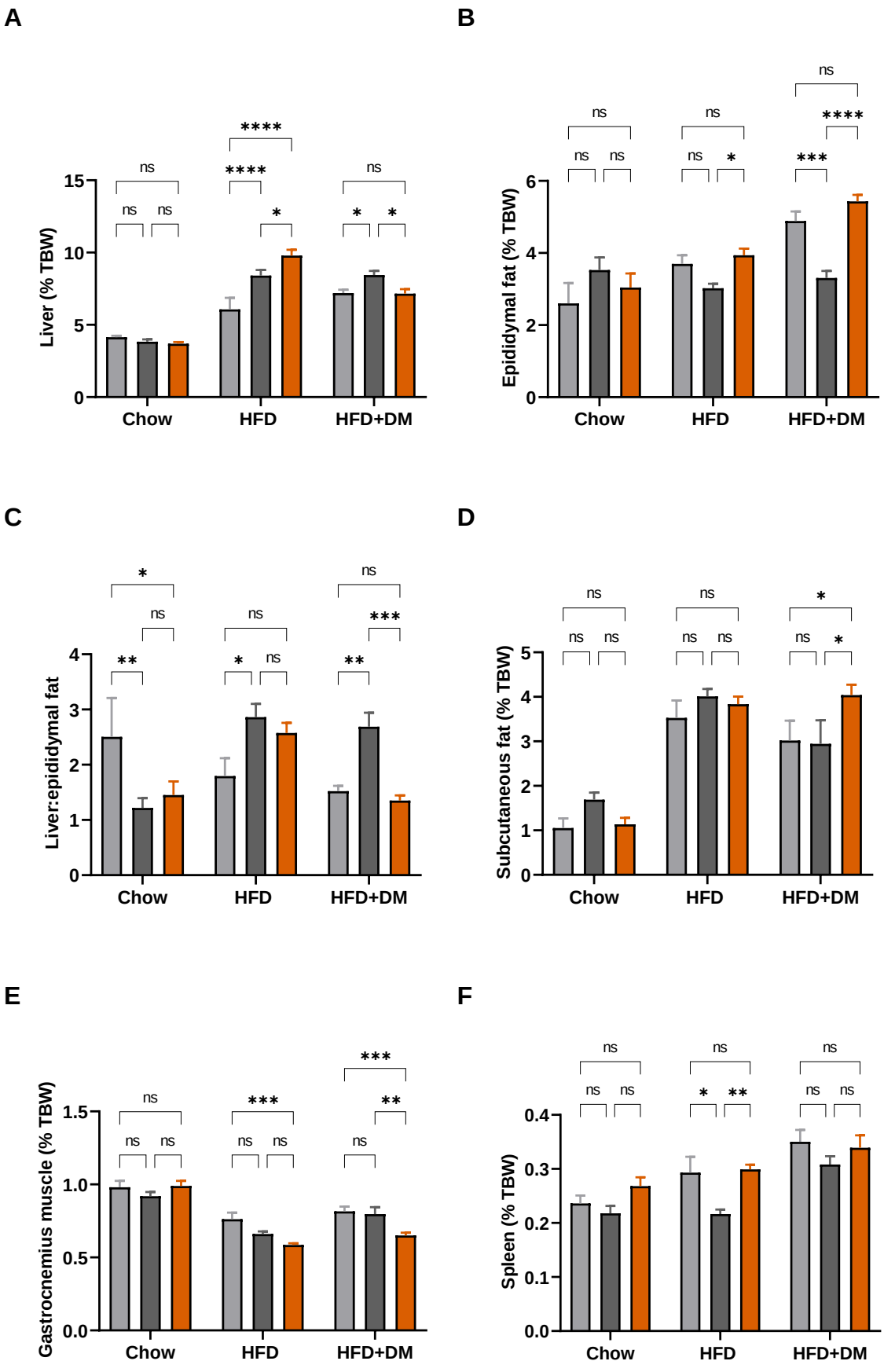
A
Liver (% TBW)
15
10
5
0
ns
****
ns
ns
****
*
ns
*
*
Chow
HFD
HFD+DM
B
Epididymal fat (% TBW)
6
4
2
0
ns
ns
ns
ns
ns
*
ns
****
***
Chow
HFD
HFD+DM
C
Liver:epididymal fat
4
3
2
1
0
*
ns
**
ns
*
ns
ns
***
**
Chow
HFD
HFD+DM
D
Subcutaneous fat (% TBW)
5
4
3
2
1
0
ns
ns
ns
ns
ns
ns
ns
*
ns
*
Chow
HFD
HFD+DM
E
Gastrocnemius muscle (% TBW)
1.5
1.0
0.5
0.0
ns
ns
ns
***
ns
ns
ns
***
**
Chow
HFD
HFD+DM
F
Spleen (% TBW)
0.4
0.3
0.2
0.1
0.0
ns
ns
ns
ns
ns
*
**
ns
ns
Chow
HFD
HFD+DM

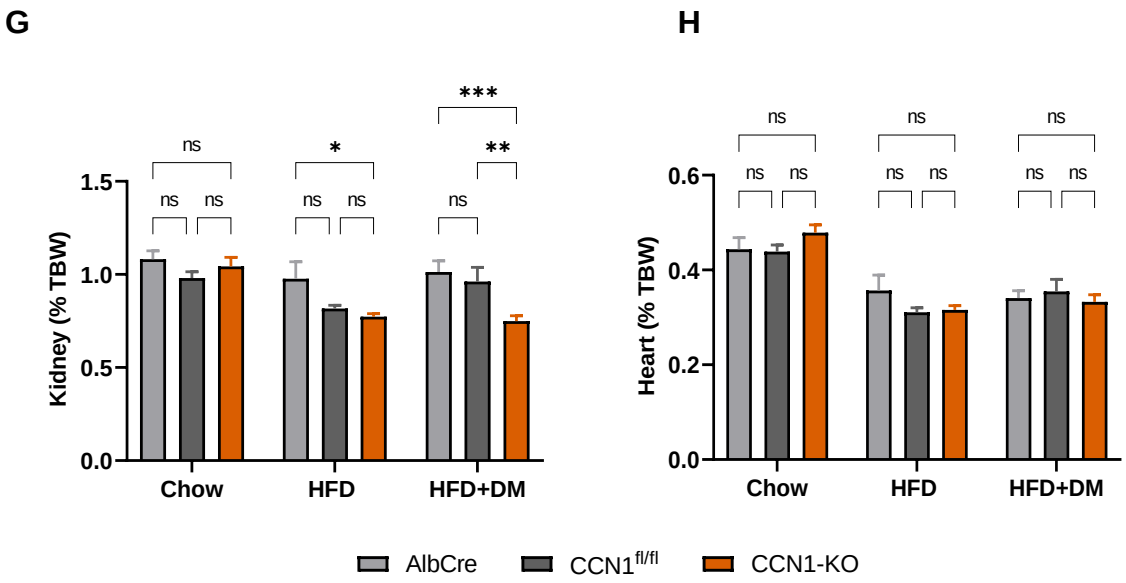

*Figure 5.10: Organ weights expressed as percentage of total body weight: liver (A), epididymal fat (B), liver to epididymal fat ratio (C), subcutaneous fat (D), gastrocnemius muscle (E), spleen (F), kidney (G), and heart (H). Data shown as mean ± SEM; n = 8 - 14. * p-value ≤ 0.05, ** p-value ≤ 0.01, *** p-value ≤ 0.001 or **** p-value ≤ 0.0001 for comparison of mouse sub-strains within the same "diet" subgroup using two-way ANOVA with Tukey's correction for multiple comparisons. TBW, total body weight; ns, not significant.*

Table 5.4: Organ wet weights (grams) at termination.

	Chow			HFD			HFD+DM		
	AlbCre	**CCN1$^{fl/fl}$**	**CCN1-KO**	**AlbCre**	**CCN1$^{fl/fl}$**	**CCN1-KO**	**AlbCre**	**CCN1$^{fl/fl}$**	**CCN1-KO**
Liver	1.39 ± 0.05	1.36 ± 0.09	1.18 ± 0.05	3.07 ± 0.51	4.58 ± 0.26	5.74 ± 0.30	3.01 ± 0.20	3.71 ± 0.33	3.51 ± 0.23
Epididymal fat	0.93 ± 0.24	1.30 ± 0.18	1.01 ± 0.16	1.77 ± 0.10	1.64 ± 0.06	2.29 ± 0.10	2.05 ± 0.16	1.46 ± 0.15	2.62 ± 0.07
Liver:epididymal fat	2.50 ± 0.70	1.22 ± 0.18	1.45 ± 0.24	1.80 ± 0.32	2.86 ± 0.24	2.58 ± 0.18	1.52 ± 0.10	2.69 ± 0.25	1.35 ± 0.09
Subcutaneous fat	0.38 ± 0.09	0.62 ± 0.09	0.38 ± 0.06	1.78 ± 0.25	2.18 ± 0.10	2.24 ± 0.12	1.33 ± 0.24	1.44 ± 0.34	1.99 ± 0.15
Gastrocnemius muscle	0.33 ± 0.003	0.33 ± 0.012	0.32 ± 0.007	0.36 ± 0.006	0.36 ± 0.006	0.34 ± 0.005	0.33 ± 0.006	0.33 ± 0.007	0.31 ± 0.007
Spleen	0.08 ± 0.005	0.08 ± 0.007	0.09 ± 0.005	0.14 ± 0.009	0.12 ± 0.005	0.17 ± 0.005	0.15 ± 0.013	0.13 ± 0.007	0.17 ± 0.013
Kidney	0.36 ± 0.009	0.35 ± 0.017	0.33 ± 0.013	0.46 ± 0.024	0.44 ± 0.011	0.45 ± 0.005	0.41 ± 0.011	0.40 ± 0.016	0.36 ± 0.018
Heart	0.16 ± 0.007	0.16 ± 0.008	0.15 ± 0.006	0.17 ± 0.009	0.17 ± 0.005	0.18 ± 0.003	0.14 ± 0.003	0.18 ± 0.003	0.16 ± 0.009
Total body weight	33.66 ± 1.57	35.74 ± 1.76	32.13 ± 1.11	48.54 ± 2.33	54.28 ± 0.84	58.31 ± 0.89	41.57 ± 1.82	43.64 ± 3.31	48.71 ± 1.71

Data shown as mean ± SEM; n = 8 - 14. Please note that as per the Methods, relevant p-values have been identified in the relevant Figures, not in the Table.

5.3.2.6 Routine fasting plasma biochemistry

5.3.2.6.1 Liver-related tests

The AST (*Figure 5.11A*) and ALT (*Figure 5.11B*) levels were markedly elevated in the HFD and HFD+DM groups compared with the Chow groups (*Table 5.5*; statistics comparing different "diet" groups not shown). In the HFD groups, the CCN1-KO mice had the largest increase in AST and ALT levels, but in the HFD+DM groups, the levels were similar. The relative changes in AST and ALT were also similar, with comparable AST to ALT ratios (*Figure 5.11C*). The ALP levels were elevated in the HFD and HFD+DM mice compared with Chow mice across all three mouse sub-strains (*Figure 5.11D*). However, the CCN1-KO mice in both the HFD and HFD+DM subgroups had significantly higher ALP increase compared with the AlbCre and $CCN1^{fl/fl}$ HFD and HFD+DM groups.

Total protein and albumin levels are measures of liver synthetic function. Total protein levels were generally stable across all groups (*Table 5.5)*. Albumin levels were significantly decreased in all HFD+DM groups compared with the Chow and HFD groups of the same mouse sub-strain (statistics comparing different "diet" groups not shown), however there was no effect from the hepatocyte CCN1 deletion (*Figure 5.11E*). Total bilirubin levels were generally very low, with no significant changes identified (*Figure 5.11F*). The automated analyser was unable to detect GGT in mouse plasma, and platelet count was not assessed either as it required stored whole blood, which was not available.

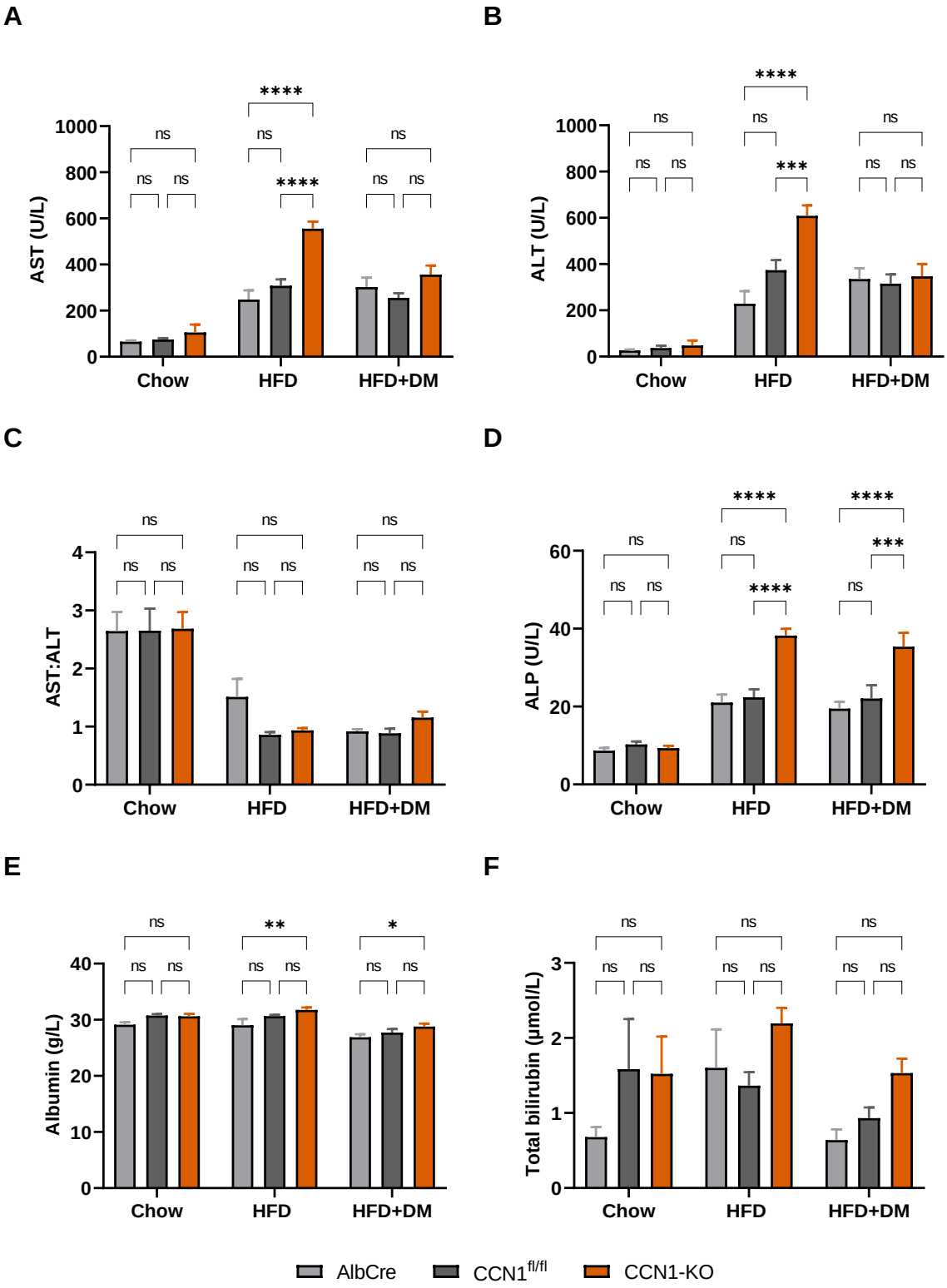

*Figure 5.11: Liver-related plasma tests: AST (A), ALT (B), AST:ALT (C), ALP (D), albumin (E), and total bilirubin (F). Data shown as mean ± SEM; n = 8 - 14. * p-value ≤ 0.05, ** p-value ≤ 0.01, *** p-value ≤ 0.001 or **** p-value ≤ 0.0001 for comparison of mouse sub-strains within the same "diet" subgroup using two-way ANOVA with Tukey's correction for multiple comparisons. ALP, alkaline phosphatase; ALT, alanine aminotransferase; AST, aspartate aminotransferase; ns, not significant.*

5.3.2.6.2 Lipid panel

Total cholesterol, HDL-c, and LDL-c were elevated in all groups that were fed a high fat diet, but to a higher degree in the HFD groups compared with the HFD+DM groups (*Figure 5.12* and *Table 5.5*; statistics comparing different "diet" groups not shown). In the HFD+DM groups, total cholesterol, HDL-c, and LDL-c were all statistically higher in the CCN1-KO mice compared with the AlbCre mice, and there was a similar trend compared with the CCN1$^{fl/fl}$ mice. Fasting triglyceride levels were lower in the HFD and HFD+DM groups compared with Chow groups, with no statistical difference between mouse sub-strains.

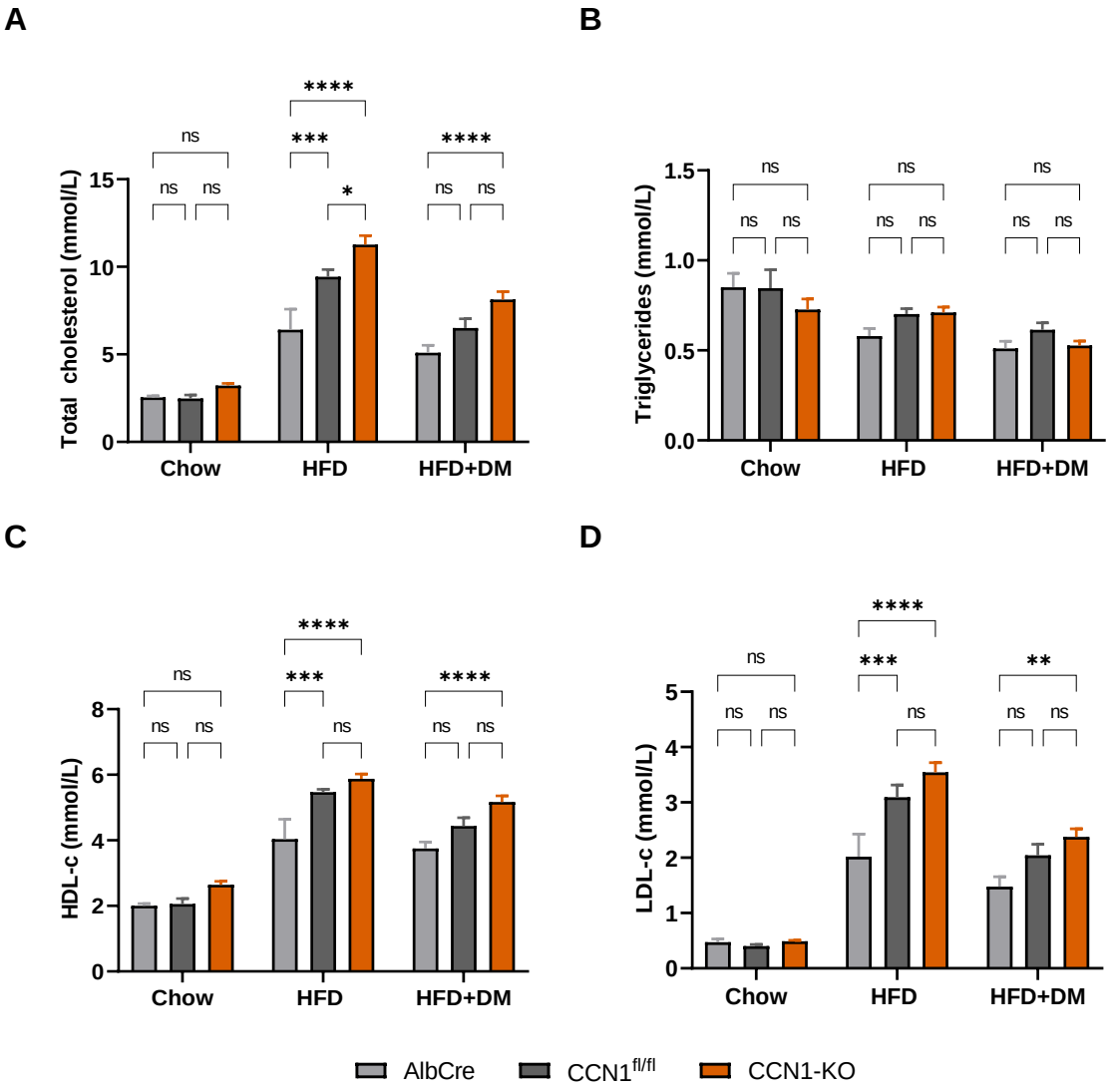

*Figure 5.12: Fasting plasma lipid panel: total cholesterol (A), triglycerides (B), HDL-c (C), and LDL-c (D). Data shown as mean ± SEM; n = 8 - 14. * p-value ≤ 0.05, ** p-value ≤ 0.01, *** p-value ≤ 0.001 or **** p-value ≤ 0.0001 for comparison of mouse sub-strains within the same "diet" subgroup using two-way ANOVA with Tukey's correction for multiple comparisons. HDL-c, high-density lipoprotein cholesterol; LDL-c, low-density lipoprotein cholesterol; ns, not significant.*

5.3.2.6.3 High sensitivity c-reactive protein

Plasma high sensitivity c-reactive protein (hsCRP) was measured as a marker of systemic inflammation. The CCN1-KO mice had a lower hsCRP compared with the AlbCre and CCN1$^{fl/fl}$ mice across all three "diet" subgroups, including in the baseline state (*Figure 5.13*).

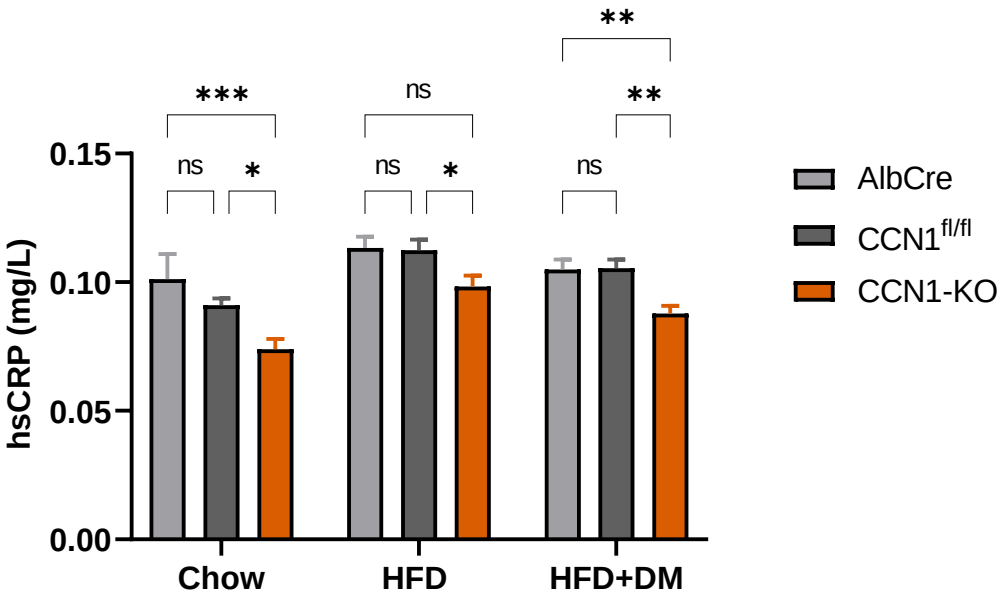

*Figure 5.13: Plasma hsCRP. Data shown as mean ± SEM; n = 8 - 14. * p-value ≤ 0.05, ** p-value ≤ 0.01 or *** p-value ≤ 0.001 for comparison of mouse sub-strains within the same "diet" subgroup using two-way ANOVA with Tukey's correction for multiple comparisons. hsCRP, high sensitivity c-reactive protein; ns, not significant.*

Table 5.5: Routine fasting plasma biochemistry.

	Chow			HFD			HFD+DM		
	AlbCre	**CCN1$^{fl/fl}$**	**CCN1-KO**	**AlbCre**	**CCN1$^{fl/fl}$**	**CCN1-KO**	**AlbCre**	**CCN1$^{fl/fl}$**	**CCN1-KO**
AST (U/L)	65.14 ± 5.23	74.87 ± 5.93	105.44 ± 34.11	247.73 ± 39.96	307.57 ± 28.04	555.70 ± 30.36	302.23 ± 40.67	255.58 ± 19.87	356.24 ± 39.03
ALT (U/L)	26.76 ± 3.39	39.90 ± 9.88	47.88 ± 21.35	229.09 ± 54.11	374.13 ± 42.87	608.65 ± 45.06	335.23 ± 46.93	315.77 ± 39.27	347.40 ± 53.20
AST:ALT	2.64 ± 0.33	2.65 ± 0.38	2.69 ± 0.29	1.51 ± 0.31	0.86 ± 0.05	0.94 ± 0.04	0.92 ± 0.03	0.88 ± 0.08	1.16 ± 0.10
ALP (U/L)	8.66 ± 0.72	10.30 ± 0.75	9.35 ± 0.57	21.03 ± 2.06	22.35 ± 2.08	38.22 ± 1.75	19.48 ± 1.72	22.09 ± 3.37	35.38 ± 3.57
Albumin (g/L)	29.13 ± 0.42	30.76 ± 0.25	30.63 ± 0.44	29.01 ± 1.10	30.65 ± 0.25	31.76 ± 0.41	26.90 ± 0.52	27.73 ± 0.62	28.78 ± 0.52
Total protein (g/L)	52.31 ± 1.39	52.18 ± 0.52	52.35 ± 0.76	55.96 ± 2.30	59.54 ± 0.90	64.75 ± 1.30	52.28 ± 1.15	54.05 ± 1.29	54.81 ± 1.57
Total bilirubin (µmol/L)	0.68 ± 0.13	1.58 ± 0.67	1.52 ± 0.50	1.60 ± 0.51	1.36 ± 0.18	2.19 ± 0.21	0.64 ± 0.14	0.93 ± 0.14	1.53 ± 0.19
Total cholesterol (mmol/L)	2.54 ± 0.09	2.48 ± 0.20	3.22 ± 0.13	6.40 ± 1.18	9.44 ± 0.41	11.3 ± 0.52	5.09 ± 0.43	6.51 ± 0.52	8.13 ± 0.45
Triglycerides (mmol/L)	0.85 ± 0.08	0.85 ± 0.10	0.73 ± 0.06	0.58 ± 0.04	0.70 ± 0.03	0.71 ± 0.03	0.51 ± 0.04	0.61 ± 0.04	0.53 ± 0.03
HDL-c (mmol/L)	2.01 ± 0.07	2.06 ± 0.17	2.64 ± 0.11	4.04 ± 0.61	5.47 ± 0.09	5.88 ± 0.15	3.75 ± 0.20	4.43 ± 0.26	5.17 ± 0.18
LDL-c (mmol/L)	0.47 ± 0.06	0.40 ± 0.03	0.49 ± 0.02	2.02 ± 0.41	3.10 ± 0.22	3.55 ± 0.17	1.48 ± 0.18	2.04 ± 0.20	2.38 ± 0.15
hsCRP (mg/L)	0.10 ± 0.010	0.09 ± 0.003	0.07 ± 0.004	0.11 ± 0.004	0.11 ± 0.004	0.10 ± 0.004	0.11 ± 0.004	0.11 ± 0.003	0.09 ± 0.003

Data shown as mean ± SEM; n = 8 - 14. ALP, alkaline phosphatase; ALT, alanine aminotransferase; AST, aspartate aminotransferase; HDL-c, high-density lipoprotein cholesterol; hsCRP, high sensitivity c-reactive protein; LDL-c, low-density lipoprotein cholesterol. Please note that as per the Methods, relevant p-values have been identified in the relevant Figures, not in the Table.

5.3.3 The effects of hepatocyte CCN1 deletion on NASH fibrosis

The gold standard for assessing the development of NASH fibrosis in humans is via a core liver biopsy, and use of standard histological staining such as H&E staining, with or without the use of a dedicated fibrosis stain, such as PSR staining or Masson's Trichrome staining[80]. We elected to use both H&E and PSR staining in assessing the main histological features of NASH: fibrosis, inflammation, hepatocyte ballooning, and steatosis. Each of these features were assessed using multiple approaches as described in the Methods (*Section 2.3.5*). In addition, other techniques, such as measurement of mRNA levels of key fibrosis and inflammation markers, were used to provide additional support to the histological outcomes.

5.3.3.1 The effects of hepatocyte CCN1 deletion on liver fibrosis

5.3.3.1.1 Assessment of liver fibrosis by histology

The primary outcome of this study was to assess the development of liver fibrosis, which, in humans, links strongly to loss of liver function and increased mortality[321-324,365]. Two different methods of assessing fibrosis were used: quantification using image analysis software and grading according to the Brunt criteria by an independent anatomical pathologist. Both methods were applied to PSR-stained liver tissue.

A) Quantification of liver fibrosis using image analysis software

The details of the methods are described in *Section 2.3.5.1*. In brief, 4 - 6 images per stained liver tissue section were taken at three magnifications (100x, 200x, and 400x) and ImageJ software was used to calculate the percent area of the PSR-positive stained tissue. The threshold settings were optimised using the HFD+DM groups, and then the same analysis settings were applied to the Chow and HFD groups.

The percent area of PSR-positive stained tissue at various magnifications is shown in *Figure 5.14*. At all three magnifications, there were very low levels (< 1%) of PSR-positive tissue in all three Chow groups, which was consistent with an absence of liver fibrosis. Some PSR-positive stained tissue was evident due to the staining of collagen fibres that normally line the blood vessel walls. Fibrosis levels in the HFD groups were intermediary, with no significant effect from the CCN1-KO, although the CCN1-KO HFD group had numerically the greatest amount of fibrosis of all the HFD groups at all magnifications. The HFD+DM groups had the greatest amount of PSR-positive tissue

compared with the Chow and HFD groups, indicating the greatest amount of liver fibrosis (statistics comparing different “diet” groups not shown). The CCN1-KO HFD+DM group displayed approximately double the percentage of PSR-positive stained tissue across all three magnifications, including at more detailed analysis of areas of the central vein and the portal tracts. Fibrosis was generally most abundant at the level of the portal tract, which was also the site of the greatest relative increase in fibrosis in the CCN1-KO HFD+DM group. Representative images are shown in *Figures 5.15 - 5.17*.

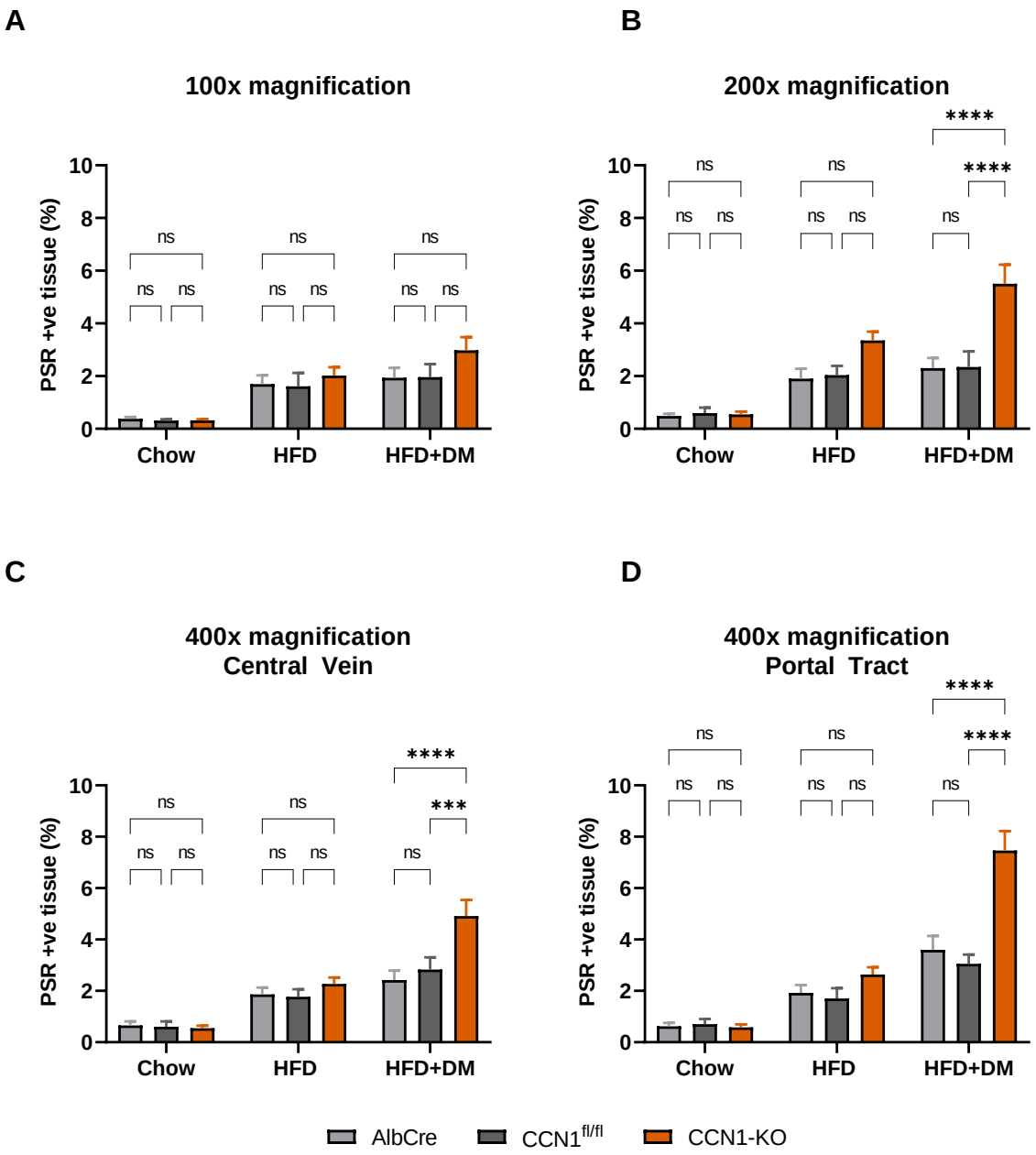

*Figure 5.14: Quantification of liver fibrosis of PSR-stained tissue with images taken at 100x magnification (A), 200x magnification (B), and 400x magnification focussing on central veins (C) and portal tracts (D). Data shown as mean ± SEM; n = 8 - 14. *** p-value ≤ 0.001 or **** p-value ≤ 0.0001 for comparison of mouse sub-strains within the same "diet" subgroup using two-way ANOVA with Tukey's correction for multiple comparisons. PSR, Picro Sirius Red; ns, not significant.*

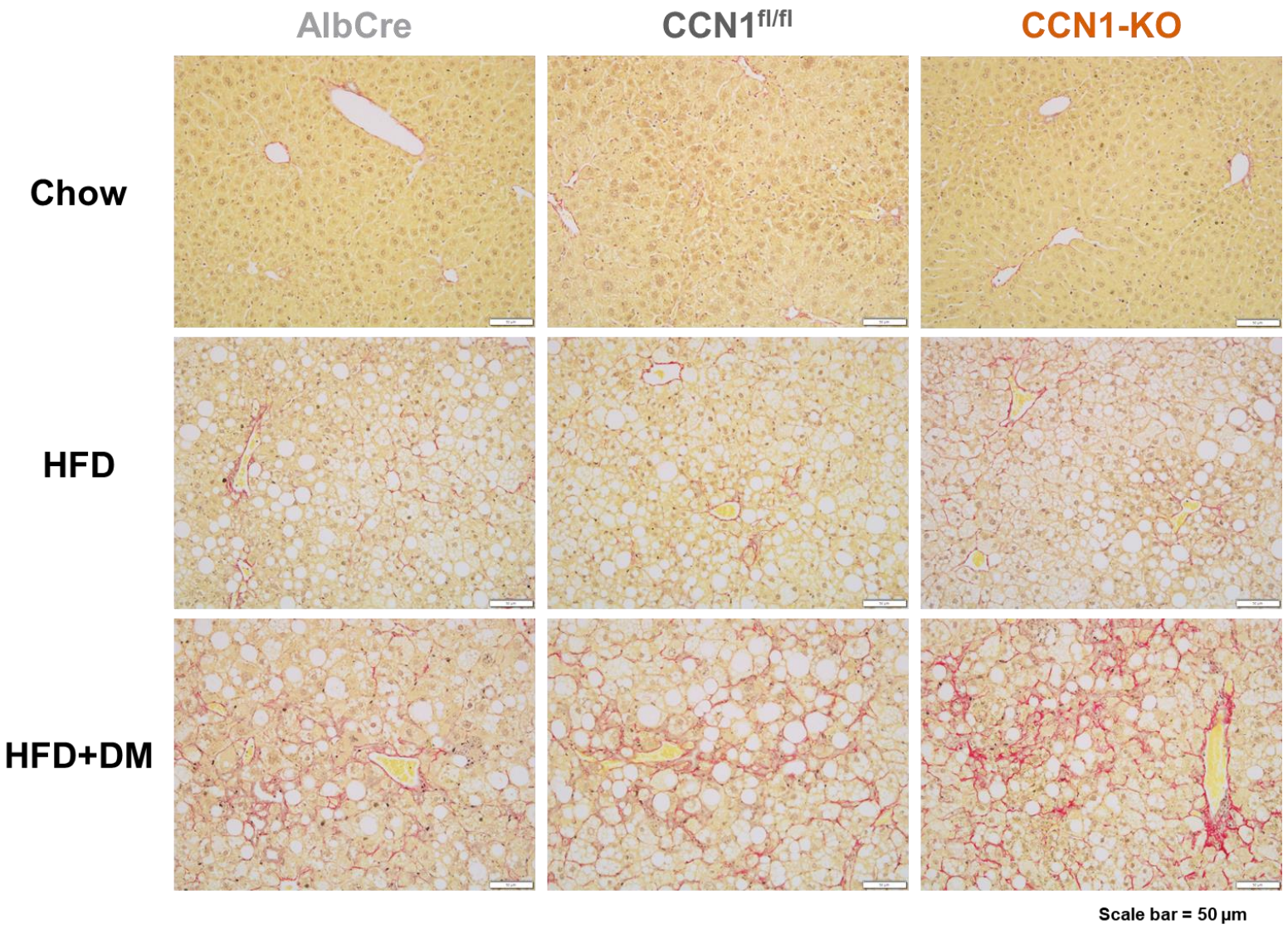

Figure 5.15: Representative histological images of PSR-stained liver tissue (200x magnification).

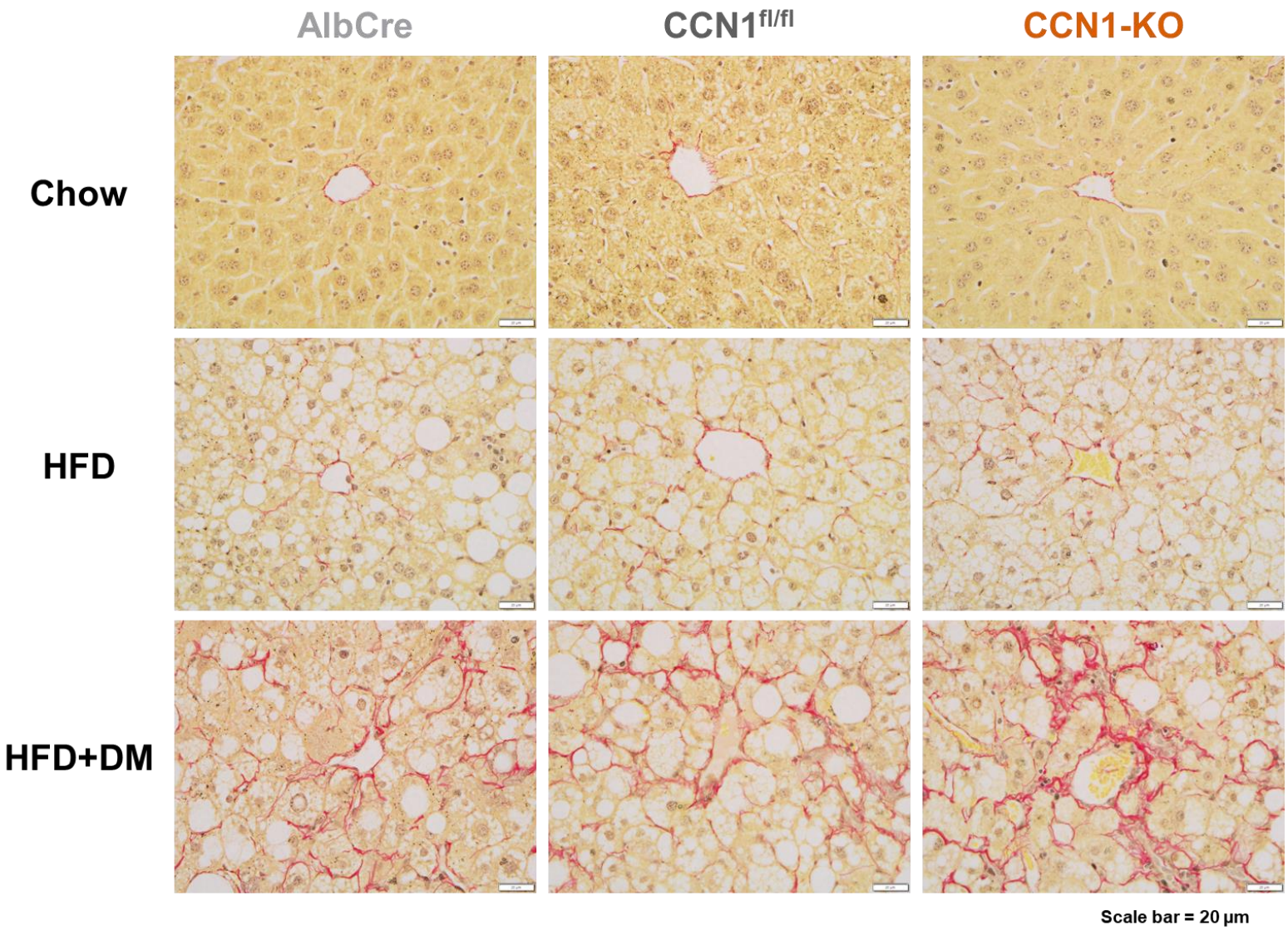

Figure 5.16: Representative histological images of central veins from PSR-stained liver tissue (400x magnification).

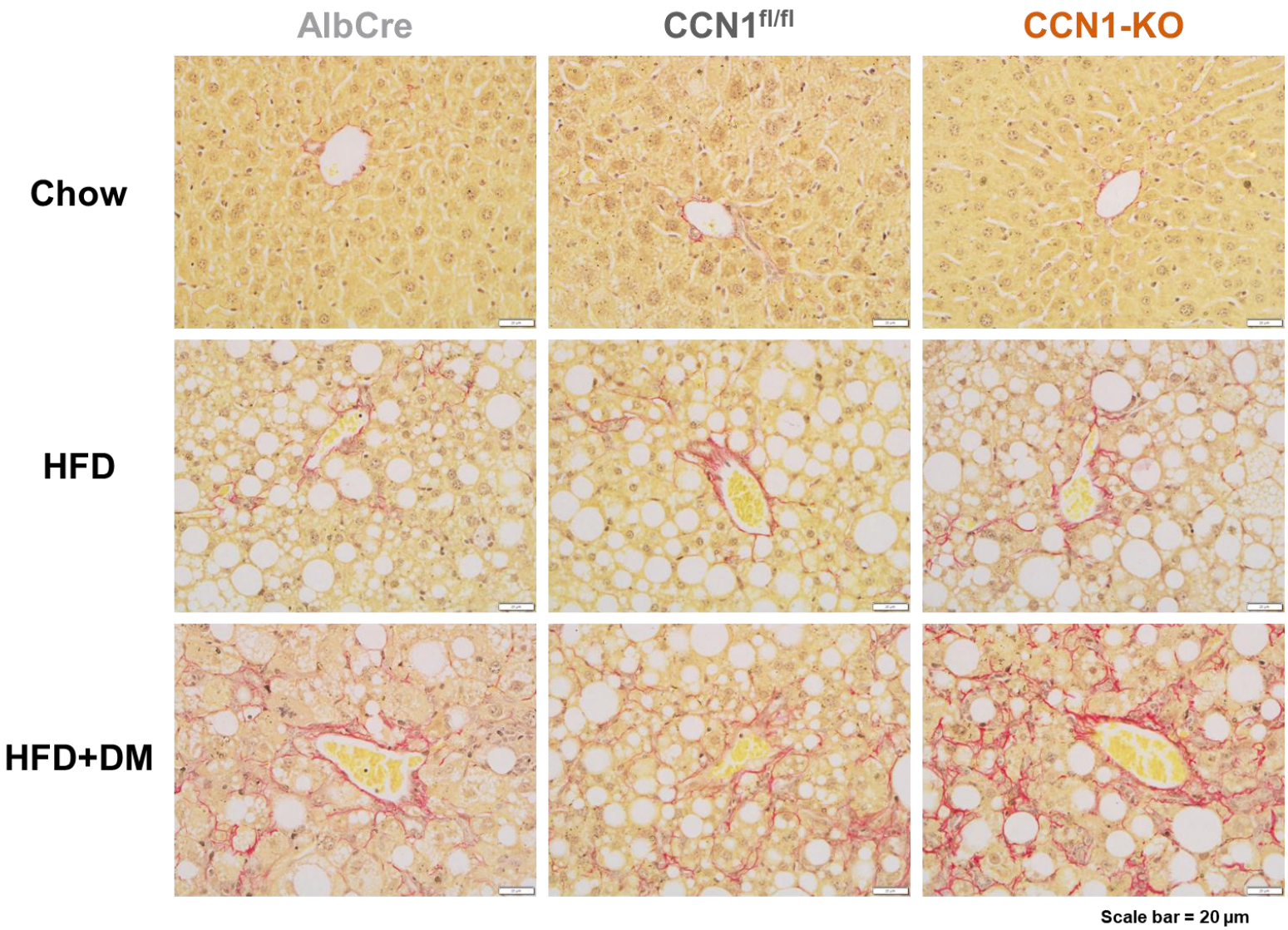

Figure 5.17: Representative histological images of portal tracts from PSR-stained liver tissue (400x magnification).

B) Grading of liver fibrosis according to the Brunt criteria

The Brunt criteria grades liver fibrosis according to its regionality, and unlike the method used in the previous section, is not quantitative. An absence of fibrosis is F0, perisinusoidal fibrosis is F1, periportal fibrosis is F2, bridging fibrosis is F3, and cirrhosis is F4. A higher stage represents more severe disease and worse prognosis. Mice from the HFD+DM groups exhibited the highest fibrosis grade, although there was no difference detected in the CCN1-KO group (AlbCre: 2.8 ± 0.2, CCN1$^{fl/fl}$: 3.3 ± 0.1, and CCN1-KO: 2.8 ± 0.2; *Figure 5.18*). There was minimal fibrosis observed in the Chow fed mice, and the HFD mice had an intermediary grade of fibrosis.

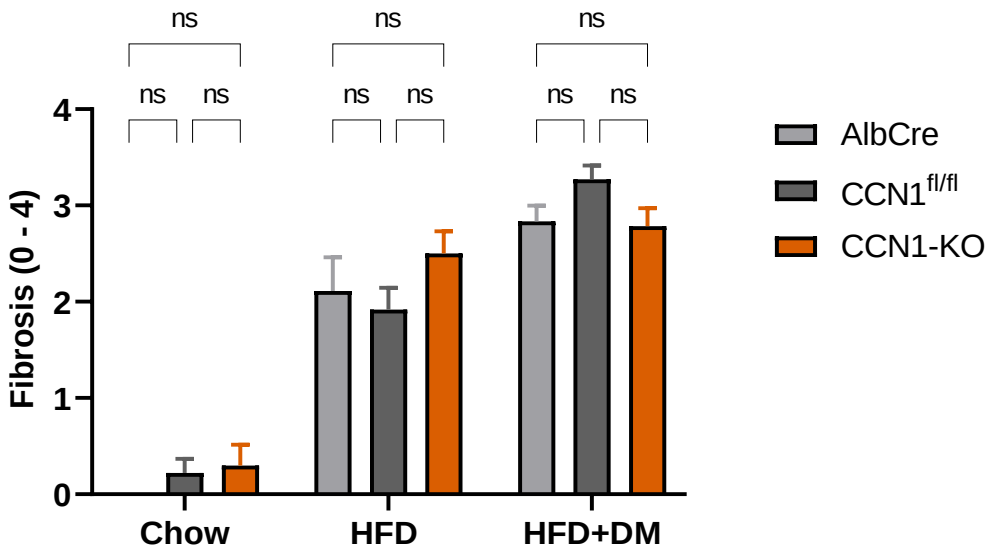

Figure 5.18: Fibrosis grade according to the Brunt criteria. Data shown as mean ± SEM; n = 8 - 14. ns (not significant), p-value > 0.05 for comparison of mouse sub-strains within the same "diet" subgroup using two-way ANOVA with Tukey's correction for multiple comparisons.

5.2.3.1.2 mRNA levels of fibrosis markers from whole liver tissue

Figure 5.19 and *Table 5.7* show the mRNA levels of fibrosis markers from whole liver tissue. In general, the expression of collagen-I, -III, -IVα1, -IVα2 and -VI, TGFβ1 and TIMP1 were increased in the HFD and HFD+DM groups compared with Chow groups (statistics comparing different "diet" groups not shown). Fibronectin mRNA level was reduced in the AlbCre and CCN1$^{fl/fl}$ HFD and HFD+DM groups, and ACTA2 mRNA level remained stable across the "diet" subgroups (*Table 5.7*). There was no significant difference in mRNA levels of the tested genes between the AlbCre groups and the CCN1$^{fl/fl}$ groups for the same "diet" subgroup, indicating that the two control sub-strains

behaved in a similar manner. The exception to this was in relation to TGFβ1 (*Figure 5.19E*) and fibronectin (*Table 5.7*) mRNA levels, where the AlbCre HFD+DM group had statistically higher expression compared with the CCN1$^{fl/fl}$ HFD+DM group.

Of particular note, there was an ~two-fold statistically significant increase in the CCN1-KO HFD+DM collagen-I (*Figure 5.19A*) and collagen-VI (*Figure 5.19D*) mRNA levels compared with both the AlbCre HFD+DM and CCN1$^{fl/fl}$ HFD+DM groups. A similar pattern was observed in collagen-III (*Figure 5.19B*), - IVα1 (*Figure 5.19C*) and -IVα2 (*Table 5.7*) mRNA levels, although these were only significant compared with the CCN1$^{fl/fl}$ HFD+DM group but not the AlbCre HFD+DM group. The CCN1-KO HFD+DM and AlbCre HFD+DM groups had similar mRNA levels of TGFβ1 (*Figure 5.19E*) and fibronectin (*Table 5.7*), and both were statistically higher than the CCN1$^{fl/fl}$ HFD+DM group. TIMP1 mRNA level was numerically higher in the CCN1-KO HFD+DM group, however this did not reach statistical significance (*Figure 5.19F*). There was no effect on ACTA2 mRNA level from the CCN1-KO (*Table 5.7*). Amongst the HFD groups, the CCN1-KO group had the highest numerical mRNA levels of the fibrosis markers compared with the AlbCre and CCN1$^{fl/fl}$ groups, however these findings were not statistically significant.

In summary, the overall pattern indicated an increase in fibrosis markers in the CCN1-KO mice, primarily observed in the HFD+DM subgroup, although this did not always meet statistical significance when using a rigorous test such as a two-way ANOVA with Tukey's correction for multiple comparisons.

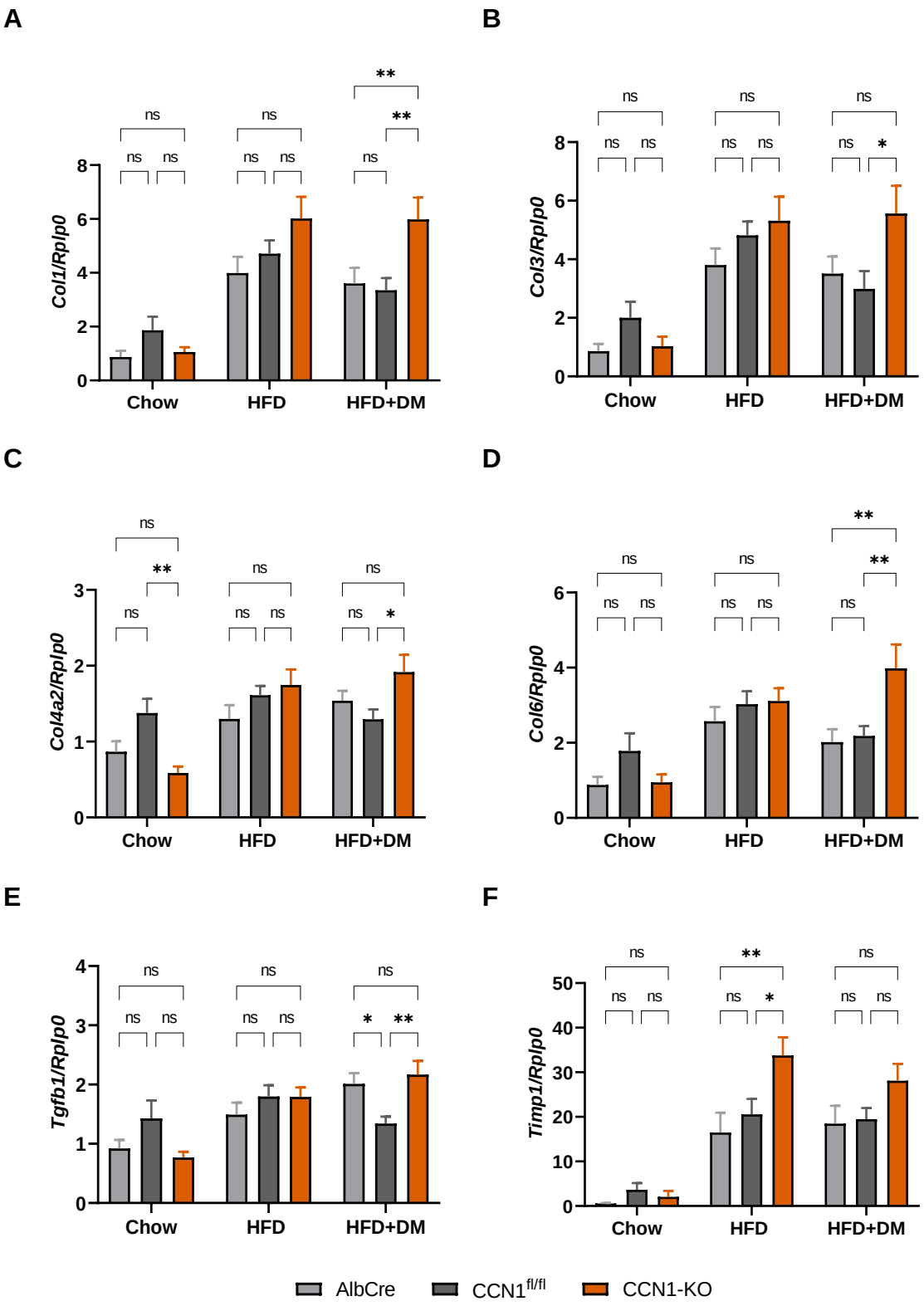

*Figure 5.19: mRNA levels of fibrosis markers Col1 (A), Col3 (B), Col4a2 (C), Col6 (D), Tgfb1 (E), and Timp1 (F). Data shown as mean ± SEM; n = 8 - 14. * p-value ≤ 0.05 or ** p-value ≤ 0.01 for comparison of mouse sub-strains within the same "diet" subgroup using two-way ANOVA with Tukey's correction for multiple comparisons. Col1, collagen-I; Col3, collagen-III; Col4a2, collagen-IVα2; Col6, collagen-VI; Rplp0, ribosomal protein, large, P0; Tgfb1, transforming growth factor β1; Timp1, tissue inhibitor of metalloproteinase 1; ns, not significant.*

5.3.3.2 The effects of hepatocyte CCN1 deletion on liver inflammation

5.3.3.2.1 Assessment of liver inflammation by histology

A) Assessment of lobular inflammation

In addition to fibrosis, a major hallmark of NASH is the development of inflammation[80]. Lobular inflammation was scored on H&E-stained tissue according to the NAS criteria (0 = absent, 1 = 1 focus, 2 = 2 - 4 foci, or 3 = > 4 foci per 200x field) by an independent anatomical pathologist (*Figure 5.20* and *Table 5.6*). The HFD+DM groups had the highest degree of lobular inflammation, with a mean of 2 - 4 foci per 200x field in each mouse sub-strain (AlbCre: 2.4 ± 0.1, CCN1$^{fl/fl}$: 2.8 ± 0.1, and CCN1-KO: 2.6 ± 0.1). The HFD groups had an intermediary level of lobular inflammation, although the CCN1$^{fl/fl}$ HFD group had less lobular inflammation compared with the AlbCre HFD and CCN1-KO HFD groups. The Chow groups all had a mean score of less than 1.

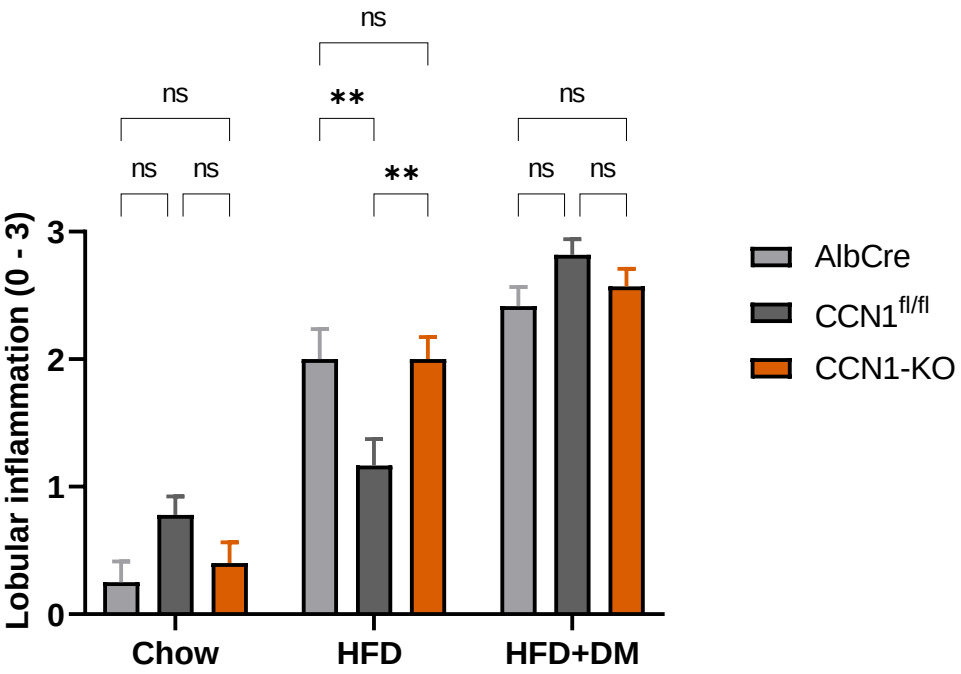

*Figure 5.20: Lobular inflammation scored according to the NAS criteria. Data shown as mean ± SEM; n = 8 - 14. ** p-value ≤ 0.01 for comparison of mouse sub-strains within the same "diet" subgroup using two-way ANOVA with Tukey's correction for multiple comparisons. ns, not significant.*

B) Assessment of portal inflammation

Portal inflammation was scored on H&E-stained tissue according to the Brunt criteria (0 = absent, 1 = mild, 2 = moderate, or 3 = severe) by an independent anatomical pathologist (*Figure 5.21* and *Table 5.6*). The HFD+DM groups had the highest degree of portal inflammation, which was graded as moderate to severe (AlbCre: 2.6 ± 0.2, CCN1$^{fl/fl}$: 2.8 ± 0.1, and CCN1-KO: 2.5 ± 0.2). The HFD groups had a mild to moderate degree of portal inflammation. The Chow groups all had low levels of portal inflammation. There was no effect from the CCN1-KO on the degree of portal inflammation.

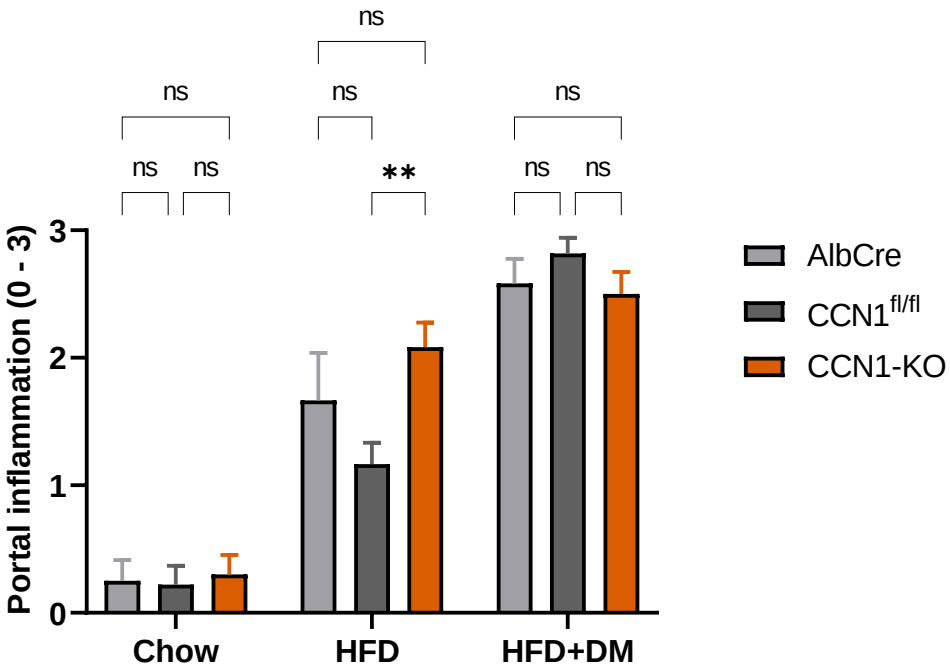

*Figure 5.21: Portal inflammation scored according to the Brunt criteria. Data shown as mean ± SEM; n = 8 - 14. ** p-value ≤ 0.010 for comparison of mouse sub-strains within the same "diet" subgroup using two-way ANOVA with Tukey's correction for multiple comparisons. ns, not significant.*

5.3.3.2.2 mRNA levels of inflammation markers from whole liver tissue

The mRNA levels of inflammation markers IL1B, CCL2, and TNF were measured (*Figure 5.22* and *Table 5.7*). Unlike the fibrosis markers, where the two control mouse sub-strains, AlbCre and CCN1$^{fl/fl}$, rendered similar results, there was a clear distinction between the AlbCre HFD+DM and CCN1$^{fl/fl}$ HFD+DM groups across all three inflammation genes: the AlbCre HFD+DM mice displayed significantly higher mRNA levels of IL1B, CCL2, and TNF compared with the CCN1$^{fl/fl}$ HFD+DM mice. The CCN1-

KO HFD+DM mice had similar expression to the CCN1$^{fl/fl}$ HFD+DM mice but significantly lower expression of IL1B and TNF compared with the AlbCre HFD+DM mice.

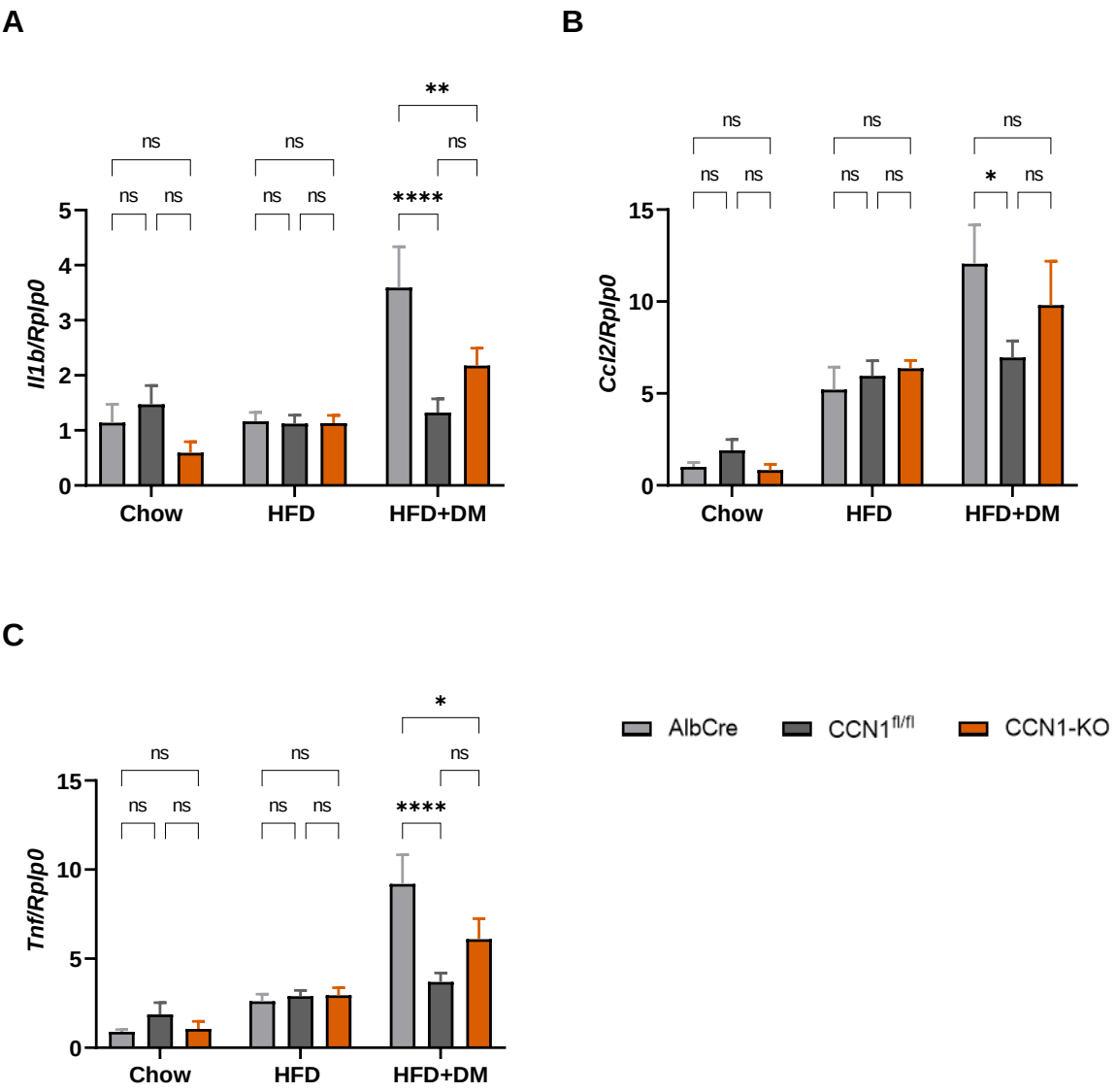

*Figure 5.22: mRNA levels of inflammation markers Il1b (A), Ccl2 (B), and Tnf (C). Data shown as mean ± SEM; n = 8 - 14. * p-value ≤ 0.05, ** p-value ≤ 0.01 or **** p-value ≤ 0.0001 for comparison of mouse sub-strains within the same "diet" subgroup using two-way ANOVA with Tukey's correction for multiple comparisons. Ccl2, C-C motif chemokine ligand 2; Il1b, interleukin-1β; Rplp0, ribosomal protein, large, P0; Tnf, tumour necrosis factor α; ns, not significant.*

5.3.3.3 The effects of hepatocyte CCN1 deletion on hepatocyte ballooning

5.3.3.3.1 Assessment of hepatocyte ballooning by histology

The development of hepatocyte ballooning is the pathognomonic histological feature of NASH[80]. Ballooning was scored on H&E-stained tissue according to the NAS criteria (0 = absent, 1 = few, or 2 = many) by an independent anatomical pathologist (*Figure 5.23* and *Table 5.6*). The CCN1-KO HFD+DM mice had lower scoring of hepatocyte ballooning compared with both the AlbCre HFD+DM and CCN1$^{fl/fl}$ HFD+DM (AlbCre: 2.0 ± 0.0, CCN1$^{fl/fl}$: 1.9 ± 0.1, and CCN1-KO: 1.4 ± 0.2). The HFD groups had an intermediary level of ballooning, and the Chow groups had minimal ballooning present.

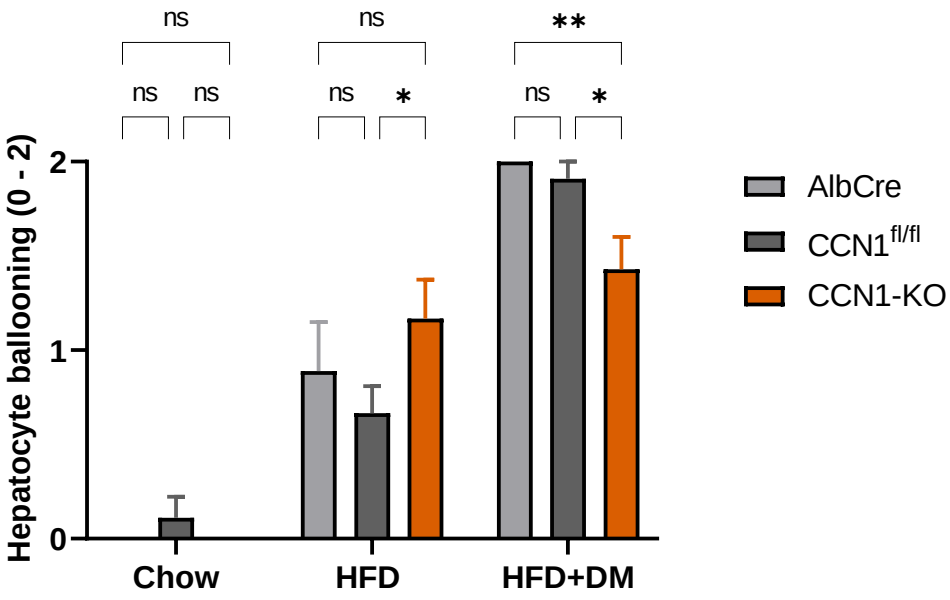

*Figure 5.23: Hepatocyte ballooning scored according to the NAS criteria. Data shown as mean ± SEM; n = 8 - 14. * p-value ≤ 0.05 or ** p-value ≤ 0.01 for comparison of mouse sub-strains within the same "diet" subgroup using two-way ANOVA with Tukey's correction for multiple comparisons. ns, not significant.*

5.3.3.4 The effects of hepatocyte CCN1 deletion on liver steatosis

5.3.3.4.1 Assessment of liver steatosis by histology

Steatosis was scored on H&E-stained tissue according to the NAS criteria (0 = < 5%, 1 = 5 - 33%, 2 = 34 - 66%, or 3 = > 66%) by an independent anatomical pathologist (*Figure 5.24* and *Table 5.6*). All Chow groups had mild steatosis, whereas all mice fed a high fat diet (HFD and HFD+DM groups) had very high levels of steatosis. There was no effect from the CCN1-KO on the degree of steatosis.

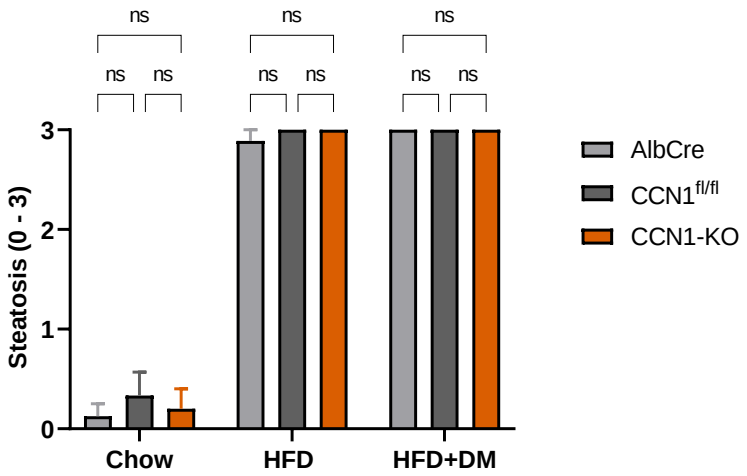

Figure 5.24: Steatosis scored according to the NAS criteria. Data shown as mean ± SEM; n = 8 - 14. ns (not significant), p-value > 0.05 for comparison of mouse sub-strains within the same "diet" subgroup using two-way ANOVA with Tukey's correction for multiple comparisons.

5.3.3.4.2 Measurement of liver triglycerides

Triglycerides were extracted from whole liver tissue and measured using a colorimetric assay[315,316]. High fat fed mice (HFD and HFD+DM groups) had higher amounts of triglyceride compared with the Chow groups (*Figure 5.25*; statistics comparing different "diet" groups not shown). There was no effect from the CCN1-KO on liver triglycerides, although there was a small but significant increase in the CCN1-KO HFD group compared with the CCN1$^{fl/fl}$ HFD group but not the AlbCre HFD group.

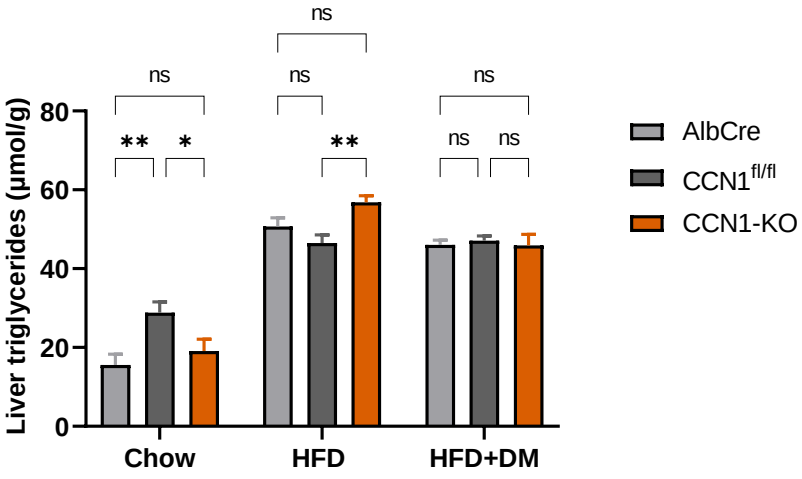

*Figure 5.25: Amount of liver triglycerides. Data shown as mean ± SEM; n = 8 - 14. * p-value ≤ 0.05 or ** p-value ≤ 0.01 for comparison of mouse sub-strains within the same "diet" subgroup using two-way ANOVA with Tukey's correction for multiple comparisons. ns, not significant.*

5.3.3.5 The effects of hepatocyte CCN1 deletion on the NAS

The NAS is calculated by the addition of scores for lobular inflammation, hepatocyte ballooning, and steatosis. As expected, the HFD+DM mice had the highest NAS, the HFD mice had an intermediary score, and the Chow mice had the lowest score (*Figure 5.26* and *Table 5.6*). Again, there was no effect observed from the CCN1-KO on this composite outcome. Representative images of the H&E-stained tissue from which the NAS was scored are shown in *Figure 5.27*.

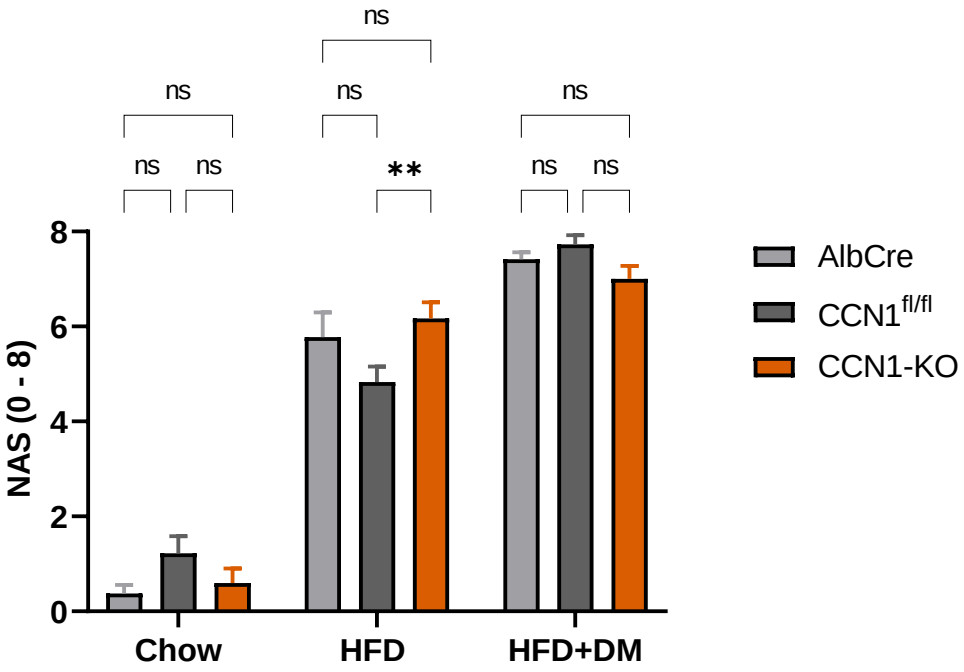

*Figure 5.26: NAS score. Data shown as mean ± SEM; n = 8 - 14. ** p-value ≤ 0.01 for comparison of mouse sub-strains within the same "diet" subgroup using two-way ANOVA with Tukey's correction for multiple comparisons. ns, not significant.*

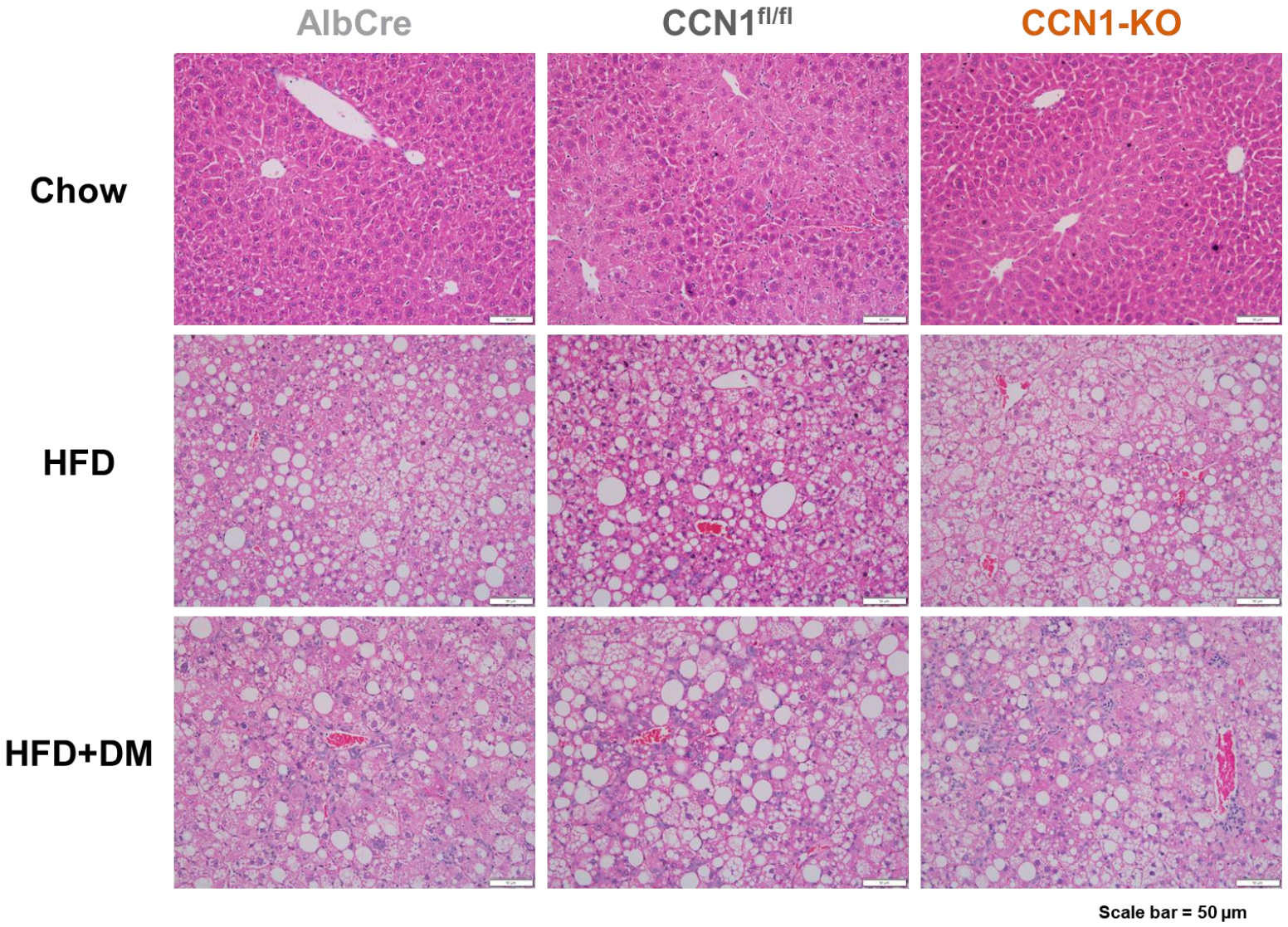

Figure 5.27: Representative histological images of H&E-stained liver tissue (200x magnification).

Table 5.6: Components of the Brunt and NAS criteria.

	Chow			HFD			HFD+DM		
	AlbCre	**CCN1$^{fl/fl}$**	**CCN1-KO**	**AlbCre**	**CCN1$^{fl/fl}$**	**CCN1-KO**	**AlbCre**	**CCN1$^{fl/fl}$**	**CCN1-KO**
Fibrosis (0 - 4)	0.0 ± 0.0	0.2 ± 0.1	0.3 ± 0.2	2.1 ± 0.4	1.9 ± 0.2	2.5 ± 0.2	2.8 ± 0.2	3.3 ± 0.1	2.8 ± 0.2
Lobular Inflammation (0 - 3)	0.3 ± 0.2	0.8 ± 0.1	0.4 ± 0.2	2.0 ± 0.2	1.2 ± 0.2	2.0 ± 0.2	2.4 ± 0.1	2.8 ± 0.1	2.6 ± 0.1
Portal Inflammation (0 - 3)	0.3 ± 0.2	0.2 ± 0.1	0.3 ± 0.2	1.7 ± 0.4	1.2 ± 0.2	2.1 ± 0.2	2.6 ± 0.2	2.8 ± 0.1	2.5 ± 0.2
Hepatocyte Ballooning (0 - 2)	0.0 ± 0.0	0.1 ± 0.1	0.0 ± 0.0	0.9 ± 0.3	0.7 ± 0.1	1.2 ± 0.2	2.0 ± 0.0	1.9 ± 0.1	1.4 ± 0.2
Steatosis (0 - 3)	0.1 ± 0.1	0.3 ± 0.2	0.2 ± 0.2	2.9 ± 0.1	3.0 ± 0.0	3.0 ± 0.0	3.0 ± 0.0	3.0 ± 0.0	3.0 ± 0.0
NAS (0 - 8)	0.4 ± 0.2	1.2 ± 0.4	0.6 ± 0.3	5.8 ± 0.5	4.8 ± 0.3	6.2 ± 0.3	7.4 ± 0.1	7.7 ± 0.2	7.0 ± 0.3

Data shown as mean ± SEM; n = 8 - 14. NAS, NAFLD activity score. Please note that as per the Methods, relevant p-values have been identified in the relevant Figures, not in the Table.

5.3.4 Potential biomarkers of NASH fibrosis in T2DM

5.3.4.1 mRNA levels of potential biomarkers

5.3.4.1.1 Other CCN family members

The mRNA levels of other CCN family members, CCN2 and CCN3 were measured (*Figure 5.28* and *Table 5.7*). CCN2 mRNA level was elevated in the CCN1-KO HFD+DM group, suggestive of a profibrotic process. There was no difference observed in CCN3 mRNA level.

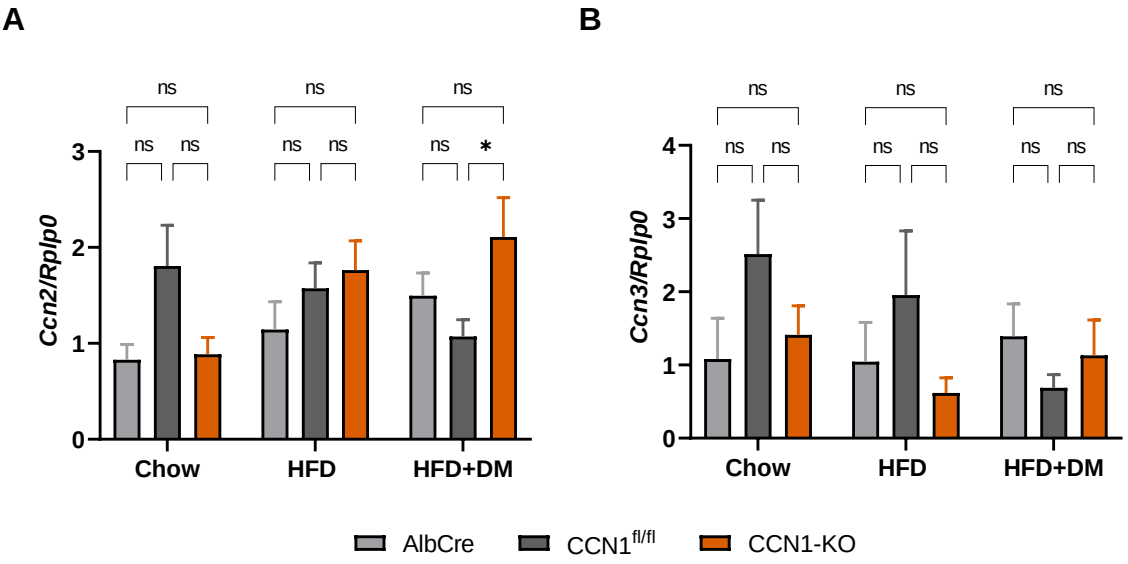

*Figure 5.28: mRNA levels of Ccn2 (A) and Ccn3 (B). Data shown as mean ± SEM; n = 8 - 14. * p-value ≤ 0.05 for comparison of mouse sub-strains within the same "diet" subgroup using two-way ANOVA with Tukey's correction for multiple comparisons. Ccn2, cellular communication network 2; Ccn3, cellular communication network 3; Rplp0, ribosomal protein, large, P0; ns, not significant.*

5.3.4.1.2 The DPP4 family

FAP is a marker of HSC activation, which are the predominant cells responsible for the deposition of ECM in the liver[67]. FAP is a member of the DPP4 family, and expresses not only DPP4 activity, but also collagenase activity.[366] There is increased mRNA level of DPP4 in liver tissue in the presence of liver disease[367], and circulating DPP4 activity is associated with hepatocyte apoptosis and fibrosis in humans with NASH and diabetes.[86] In this study, the mRNA level of FAP incrementally rose in the CCN1-KO mice from Chow to HFD to HFD+DM, consistent with increasing HSC activation (*Figure 5.29* and *Table 5.7*). In contrast, there was no progressive rise in the AlbCre or CCN1$^{fl/fl}$ mouse sub-strains. The CCN1-KO mice had a lower DPP4 mRNA level at baseline, with no subsequent change with HFD or HFD+DM. DPP4 mRNA

level also remained low in the AlbCre and CCN1$^{fl/fl}$ HFD and HFD+DM groups. These findings were inconsistent with the histology data quantifying PSR-stained liver tissue and mRNA levels of fibrosis markers indicating higher severity of fibrosis in the CCN1-KO HFD+DM group, and therefore higher levels of FAP and DPP4 compared with the control sub-strains were expected.

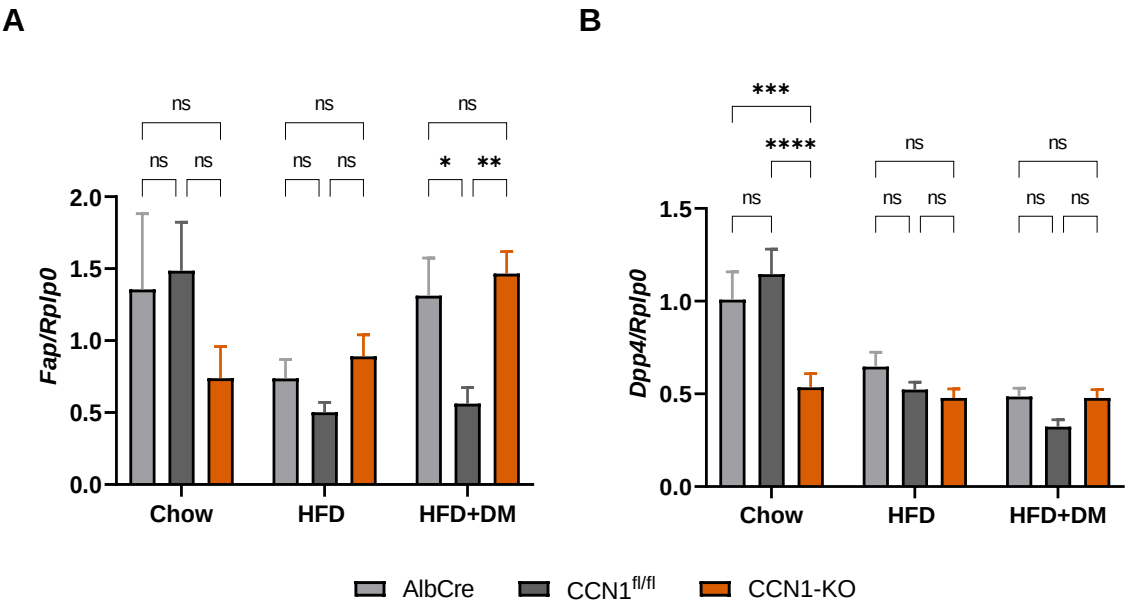

*Figure 5.29: mRNA levels of Fap (A) and Dpp4 (B). Data shown as mean ± SEM; n = 8 - 14. * p-value ≤ 0.05, ** p-value ≤ 0.01, *** p-value ≤ 0.001 or **** p-value ≤ 0.0001 for comparison of mouse sub-strains within the same "diet" subgroup using two-way ANOVA with Tukey's correction for multiple comparisons. Dpp4, dipeptidyl-peptidase 4; Fap, fibroblast activating protein; Rplp0, ribosomal protein, large, P0; ns, not significant.*

Table 5.7: mRNA levels normalised to the housekeeper gene and expressed as fold change (reference group = AlbCre Chow + CCN1$^{fl/fl}$ Chow).

	Chow			HFD			HFD+DM		
	AlbCre	**CCN1$^{fl/fl}$**	**CCN1-KO**	**AlbCre**	**CCN1$^{fl/fl}$**	**CCN1-KO**	**AlbCre**	**CCN1$^{fl/fl}$**	**CCN1-KO**
Col1	0.87 ± 0.22	1.86 ± 0.51	1.06 ± 0.18	3.99 ± 0.61	4.71 ± 0.49	6.02 ± 0.81	3.60 ± 0.58	3.35 ± 0.45	5.98 ± 0.82
Col3	0.87 ± 0.25	2.00 ± 0.55	1.03 ± 0.33	3.80 ± 0.57	4.82 ± 0.47	5.32 ± 0.82	3.51 ± 0.59	2.99 ± 0.60	5.56 ± 0.95
Col4a1	0.84 ± 0.09	1.31 ± 0.18	0.82 ± 0.13	2.15 ± 0.29	2.50 ± 0.38	3.42 ± 0.39	2.99 ± 0.38	2.22 ± 0.29	3.57 ± 0.37
Col4a2	0.87 ± 0.14	1.38 ± 0.19	0.59 ± 0.08	1.30 ± 0.18	1.61 ± 0.12	1.75 ± 0.20	1.54 ± 0.13	1.29 ± 0.13	1.92 ± 0.23
Col6	0.88 ± 0.22	1.78 ± 0.47	0.95 ± 0.21	2.57 ± 0.38	3.03 ± 0.34	3.11 ± 0.34	2.02 ± 0.34	2.18 ± 0.26	3.98 ± 0.64
Tgfb1	0.92 ± 0.14	1.43 ± 0.30	0.77 ± 0.10	1.49 ± 0.20	1.80 ± 0.19	1.79 ± 0.16	2.01 ± 0.18	1.34 ± 0.12	2.17 ± 0.23
Fn1	0.96 ± 0.10	1.16 ± 0.14	0.53 ± 0.08	0.68 ± 0.05	0.56 ± 0.02	0.49 ± 0.04	0.60 ± 0.03	0.34 ± 0.04	0.54 ± 0.04
Acta2	0.92 ± 0.50	2.73 ± 0.73	0.88 ± 0.23	0.93 ± 0.33	2.21 ± 0.61	1.04 ± 0.09	1.18 ± 0.22	3.67 ± 2.82	1.40 ± 0.29
Timp1	0.55 ± 0.15	3.64 ± 1.50	2.07 ± 1.32	16.48 ± 4.45	20.57 ± 3.46	33.75 ± 4.12	18.50 ± 3.97	19.49 ± 2.47	28.09 ± 3.83
Il1b	1.14 ± 0.33	1.47 ± 0.34	0.59 ± 0.20	1.16 ± 0.16	1.12 ± 0.15	1.13 ± 0.14	3.60 ± 0.74	1.32 ± 0.25	2.18 ± 0.32
Ccl2	1.00 ± 0.24	1.91 ± 0.58	0.84 ± 0.30	5.21 ± 1.22	5.96 ± 0.82	6.36 ± 0.43	12.05 ± 2.12	6.95 ± 0.90	9.81 ± 2.39
Tnf	0.89 ± 0.12	1.87 ± 0.66	1.05 ± 0.43	2.60 ± 0.41	2.89 ± 0.32	2.94 ± 0.43	9.19 ± 1.64	3.70 ± 0.50	6.09 ± 1.15
Ccn2	0.83 ± 0.16	1.81 ± 0.43	0.89 ± 0.18	1.14 ± 0.29	1.57 ± 0.27	1.76 ± 0.31	1.50 ± 0.24	1.07 ± 0.17	2.11 ± 0.41
Ccn3	1.08 ± 0.56	2.51 ± 0.74	1.41 ± 0.40	1.04 ± 0.54	1.95 ± 0.88	0.62 ± 0.21	1.39 ± 0.44	0.69 ± 0.18	1.13 ± 0.49
Dpp4	1.01 ± 0.15	1.15 ± 0.13	0.54 ± 0.07	0.65 ± 0.08	0.52 ± 0.04	0.48 ± 0.05	0.49 ± 0.05	0.32 ± 0.04	0.48 ± 0.04
Fap	1.36 ± 0.53	1.49 ± 0.34	0.74 ± 0.22	0.74 ± 0.13	0.50 ± 0.07	0.89 ± 0.15	1.31 ± 0.26	0.56 ± 0.11	1.47 ± 0.15

Data shown as mean ± SEM; n = 8 - 14. *Acta2*, α smooth muscle actin; *Ccl2*, C-C motif chemokine ligand 2; *Ccn2*, cellular communication network 2; *Ccn3*, cellular communication network 3; *Col1*, collagen-I; *Col3*, collagen-III; *Col4a1*, collagen-IVα1; *Col4a2*, collagen-IVα2; *Col6*, collagen-VI; *Dpp4*, dipeptidyl-peptidase 4; *Fap*, fibroblast activation protein; *Fn1*, fibronectin; *Il1b*, interleukin-1β; *Tgfb1*, transforming growth factor β1; *Timp1*, tissue inhibitor of metalloproteinase 1; *Tnf*, tumour necrosis factor α. Please note that as per the Methods, relevant p-values have been identified in the relevant Figures, not in the Table.

5.3.4.2 Plasma cytokeratin-18

CK-18 has been proposed as a potential biomarker for NASH fibrosis. Plasma concentrations of CK-18 were generally higher in the HFD+DM groups, but there was no effect observed in the CCN1-KO HFD+DM group compared with the control strains (*Figure 5.30*).

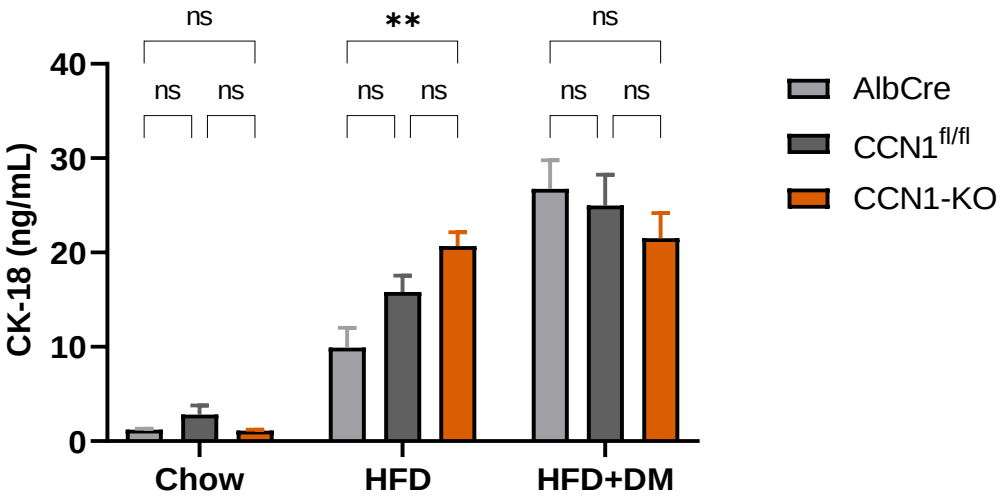

*Figure 5.30: Plasma cytokeratin-18 quantification. Data shown as mean ± SEM; n = 8 - 14. ** p-value ≤ 0001 for comparison of mouse sub-strains within the same "diet" subgroup using two-way ANOVA with Tukey's correction for multiple comparisons. CK-18, cytokeratin-18; ns, not significant.*

5.3.5 Pre-clinical *in vivo* mouse imaging

5.3.5.1 Liver ultrasound

It has been reported in the literature that liver ultrasound can be used as a novel non-invasive method for assessing liver fibrosis in mice[301,303] but unfortunately attempts to replicate this were unsuccessful. The recommended ultrasound images were captured according to the published methods; however, the analysis of the data is complex and requires specialised software and external assistance. Ultrasound images taken at week 25 of high fat fed mice demonstrated hyperechoic liver tissue and hepatomegaly. Representative images are shown in *Figure 5.31*.

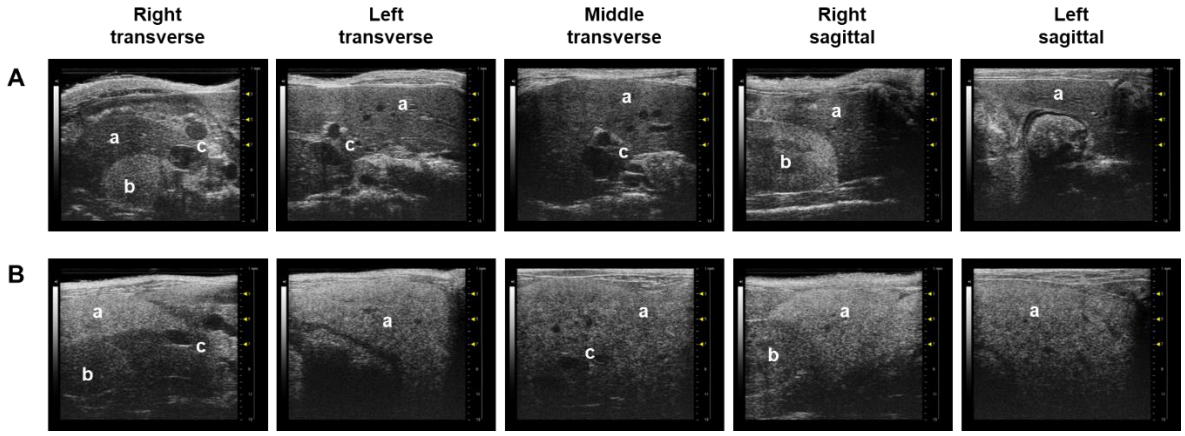

Figure 5.31: Representative liver ultrasound images taken at week 25 of a chow fed mouse (A) and an HFD+DM mouse (B). a, liver tissue; b, right kidney; c, blood vessels.

5.4 Discussion

5.4.1 Summary of main findings

The CCN1 Study demonstrated that targeting hepatocyte CCN1 worsened the development of NASH fibrosis induced by high fat feeding followed by diabetes. Quantitative histological analysis showed an increased amount of liver fibrosis in the CCN1-KO HFD+DM mice compared with the control sub-strain mice (AlbCre HFD+DM and $CCN1^{fl/fl}$ HFD+DM groups), with supporting data from increased mRNA levels of fibrosis markers in liver tissue. There were no differences observed in the CCN1-KO HFD+DM mice in the components of the NAS or Brunt criteria, although these scoring systems have not been validated in mice. In addition, a systemic metabolic phenotype was identified in the CCN1-KO HFD+DM mice, characterised by greater body weight and lower blood glucose levels.

5.4.2 More severe hepatic fibrosis in mice with deletion of hepatocyte CCN1

The quantitative histological assessment of PSR-stained liver tissue and collagen mRNA level data indicate that the absence of hepatocyte CCN1 causes increased liver fibrosis. This finding was most clear in the CCN1-KO HFD+DM group rather than the CCN1-KO HFD group. The FaD model was originally developed with the evidence that T2DM exacerbates the liver fibrosis phenotype compared with high fat feeding alone. CCN1 has previously been found to be an important factor in the induction of senescence of activated HSCs to aid prevention of increased liver fibrosis[246] and future studies should examine HSC activation status and degree of senescence, which may potentially be altered in the CCN1-KO HFD+DM mice.

It may well be that in the presence of relative insulin deficiency, hepatic insulin signalling is selectively impaired and hepatocyte CCN1 deletion may exacerbate this finding. Indeed, it has previously been shown using this current model that MAPK signalling through ERK phosphorylation is markedly increased in HFD+DM compared with Chow fed mice[144], and future studies should examine MAPK signalling in the CCN1-KO HFD+DM mice. Overall, it is predicted that HSC senescence will be decreased in the CCN1-KO HFD+DM mice, and the number of activated HSCs will be increased. In this case, the hepatocyte CCN1 deletion may not substantially impact the increased phosphorylation of ERK already seen in HFD+DM, but the lack of HSC senescence and/or increased HSC activation may further contribute to worsening liver fibrosis.

There was a trend to elevation of TIMP1 mRNA level in the mice with hepatocyte CCN1 deletion compared with the control sub-strains (~50%). TIMP1 inhibits the actions of MMPs, thereby preventing degradation of ECM and worsening fibrosis[170]. TIMP1 is produced predominantly by activated HSCs[171,374,375], and thus it would be expected to be further increased in mice with a hepatocyte CCN1 deletion which are hypothesised to have greater number of activated HSCs. In addition to preventing ECM degradation, TIMP1 also promotes fibrogenesis through the inhibition of apoptosis of activated HSCs[173,174]. TIMP1 mRNA level is regulated by several pro-inflammatory cytokines, including IL1B, TNF, and TGFβ[172]. This study did not show up-regulation of these inflammatory markers at the mRNA level, suggesting that other pathways, such as greater number of activated HSCs, may be involved. Another potential indirect pathway may involve CCN2, which was up-regulated in the CCN1-KO HFD+DM group. CCN2 has been shown to promote fibrosis though increasing the expression of TIMP1[273].

There were significant increases in mRNA levels of collagen-I, -III, -IVα2 and -VI in the CCN1-KO HFD+DM mice compared with the control sub-strains. Collagen-I and -VI are the main collagens deposited in increased fibrosis. Collagen-VI production is tightly linked to activated HSCs. It is unclear in this study whether absence of CCN1 is inducing changes in collagen-VI via effects on hepatocytes or effects on HSCs. Further studies assessing protein levels of the collagens are needed.

The antifibrotic properties of CCN1 in the liver are related to the induction of senescence of activated HSCs[246]. This prevents further proliferation of activated HSCs, induces up-regulation of MMPs with down-regulation of collagens and TGFβ1, and signals for removal of senescent cells by natural killer cells[286]. Further studies examining the activated and senescent forms of HSCs are required. This study did not demonstrate increased mRNA levels of ACTA2 or FAP, both markers of activated HSCs, however these genes may undergo post-transcriptional or post-translational modification and assessment of protein levels may be more valuable.

5.4.3 Identification of a systemic phenotype in CCN1-KO HFD+DM mice

The systemic phenotype identified in the CCN1-KO HFD+DM group was characterised by increased fat deposition in subcutaneous and epididymal fat stores, with lesser hyperglycaemia. The insulin resistance and pancreatic β cell effectiveness were trending to increases in each but were not statistically significant. The data suggest that the CCN1-KO HFD+DM mice are less insulin deficient than the controls and can overcome the insulin resistance to improve the blood glucose levels. The reason for this is unclear; it may be that the mice with hepatocyte CCN1 deletion were less susceptible to the toxic effects of STZ on the pancreatic β cells than the controls, as even after one week of STZ administration the hyperglycaemia was less despite receiving the same weight-based dose of STZ as the control mice. Alternatively, mice with hepatocyte CCN1 deletion may exhibit enhanced pancreatic β cell recovery. To confirm such effects would require a repeat of the same study with analysis of the pancreas. If the changes in glucose and insulin were replicated, then consideration of using other methods to induce diabetes in the model, such as with alloxan or use of mice with genetically-induced diabetes, would be helpful in excluding STZ as the culprit.

In turn, the relative hyperinsulinaemia may be contributing to the increased fat deposition in the CCN1-KO HFD+DM mice. The mice in this group had baseline body weights equivalent to the other mice in the study. However, they exhibited greater total weight gain over the course of the study (versus the AlbCre and $CCN1^{fl/fl}$ HFD+DM groups), greater fat mass by body composition (versus the AlbCre HFD+DM group), and greater epididymal (versus the $CCN1^{fl/fl}$ HFD+DM group) and subcutaneous (versus the AlbCre and $CCN1^{fl/fl}$ HFD+DM groups) fat depots. Insulin plays an

important role in fat accumulation, through promotion of lipid uptake and storage, stimulation of lipogenesis, and inhibition of lipolysis[376]. Interestingly, the liver weight was not further elevated in the CCN1-KO HFD+DM mice compared with the control mice, nor were the amount of liver triglyceride or plasma triglyceride levels. This may suggest that the effects of insulin on lipid pathways are more affected in some tissues compared with others.

Whilst specific caloric intake and energy expenditure measurements were not undertaken, food intake and mouse activity were grossly monitored. They were not noticeably different between the different sub-strains of mice and are thus unlikely to explain the differences in body weight and fat composition. Future studies might include use of BioDAQ Food and Water intake monitoring system and/or Promethion metabolic cages to objectively measure these variables.

The mice with hepatocyte CCN1 deletion also demonstrated an interesting phenotype where the hsCRP levels were lower than the control mice. This finding was independent of the “diet” subtype and was observed in the Chow fed mice, the HFD mice, and the HFD+DM mice. As CRP is synthesised predominantly by hepatocytes, the data suggest that hepatocyte CCN1 may be necessary for production of normal CRP levels. Interestingly, CRP has been shown to induce CCN1 in vascular endothelial cells[377], although no studies have reported systemic CRP dependence on liver CCN1.

It is possible that the systemic phenotype of the CCN1-KO HFD+DM mice contributed to, or primarily caused the increased liver fibrosis. However, this is less likely than a direct hepatic fibrotic effect, as there was no increase in liver inflammatory markers in the CCN1-KO HFD+DM mice, suggesting that some more direct profibrotic effect of hepatocyte CCN1 absence occurred. In addition, the mice were less hyperglycaemic rather than more. Previous use of this model has demonstrated that within the HFD+DM mice, greater insulin resistance links to more severe fibrosis[145], but in the current study the hepatocyte CCN1 deletion in the HFD+DM mice did not cause statistically significant greater insulin resistance.

5.4.4 Liver tissue CCN1 levels with hepatocyte CCN1 deletion

In the mice with hepatocyte CCN1 deletion, the CCN1 mRNA level from whole liver tissue was reduced by more than 80% across each of the Chow, HFD, and HFD+DM groups when compared with both control mouse groups. Although the lack of good quality commercial antibodies for mouse CCN1 have made it challenging to provide much protein data, one antibody did detect a faint band of the correct molecular mass that showed that CCN1 protein level was lower in the CCN1-KO liver tissue (shown in *Section 2.3.1.4*). Overall, this indicates successful deletion of hepatocyte CCN1 using the CreLoxP system. Residual CCN1 expression is probably derived from non-hepatocyte cells.

5.4.5 Comparison of the two control HFD+DM groups

Unlike The CCN2 Study, where there were several systemic differences between the AlbCre HFD+DM mice and the $CCN2^{fl/fl}$ HFD+DM mice, the two control groups in The CCN1 Study had a similar overall phenotype. An exception to this was in the mRNA levels of liver tissue inflammatory markers, where the AlbCre HFD+DM group had approximately double the expression of the $CCN1^{fl/fl}$ HFD+DM group in IL1B, CCL2, and TNF. A similar pattern was observed for the AlbCre HFD+DM group in The CCN2 Study. This suggests that the AlbCre mice generate a greater inflammatory response in the liver when exposed to HFD+DM conditions. The implications of this are unclear, as both control sub-strains developed similar amounts of liver fibrosis on histological analysis and similar increases in mRNA levels of fibrosis markers. It is possible that the AlbCre mice have increased protein misfolding of albumin in the liver leading to greater ER stress, but further studies are needed to support this. Nevertheless, it is important to acknowledge the differences between the control groups under HFD+DM conditions, so as not to misinterpret the data when making comparisons to the CCN1-KO HFD+DM group.

5.4.6 Conclusion

The CCN1 Study primarily addressed if hepatocyte CCN1 deletion worsens liver fibrosis in the HFD+DM model. The quantitative PSR histological data and mRNA levels for ECM components support the main hypothesis that was being tested. The novelty of the current research is that findings of a lack of hepatocyte CCN1 led to increased fibrosis in this clinically relevant metabolic model of high fat feeding with

diabetes. While other researchers in the CCN1 field have also found the lack of CCN1 exacerbates liver fibrosis, the models used were not metabolic in type and were based on CCl_4 exposure or bile duct ligation[286]. The current work now extends the CCN1 findings to this translational metabolic model and it suggests that hepatocyte CCN1 has an important counter-regulatory role to limit liver fibrosis.

Chapter 6: Circulating CCNs as Potential Biomarkers of Diabetes-Related Complications

6.1 Introduction

Development of diabetes-related complications causes increased morbidity and mortality in individuals with T2DM. Routine screening for some complications is recommended for early detection of complications[13,29,33]. While some biomarkers can predict development of complications before they occur, such as HbA1c, hsCRP, and albuminuria, some of these are not specific for one tissue, and overall, there are few markers with proven clinical utility.

The CCN proteins are key signalling and regulatory molecules implicated in normal physiology and pathological states[240]. They stimulate mitosis, adhesion, apoptosis, ECM production, growth arrest and migration[240]. Different CCNs may be involved in different stages of the development of diabetes and its complications[272]. While there is evidence that some CCNs may be mediators of certain complications at a tissue or organ level, whether circulating CCNs can predict certain diabetes complications, is an albeit related, but different issue. The aim of this study was to determine if circulating levels of CCN1, CCN2, and CCN3, enabling readily accessible systemic CCN levels, can be used as potential biomarkers of diabetes-related complications, including NASH fibrosis, in clinical and pre-clinical studies.

6.2 Methods

The Diabetes and Steatohepatitis (DaSH) Study was a cross-sectional study of individuals with T2DM attending the RPAH Diabetes Centre (described in detail in *Section 2.4.1*). Circulating levels of CCN1, CCN2 and CCN3 were measured using commercial kits from historical blood samples collected in The DaSH Study. Univariate (Spearman's test) and multivariate stepwise linear and logistic regression analyses were used to determine correlations between human circulating CCN concentrations and NASH fibrosis, as well as other clinical, biochemical, or radiological characteristics.

The CCN2 Study and The CCN1 Study used a translatable mouse model of high fat feeding and diabetes to study the effects of hepatocyte-specific gene deletion of CCN2 and CCN1 on the development and progression of NASH fibrosis (described in detail in *Section 2.3*). Circulating levels of CCN1, CCN2 and CCN3 were measured using

commercial kits from plasma samples collected from the mice in these pre-clinical studies (described in detail in *Section 2.4.2*). Univariate (Pearson's test) analyses were used to determine correlations between mouse circulating CCN concentrations and severity of liver fibrosis, as well as other metabolic, biochemical, or histological characteristics. All correlative statistics were performed using SPSS version 26.0 (IBM, Armonk, NY, USA).

6.3 Results

6.3.1 Circulating CCNs in The DaSH Study

6.3.1.1 Clinical and biochemical characteristics

The baseline characteristics of participants in The DaSH Study have been reported previously[86,87,317]. Out of the 108 participants included in the original study, two participants were excluded from this study as they had T1DM. *Table 6.1* and *Table 6.2* show the clinical and biochemical characteristics of the 106 participants included in this sub-study cohort. One patient did not have a height recorded and thus BMI could not be calculated, and a valid Fibroscan® reading could not be obtained from four patients.

Table 6.1: Clinical characteristics of participants in The DaSH Study.

	All Participants	
Gender, % male (n)	64.7 (66)	n = 106
Age, years (range)	62.6 ± 9.6 (40 - 82)	n = 106
Duration of diabetes, years (range)	11.2 ± 8.5 (0 - 41)	n = 106
Insulin-requiring, % (n)	35.8 (38)	n = 106
Presence of ≥ one diabetes-related complication, % (n)	75.5 (80)	n = 106
Presence of ≥ one microvascular complication, % (n)	70.8 (75)	n = 106
Peripheral neuropathy	51.9 (55)	n = 106
Diabetic retinopathy	19.8 (21)	n = 106
Diabetic nephropathy	38.7 (41)	n = 106
Diabetic foot ulcer/amputation	10.4 (11)	n = 106
Presence of ≥ one macrovascular complication, % (n)	24.5 (26)	n = 106
Ischaemic heart disease	19.8 (21)	n = 106
Peripheral vascular disease	6.6 (7)	n = 106
Cerebrovascular accident	8.5 (9)	n = 106
NAFLD	87.7 (93)	n = 106
LSM, kPa	5.8 [4.4 - 8.4]	n = 102
LSM ≥ 10.3 kPa	18.6 (19)	n = 102
Body weight, kg	89.2 ± 22.1	n = 106
BMI, kg/m^2	31.4 ± 6.2	n = 105
Overweight/obese, % (n)	87.6 (92)	n = 105
History of hypertension, % (n)	79.2 (84)	n = 106
SBP, mmHg	136.8 ± 16.0	n = 106
DBP, mmHg	78.4 ± 10.5	n = 106
History of dyslipidaemia, % (n)	90.6 (96)	n = 106

Data expressed as mean ± SD, % (n) or median [IQR]. BMI, body mass index; DBP, diastolic blood pressure; LSM, liver stiffness measurement; NAFLD, non-alcoholic fatty liver disease; SBP, systolic blood pressure.

Table 6.2: Biochemical characteristics of participants in The DaSH Study.

	All Participants	
HbA1c, % NGSP units	7.5 ± 1.2	n = 106
ALP, U/L	78.2 ± 26.6	n = 106
GGT, U/L	38.3 ± 40.2	n = 106
ALT, U/L	32.6 ± 22.0	n = 106
AST, U/L	26.5 ± 12.0	n = 103
Albumin, g/L	45.9 ± 2.9	n = 106
Platelet count, x 10^9/L	255.3 ± 71.2	n = 106
Ferritin, µg/L	95.0 ± 99.9	n = 106
Total cholesterol, mmol/L	4.1 ± 1.0	n = 106
Triglycerides, mmol/L	1.8 ± 1.2	n = 106
HDL-c, mmol/L	1.2 ± 0.4	n = 106
LDL-c, mmol/L	2.1 ± 0.8	n = 102
Creatinine, µmol/L	78.6 ± 20.9	n = 106
eGFR, mL/min/1.73m^2	88.1 ± 21.1	n = 106
UACr, mg/mmol Cr	10.9 ± 32.7	n = 105

Data expressed as mean ± SD. ALP, alkaline phosphatase; ALT, alanine aminotransferase; AST, aspartate aminotransferase; eGFR, estimated glomerular filtration rate; GGT, gamma-glutamyl transferase; HbA1c, haemoglobin A1c; HDL-c, high-density lipoprotein-cholesterol; LDL-c, low-density lipoprotein cholesterol; NGSP, National Glycohemoglobin Standardization Program; UACr, urine albumin to creatinine ratio.

6.3.1.2 Circulating CCN concentrations

The concentrations of each of the CCNs measured are listed in *Table 6.3*. Some serum and plasma samples were unavailable for testing.

Table 6.3: Median and interquartile ranges for circulating CCN1, CCN2, and CCN3.

	CCN1 (pg/mL)	**CCN2 (ng/mL)**	**CCN3 (ng/mL)**	
	Serum	**Serum**	**Serum**	**Plasma**
	n = 92	n = 92	n = 93	n = 100
Median	225.0	744.8	15.7	17.6
25% Percentile	187.2	512.4	11.7	13.6
75% Percentile	267.7	1125.6	28.1	27.5

A univariate analysis was performed to assess the correlation between the circulating CCNs, and the results are shown in *Table 6.4*. Serum CCN1 concentration did not correlate with measures of CCN2 or CCN3, although the p-values for each of these interactions were between 0.068 - 0.090. Serum CCN2 concentration positively correlated with plasma CCN3 concentration (r = 0.226, p = 0.034), and serum and plasma CCN3 concentrations correlated strongly with each other (r = 0.917, p < 0.001). The results of the circulating CCN2 concentrations measured using the R&D assay have not been described here, as they did not make plausible biological sense and the results were not consistent with data from the literature.

Table 6.4: Correlation matrix for circulating CCN1, CCN2, and CCN3.

		CCN1	**CCN2**	**CCN3**	
		Serum	**Serum**	**Serum**	**Plasma**
CCN1	**Serum**				
CCN2	**Serum**	0.191 (p = 0.068)			
CCN3	**Serum**	0.190 (p = 0.070)	0.170 (p = 0.105)		
	Plasma	0.182 (p = 0.090)	0.226 (p = 0.034)	0.917 (p < 0.001)	

Data expressed as Spearman r (p-value). Significant correlations (p-value ≤ 0.05) are highlighted in green.

6.3.1.3 Circulating CCNs and general metabolic variables

A higher serum CCN1 concentration was associated with older age, female gender, lower body weight, lower WC, lower WHR and higher HDL-c (*Table 6.5* and *Figure 6.1*). This data suggests that CCN1 may be a serological biomarker of reduced metabolic syndrome presence in individuals with T2DM. There was no association with duration of diabetes or HbA1c.

Circulating CCN2 concentration was associated with a lower BMI (r = -0.258, p = 0.014). There were no significant correlates between serum or plasma CCN3 concentrations and metabolic variables.

Table 6.5: Univariate correlations between circulating CCNs and metabolic variables.

	CCN1	CCN2	CCN3	
n = 92 - 106	**Serum**	**Serum**	**Serum**	**Plasma**
Age	0.213 (p = 0.041)	0.107 (p = 0.310)	0.060 (p = 0.567)	0.113 (p = 0.261)
Gender	-0.264 (p = 0.011)	-0.053 (p = 0.619)	-0.084 (p = 0.426)	-0.066 (p = 0.516)
Duration of diabetes	0.044 (p = 0.674)	0.082 (p = 0.438)	-0.039 (p = 0.710)	-0.046 (p = 0.650)
HbA1c	-0.006 (p = 0.955)	-0.034 (p = 0.749)	-0.051 (p = 0.629)	0.014 (p = 0.888)
Insulin therapy	0.132 (p = 0.209)	-0.057 (p = 0.591)	-0.002 (p = 0.984)	0.011 (p = 0.911)
Body weight	-0.260 (p = 0.012)	-0.175 (p = 0.095)	-0.005 (p = 0.963)	0.004 (p = 0.967)
BMI	-0.165 (p = 0.118)	-0.258 (p = 0.014)	-0.014 (p = 0.896)	0.001 (p = 0.990)
WC	-0.261 (p = 0.013)	-0.121 (p = 0.253)	-0.054 (p = 0.610)	-0.032 (p = 0.756)
WHR	-0.271 (p = 0.009)	-0.012 (p = 0.911)	-0.140 (p = 0.182)	-0.124 (p = 0.221)
Hypertension	0.069 (p = 0.512)	0.054 (p = 0.609)	-0.106 (p = 0.313)	-0.062 (p = 0.541)
SBP	0.099 (p = 0.348)	-0.058 (p = 0.584)	0.014 (p = 0.896)	-0.019 (p = 0.852)
DBP	-0.011 (p = 0.915)	-0.006 (p = 0.956)	-0.022 (p = 0.833)	0.014 (p = 0.890)
Dyslipidaemia	0.046 (p = 0.663)	-0.150 (p = 0.154)	0.076 (p = 0.467)	0.021 (p = 0.837)
Total cholesterol	0.182 (p = 0.082)	0.072 (p = 0.496)	0.069 (p = 0.513)	0.099 (p = 0.327)
Triglycerides	-0.050 (p = 0.634)	0.187 (p = 0.074)	-0.025 (p = 0.814)	0.031 (p = 0.760)
HDL-c	0.321 (p = 0.002)	0.027 (p = 0.795)	-0.013 (p = 0.902)	-0.066 (p = 0.514)
LDL-c	0.137 (p = 0.202)	-0.093 (p = 0.386)	0.030 (p = 0.779)	0.049 (p = 0.633)

Data expressed as Spearman r (p-value). Significant correlations (p-value ≤ 0.05) are highlighted in green. BMI, body mass index; DBP, diastolic blood pressure; HbA1c, haemoglobin A1c; HDL-c, high-density lipoprotein-cholesterol; LDL-c, low-density lipoprotein cholesterol; SBP, systolic blood pressure; WC, waist circumference; WHR, waist to hip ratio.

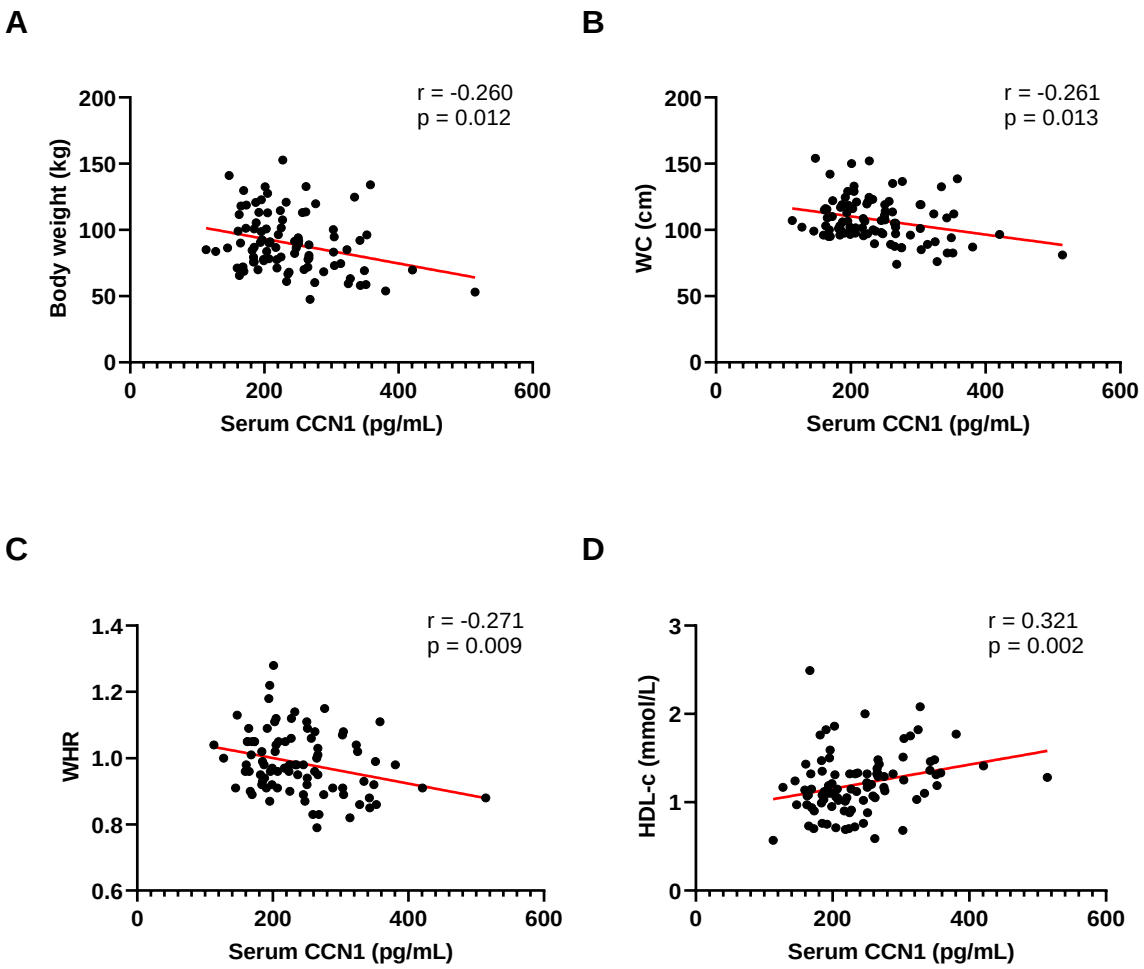

Figure 6.1: Serum CCN1 correlations with metabolic parameters: body weight (A), WC (B), WHR (C), and HDL-c (D). HDL-c, high-density lipoprotein cholesterol; WC, waist circumference; WHR, waist to hip ratio.

6.3.1.4 Circulating CCNs and diabetes-related complications

There was a total of 80 participants that had a least one diabetes-related complication, including 75 that had at least one microvascular complication and 26 that had at least one macrovascular complication (*Table 6.6*). Two participants had advanced liver fibrosis with no other diabetes-related complications. The definitions of diabetes-related complications applied in this study are listed in *Table 6.7*.

Serum CCN1 concentrations did not correlate with the presence of any diabetes-related complication. There was a positive association with BNP, however the significance of this is unclear. Unfortunately, we did not have information on the presence or history of congestive cardiac failure, which is closely associated with elevated BNP concentrations[378]. There have not been any previous reports of CCN1

being linked to cardiac disease in diabetes[272]. In mice, CCN1 is essential for normal cardiac development[379].

Serum CCN2 concentration was positively associated with an abnormal monofilament test (r = 0.236, p = 0.024). There have not been any previous reports on CCNs in diabetic peripheral neuropathy[272] and further clarification in this area is needed, including assessment for correlations with objective measures such as biothesiometer readings. A higher serum CCN2 concentration was associated with increased likelihood of having a reduced eGFR (r = 0.296, p = 0.004; *Figure 6.3*), which is consistent with its known profibrotic role in DKD[380]. There was also a strong positive correlation with higher BNP (r = 0.338, p = 0.001; *Figure 6.2*), again consistent with previous research demonstrating a link between CCN2 and cardiovascular disease[272]. The correlation with presence of diabetic retinopathy was did not quite reach statistical significance (r = 0.197, p = 0.064), however CCN2 has previously been associated with this microvascular complication too[272].

Plasma CCN3 concentration was associated with a lower eGFR (continuous and categorical) and a higher UACr, suggesting that it may be a predictor of kidney disease in individuals with T2DM (*Figure 6.2* and *Figure 6.3*). Biologically, this is consistent with the understanding that CCN3 is an antifibrotic protein, and is increased in DKD as it inhibits the profibrotic actions of CCN2[272]. It is also not surprising that circulating CCN2 concentrations correlate very strongly with circulating CCN3 concentrations (*Table 6.4*), although if CCN3 was able to overcome CCN2, then a negative correlation might also be expected.

Table 6.6: Univariate correlations between circulating CCNs and diabetes-related complications.

		CCN1	CCN2	CCN3	
	n	**Serum**	**Serum**	**Serum**	**Plasma**
Presence of ≥ one diabetes-related complication	80	-0.066 (p = 0.534)	0.006 (p = 0.954)	-0.033 (p = 0.754)	-0.099 (p = 0.328)
Presence of ≥ one microvascular complication	75	-0.044 (p = 0.680)	0.089 (p = 0.397)	-0.038 (p = 0.721)	-0.111 (p = 0.271)
Presence of ≥ one macrovascular complication	26	-0.053 (p = 0.617)	0.006 (p = 0.957)	0.007 (p = 0.950)	0.023 (p = 0.823)
Peripheral neuropathy (AMT or Sx of PN)	55	-0.009 (p = 0.935)	0.059 (p = 0.579)	-0.060 (p = 0.570)	-0.126 (p = 0.213)
Abnormal monofilament test	21	-0.036 (p = 0.732)	0.236 (p = 0.024)	0.093 (p = 0.377)	0.164 (p = 0.103)
Symptoms of peripheral neuropathy	52	-0.007 (p = 0.947)	0.031 (p = 0.771)	-0.075 (p = 0.475)	-0.174 (p = 0.083)
Diabetic nephropathy (eGFR < 60 or albuminuria)	41	-0.018 (p = 0.866)	0.048 (p = 0.648)	0.129 (p = 0.219)	0.189 (p = 0.060)
eGFR < 60	9	-0.052 (p = 0.621)	0.296 (p = 0.004)	0.213 (p = 0.041)	0.226 (p = 0.024)
eGFR (continuous variable)	-	0.019 (p = 0.854)	-0.172 (p = 0.101)	-0.148 (p = 0.156)	-0.218 (p = 0.029)
Albuminuria	38	0.018 (p = 0.868)	-0.031 (p = 0.771)	0.118 (p = 0.261)	0.162 (p = 0.108)
UACr (continuous variable)	-	0.089 (p = 0.403)	0.023 (p = 0.830)	0.144 (p = 0.171)	0.202 (p = 0.044)
Diabetic retinopathy	21	-0.045 (p = 0.674)	0.197 (p = 0.064)	0.055 (p = 0.610)	-0.010 (p = 0.919)
Diabetic foot ulcer/amputation	11	-0.019 (p = 0.858)	-0.054 (p = 0.612)	0.115 (p = 0.271)	0.101 (p = 0.318)
Ischaemic heart disease	21	-0.030 (p = 0.776)	-0.008 (p = 0.940)	-0.019 (p = 0.859)	0.015 (p = 0.886)
BNP (continuous variable)	-	0.246 (p = 0.018)	0.338 (p = 0.001)	0.071 (p = 0.504)	0.116 (p = 0.283)
Peripheral vascular disease	7	-0.012 (p = 0.912)	0.120 (p = 0.258)	0.018 (p = 0.863)	0.104 (p = 0.307)
Cerebrovascular accident	9	0.100 (p = 0.343)	-0.123 (p = 0.242)	0.068 (p = 0.519)	0.040 (p = 0.696)

Data expressed as Spearman r (p-value). Significant correlations (p-value ≤ 0.05) are highlighted in green. AMT, abnormal monofilament test; BNP, brain natriuretic peptide; eGFR, estimated glomerular filtration rate; Sx of PN, symptoms of peripheral neuropathy; UACr, urine albumin to creatinine ratio.

Table 6.7: Definitions of diabetes-related complications.

Complication	Definition
Any diabetes-related complication	Any micro- or macrovascular complication, or advanced liver fibrosis
Microvascular complication	Peripheral neuropathy or diabetic nephropathy or diabetic retinopathy
Peripheral neuropathy	Symptoms of peripheral neuropathy or abnormal monofilament test
Diabetic nephropathy	eGFR < 60 mL/min/1.73m^2 or albuminuria (UACr > 3.5 mg/mmol Cr in females or UACr > 2.5 mg/mmol/Cr in males)
Diabetic retinopathy	Any degree of retinopathy based on dilated eye examination
Diabetic foot ulcer/amputation	Current or previous foot ulcer of lower limb amputation
Ischaemic heart disease	Acute myocardial infarction or revascularisation
Peripheral vascular disease	Abnormal peripheral vascular assessment
Cerebrovascular accident	Stroke or transient ischaemic attack
Advanced liver fibrosis	LSM ≥ 10.3 kPa

eGFR, estimated glomerular filtration rate; LSM, liver stiffness measurement; UACr, urine albumin to creatinine ratio.

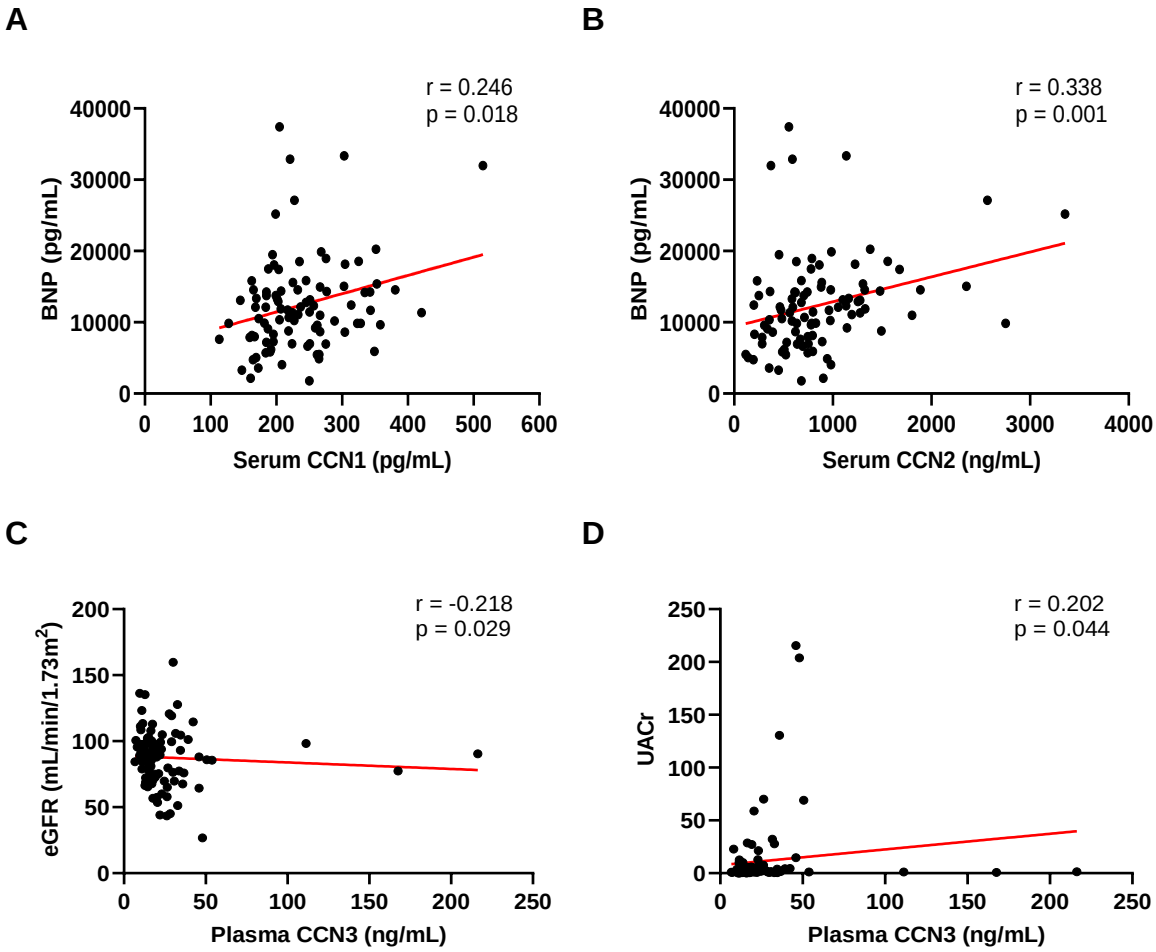

Figure 6.2: Circulating CCN correlations with diabetes-related complications: CCN1 and BNP (A), CCN2 and BNP (B), CCN3 and eGFR (C), and CCN3 and UACr (D). BNP, brain natriuretic peptide; eGFR, estimated glomerular filtration rate; UACr, urine albumin to creatinine ratio.

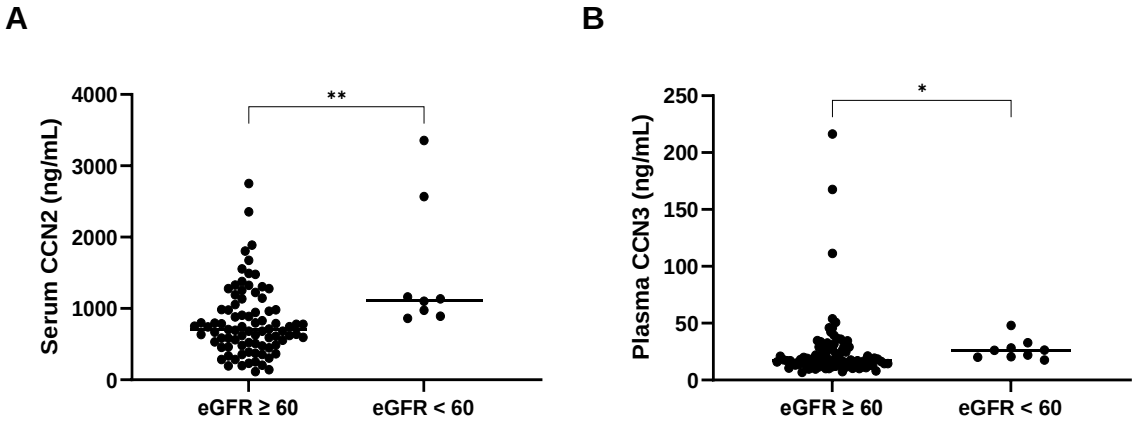

*Figure 6.3: Stratification of circulating CCN2 (A) and CCN3 (B) by eGFR. Data shown as individual values with median (black line). * p-value ≤ 0.05 or ** p-value ≤ 0.01 using Mann-Whitney test. eGFR, estimated glomerular filtration rate.*

6.3.1.5 Circulating CCNs and NASH fibrosis

There was no significant difference in the median concentration of CCN1, CCN2, or CCN3 when stratified by the presence of advanced liver fibrosis (*Table 6.8*). Univariate correlations were performed to establish whether circulating CCNs could be used as potential biomarkers for NASH fibrosis in individuals with T2DM (*Table 6.9*). Blood concentrations of CCN1, CCN2, or CCN3 did not correlate with the presence of advanced liver fibrosis, as determined by transient elastography with an LSM cut-off ≥10.3 kPa or when LSM was included as a continuous variable. However, serum CCN1 concentrations correlated positively with both DPP4 activity, FAP and HA concentrations, and CCN3 (serum and plasma) correlated with FAP, PIIINP, AST:ALT and FIB-4 (*Figure 6.4*). This suggests that CCN1 and CCN3 may have value as biomarkers for NASH fibrosis.

Table 6.8: Circulating CCN concentrations according to absence (LSM < 10.3 kPa) or presence (LSM ≥ 10.3 kPa) of advanced liver fibrosis.

		LSM < 10.3 kPa		**LSM ≥ 10.3 kPa**		**p-value***
CCN1 (pg/mL)	**Serum**	225.0 [186.5 - 269.9]	n = 70	230.0 [201.0 - 283.0]	n = 18	0.507
CCN2 (ng/mL)	**Serum**	727.3 [486.8 - 1108.9]	n = 70	886.8 [530.3 - 1413.5]	n = 18	0.202
CCN3 (ng/mL)	**Serum**	14.8 [10.9 - 27.3]	n = 71	17.9 [14.3 - 29.9]	n = 18	0.216
	Plasma	17.4 [13.6 - 29.1]	n = 79	20.5 [17.4 - 27.3]	n = 17	0.160

Data expressed as median [IQR]. * Mann-Whitney test. LSM, liver stiffness measurement.

Table 6.9: Univariate correlations between circulating CCNs and liver-related variables.

	CCN1	CCN2	CCN3	
n = 92 - 106	**Serum**	**Serum**	**Serum**	**Plasma**
LSM ≥ 10.3 kPa	0.072 (p = 0.504)	0.138 (p = 0.201)	0.133 (p = 0.215)	0.145 (p = 0.158)
LSM	0.094 (p = 0.385)	0.043 (p = 0.694)	0.021 (p = 0.843)	-0.008 (p = 0.941)
ALT	-0.072 (p = 0.492)	-0.022 (p = 0.836)	-0.104 (p = 0.320)	-0.130 (p = 0.196)
AST	0.013 (p = 0.905)	-0.033 (p = 0.758)	0.052 (p = 0.627)	-0.034 (p = 0.739)
AST:ALT	0.134 (p = 0.209)	0.043 (p = 0.688)	0.286 (p = 0.006)	0.223 (p = 0.028)
NFS	-0.080 (p = 0.458)	-0.138 (p = 0.200)	0.054 (p = 0.615)	0.116 (p = 0.262)
FIB-4	-0.041 (p = 0.702)	0.197 (p = 0.064)	0.102 (p = 0.337)	0.206 (p = 0.043)
HA	0.274 (p = 0.008)	0.163 (p = 0.122)	0.075 (p = 0.473)	0.086 (p = 0.395)
TIMP1	0.034 (p = 0.744)	0.206 (p = 0.049)	0.081 (p = 0.442)	0.124 (p = 0.219)
PIIINP	0.148 (p = 0.159)	0.019 (p = 0.858)	0.267 (p = 0.010)	0.293 (p = 0.003)
CK-18	-0.030 (p = 0.774)	0.042 (p = 0.691)	0.098 (p = 0.348)	0.075 (p = 0.457)
DPP4 activity	0.357 (p < 0.001)	0.146 (p = 0.164)	0.013 (p = 0.898)	0.082 (p = 0.416)
FAP	0.276 (p = 0.008)	0.102 (p = 0.335)	0.282 (p = 0.006)	0.332 (p = 0.001)

Data expressed as Spearman r (p-value). Significant correlations (p-value ≤ 0.05) are highlighted in green. ALT, alanine aminotransferase; AST, aspartate aminotransferase; AST:ALT, AST to ALT ratio; CK-18, cytokeratin-18; DPP4, dipeptidyl-peptidase 4; FAP, fibroblast activation protein; FIB-4, fibrosis-4 index; HA, hyaluronic acid; LSM, liver stiffness measurement; NFS, NAFLD fibrosis score; PIIINP, type III procollagen N-terminal peptide; TIMP1, tissue inhibitor of metalloproteinase 1.

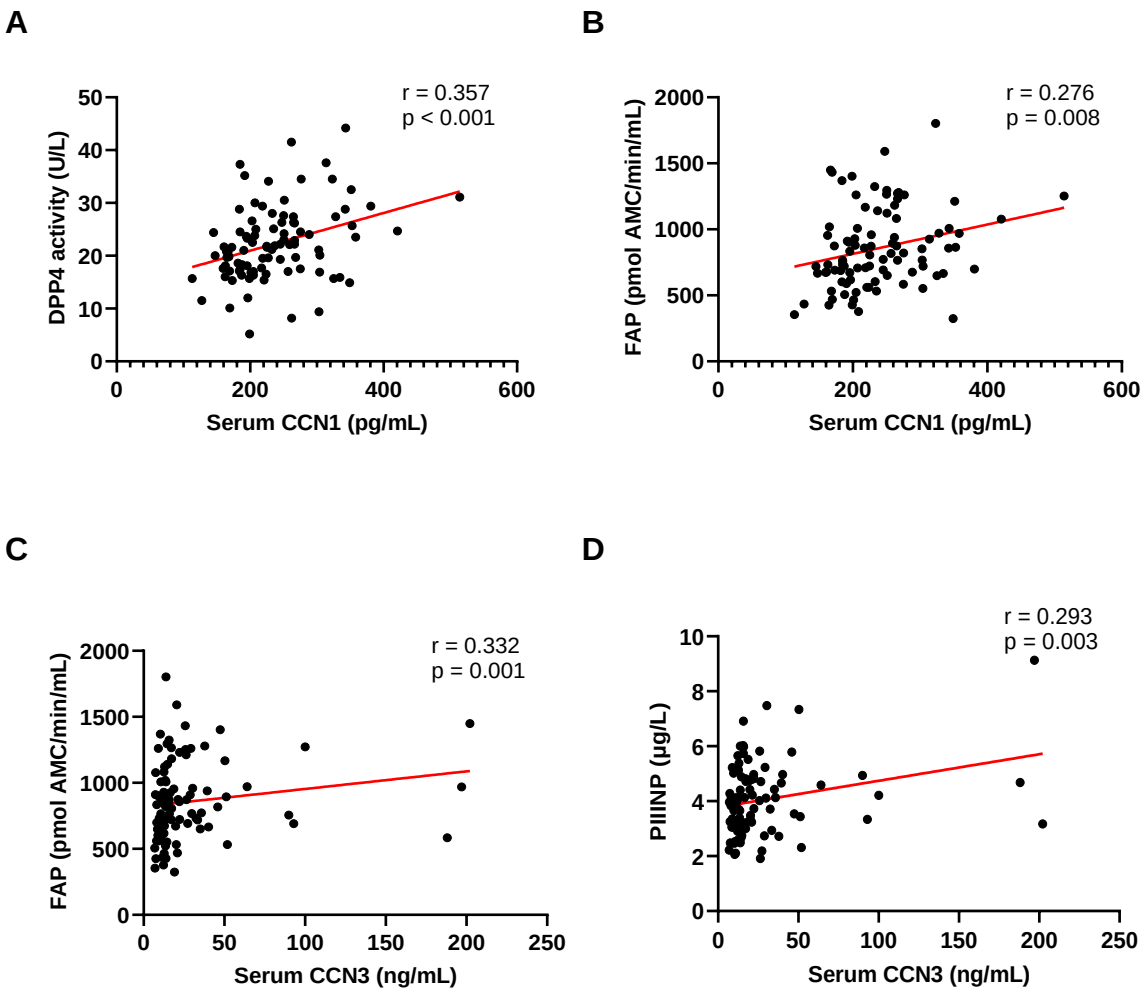

Figure 6.4: Serum CCN1 correlations with DPP4 activity (A) and FAP (B), and serum CCN3 correlations with FAP (C) and PIIINP (D). DPP4, dipeptidyl-peptidase 4; FAP, fibroblast activation protein; PIIINP, type III procollagen N-terminal peptide.

6.3.1.6 Identifying predictors of NASH fibrosis

Univariate and multivariate analyses were performed to identify if other variables or combinations of variables, apart from CCNs, may be useful in predicting advanced fibrosis. Correlative analysis was performed with Fibroscan® reading as a categorical variable of < or ≥ 10.3 kPa, and separately as a continuous variable. Variables with p-values > 0.05 but ≤ 0.1 were included in the multivariate analysis. The variables associated with advanced liver fibrosis are listed in *Table 6.10*. On multivariate logistic regression, an LSM ≥ 10.3 kPa was best predicted by a combination of triglyceride level, waist circumference, duration of diabetes, and hyaluronic acid (p-value < 0.001; *Table 6.11*). On multivariate linear regression, a higher LSM was best predicted by a combination of diabetic foot ulcer/amputation, insulin therapy, TSH, AST, ALT, and platelet count (p-value < 0.001; *Table 6.11*).

Table 6.10: Univariate correlations between Fibroscan® reading and clinical and biochemical variables with p-value ≤ 0.01.

	LSM ≥ 10.3 kPa			LSM continuous variable	
Variable	**Spearman R**	**p-value**	**Variable**	**Spearman R**	**p-value**
Sex	0.230	0.020*	Sex	0.352	<0.001
Weight[a]	0.307	0.002	Weight[a]	0.405	<0.001
BMI[a]	0.232	0.019	BMI[a]	0.299	0.002
WC	0.325	0.001*	WC	0.416	<0.001
WHR[a]	0.273	0.006	WHR[a]	0.361	<0.001
SBP	0.184	0.065*	SBP	0.175	0.079
Duration of diabetes	0.255	0.010*	Insulin therapy	0.279	0.004
Insulin therapy	0.215	0.030*	HbA1c	0.325	0.001
HbA1c	0.204	0.040*	Any diabetes-related complication[a]	0.234	0.018
Any diabetes-related complication[a]	0.280	0.004	Total # of microvascular complications[a]	0.289	0.003
Total # of microvascular complications[a]	0.326	0.001	Diabetic nephropathy	0.267	0.007
Diabetic nephropathy	0.245	0.013*	Albuminuria[a]	0.283	0.004
eGFR < 60[a]	0.206	0.038	UACr[a]	0.232	0.019
Albuminuria[a]	0.248	0.013	Diabetic foot ulcer/amputation	0.246	0.013
UACr[a]	0.237	0.017	Any macrovascular complication	0.169	0.090
Abnormal monofilament test	0.208	0.036*	PVD[a]	0.185	0.064
Diabetic foot ulcer/amputation	0.321	0.001*	Steatosis	0.175	0.079
Any macrovascular complication	0.240	0.015*	OSA	0.168	0.091
PVD[a]	0.168	0.093	Creatinine[a]	0.235	0.018
GGT	0.318	0.001*	GGT	0.293	0.003
ALT	0.196	0.048*	ALT	0.221	0.026
AST	0.181	0.073*	AST	0.213	0.034
Platelet count	-0.302	0.002*	AST:ALT[a]	-0.175	0.083
Total cholesterol	0.210	0.034*	Platelet count	-0.301	0.002
Triglycerides	0.215	0.030*	Triglycerides	0.207	0.037
NFS[a]	0.294	0.003	HDL-c	-0.188	0.059
HA	0.284	0.004*	Uric acid	0.230	0.020
TIMP1	0.204	0.039*	TSH	-0.259	0.009
PIIINP	0.442	<0.001*	fT4[a]	0.193	0.052
DPP4 activity	0.218	0.028*	25-OH Vit D	-0.174	0.080
FAP	0.261	0.008*	NFS[a]	0.251	0.013
			HA	0.312	0.001
			TIMP1	0.255	0.010

			PIIINP	0.487	<0.001
			CK-18	0.264	0.007
			DPP4 activity	0.166	0.095

* p-value ≤ 0.1 for inclusion in multivariate regression analysis. [a] not included in multivariate regression analysis due to multicollinearity. 25-OH VitD, 25-hydroxy vitamin D; ALT, alanine aminotransferase; AST, aspartate aminotransferase; AST:ALT, AST to ALT ratio; BMI, body mass index; CK-18, cytokeratin-18; DPP4, dipeptidyl-peptidase 4; eGFR, estimated glomerular filtration rate; FAP, fibroblast activation protein; fT4, free thyroxine; GGT, gamma-glutamyl transferase; HA, hyaluronic acid; HbA1c, haemoglobin A1c; HDL-C, high-density lipoprotein cholesterol; LSM, liver stiffness measurement; NFS, NAFLD fibrosis score; OSA, obstructive sleep apnoea; PIIINP, type III procollagen N-terminal peptide; PVD, peripheral vascular disease; SBP; systolic blood pressure; TIMP1, tissue inhibitor of metalloproteinase 1; TSH, thyroid stimulating hormone; UACr, urine albumin to creatinine ratio; WC, waist circumference; WHR, waist to hip ratio.

Table 6.11: Multivariate regression analysis.

LSM ≥ 10.3 kPa			**LSM continuous variable**		
Variable	**Beta**	**p-value**	**Variable**	**Beta**	**p-value**
Constant	-13.556	<0.001	Constant	14.592	<0.001
Triglycerides	0.791	0.024	Diabetic foot ulcer/amputation	5.677	0.016
WC	0.076	0.002	Insulin therapy	4.334	0.006
Duration of diabetes	0.076	0.044	TSH	-1.685	0.007
HA	0.014	0.004	AST	0.290	0.011
			ALT	-0.146	0.022
			Platelet count	-0.034	0.001
Summary:			**Summary:**		
$\chi^2 = 35.824$			F = 7.139		
$R^2 = 0.491$			$R^2 = 0.318$		
p-value < 0.001			p-value < 0.001		

ALT, alanine aminotransferase; AST, aspartate aminotransferase; HA, hyaluronic acid; LSM, liver stiffness measurement; TSH, thyroid stimulating hormone; WC, waist circumference.

6.3.2 Circulating CCNs in pre-clinical mouse studies

The circulating concentrations of CCN1, CCN2, and CCN3 in The CCN2 Study and The CCN1 Study were measured using commercial kits, to determine if there was an association with the development of NASH fibrosis. The metabolic, biochemical, and histological characteristics have been described in detail in *Chapter 4* (The CCN2 Study) and *Chapter 5* (The CCN1 Study). The focus of the correlation analyses was in the HFD+DM groups, as these were the groups in which significant NASH fibrosis developed. Correlation results of the HFD and Chow groups were not performed as these groups did not develop NASH fibrosis.

6.3.2.1 Circulating CCNs in The CCN2 Study

6.3.2.1.1 Circulating CCN concentrations

There was no effect from the hepatocyte specific gene deletion of CCN2 on the systemic concentrations of plasma CCN2 (*Figure 6.5*). Plasma CCN2 levels were similar across all nine study groups. Plasma CCN1 concentrations were significantly higher in the CCN2-KO HFD and CCN2-KO HFD+DM groups compared with the corresponding AlbCre groups of the same “diet”, but not compared with the $CCN2^{fl/fl}$ groups. The plasma concentration of antifibrotic CCN3 was increased in the CCN2-KO HFD+DM group which may be consistent with the reduced amount of liver fibrosis observed in this group. Baseline (Chow groups) CCN concentrations were similar across all three sub-strains of mice.

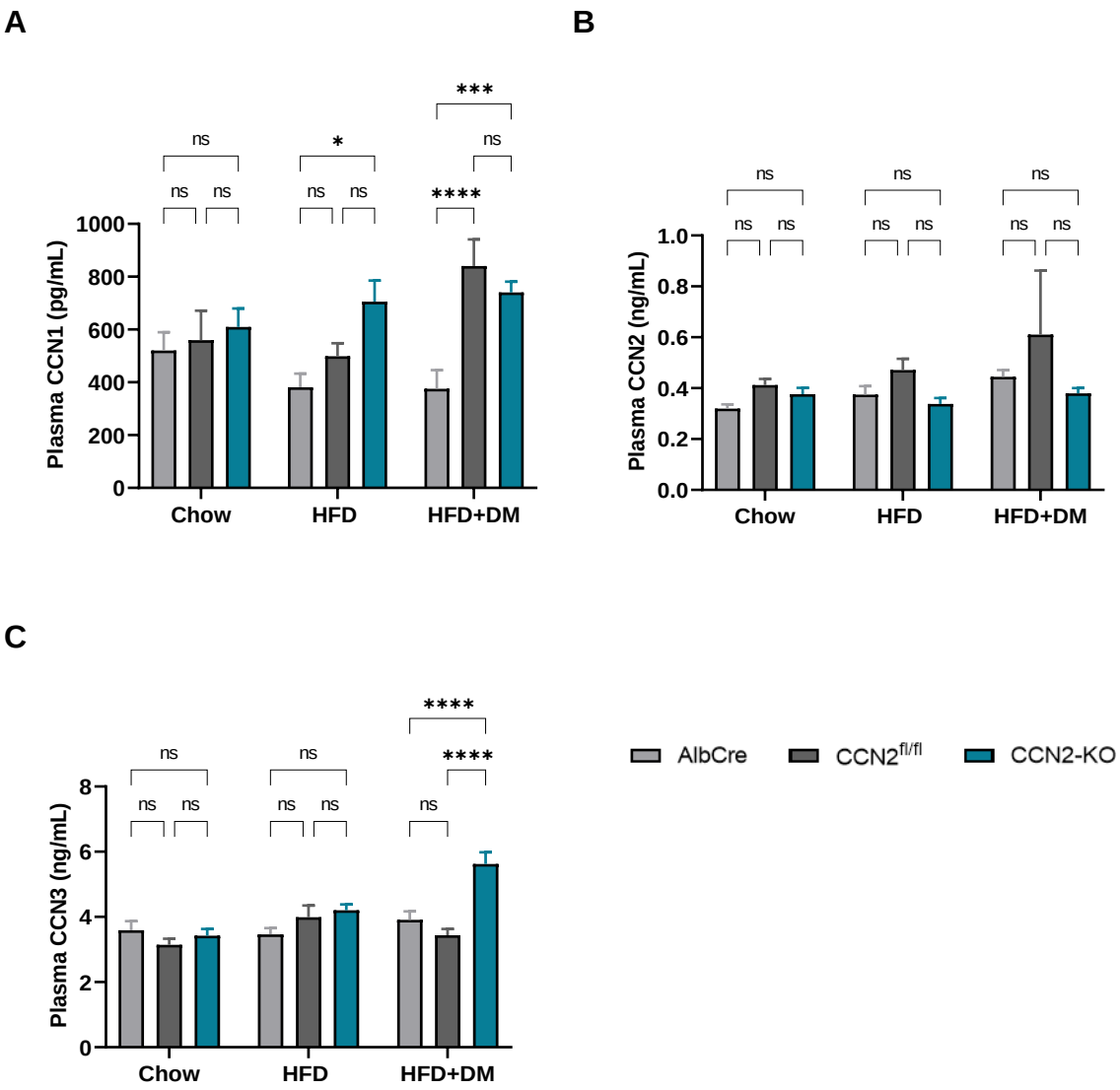

*Figure 6.5: Mouse plasma CCN1 (A), CCN2 (B), and CCN3 (C) concentrations from The CCN2 Study. Data shown as mean ± SEM; n = 7 - 13. * p-value ≤ 0.05, *** p-value ≤ 0.001 or **** p-value ≤ 0.0001 for comparison of mouse sub-strains within the same "diet" subgroup using two-way ANOVA with Tukey's correction for multiple comparisons. ns, not significant.*

6.3.2.1.2 Circulating CCN correlations with liver fibrosis

Plasma concentrations of CCN1, CCN2, or CCN3 did not correlate with the amount of liver fibrosis detected by PSR staining in any of the three HFD+DM groups in The CCN2 Study (*Table 6.12*). This is consistent with the lack of correlation identified in The DaSH Study and suggests that circulating CCNs may not be useful biomarkers for the presence of liver fibrosis.

Table 6.12: Univariate correlations between plasma CCNs and amount of liver fibrosis.

	Plasma CCN1	Plasma CCN2	Plasma CCN3
AlbCre HFD+DM			
% PSR +ve tissue 100x	0.200 (p = 0.605)	-0.067 (p = 0.853)	-0.083 (p = 0.820)
% PSR +ve tissue 200x	-0.018 (p = 0.962)	0.233 (p = 0.517)	0.287 (p = 0.421)
% PSR +ve tissue 400x CV	0.062 (p = 0.874)	0.298 (p = 0.403)	0.023 (p = 0.950)
% PSR +ve tissue 400x PT	-0.185 (p = 0.633)	-0.058 (p = 0.873)	0.164 (p = 0.652)
CCN2$^{fl/fl}$ HFD+DM			
% PSR +ve tissue 100x	0.092 (p = 0.828)	0.667 (p = 0.035)	0.365 (p = 0.300)
% PSR +ve tissue 200x	0.047 (p = 0.912)	0.493 (p = 0.148)	0.299 (p = 0.402)
% PSR +ve tissue 400x CV	-0.435 (p = 0.281)	0.091 (p = 0.802)	-0.096 (p = 0.792)
% PSR +ve tissue 400x PT	-0.378 (p = 0.355)	0.311 (p = 0.587)	0.040 (p = 0.913)
CCN2-KO HFD+DM			
% PSR +ve tissue 100x	-0.193 (p = 0.570)	-0.309 (p = 0.304)	0.133 (p = 0.665)
% PSR +ve tissue 200x	-0.026 (p = 0.940)	-0.355 (p = 0.234)	0.202 (p = 0.509)
% PSR +ve tissue 400x CV	-0.119 (p = 0.728)	-0.204 (p = 0.504)	0.164 (p = 0.593)
% PSR +ve tissue 400x PT	-0.078 (p = 0.821)	-0.178 (p = 0.560)	0.303 (p = 0.314)

Data expressed as Pearson r (p-value). Significant correlations (p-value ≤ 0.05) are highlighted in green.

CV, central vein; PSR, Picro Sirius Red; PT, portal tract.

6.3.2.1.3 Identifying predictors of NASH fibrosis

An attempt was made to identify metabolic, biochemical, or histological characteristics that may predict the amount of liver fibrosis identified in the HFD+DM groups. There was no logical series of variables with statistical significance that correlated with the percent of PSR-positive staining (200x magnification) in the $CCN2^{fl/fl}$ HFD+DM and CCN2-KO HFD+DM groups. In the AlbCre HFD+DM group, more fibrosis was associated with lower final weight, higher termination BGL, lower fat mass and higher lean mass (by termination tissue weights and body composition data), lower liver CCN1 mRNA level, and higher grade of portal inflammation and fibrosis by Brunt criteria (all $p < 0.05$)[80,81].

6.3.2.1.4 Correlates of other variables with circulating CCNs

<u>The AlbCre HFD+DM group</u>

A higher plasma CCN1 concentration was associated with greater hyperglycaemia ($r = 0.835$, $p = 0.005$) and lower insulin ($r = -0.658$, $p = 0.076$) and c-peptide ($r = -0.759$, $p = 0.029$) levels, consistent with pancreatic damage and metabolic dysregulation. It also correlated with a lower ALP ($r = -0.853$, $p = 0.003$), AST:ALT ($r = -0.787$, $p = 0.012$) and bilirubin ($r = -0.771$, $p = 0.015$), which may be indicative of lesser liver damage. Plasma CCN2 concentration was correlated with liver CCN1 ($r = -0.633$, $p = 0.049$) and ACTA2 ($r = -0.809$, $p = 0.005$) mRNA levels. A higher plasma CCN3 concentration was associated with lower scores for steatosis ($r = -0.656$, $p = 0.039$), hepatocyte ballooning ($r = -0.680$, $p = 0.030$) and NAS ($r = -0.711$, $p = 0.021$) on histological assessment.

<u>The $CCN2^{fl/fl}$ HFD+DM group</u>

Higher plasma CCN1 concentration was associated with variables suggestive of lesser liver damage, including lower liver collagen-VI ($r = -0.688$, $p = 0.040$) and FAP ($r = -0.806$, $p = 0.009$) mRNA levels, and lower scores for lobular inflammation ($r = -0.905$, $p = 0.001$), hepatocyte ballooning ($r = -0.729$, $p = 0.026$) and total NAS ($r = -0.866$, $p = 0.003$). It was also associated with a significantly higher plasma CCN3 concentration ($r = 0.714$, $p = 0.047$) and a trend towards a higher plasma CCN2 concentration ($r = 0.694$, $p = 0.056$). Plasma CCN2 concentration was positively associated with ALP ($r = 0.666$, $p = 0.025$) and percent of PSR-positive tissue at 100x magnification ($r =$

0.667, p = 0.035). There was a trend for reduced liver FAP mRNA level with higher plasma CCN3 concentration (r = -0.594, p = 0.054).

The CCN2-KO HFD+DM group

Plasma CCN1 concentrations were associated with lower insulin (r = -0.722, p = 0.012) and c-peptide (r = -0.742, p = 0.009) levels, as well as lower liver mRNA levels of collagen-IVα2 (r = -0.691, p = 0.019) and TNF (r = -0.611, p = 0.046). Plasma CCN2 concentration was correlated with liver CCN1 mRNA level (r = 0.629, p = 0.021), whilst plasma CCN3 concentration was associated with liver CCN3 mRNA level (r = 0.608, p = 0.028).

6.3.2.2 Circulating CCNs in The CCN1 Study

6.3.2.2.1 Circulating CCN concentrations

There was a systemic effect on plasma CCN1 concentrations in mice with a hepatocyte-specific CCN1 gene deletion: plasma CCN1 concentrations were significantly lower in the CCN1-KO HFD and CCN1-KO HFD+DM groups compared with the corresponding AlbCre groups of the same "diet", and numerically lower compared with the $CCN1^{fl/fl}$ groups (*Figure 6.6*). Plasma CCN2 concentrations were significantly lower in the CCN1-KO HFD+DM group compared with the other two control HFD+DM groups, despite increased liver fibrosis observed in this group, suggesting that other non-circulating CCN2-mediated pathways may be responsible for fibrosis development. Plasma CCN3 levels were similar across all nine study groups, and baseline (Chow groups) CCN concentrations were similar across the three mouse sub-strains.

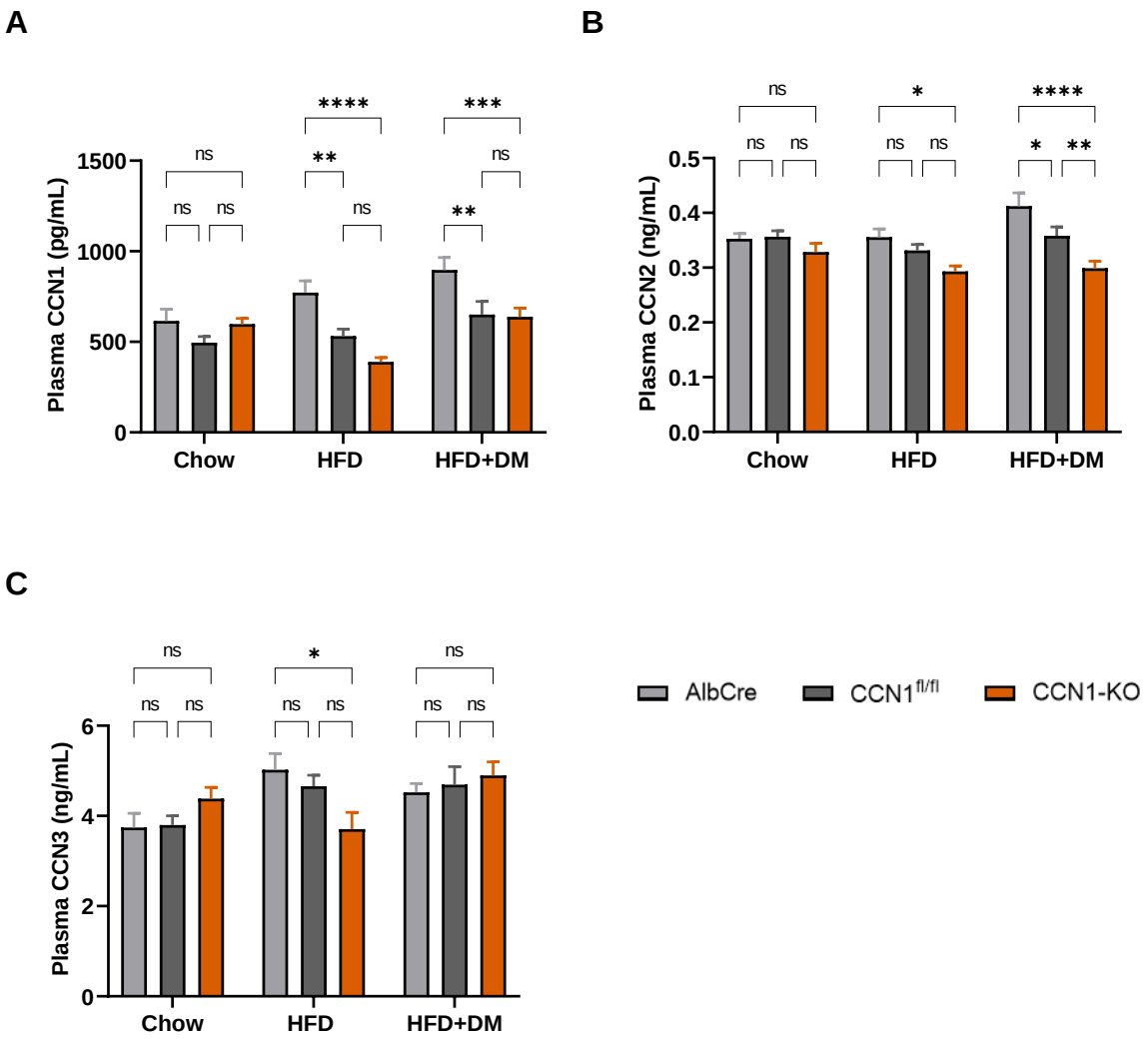

*Figure 6.6: Mouse plasma CCN1 (A), CCN2 (B), and CCN3 (C) concentrations from The CCN1 Study. Data shown as mean ± SEM; n = 7 - 14. * p-value ≤ 0.05, ** p-value ≤ 0.01, *** p-value ≤ 0.001 or **** p-value ≤ 0.0001 for comparison of mouse sub-strains within the same "diet" subgroup using two-way ANOVA with Tukey's correction for multiple comparisons. ns, not significant.*

6.3.2.2.2 Circulating CCN correlations with liver fibrosis

Plasma concentrations of CCN1, CCN2, or CCN3 did not correlate with the amount of liver fibrosis detected by PSR staining in the CCN1$^{fl/fl}$ HFD+DM or the CCN1-KO HFD+DM groups in The CCN1 Study (*Table 6.13*). There was an unexpected negative correlation in the AlbCre HFD+DM group with plasma CCN2 concentration, which was discordant from the findings in The CCN2 Study (*Table 6.12*). There was also a negative correlation with plasma CCN1 concentration, but only at the high-powered magnification of the PSR assessment. Again, this data suggests that circulating CCNs may not be useful biomarkers for the presence of liver fibrosis.

Table 6.13: Univariate correlations between plasma CCNs and amount of liver fibrosis.

	Plasma CCN1	Plasma CCN2	Plasma CCN3
AlbCre HFD+DM			
% PSR +ve tissue 100x	-0.501 (p = 0.117)	-0.674 (p = 0.046)	-0.350 (p = 0.265)
% PSR +ve tissue 200x	-0.495 (p = 0.122)	-0.728 (p = 0.026)	-0.323 (p = 0.306)
% PSR +ve tissue 400x CV	-0.685 (p = 0.020)	-0.487 (p = 0.184)	0.026 (p = 0.937)
% PSR +ve tissue 400x PT	-0.643 (p = 0.033)	-0.673 (p = 0.047)	-0.326 (p = 0.300)
CCN1$^{fl/fl}$ HFD+DM			
% PSR +ve tissue 100x	-0.351 (p = 0.320)	-0.111 (p = 0.776)	0.273 (p = 0.417)
% PSR +ve tissue 200x	-0.333 (p = 0.348)	-0.081 (p = 0.836)	0.341 (p = 0.305)
% PSR +ve tissue 400x CV	-0.389 (p = 0.267)	-0.472 (p = 0.200)	0.024 (p = 0.945)
% PSR +ve tissue 400x PT	-0.362 (p = 0.304)	0.074 (p = 0.849)	0.472 (p = 0.143)
CCN1-KO HFD+DM			
% PSR +ve tissue 100x	-0.195 (p = 0.523)	-0.201 (p = 0.510)	0.116 (p = 0.694)
% PSR +ve tissue 200x	-0.285 (p = 0.346)	-0.259 (p = 0.392)	-0.008 (p = 0.978)
% PSR +ve tissue 400x CV	-0.067 (p = 0.827)	-0.231 (p = 0.447)	0.257 (0.375)
% PSR +ve tissue 400x PT	-0.200 (p = 0.513)	-0.282 (p = 0.351)	-0.098 (p = 0.740)

Data expressed as Pearson r (p-value). Significant correlations (p-value ≤ 0.05) are highlighted in green.

CV, central vein; PSR, Picro Sirius Red; PT, portal tract.

6.3.2.2.3 Identifying predictors of NASH fibrosis

The amount of liver fibrosis (% PSR +ve tissue 200x) was positively correlated with the grade of fibrosis by Brunt criteria[80] in the CCN1$^{fl/fl}$ HFD+DM ($r = 0.643$, $p = 0.033$) and CCN1-KO HFD+DM ($r = 0.648$, $p = 0.012$) groups but not the AlbCre HFD+DM group ($r = 0.283$, $p = 0.372$). In the AlbCre HFD+DM group, more fibrosis was associated with higher final weight and higher liver mRNA levels of collagen-I, collagen-IVα2, TGFβ1, and TIMP1 (all $p < 0.05$).

6.3.2.2.4 Correlates of other variables with circulating CCNs

<u>The AlbCre HFD+DM group</u>

A higher plasma CCN1 concentration was associated with lower weight gain ($r = -0.757$, $p = 0.007$), reduced fat mass ($r = -0.677$, $p = 0.022$), better insulin sensitivity (glucose:insulin ratio: $r = 0.706$, $p = 0.015$; AUC ITT: $r = -0.660$, $p = 0.027$), but higher glucose level ($r = 0.692$, $p = 0.018$). There was also a trend to less severe lobular inflammation ($r = -0.552$, $p = 0.078$) and NAS score ($r = -0.552$, $p = 0.078$) on histology assessment. Plasma CCN2 concentration correlated with an improved metabolic phenotype (lower final body weight: $r = -0.791$, $p = 0.011$; lower fasting plasma insulin: $r = -0.675$, $p = 0.046$; lower fat mass: $r = -0.801$, $p = 0.009$; higher lean mass: $r = 0.796$, $p = 0.010$) and lower mRNA levels of fibrosis markers (collagen-I: $r = -0.827$, $p = 0.006$; collagen-III: $r = -0.791$, $p = 0.011$; collagen-IVα2: $r = -0.802$, $p = 0.009$; collagen-VI: $r = -0.697$, $p = 0.037$; TGFβ1: $r = -0.677$, $p = 0.045$; TIMP1: $r = -0.683$, $p = 0.042$). There was an inverse relationship between plasma CCN3 concentration and liver weight ($r = -0.703$, $p = 0.011$) and liver triglyceride concentration ($r = -0.620$, $p = 0.031$).

<u>The CCN1$^{fl/fl}$ HFD+DM group</u>

Plasma CCN1 concentration was associated with a lower fasting plasma c-peptide level ($r = -0.650$, $p = 0.042$) and improved insulin sensitivity (glucose:insulin ratio: $r = 0.677$, $p = 0.032$; AUC ITT: $r = 0.621$, $p = 0.055$). It was also associated with a lower ALT ($r = -0.731$, $p = 0.016$) but higher AST:ALT ($r = 0.749$, $p = 0.013$) and higher liver FAP mRNA level ($r = 0.657$, $p = 0.039$). Plasma CCN2 concentration was correlated with lower weight gain ($r = -0.884$, $p = 0.002$), higher mean BGL ($r = 0.808$ $p = 0.008$), lower fasting plasma insulin level ($r = -0.677$, $p = 0.045$), improved insulin resistance (glucose:insulin ratio: $r = 0.697$, $p = 0.037$; AUC ITT: $r = -0.711$, $p = 0.032$), lower fat mass ($r = -0.925$, $p < 0.001$), and higher lean mass ($r = 0.922$, $p < 0.001$). There was

also a negative association with ALP (r = -0.802, p = 0.009), blood lipids (total cholesterol: r = -0.769, p = 0.015; HDL-c: r = -0.745, p = 0.021; LDL-c: r = -0.682, p = 0.043) and collagen-I (r = -0.699, p = 0.036) and collagen-VI (r = -0.854, p = 0.003) mRNA levels. Plasma CCN3 concentration was also negatively correlated with collagen-VI mRNA level (r = -0.647, p = 0.031).

The CCN1-KO HFD+DM group

Plasma CCN1 concentration was associated with lower weight gain (r = -0.636, p = 0.019), lower fat mass (r = -0.691, p = 0.013), higher lean mass (r = 0.664, p = 0.019), lower liver mass (r = -0.672, p = 0.012) and liver triglyceride concentration (r = -0.616, p = 0.025), lower blood lipids (total cholesterol: r = -0.656, p = 0.015; HDL-c: r = -0.620, p = 0.024; LDL-c: r = -0.562, p = 0.046), and higher liver DPP4 mRNA level (r = 0.606, p = 0.028). Plasma CCN2 concentration was associated with lower weight gain (r = -0.636, p = 0.019), lower fat mass (r = -0.800, p = 0.002), and higher lean mass (r = 0.779, p = 0.003). There was a positive relationship with ALT (r = 0.626, p = 0.022) and AST (r = 0.649, p = 0.016), and an inverse relationship with total cholesterol (r = -0.571, p = 0.041) and HDL-c (r = -0.714, p = 0.006). Plasma CCN3 concentration was inversely associated with liver triglyceride level (r = -0.606, p = 0.022).

6.4 Discussion

6.4.1 Predicting diabetes-related complications with circulating CCNs in individuals with T2DM

The DaSH cohort consisted of individuals with relatively well-controlled, long-standing T2DM, with high rates of diabetes-related complications, obesity, hypertension, and dyslipidaemia. The prevalence of advanced liver fibrosis by transient elastography was 19%. Whilst the measurements of blood CCN1, CCN2 or CCN3 were not able directly predict the presence of specific diabetes-related complications in this relatively small cohort, some interesting correlations were noted.

Firstly, a higher blood CCN1 concentration was associated with a lower body weight and waist circumference, and higher HDL-c. Individually, these variables are tightly linked to cardiovascular risk, but together they suggest that there may be an impact of CCN1 on the metabolic phenotype. There have not been any reports in the literature linking circulating CCN1 with obesity or metabolic syndrome[272] and further studies in

this area are warranted. A higher circulating CCN2 level was associated with variables linked to peripheral neuropathy, diabetic nephropathy, and cardiac disease, and this has previously been described in the literature[272]. Circulating CCN3 correlated with markers of diabetic nephropathy. CCN2 and CCN3 have a “ying-yang” relationship in some organ pathologies, and CCN3 was previously demonstrated to have an inhibitory effect on CCN2 to prevent renal fibrosis[381].

The circulating concentrations of neither CCN1, CCN2, nor CCN3 correlated with the presence of advanced liver fibrosis as determined by an LSM threshold of ≥ 10.3 kPa. The rationale and limitations for using a conservative cut-off were discussed earlier in The DLC Audit (*Chapter 3*). The lack of a significant difference in circulating CCN concentration between individuals with and without advanced liver fibrosis suggests that these measures may not be sensitive enough to be used as novel blood biomarkers, at least not on their own. However, the association of CCN1 with DPP4 activity, FAP, and HA, and of CCN3 with FAP, PIIINP, and FIB-4, suggests there may be a link of some of these blood CCN measures with NASH fibrosis.

In further attempts to study the predictors of advanced liver fibrosis in The DaSH cohort, univariate and multivariate logistic and linear regression analyses were performed. Interestingly, yet another novel combination of variables was identified in the multivariate analyses, different from currently used clinical risk scores and from The DLC Audit. In this cohort, advanced liver fibrosis was best predicted by higher triglycerides, waist circumference, and HA, and longer duration of diabetes. These variables generally make plausible clinical sense. The combination of variables in the linear regression analysis are more difficult to explain. Association with foot disease has previously been reported[337], and AST and platelet count are included in several of the validated clinical risk scores. Insulin therapy may be a surrogate for the presence of more severe diabetes. Surprisingly, there was an inverse relationship with ALT and TSH, both variables that generally have positive correlations with NAFLD and NASH[382,383]. There is conflicting data around the relationship between TSH and NAFLD, with some studies reporting on a positive association[384] and others concluding a lack of association[385], but none have reported on an inverse relationship.

6.4.2 Predicting liver fibrosis with circulating CCNs in mice

As major organ contributions (such as from the liver) to circulating concentrations of CCNs and clearance of CCNs from the blood have not been defined in mice or humans, it was unclear what to expect in these animal studies. The hepatocyte CCN2 deletion did not affect systemic levels of CCN2, but there was a significant increase in the CCN3 concentration in the CCN2-KO HFD+DM mice. Elevated CCN3 may represent an indirect mechanism for reduced fibrosis, through its inhibitory actions on CCN2[381]. Conversely, there was some data to suggest that hepatocyte CCN1 deletion may have had a systemic effect on circulating CCN1 concentrations. The levels of CCN1 were lower in the CCN1-KO groups compared with the AlbCre groups under HFD and HFD+DM conditions, but not when compared with the $CCN1^{fl/fl}$ groups. There was also lower circulating CCN2 concentrations in the CCN1-KO groups, possibly indicating that the increased fibrosis was independent of circulating CCN2 actions. There were no changes in plasma CCN3 levels.

None of the measured circulating CCNs positively correlated with the amount of liver fibrosis by PSR staining in either animal study. There was also a lack of other predictors of liver fibrosis that were consistent between the six groups of HFD+DM mice (representing five different sub-strains of mice).

When examining other variables that correlated with circulating CCNs, overall patterns observed included that circulating CCN1 generally correlated with an improved metabolic phenotype. Circulating CCN2 also correlated with improved metabolic phenotype, but correlations with liver outcomes were frequently discordant. For example, circulating CCN2 correlation with reduced mRNA levels of fibrosis markers contradicts what is already known about CCN2. Circulating CCN3 tended to correlate with outcomes suggestive of less liver damage.

Identifying significant correlations in the animal studies was challenging. In part this may have been due to the small sample sizes within each group. Another factor that may have confounded the findings was the discordance in the outcomes from the AlbCre groups in the two studies. Potential reasons for this are discussed in *Section 7.2.2*. This provides justification for using two control sub-strains (AlbCre and homozygous floxed mice) in studies using the CreLoxP system. In addition, the quality

(and specificity) of CCN antibodies used in the commercial ELISA kits may be an issue and a presumption was made that these kits were able to measure what was described by the kit manufacturer.

6.4.3 Conclusion

Overall, circulating levels of CCNs alone are not good predictors of the presence of NASH fibrosis. However, based on the small clinical and pre-clinical studies presented here, they do link with metabolic phenotype and with some microvascular complications. In particular, higher CCN1 associates with fewer metabolic syndrome features, and hepatocyte CCN1 may contribute to similar features. The circulating CCNs may have better utility predicting diabetes-related complications if they were combined with other biomarkers or clinical risk scores, and in more severe microvascular complications of diabetes. Further testing of this in prospective studies with larger cohorts is needed.

Chapter 7: General Discussion and Conclusions

7.1 Summary of Key Findings

This thesis presents novel research from both clinical and pre-clinical studies on the development of NASH with fibrosis in the setting of T2DM. This is an area of emerging interest as rising prevalence as well as enhanced awareness of the potential adverse clinical outcomes posed by these concomitant diseases is recognised. There is a great need to better understand the natural history and pathophysiology, to develop better screening algorithms and diagnostic tools, and to discover new therapeutic targets to improve the outcomes for individuals with NASH fibrosis and diabetes.

The key findings from each of the studies in this thesis are summarised below. A comprehensive discussion of the key findings has been provided within each of the preceding four results chapters. This final chapter will discuss how the studies have collectively addressed the thesis aims and provide a general discussion, including strengths, limitations, and future directions arising from this thesis.

The results from The Diabetes and Liver Clinic Audit presented in *Chapter 3* provided evidence that a dedicated multidisciplinary clinic can enhance the assessment for NASH fibrosis. The prevalence of advanced liver fibrosis determined by transient elastography with a conservative Fibroscan® threshold of 10.3 kPa was 28%. This was almost 10% higher than a historic cohort of randomly recruited individuals with diabetes from the same tertiary diabetes centre. The increased prevalence compared with the historic cohort, and from other similar observational studies, is attributed to our pre-selection of individuals on biochemical or radiological evidence of NAFLD. In doing this, it was possible to direct limited resources to those who were at relatively higher risk, compared using the more general approach of screening all people with T2DM for NAFLD and NASH fibrosis. However, it is acknowledged that many metabolic-focused centres, such as diabetes centres, may not have the resources to establish such a specialised clinic, and thus the use of clinical risk scores using readily available clinical and biochemical variables has an important role in further stratifying those at greatest risk. In The DLC Audit, the use of the NFS had a marginally better NPV compared with the FIB-4, but sensitivity and specificity of both were suboptimal. This highlights the need to develop more accurate clinical risk scores, specifically designed for individuals with diabetes and NAFLD. This study identified that the

combination of lower LDL-c, and higher BMI, ALT, and ALP best predicted the presence of advanced fibrosis, and this novel statistical model outperformed both the NFS and the FIB-4. Further studies validating this model in other cohorts are required.

Having established the scope of the clinical problem, the following two results chapters proceeded to use an established pre-clinical model of NASH fibrosis and diabetes to examine the role of two members of the CCN family that have been implicated in NASH fibrosis. The CCN2 Study, presented in *Chapter 4,* confirmed the hypothesis that hepatocyte deletion of CCN2, a profibrotic gene/protein, would protect against the development of NASH fibrosis. Indeed, mice with hepatocyte CCN2 deletion exhibited a reduced amount of liver fibrosis on quantitative histological analysis, with supporting evidence from reduction in mRNA levels of key ECM components. Conversely, The CCN1 Study, presented in *Chapter 5*, confirmed the hypothesis that hepatocyte deletion of CCN1, an antifibrotic gene/protein, would worsen the development of NASH fibrosis. Mice with hepatocyte CCN1 deletion exhibited increased liver fibrosis on quantitative histological analysis, with supporting evidence from increased mRNA levels of key ECM components. The independent pathologist's data supported the model but was not able to detect the more subtle findings seen in quantitative image analysis of liver fibrosis in the knockout mice. Nor were differences observed in the other components of the NAS and Brunt criteria, however, these scoring systems have not been validated in pre-clinical settings (discussed in *Section 7.2.3*).

Interestingly, mice with the hepatocyte CCN1 deletion also displayed metabolic alterations characterised predominantly by greater weight gain and fat mass, with lesser hyperglycaemia, indicating that the tissue-specific gene deletion had a systemic effect on the mice. There was no such systemic effect identified in the hepatocyte CCN2 deletion mice.

Finally, based on the existing literature implicating the CCNs in diabetes-related complications, including NASH fibrosis, it was proposed that circulating CCNs could be used as potential blood biomarkers. *Chapter 6* reported on the measurement of CCN1, CCN2, and CCN3 in blood samples from The DaSH Study, of which 19% had advanced liver fibrosis. Whilst none of the measured CCNs correlated with advanced fibrosis by transient elastography, there were associations between CCN1 and CCN3

with other biomarkers of NASH fibrosis (CCN1: FAP, DPP4 activity, and HA; CCN3: FAP and PIIINP). Higher CCN1 concentration was associated with an improved metabolic phenotype, whereas CCN2 concentration was associated with markers of peripheral neuropathy, kidney disease and heart disease, whilst CCN3 concentration was associated with kidney disease. Plasma measurements of CCN1, CCN2, and CCN3 in the mice from the pre-clinical studies did not reveal any correlation with severity of liver fibrosis.

7.2 Links Observed Between the Clinical and Pre-clinical Studies

7.2.1 CCN1 and the metabolic syndrome

The CCN1-KO HFD+DM mice exhibited an unexpected phenotype with a 'worse metabolic state', suggesting that the tissue-specific gene deletion had a systemic effect. It is important to note that the overall circulating concentrations of CCN1 in the CCN1-KO HFD+DM mice were the same as in one mouse control sub-strain but were reduced compared to the other control, but that the metabolic phenotype between the two control sub-strains was similar. The findings suggest that reduced hepatocyte CCN1 expression has deleterious effects on the systemic metabolic phenotype. This concept is consistent with observations in The DaSH Study, where a higher circulating CCN1 level was associated with the improved metabolic phenotypes of lower body weight and waist circumference, and higher HDL-c. Whether increasing CCN1 concentration can be used to prevent or treat NASH fibrosis and improve metabolic parameters, is still to be elucidated.

7.2.2 CCN2, CCN1 and TIMP1

The effects of hepatocyte CCN2 and CCN1 on TIMP1 mRNA levels were investigated in the animal studies. Deletion of hepatocyte CCN2 led to a trend in reduced TIMP1, which may partially explain the reduced fibrosis through less inhibition of MMPs that degrade ECM. Consistent with the paradigm developed in these findings, deletion of hepatocyte CCN1 led to a trend in increased TIMP1, which again, may partially explain the increased fibrosis through increased inhibition of MMPs. It is unclear if the changes in TIMP1 levels are a direct effect of the hepatocyte gene deletion, or if they result from the CCN effects on activated HSCs, which are the main producers of TIMP1. Nevertheless, there is an interesting relationship between CCN2 and CCN1, and

TIMP1. The CCNs have been proposed here as potential biomarkers of NASH fibrosis, while circulating TIMP1 is a component of the validated ELF Test (*Section 1.4.3.2.1*) that is used internationally in screening algorithms for NASH fibrosis. Interestingly, The DaSH Study uncovered a positive correlation between circulating CCN2 and circulating TIMP1 levels. Although circulating CCN2 did not correlate with advanced liver fibrosis by transient elastography, inclusion of CCN2 in existing fibrosis panels such as the ELF Test may improve its predictive performance.

7.2.3 ALP and NASH fibrosis

The statistical model reported in The DLC Audit found that advanced liver fibrosis was best predicted by a combination of variables that included higher ALP. This was unexpected, as generally AST and ALT have greater value in predicting liver damage. Similar findings of higher ALP association with NASH fibrosis have been reported in other small cross-sectional studies[348,349]. Interestingly, the animal studies also demonstrated changes in ALP that appeared to be related to the severity of NASH fibrosis under HFD+DM conditions. In The CCN2 Study, there was reduced ALP in the CCN2-KO HFD+DM group which showed less liver fibrosis, compared with the control sub-strains. Conversely, in The CCN1 Study, there was increased ALP in the CCN1-KO HFD+DM group which exhibited more liver fibrosis. The elevation of ALP is generally observed in cholestatic liver diseases, but here it is shown in three different studies to be linked with NASH fibrosis. It is possible that a ductular reaction[350] associated with liver fibrosis resulted in bile duct injury and release of ALP into the serum. Histological evidence of a ductular reaction was observed in liver tissue from HFD+DM mice but it was not formally quantified. Further research is needed to establish the relevance of this unusual finding, including confirmation of liver-derived ALP, and not bone-derived ALP.

7.3 Strengths of this Thesis

7.3.1 The clinically relevant FaD model of NASH fibrosis

Scientific research in the development and progression of NASH fibrosis has been hampered by the lack of clinically relevant animal models that closely reflect the metabolic changes and histological features as they occur in humans. In addition, many frequently used models do not include a component of diabetes; whilst diabetes

is not specifically essential to the development of NASH fibrosis, it has been well established that diabetes is an independent risk factor for more severe disease in humans[67].

The FaD model was first published by this laboratory in 2011[145] as a highly translatable and clinically relevant animal model. It has since been used to contribute to further important research in NASH fibrosis in published[144] and unpublished studies. This thesis combined the use of the FaD model with tissue-specific gene deletions, highlighting the interaction between the environment and genetics to study NASH fibrosis in diabetes. The FaD model begins with inducing obesity by high fat feeding of mice aged four to seven weeks for a total of 26 weeks. Mice are not considered to be mature adults until the age of three months; however, they have reached sexual maturity by ~five weeks and thus this model aims to study the effects of obesity induced in adult mice, and not in juvenile mice[386]. Mice generally begin to exhibit changes associated with old age after the age of six months[386], but in this study mice were terminated by ~seven months of age, thereby limiting the effects of confounding age-related changes.

The high fat diet used in the FaD model was comprised of 45% kcal fat and 0.26% added cholesterol. High fat diets are frequently used to achieve obesity and insulin resistance in animal models, but the effects can be unreliable. This may be related to adaptation to reduce oral intake and resistance to the development of metabolic abnormalities[235], which may be more pronounced in certain mouse strains[387]. In response to this, researchers have developed methods of “force feeding” through oral gavage or gastrostomy feeding tubes or using genetically manipulated mice that exhibit hyperphagia[235], methods which are not relevant to human disease. Percentages of more than 60% kcal fat have been used in some diets, an amount that far exceeds human dietary intake in the majority of the population[212]. The WHO currently recommends that the total amount of fat consumed by an individual should be less than 30% of their total energy intake, as amounts greater than this will contribute to unhealthy weight gain[388]. To put this into perspective, recent data of American adults reports that the mean total fat intake as a percentage of total energy intake and adjusted for age was almost 36%[389]. A panel of experts in obesity research propose that a tolerated high fat human diet may consist of ~50 - 60% kcal fat[390], which

is almost double the recommended intake. In contrast, the relative difference of a Chow diet, containing 12% kcal fat, and a high fat diet of 60% kcal fat, is much larger and has questionable relevance to human physiology[390].

The amount of added cholesterol used in dietary animal studies has also been heavily scrutinised. Cholesterol increases the disease severity of NASH[215] but amounts used in some studies are much greater than a standard human diet. The amount used in the FaD model is relatively high for rodents but remains within the threshold of less than 0.5% which is recommended to maintain human relevance[212].

In general, the rationale for using diets that have such excessive amounts of fat or cholesterol relate to the convenience of such diets in rapidly causing metabolic derangements. This has advantageous effects such as less time required to perform a study, which can reduce the financial costs associated with long-term animal care, and increased research productivity[390]. Mice also tend to develop a more severe phenotype. However, these factors are at the expense of maintaining clinical applicability. The composition of the diet used in the FaD model remains highly relevant to human disease and importantly avoids many of the criticisms raised in other studies that use less relevant diets.

After 15 weeks of *ad libitum* high fat feeding, mice in the FaD model diabetes were then induced with diabetes using multiple low dose intraperitoneal injections of STZ. This mimics the progression of human disease, whereby the initial onset of obesity leads to insulin resistance and hyperinsulinaemia, followed then by the development of relative insulin deficiency and subsequent elevation of glucose levels to the diabetes range. Most of the mice required only two doses of STZ (65 mg/kg/day) given on consecutive days to achieve hyperglycaemia. Studies of much higher daily and cumulative doses of STZ to induce diabetes result in complete pancreatic β cell destruction, and a phenotype of absolute insulin deficiency that is typical of T1DM[230]. Whilst this model maintains glucose levels in the diabetes range throughout the ten weeks of diabetes, there is improvement in levels, likely related to recovery of pancreatic β cells over time. This pattern of glycaemia is frequently observed in animal models using STZ to induce diabetes[391-393].

Measurement of fasting plasma insulin and c-peptide levels indicate that mice in this study retained pancreatic β cell function to produce similar amounts of insulin as Chow fed mice, consistent with a relative insulin deficiency. Although these mice do not display overt hyperinsulinaemia at termination, data from fasting whole blood measurements taken at week 16, before the induction of diabetes, indicates that the mice were hyperinsulinaemic for more than half of the duration of the study. This model was not able to consistently demonstrate significant insulin resistance in the HFD+DM groups using multiple surrogate markers and calculated measures. However, the gold standard of hyperinsulinaemic euglycaemic clamp was not performed, and in future, this may be able to confirm the presence of insulin resistance in these obese and hyperglycaemic mice.

At high doses, STZ is known to cause toxicity outside of the pancreas[394]. Of main concern in this study is the effects of liver toxicty[231,395]. However, the initial publication from this laboratory reported on the amelioration of liver fibrosis in HFD+DM mice that were treated with insulin to achieve normoglycaemia[145]. This data provides evidence that the low dose STZ was not the cause of the liver fibrosis observed in the FaD model and reiterates that hyperglycaemia and diabetes increase the severity of disease.

These two animal studies recapitulate that the FaD model reliably produces NASH fibrosis, with a metabolic phenotype that closely resembles human disease. This is the first time that the FaD model has been assessed according to the NAS and Brunt criteria[80,81] by an independent anatomical pathologist with experience in mouse liver histology. Importantly, the ~200 specimens were de-identified for the analysis. Each of the Chow groups scored lowly in each of the individual criteria of fibrosis, lobular inflammation, portal inflammation, hepatocyte ballooning, steatosis, and total NAS. The HFD+DM groups had the highest scores for each of these criteria, whilst the HFD groups had intermediary scores, except for steatosis where all mice fed a high fat diet scored highly. This data provides further evidence that the addition of diabetes to a high fat feeding worsens the phenotype of NASH fibrosis. In addition, the sequential elevation in plasma measurement of CK-18, a proposed biomarker of NASH fibrosis, provides further evidence of the robustness of the FaD model. The mRNA levels of

collagens and related fibrotic genes change in the expected directions according to the metabolic stress that each group of mice was exposed to.

A comprehensive method for quantification of the amount of PSR-positive stained tissue using image analysis software was developed. This method was more sensitive at detecting changes in fibrosis severity compared with the independent pathologist's assessment. The use of automated technology enhances the practicality of this otherwise time-intensive method of capturing 20 images per mouse at multiple magnifications and focussing on different zones of the liver. However, assessment of a relatively large amount of tissue increases the reliability of the findings.

The main priority of the two animal studies was to examine the effects on development of NASH fibrosis in mice with hepatocyte gene deletions of CCN2 or CCN1 exposed to the FaD model of high fat feeding with diabetes. Assessment of mice fed a high fat diet alone was not the primary aim, but these groups were used to highlight the increased severity of disease when a high fat diet was combined with diabetes. A diabetes-only group was not performed in this study as they have been reported on in previous research from this laboratory and do not develop the metabolic features that are characteristic of NASH, nor do they develop significant liver fibrosis[145]. The findings in the HFD groups are generally as expected: lesser severity of fibrosis and inflammatory endpoints compared with HFD+DM groups, although this was not always statistically significant. Plasma studies of liver enzymes were somewhat discordant in the HFD groups, as they were either similar to, or higher than the HFD+DM groups, despite the lesser liver fibrosis. However, liver enzyme tests are a non-specific measure of liver damage and therefore the discordance may not be clinically relevant, especially when more reliable histological endpoints are available. The gene deletion of CCN2 had no observed effect within the HFD groups in The CCN2 Study. In The CCN1 Study, there were some minor effects with the hepatocyte CCN1 deletion exacerbating the liver and metabolic phenotype, but these changes rarely reached statistical significance. It is possible that the phenotype of the HFD mice was not severe enough to show subtle differences induced by the gene deletion.

A two-way ANOVA with correction for multiple comparisons was a rigorous statistical test for data consisting of two independent variables (mouse sub-strain and "diet").

One could argue that a less robust statistical test, such as a one-way ANOVA, may have been sufficient, as the primary aim was to compare mice exposed to same metabolic conditions. Although the data from this thesis adds to the model's reliability, this model has already been validated and published before, and so statistical tests between Chow, HFD, and HFD+DM were observed but not routinely reported in the current research. Nevertheless, even though it was difficult to demonstrate statistical significance in many outcomes because of the multiple interactions, the two-way ANOVA proved to be most appropriate statistical test, and reduced the risk of type I statistical error being seen in these studies[396].

7.3.2 The use of two control sub-strains when using the CreLoxP system

A major strength of this thesis is the use of two control sub-strains for comparison with the knockout sub-strain. Many studies that use the CreLoxP system report on only a single control sub-strain, yet debate remains regarding which sub-strain is an appropriate control. Evidence from this thesis shows that the two control sub-strains can sometimes have different phenotypes, and this has potential to significantly affect the interpretation of the data. The Jackson Laboratory details three options for control sub-strains when using the CreLoxP system[290]. Firstly, the homozygous LoxP is the control used in the $CCN2^{fl/fl}$ and $CCN1^{fl/fl}$ mice. These mice have the 34 bp LoxP sites flanking the gene of interest, but without the presence of Cre recombinase will not display a phenotype. The second option was the Cre transgene control, or in this case, the AlbCre mouse. Theoretically, these mice do not contain the LoxP sites that determine the site of recombination, and thus are frequently used as controls. However, several potential problems have been identified with these mice, which will be discussed below. The final suggestion is the Cre, heterozygous floxed control, which carries the Cre transgene and a single floxed allele of the gene of interest. Presumably, this is only a suitable control if a heterozygous deletion of the gene of interest does not produce a phenotype. Alternatively, some studies simply use the C57BL/6 wild-type strain as a control.

The Cre transgene control is frequently used in animal studies, but researchers should be aware of potential problems with them[373]. Firstly, Cre itself can produce its own phenotype. The random insertion of Cre may inadvertently disrupt an endogenous gene, causing unexpected and unrelated effects. In addition, Cre expression can be

high enough to affect normal cell physiology, a phenomenon called “Cre toxicity”[397,398]. There may also be naturally occurring “cryptic” LoxP sites, which closely resemble a LoxP site[399,400]. If the Cre recognises a cryptic LoxP, DNA damage at that site can occur. Secondly, although promoters are thought to be tissue-specific, Cre can be expressed in other tissues. For example, the RIP-Cre is expected to cause a gene deletion within pancreatic β cells, but a recent report showed unexpected Cre activity in the brain[401]. And finally, there can be mosaic Cre activity where there is incomplete deletion of floxed alleles. This may arise from Cre not being expressed in every cell in the target organ (e.g., not all hepatocytes expressed Cre), or alternatively there may be a failure of complete recombination.

Some of the above-mentioned concerns are more relevant to this thesis than others, noting that the AlbCre mice used in this thesis were purchased commercially from The Jackson Laboratory. Problems specific to creating new Cre transgenic mice or germline expression of Cre have not been discussed. Nevertheless, the main approach for addressing these concerns in the current animal studies was careful observation for unexpected phenotypes and the use of two control sub-strains, enabling comparison of the AlbCre sub-strain with the homozygous floxed sub-strain. Future studies that include the use of a Cre reporter strain, which can express a visible marker (e.g., fluorescent tag) in cells or tissue that express Cre activity may provide a more accurate method of confirming appropriate Cre activity[373,402].

7.3.3 The use of two methods for fibrosis assessment

The histological assessment by the pathologist was not able to detect a change in the fibrosis stage in the CCN2-KO and CCN1-KO HFD+DM mice, despite significant changes in the amount of PSR-positive staining by quantitative analysis. One consideration is that the two different methods used to assess liver fibrosis are measuring different things: the Brunt criteria used to grade fibrosis is a measure of regionality of fibrosis, where F0 is the absence of fibrosis, F1 is perisinusoidal, F2 is periportal, F3 is bridging and F4 is cirrhosis[80]. As the grade increases, more fibrosis is present, however there is no specific quantitative aspect to this grading system, and it is semi-quantitative at best. The fibrosis grade correlates well with clinical outcomes in humans, but whilst this system is frequently used in pre-clinical models, it has not been validated in animals. It may be that larger differences in fibrosis are required to

be able to detect this using the Brunt criteria. For example, a longer duration model of 40 weeks routinely induces F4 fibrosis with occasional HCC (unpublished data) and use of a hepatocyte CCN2 or CCN1 deletion in this model may be able to show a significant change in fibrosis using the Brunt criteria.

Another drawback of using the NAS and Brunt criteria is that by convention, the specimen is graded as the highest grade present, rather than the average grade of the sample. For example, in a mouse specimen containing 20 portal tracts, if 19 portal tracts are F0/F1, but one portal tract is F2, then the sample is graded as F2. This may explain the discrepancy between the amount of fibrosis by PSR staining compared with the grading of fibrosis by the pathologist in the HFD groups.

Alternatively, using PSR staining in combination with image software analysis provides a quantitative assessment of the amount of fibrosis. To improve the accuracy of this measurement, multiple images of each histological section were taken, at multiple magnifications, and focusing on multiple regions. In total, 20 images, covering a large range of each specimen, were taken: four images at 100x magnification, four images at 200x magnification, six images of six central veins at 400x magnification, and six images of six portal tracts at 400x magnification. PSR staining is frequently used to study fibrosis, but many studies do not perform such stringent analysis to quantify the amount of fibrosis.

One problem that was encountered in the quantitative PSR analysis was the effects of nuclei counterstaining. Standard protocols include a step for counterstaining nuclei with haematoxylin to aid in cellular identification. The image analysis software was detecting the brown-coloured nuclei as PSR-positive tissue, which was falsely increasing the amount of fibrosis. This had a greater effect on Chow fed groups compared with high fat fed groups: normal hepatocytes have nuclei with much larger surface areas compared with hepatocytes of high fat fed mice, which have nuclei that are pushed to the periphery by fat droplets and have a much smaller surface area. To overcome this issue, two sets of consecutive tissue sections were stained, one with nuclei counterstaining and one without. The non-counterstained sections were used for fibrosis quantification, whilst the counterstained sections were used for cellular identification and representative images.

7.3.4 The value of clinical cohort studies: The DLC Audit and The DaSH Study

The two clinical cohorts used in this thesis provide valuable information in the study of individuals with diabetes and liver disease. The CPC RPAH DLC clinic is the first of its kind in Australasia. Patients undergo thorough clinical assessment, with access to transient elastography for liver fibrosis assessment, which is not otherwise readily accessible in Australia. It provides opportunity for coordinated screening of complications in those with advanced liver fibrosis, and access to relevant clinical trials of potential therapeutic interventions. In the future, serial assessment of these patients will allow a better understanding of the natural history of NAFLD in individuals with diabetes.

Over recent years, international guidelines for screening of NAFLD/NASH fibrosis in the diabetes population have been developed[199-201], in recognition of the increasing burden of disease and the need to provide guidance to primary care physicians, endocrinologists and hepatologists. The CPC RPAH DLC clinic was established before most of the international guidelines were published, and this provides significant validation for the clinic. Australia is yet to establish its own clinical guideline, and real-world data from clinics such as this will aid in the development of relevant and practical recommendations to improve patient outcomes.

The novelty of The DaSH Study cohort lies in the bio-banked blood samples with corresponding clinical data, including liver assessment, of a cohort of individuals with diabetes. Other potential biomarkers have been tested in this cohort before and provided some novel results, including in FAP[87] and DPP4 activity[86]. This thesis reports on the measurement of circulating CCNs as potential novel blood biomarkers. Although CCN1, CCN2, or CCN3 did not correlate directly with the presence of advanced fibrosis by transient elastography, overall, the cohort had relatively mild disease and few individuals had severe disease. Measurement of circulating CCNs in a larger cohort selected for moderate to advanced liver fibrosis and T2DM might yield better results.

7.4 Limitations of this Thesis

7.4.1 Evidence for the gene deletion of CCN2 and CCN1

A limitation of this study was that *in situ* hybridisation was not performed to confirm the location of the gene deletion. It is also assumed that deletion of a single module of CCN2 and CCN1 will result in knockdown of all functional hepatocyte CCN2 and CCN1 proteins. The homozygous floxed mice were created by Professor Andrew Leask and donated to our laboratory and thus there was no control over the insertion sites of the LoxP sequences. Importantly, the deleted sequences were in-frame mutations that resulted in a stop codon. Data prepared by Dr Xiaoyu Wang prior to the commencement of this thesis and during the generation and confirmation of the gene knockout mice clearly showed reductions at the DNA, mRNA, and protein levels in the livers of chow fed CCN2-KO and also in the CCN1-KO mice.

In The CCN2 Study, it would have been helpful to achieve a greater reduction in liver CCN2 in the CCN2-KO mice than the ~40 - 60% reduction that was shown here. If so, then it may have been possible to achieve even greater prevention of liver fibrosis. Continued production of CCN2 by non-hepatocyte liver cells may be responsible for this and deletion of CCN2 in all liver cells, including HSCs, might yield greater effects on fibrosis prevention.

There was a reduction of > 80% of liver CCN1 mRNA level in the CCN1-KO mice in The CCN1 Study. There were challenges in detecting the CCN1 protein and the Western immunoblot analysis of mice from chow fed mice appeared to show a reduced level of CCN1 protein. Although several commercial antibodies were trialled, the antibody used in the Western immunoblot shown in *Chapter 2* detected a very faint band that corresponded to the molecular mass for monomeric CCN1and showed the expected reduction in the CCN1-KO mice compared with the AlbCre mice. A prominent band at a higher molecular mass was also detected and this darker band may represent dimeric CCN1 protein. It showed the same trend of reduction in the CCN1-KO mice but was not further investigated and remained to be confirmed.

7.4.2 Generalisability of the pre-clinical findings

The effect of gender on development of NASH fibrosis was not explored as only male mice were used in the animal studies. Both human and animal studies suggest that NAFLD is a sexually dimorphic disease[403,404]. In humans, NAFLD affects men more than women, but post-menopausal women are more likely to develop more severe steatosis and liver fibrosis[403]. Similar findings have been reported in models of oestrogen deficiency in zebrafish[405] and mice[406]. These findings implicate oestrogen as a protective hormone for NASH fibrosis and research is ongoing regarding its therapeutic value[404].

However, gender is not included as a component of any of the validated clinical risk scores for liver fibrosis and nor was it statistically significant in the multivariate analyses of the two clinical cohorts used in this thesis. At the time of application for animal ethics approval for The CCN2 Study and The CCN1 Study, use of both genders of mice was not mandated, as it is now. Historically, use of male animals was preferred by researchers to mitigate the impact of the female oestrous cycle that may confound results and increase the number of controls required. Also relevant to this study is the resistance to diabetes induction by STZ in female C57BL/6 mice[407]. It may be reasonable to hypothesise that if pre-menopausal females had been used in this study, they would have developed less fibrosis than the male mice, related to oestrogen protection and less severe diabetes, and consequently the effects of the CCN2 or CCN1 deletion may have been less pronounced. However, future studies should endeavour to include female mice to improve the general applicability of the findings.

Each of the mouse sub-strains used in the animal studies were bred on a C57BL/6J background, the most common strain used in animal research of dietary induced metabolic changes. The benefits include their susceptibility to developing diet-induced obesity and diabetes[289]. However, inbred mouse strains do not exhibit the genetic diversity of humans, and future studies should also incorporate other inbred and outbred mouse strains for a better understanding of the effect of genetic diversity on development of NASH fibrosis.

7.4.3 Utilisation of pre-clinical *in vivo* imaging

The Pre-clinical Imaging Core Research Facility in the Charles Perkins Centre at the University of Sydney houses a wide range of modality options to conduct *in vivo* studies in small animals. Unfortunately, this thesis was not able to fully utilise the pre-clinical imaging facilities. The results of the liver ultrasound were not presented in this thesis as there were difficulties with the data analysis, which required external assistance. Whether a radiomics approach can be used to reliably identify liver fibrosis in live mice is still unknown but ultrasound would be a useful non-invasive tool if it were validated. The ultrasound images were easily acquired with short anaesthesia times (under 15 minutes) and the procedure was well-tolerated by the mice.

Assessment by MRI was abandoned as high fat fed mice became too obese to fit inside the MRI chamber for serial assessment. A further imaging modality that was not explored due to the temporary closure of the facility during the COVID-19 pandemic was MRS. A study in humans has reported that ^{1}Hydrogen (^{1}H) MRS features correlated well with biopsy-proven fibrosis in individuals with chronic hepatitis[408]. Others have used ^{1}H MRS in mice to quantify liver fat[409,410] and ^{31}Phosphorous (^{31}P) MRS in rats to assess liver fibrosis[411]. The benefit of pre-clinical imaging is that real-time non-invasive assessment can be performed, which would otherwise require termination of an animal for each single time-point analysis. Imaging modalities can be repeated throughout the study and provide information on progression or regression of disease. Incorporating pre-clinical imaging into future animal studies has the potential to reduce the overall number of mice required in animal research, which is one of the three R's in the Australian Code for animal research[412].

7.4.4 Generalisability of the clinical findings

Whilst both clinical cohorts studied in this thesis have reported on novel and important data that adds to what is already known about NASH fibrosis and diabetes, a limitation is the size of each cohort. There were just under 100 individuals in each study, and this affects the general application of the results to a wider population. Data collection from The DLC Audit is currently ongoing, however this audit has been significantly impacted by the COVID-19 pandemic with the temporary cessation of face-to-face clinical assessments. Larger studies of a longitudinal nature are required, which will aid in further characterisation of individuals with NASH fibrosis and in defining the

natural history of the disease. The statistical models proposed in The DLC Audit and The DaSH Study could then be validated in these larger cohorts.

In the absence of national guidelines, controversy remains regarding the best screening algorithm for NAFLD/NASH in T2DM. The development of accurate screening tests, such as novel blood biomarkers, could be used in addition to clinical risk scores to enhance diagnostic and prognostic value. Prospective studies with relevant ethical approval to collect and store human blood samples will be useful in the future testing of potential biomarkers for NASH fibrosis.

7.5 Future Directions

Many of the future directions were already discussed in previous sections of this thesis. This final section will focus on two of the broader aspects of potential future research studies that arose from the findings of this thesis.

7.5.1 Identifying mechanisms by which hepatocyte CCN2 and CCN1 affect liver fibrosis

The CCN2 Study and The CCN1 Study have so far focussed on a phenotypic description of the relevant hepatocyte gene deletions. Having confirmed the hypotheses, the next step is to consider whether CCN2 or CCN1 are mediators, or markers of liver fibrosis development or fibrosis regression. To do this, further research into potential mechanisms will be required.

In examining the role of hepatocyte CCN2, further lines of investigation mentioned already in this thesis (discussed in *Section 4.4*) include assessment of the MAPK signalling pathways, the further exploration of the relationship between CCN2 and TIMP1 and collagen proteins, and the interaction of CCN2 with activated HSCs. Targeting CCN2 in other liver cells, such as HSCs, either in addition to or independently of the hepatocyte, may improve outcomes in the prevention of liver fibrosis. The protocol used is primarily a study of the prevention of liver fibrosis, and future studies should aim to examine whether established liver fibrosis can be reversed or at least progression prevented. This could be performed using time-

targeted inducible gene deletions with the CreLoxP system, or with administration of an anti-CCN2 agent after the development of liver fibrosis in a longer-term study.

Important future studies in The CCN1 Study will involve detailed assessment of the role played by the HSCs, in relation to senescence and apoptosis pathways. Previous studies of hepatocyte CCN1 gene deletion in a toxin-induced model of NASH showed a deficit of HSC senescence using senescence-associated β-galactosidase staining[286]. Further investigation of the systemic phenotype in the CCN1-KO HFD+DM mice is also required and will include consideration of whether this systemic phenotype is an indirect contributor to the development of liver fibrosis. In the first instance, repeating the current study would determine whether the systemic phenotype can be replicated.

7.5.2 Considerations of CCN2 and CCN1 as potential therapeutic targets

The findings presented in the pre-clinical studies in this thesis suggest that inhibition of liver CCN2 or treatment with CCN1 may be of therapeutic value in the prevention, and possibly treatment, of NASH fibrosis.

7.5.2.1 Inhibition of CCN2 to reduce liver fibrosis

CCN2 has been studied as a therapeutic target in pre-clinical and clinical studies. In the kidney, rodent studies have demonstrated that a reduction in CCN2 achieved by injections of antisense oligonucleotides was able to reduce histological fibrosis and expression of relevant fibrosis markers[413-415]. Other studies have used small interfering RNA (siRNA) to silence CCN2 gene expression in models of renal allograft nephropathy[416] and unilateral ureteral obstruction[417]. A small phase 1 clinical trial of a monoclonal antibody against CCN2 (FG-3019; FibroGen, San Francisco, CA, USA) in individuals with microalbuminuric diabetic kidney disease showed promise in reducing UACr[418]. The medication was administered intravenously every fortnight for two months and was well tolerated. A subsequent phase 2 clinical was terminated early[419]. There are no current clinical trials of FG-3019 in the renal field listed on ClinicalTrials.gov.

The most promising therapeutic use for FG-3019 exists for the treatment of idiopathic pulmonary fibrosis (IPF). A phase 2 clinical trial (PRAISE) was published in 2020

reporting on the attenuation of progression of IPF in patients who had been randomised to receive intravenous infusions of FG-3019 (pamrevlumab) every 3 weeks for 48 weeks[420]. A phase 3 double-blinded RCT (ZEPHYRUS I)[421] with open-label extension phase (ZEPHYRUS II)[422] are currently underway. There have been no safety concerns identified. Other active clinical trials listed on ClinicalTrials.gov include studies of FG-3019 in pancreatic cancer and Duchenne Muscular Dystrophy.

Another drug targeting CCN2 through RNA interference, RXI-109 (Phio Pharmaceuticals (formerly RXi Pharmaceuticals), Marlborough, MA, USA) has undergone phase 2 clinical trials in individuals with hypertrophic[423] and keloid[424] scarring. It is administered intra-dermally, but results are yet to be published. There is also interest in intravitreal injection of this agent for the treatment of eye disease[425,426].

Similar techniques of antisense oligonucleotides, siRNA, and neutralising antibodies have been investigated in pre-clinical studies of liver fibrosis. One study showed reduction of collagen-I expression but not fibrosis with intra-portal administration of CCN2 antisense oligonucleotides in a CCl_4-induced mouse model of liver fibrosis[427]. Other studies using siRNA in toxin-induced liver fibrosis in rats reported improvements in fibrosis marker expression and liver fibrosis[428,429]. Our laboratory used intraperitoneal administration of a polyclonal neutralising antibody against CCN2 to show partial protection from the development of liver fibrosis in the clinically relevant FaD model[144]. A phase 2 clinical trial of FG-3019 plus the antiviral agent, entecavir, in individuals with liver fibrosis due to chronic hepatitis B infection, was terminated early as entecavir had an unexpected positive effect on fibrosis regression[430]. No further studies examining treatment of humans with liver fibrosis with inhibition of CCN2 have been reported.

7.5.2.2 Treatment with CCN1 to reduce liver fibrosis

There is considerably less research on the use of CCN1 as a therapeutic target. In a mouse model of worsened fibrosis due to mutant CCN1 that is unable to bind to integrins, administration of CCN1 was able to reverse the damage; this was demonstrated in studies of wound healing with topical application of CCN1 protein[262], and in colitis with intraperitoneal injection of purified CCN1[431].

7.5.2.3 Targeted therapeutic strategies

Many of the above-mentioned studies have utilised systemic administration of a potential therapeutic agent. However, the CCNs have a diverse range of functions in many cells and tissues, and unwanted off-target side effects may limit their utility. But CCNs are generally lowly expressed under normal conditions and become highly expressed in response to inflammation and tissue damage. Theoretically, it is likely that the sites of pathology will be preferentially targeted by systemically administered therapeutic agents, and that the normal functions of unaffected organs and tissues will be minimally impacted[252].

The homologous structure of the CCN family proteins makes the development of humanised monoclonal antibodies challenging. Targeting the hinge region, which is unique to each CCN member, may offer better specificity and less side effects[252]. The fact that FG-3019 has promising data for therapeutic effectiveness for IPF without significant side effects[420] gives promise that this type of drug design can potentially be used in other fibrotic diseases.

Some technologies, such as siRNA and antisense oligonucleotides can have relatively good specificity through careful design of nucleotide sequences[252]. The choice of vector can also affect the effectiveness of drug delivery and potential side effects. Adeno-associated virus (AAV) is the most preferable vector for gene therapy involving the liver. They carry long-term gene expression and do not have the significant immunogenic and genetic side effects associated with other viral vectors[432]. Non-viral vectors, such as nanoparticles, are another potential option that are less likely to generate an immune response. Nanoparticles have been used to deliver CCN2 siRNA to treat liver fibrosis in cell-based and animal studies but have not yet been tested in humans[433,434].

Another novel approach to targeting CCN2 is via injection of protein peptides. Several peptides are under development by BLR Bio that target CCN2 through manipulations in CCN3. Certain peptides have been designed to target kidney diseases, whilst others have anti-cancer[435] and/or antifibrotic properties. These remain under investigation in pre-clinical studies and have not yet been tested in humans[436].

7.5.2.4 Reflections on therapy from The CCN2 Study and The CCN1 Study

Based on the results presented in the animal studies from this thesis, CCN2 and CCN1 are potential targets for the prevention of NASH fibrosis in diabetes. Future studies could aim to test methods of gene therapy for inhibiting CCN2 to establish if NASH fibrosis can be prevented, or even treated, using a clinically relevant mouse model. Studies of administering CCN1 protein and determining effect on NASH fibrosis would also be useful. As individually targeting CCN2 or CCN1 is likely to result in partial, rather than complete amelioration of fibrosis, models that simultaneously target CCN2 and CCN1 may offer a more effective therapeutic strategy.

7.6 Concluding Remarks

The growing burden of disease posed by NASH fibrosis in individuals with T2DM highlights the need for increasing clinical and pre-clinical research into this area. Research from this thesis has described the clinical problem and local prevalence in The DLC Audit. Potential candidates implicated in the pathogenesis of NASH fibrosis have been explored in novel pre-clinical mechanistic studies, with results suggesting that each of CCN2 and CCN1 indeed have promise as therapeutic targets. Finally, the role of circulating CCNs as novel biomarkers for screening of NASH fibrosis has been investigated. It is anticipated that in future years, answering key questions related to pathophysiology using clinically relevant animal models will lead to development of novel therapies for prevention and treatment of NASH fibrosis. Subsequent translation of such pre-clinical research to the clinical setting, likely across decades, will predictably lead to improved outcomes for people who have NASH fibrosis with T2DM.

References

1. American Diabetes Association Professional Practice Committee. 2. Classification and Diagnosis of Diabetes: Standards of Medical Care in Diabetes—2022. *Diabetes Care.* 2021;45(Supplement_1):S17-S38.
2. Kahn CR. Insulin Action, Diabetogenes, and the Cause of Type II Diabetes. *Diabetes.* 1994;43(8):1066-1085.
3. World Health Organization. *Classification of diabetes mellitus.* Geneva: World Health Organization; 2019.
4. Australian Institute of Health and Welfare. *Diabetes: Australian facts.* Canberra: Australian Institute of Health and Welfare;2022.
5. Australian Bureau of Statistics. https://www.abs.gov.au/statistics/health/causes-death/causes-death-australia/2020. Published 2020. Accessed 13/10/2022.
6. Diabetes NSW & ACT. https://diabetesnsw.com.au/diabetes/#facts. Accessed 13/10/2022.
7. Sun H, Saeedi P, Karuranga S, et al. IDF Diabetes Atlas: Global, regional and country-level diabetes prevalence estimates for 2021 and projections for 2045. *Diabetes Research and Clinical Practice.* 2022;183:109119.
8. International Diabetes Federation. *IDF Diabetes Atlas.* 10th ed. Brussels: International Diabetes Federation; 2021.
9. Reinehr T. Type 2 diabetes mellitus in children and adolescents. *World J Diabetes.* 2013;4(6):270-281.
10. World Health Organization. *Global report on diabetes.* Geneva: World Health Organization; 2016.
11. Chen L, Magliano DJ, Balkau B, et al. AUSDRISK: an Australian Type 2 Diabetes Risk Assessment Tool based on demographic, lifestyle and simple anthropometric measures. *Medical Journal of Australia.* 2010;192(4):197-202.
12. Australian Diabetes Society. Australian type 2 diabetes management algorithm. https://treatment.diabetessociety.com.au/documents/t2d-mgmt-algorithm-625.pdf. Published 2022. Accessed 14/10/2022.
13. American Diabetes Association Professional Practice Committee. 10. Cardiovascular Disease and Risk Management: Standards of Medical Care in Diabetes—2022. *Diabetes Care.* 2021;45(Supplement_1):S144-S174.
14. Harding JL, Shaw JE, Peeters A, Guiver T, Davidson S, Magliano DJ. Mortality Trends Among People With Type 1 and Type 2 Diabetes in Australia: 1997–2010. *Diabetes Care.* 2014;37(9):2579-2586.
15. Gaede P, Lund-Andersen H, Parving HH, Pedersen O. Effect of a multifactorial intervention on mortality in type 2 diabetes. *N Engl J Med.* 2008;358(6):580-591.
16. Intensive Blood Glucose Control and Vascular Outcomes in Patients with Type 2 Diabetes. *New England Journal of Medicine.* 2008;358(24):2560-2572.
17. Effects of Intensive Glucose Lowering in Type 2 Diabetes. *New England Journal of Medicine.* 2008;358(24):2545-2559.
18. Duckworth W, Abraira C, Moritz T, et al. Glucose Control and Vascular Complications in Veterans with Type 2 Diabetes. *New England Journal of Medicine.* 2009;360(2):129-139.
19. Zoungas S, Chalmers J, Neal B, et al. Follow-up of Blood-Pressure Lowering and Glucose Control in Type 2 Diabetes. *New England Journal of Medicine.* 2014;371(15):1392-1406.

20. Nine-Year Effects of 3.7 Years of Intensive Glycemic Control on Cardiovascular Outcomes. *Diabetes Care.* 2016;39(5):701-708.
21. Hayward RA, Reaven PD, Wiitala WL, et al. Follow-up of Glycemic Control and Cardiovascular Outcomes in Type 2 Diabetes. *New England Journal of Medicine.* 2015;372(23):2197-2206.
22. Intensive blood-glucose control with sulphonylureas or insulin compared with conventional treatment and risk of complications in patients with type 2 diabetes (UKPDS 33). UK Prospective Diabetes Study (UKPDS) Group. *Lancet.* 1998;352(9131):837-853.
23. Holman RR, Paul SK, Bethel MA, Matthews DR, Neil HAW. 10-Year Follow-up of Intensive Glucose Control in Type 2 Diabetes. *New England Journal of Medicine.* 2008;359(15):1577-1589.
24. Ray KK, Seshasai SRK, Wijesuriya S, et al. Effect of intensive control of glucose on cardiovascular outcomes and death in patients with diabetes mellitus: a meta-analysis of randomised controlled trials. *Lancet (London, England).* 2009;373(9677):1765-1772.
25. Boussageon R, Bejan-Angoulvant T, Saadatian-Elahi M, et al. Effect of intensive glucose lowering treatment on all cause mortality, cardiovascular death, and microvascular events in type 2 diabetes: meta-analysis of randomised controlled trials. *BMJ.* 2011;343:d4169.
26. Kelly TN, Bazzano LA, Fonseca VA, Thethi TK, Reynolds K, He J. Systematic review: glucose control and cardiovascular disease in type 2 diabetes. *Ann Intern Med.* 2009;151(6):394-403.
27. Forbes JM, Cooper ME. Mechanisms of Diabetic Complications. *Physiological Reviews.* 2013;93(1):137-188.
28. Lee R, Wong TY, Sabanayagam C. Epidemiology of diabetic retinopathy, diabetic macular edema and related vision loss. *Eye Vis (Lond).* 2015;2:17.
29. American Diabetes Association Professional Practice Committee. 12. Retinopathy, Neuropathy, and Foot Care: Standards of Medical Care in Diabetes—2022. *Diabetes Care.* 2021;45(Supplement_1):S185-S194.
30. Mohamed Q, Gillies MC, Wong TY. Management of diabetic retinopathy: a systematic review. *Jama.* 2007;298(8):902-916.
31. Lightman S, Towler HM. Diabetic retinopathy. *Clin Cornerstone.* 2003;5(2):12-21.
32. Mitchell P, Foran S, Assistance E, Foran J. Guidelines for the Management of Diabetic Retinopathy. 2008.
33. American Diabetes Association Professional Practice Committee. 11. Chronic Kidney Disease and Risk Management: Standards of Medical Care in Diabetes—2022. *Diabetes Care.* 2021;45(Supplement_1):S175-S184.
34. Alicic RZ, Rooney MT, Tuttle KR. Diabetic Kidney Disease: Challenges, Progress, and Possibilities. *Clin J Am Soc Nephrol.* 2017;12(12):2032-2045.
35. Griffin TP, O'Shea PM, Smyth A, et al. Burden of chronic kidney disease and rapid decline in renal function among adults attending a hospital-based diabetes center in Northern Europe. *BMJ Open Diabetes Research & Care.* 2021;9(1):e002125.
36. White S, Chadban S. Diabetic kidney disease in Australia: current burden and future projections. *Nephrology (Carlton).* 2014;19(8):450-458.
37. Bakris GL, Agarwal R, Anker SD, et al. Effect of Finerenone on Chronic Kidney Disease Outcomes in Type 2 Diabetes. *New England Journal of Medicine.* 2020;383(23):2219-2229.

38. Said G. Diabetic neuropathy--a review. *Nat Clin Pract Neurol.* 2007;3(6):331-340.
39. Stratton IM, Adler AI, Neil HAW, et al. Association of glycaemia with macrovascular and microvascular complications of type 2 diabetes (UKPDS 35): prospective observational study. *BMJ.* 2000;321(7258):405-412.
40. American Diabetes Association Professional Practice Committee. 4. Comprehensive Medical Evaluation and Assessment of Comorbidities: Standards of Medical Care in Diabetes—2022. *Diabetes Care.* 2021;45(Supplement_1):S46-S59.
41. World Health Organization. Obesity and overweight. World Health Organisation. https://www.who.int/news-room/fact-sheets/detail/obesity-and-overweight. Published 2021. Accessed 15/10/2022.
42. Razak F, Anand SS, Shannon H, et al. Defining Obesity Cut Points in a Multiethnic Population. *Circulation.* 2007;115(16):2111-2118.
43. World Obesity Federation. *World Obesity Atlas 2022.* London World Obesity Federation;2022.
44. Waters H, Graf M. *America's Obesity Crisis: The Health and Economic Costs of Excess Weight.* New York: Milken Institute;2018.
45. Australian Institute of Health and Welfare. *Overweight and obesity.* Canberra: Australian Institute of Health and Welfare;2022.
46. Australian Bureau of Statistics. *National Health Survey: First results.* Canberra: Australian Bureau of Statistics;2017-18.
47. Collective for Action on Obesity. *Weighing in: Australia's growing obesity epidemic.* Collective for Action on Obesity; 2019.
48. Di Angelantonio E, Bhupathiraju SN, Wormser D, et al. Body-mass index and all-cause mortality: individual-participant-data meta-analysis of 239 prospective studies in four continents. *The Lancet.* 2016;388(10046):776-786.
49. Dai H, Alsalhe TA, Chalghaf N, Riccò M, Bragazzi NL, Wu J. The global burden of disease attributable to high body mass index in 195 countries and territories, 1990-2017: An analysis of the Global Burden of Disease Study. *PLoS Med.* 2020;17(7):e1003198.
50. Bhaskaran K, Dos-Santos-Silva I, Leon DA, Douglas IJ, Smeeth L. Association of BMI with overall and cause-specific mortality: a population-based cohort study of 3·6 million adults in the UK. *Lancet Diabetes Endocrinol.* 2018;6(12):944-953.
51. Malnick SDH, Knobler H. The medical complications of obesity. *QJM: An International Journal of Medicine.* 2006;99(9):565-579.
52. Finer N. Medical consequences of obesity. *Medicine.* 2015;43(2):88-93.
53. Rueda-Clausen CF, Ogunleye AA, Sharma AM. Health Benefits of Long-Term Weight-Loss Maintenance. *Annu Rev Nutr.* 2015;35:475-516.
54. Blüher M. Obesity: global epidemiology and pathogenesis. *Nature Reviews Endocrinology.* 2019;15(5):288-298.
55. Loos RJ. The genetics of adiposity. *Curr Opin Genet Dev.* 2018;50:86-95.
56. Walter S, Mejía-Guevara I, Estrada K, Liu SY, Glymour MM. Association of a Genetic Risk Score With Body Mass Index Across Different Birth Cohorts. *Jama.* 2016;316(1):63-69.
57. Grundy SM, Cleeman JI, Daniels SR, et al. Diagnosis and management of the metabolic syndrome: an American Heart Association/National Heart, Lung, and Blood Institute Scientific Statement. *Circulation.* 2005;112(17):2735-2752.

58. Alberti KG, Eckel RH, Grundy SM, et al. Harmonizing the metabolic syndrome: a joint interim statement of the International Diabetes Federation Task Force on Epidemiology and Prevention; National Heart, Lung, and Blood Institute; American Heart Association; World Heart Federation; International Atherosclerosis Society; and International Association for the Study of Obesity. *Circulation.* 2009;120(16):1640-1645.
59. World Health Organization. Definition, diagnosis and classification of diabetes mellitus and its complications : report of a WHO consultation. Part 1, Diagnosis and classification of diabetes mellitus. In. Geneva: World Health Organization; 1999.
60. Mescher AL. Organs Associated with the Digestive Tract. In: *Junqueira's Basic Histology Text and Atlas, 16e.* New York, NY: McGraw Hill; 2021.
61. Ghany MG, Hoofnagle JH. Approach to the Patient with Liver Disease. In: Jameson JL, Fauci AS, Kasper DL, Hauser SL, Longo DL, Loscalzo J, eds. *Harrison's Principles of Internal Medicine, 20e.* New York, NY: McGraw-Hill Education; 2018.
62. Wong VW, Chan WK, Chitturi S, et al. Asia-Pacific Working Party on Non-alcoholic Fatty Liver Disease guidelines 2017-Part 1: Definition, risk factors and assessment. *J Gastroenterol Hepatol.* 2018;33(1):70-85.
63. Cohen JC, Horton JD, Hobbs HH. Human Fatty Liver Disease: Old Questions and New Insights. *Science.* 2011;332(6037):1519-1523.
64. Eslam M, Sanyal AJ, George J, et al. MAFLD: A Consensus-Driven Proposed Nomenclature for Metabolic Associated Fatty Liver Disease. *Gastroenterology.* 2020;158(7):1999-2014.e1991.
65. Younossi ZM, Paik JM, Al Shabeeb R, Golabi P, Younossi I, Henry L. Are there outcome differences between NAFLD and metabolic-associated fatty liver disease? *Hepatology.* 2022;76(5):1423-1437.
66. Cotter TG, Rinella M. Nonalcoholic Fatty Liver Disease 2020: The State of the Disease. *Gastroenterology.* 2020;158(7):1851-1864.
67. Williams KH, Shackel NA, Gorrell MD, McLennan SV, Twigg SM. Diabetes and nonalcoholic Fatty liver disease: a pathogenic duo. *Endocr Rev.* 2013;34(1):84-129.
68. Younossi Z, Anstee QM, Marietti M, et al. Global burden of NAFLD and NASH: trends, predictions, risk factors and prevention. *Nature Reviews Gastroenterology & Hepatology.* 2018;15(1):11-20.
69. Mahady SE, Adams LA. Burden of non-alcoholic fatty liver disease in Australia. *J Gastroenterol Hepatol.* 2018;33 Suppl 1:1-11.
70. Abdelmalek MF, Diehl AM. Nonalcoholic Fatty Liver Diseases and Nonalcoholic Steatohepatitis. In: Jameson JL, Fauci AS, Kasper DL, Hauser SL, Longo DL, Loscalzo J, eds. *Harrison's Principles of Internal Medicine, 20e.* New York, NY: McGraw-Hill Education; 2018.
71. Gill R, Kakar S. Liver and Gallbladder. In: *Robbins & Cotran Pathologic Basis of Disease.* 10th ed. Philadelphia: Elsevier; 2021.
72. Villeret F, Dumortier J, Erard-Poinsot D. How will NAFLD change the liver transplant landscape in the 2020s? *Clinics and Research in Hepatology and Gastroenterology.* 2022;46(1):101759.
73. Younossi ZM, Stepanova M, Ong J, et al. Nonalcoholic Steatohepatitis Is the Most Rapidly Increasing Indication for Liver Transplantation in the United States. *Clinical Gastroenterology and Hepatology.* 2021;19(3):580-589.e585.

74. Calzadilla-Bertot L, Jeffrey GP, Jacques B, et al. Increasing Incidence of Nonalcoholic Steatohepatitis as an Indication for Liver Transplantation in Australia and New Zealand. *Liver Transplantation.* 2019;25(1):25-34.
75. Valery PC, Laversanne M, Clark PJ, Petrick JL, McGlynn KA, Bray F. Projections of primary liver cancer to 2030 in 30 countries worldwide. *Hepatology.* 2018;67(2):600-611.
76. Estes C, Razavi H, Loomba R, Younossi Z, Sanyal AJ. Modeling the epidemic of nonalcoholic fatty liver disease demonstrates an exponential increase in burden of disease. *Hepatology.* 2018;67(1):123-133.
77. Adams LA, Roberts SK, Strasser SI, et al. Nonalcoholic fatty liver disease burden: Australia, 2019-2030. *J Gastroenterol Hepatol.* 2020;35(9):1628-1635.
78. Targher G, Byrne CD, Tilg H. NAFLD and increased risk of cardiovascular disease: clinical associations, pathophysiological mechanisms and pharmacological implications. *Gut.* 2020;69(9):1691-1705.
79. Brunt EM, Kleiner DE, Carpenter DH, et al. NAFLD: Reporting Histologic Findings in Clinical Practice. *Hepatology.* 2021;73(5):2028-2038.
80. Brunt EM, Janney CG, Di Bisceglie AM, Neuschwander-Tetri BA, Bacon BR. Nonalcoholic steatohepatitis: a proposal for grading and staging the histological lesions. *Am J Gastroenterol.* 1999;94(9):2467-2474.
81. Kleiner DE, Brunt EM, Van Natta M, et al. Design and validation of a histological scoring system for nonalcoholic fatty liver disease. *Hepatology.* 2005;41(6):1313-1321.
82. Nalbantoglu ILK, Brunt EM. Role of liver biopsy in nonalcoholic fatty liver disease. *World J Gastroenterol.* 2014;20(27):9026-9037.
83. Musso G, Gambino R, Cassader M, Pagano G. Meta-analysis: Natural history of non-alcoholic fatty liver disease (NAFLD) and diagnostic accuracy of non-invasive tests for liver disease severity. *Annals of Medicine.* 2011;43(8):617-649.
84. Wong VW-S, Adams LA, de Lédinghen V, Wong GL-H, Sookoian S. Noninvasive biomarkers in NAFLD and NASH — current progress and future promise. *Nature Reviews Gastroenterology & Hepatology.* 2018;15(8):461-478.
85. Kwok R, Tse YK, Wong GL, et al. Systematic review with meta-analysis: non-invasive assessment of non-alcoholic fatty liver disease--the role of transient elastography and plasma cytokeratin-18 fragments. *Aliment Pharmacol Ther.* 2014;39(3):254-269.
86. Williams KH, Vieira De Ribeiro AJ, Prakoso E, et al. Circulating dipeptidyl peptidase-4 activity correlates with measures of hepatocyte apoptosis and fibrosis in non-alcoholic fatty liver disease in type 2 diabetes mellitus and obesity: A dual cohort cross-sectional study. *Journal of Diabetes.* 2015;7(6):809-819.
87. Williams KH, Viera de Ribeiro AJ, Prakoso E, et al. Lower serum fibroblast activation protein shows promise in the exclusion of clinically significant liver fibrosis due to non-alcoholic fatty liver disease in diabetes and obesity. *Diabetes Research and Clinical Practice.* 2015;108(3):466-472.
88. Lonardo A, Bellini M, Tondelli E, et al. Nonalcoholic steatohepatitis and the "bright liver syndrome": should a recently expanded clinical entity be further expanded? *Am J Gastroenterol.* 1995;90(11):2072-2074.
89. Saverymuttu SH, Joseph AE, Maxwell JD. Ultrasound scanning in the detection of hepatic fibrosis and steatosis. *Br Med J (Clin Res Ed).* 1986;292(6512):13-15.

90. Mottin CC, Moretto M, Padoin AV, et al. The role of ultrasound in the diagnosis of hepatic steatosis in morbidly obese patients. *Obes Surg.* 2004;14(5):635-637.
91. Yoneda M, Yoneda M, Mawatari H, et al. Noninvasive assessment of liver fibrosis by measurement of stiffness in patients with nonalcoholic fatty liver disease (NAFLD). *Dig Liver Dis.* 2008;40(5):371-378.
92. Friedrich-Rust M, Romen D, Vermehren J, et al. Acoustic radiation force impulse-imaging and transient elastography for non-invasive assessment of liver fibrosis and steatosis in NAFLD. *European Journal of Radiology.* 2012;81(3):e325-e331.
93. Kumar R, Rastogi A, Sharma MK, et al. Liver stiffness measurements in patients with different stages of nonalcoholic fatty liver disease: diagnostic performance and clinicopathological correlation. *Dig Dis Sci.* 2013;58(1):265-274.
94. Dowman JK, Tomlinson JW, Newsome PN. Systematic review: the diagnosis and staging of non-alcoholic fatty liver disease and non-alcoholic steatohepatitis. *Aliment Pharmacol Ther.* 2011;33(5):525-540.
95. Borra RJ, Salo S, Dean K, et al. Nonalcoholic fatty liver disease: rapid evaluation of liver fat content with in-phase and out-of-phase MR imaging. *Radiology.* 2009;250(1):130-136.
96. Springer F, Machann J, Claussen CD, Schick F, Schwenzer NF. Liver fat content determined by magnetic resonance imaging and spectroscopy. *World J Gastroenterol.* 2010;16(13):1560-1566.
97. Singh S, Venkatesh SK, Wang Z, et al. Diagnostic performance of magnetic resonance elastography in staging liver fibrosis: a systematic review and meta-analysis of individual participant data. *Clin Gastroenterol Hepatol.* 2015;13(3):440-451.e446.
98. Marra F, Svegliati-Baroni G. Lipotoxicity and the gut-liver axis in NASH pathogenesis. *J Hepatol.* 2018;68(2):280-295.
99. Donnelly KL, Smith CI, Schwarzenberg SJ, Jessurun J, Boldt MD, Parks EJ. Sources of fatty acids stored in liver and secreted via lipoproteins in patients with nonalcoholic fatty liver disease. *The Journal of Clinical Investigation.* 2005;115(5):1343-1351.
100. Hudgins LC, Hellerstein MK, Seidman CE, Neese RA, Tremaroli JD, Hirsch J. Relationship between carbohydrate-induced hypertriglyceridemia and fatty acid synthesis in lean and obese subjects. *Journal of Lipid Research.* 2000;41(4):595-604.
101. Parks EJ. Dietary carbohydrate's effects on lipogenesis and the relationship of lipogenesis to blood insulin and glucose concentrations. *British Journal of Nutrition.* 2002;87(S2):S247-S253.
102. Ferramosca A, Zara V. Modulation of hepatic steatosis by dietary fatty acids. *World J Gastroenterol.* 2014;20(7):1746-1755.
103. Nolan CJ, Ruderman NB, Kahn SE, Pedersen O, Prentki M. Insulin Resistance as a Physiological Defense Against Metabolic Stress: Implications for the Management of Subsets of Type 2 Diabetes. *Diabetes.* 2015;64(3):673-686.
104. Tilg H, Hotamisligil GS. Nonalcoholic fatty liver disease: Cytokine-adipokine interplay and regulation of insulin resistance. *Gastroenterology.* 2006;131(3):934-945.
105. Ameer F, Scandiuzzi L, Hasnain S, Kalbacher H, Zaidi N. De novo lipogenesis in health and disease. *Metabolism.* 2014;63(7):895-902.

106. Strable MS, Ntambi JM. Genetic control of de novo lipogenesis: role in diet-induced obesity. *Critical Reviews in Biochemistry and Molecular Biology.* 2010;45(3):199-214.
107. Postic C, Girard J. Contribution of de novo fatty acid synthesis to hepatic steatosis and insulin resistance: lessons from genetically engineered mice. *The Journal of Clinical Investigation.* 2008;118(3):829-838.
108. Ip E, Farrell GC, Robertson G, Hall P, Kirsch R, Leclercq I. Central role of PPARalpha-dependent hepatic lipid turnover in dietary steatohepatitis in mice. *Hepatology.* 2003;38(1):123-132.
109. Xu A, Wang Y, Keshaw H, Xu LY, Lam KS, Cooper GJ. The fat-derived hormone adiponectin alleviates alcoholic and nonalcoholic fatty liver diseases in mice. *J Clin Invest.* 2003;112(1):91-100.
110. Fujita K, Nozaki Y, Wada K, et al. Dysfunctional very-low-density lipoprotein synthesis and release is a key factor in nonalcoholic steatohepatitis pathogenesis. *Hepatology.* 2009;50(3):772-780.
111. Musso G, Gambino R, De Michieli F, et al. Dietary habits and their relations to insulin resistance and postprandial lipemia in nonalcoholic steatohepatitis. *Hepatology.* 2003;37(4):909-916.
112. Schuster S, Cabrera D, Arrese M, Feldstein AE. Triggering and resolution of inflammation in NASH. *Nature Reviews Gastroenterology & Hepatology.* 2018;15(6):349-364.
113. Farrell GC, van Rooyen D, Gan L, Chitturi S. NASH is an Inflammatory Disorder: Pathogenic, Prognostic and Therapeutic Implications. *Gut Liver.* 2012;6(2):149-171.
114. Arrese M, Cabrera D, Kalergis AM, Feldstein AE. Innate Immunity and Inflammation in NAFLD/NASH. *Digestive Diseases and Sciences.* 2016;61(5):1294-1303.
115. Bieghs V, Trautwein C. Innate immune signaling and gut-liver interactions in non-alcoholic fatty liver disease. *Hepatobiliary Surg Nutr.* 2014;3(6):377-385.
116. Alegre F, Pelegrin P, Feldstein AE. Inflammasomes in Liver Fibrosis. *Semin Liver Dis.* 2017;37(2):119-127.
117. Tosello-Trampont AC, Landes SG, Nguyen V, Novobrantseva TI, Hahn YS. Kuppfer cells trigger nonalcoholic steatohepatitis development in diet-induced mouse model through tumor necrosis factor-α production. *J Biol Chem.* 2012;287(48):40161-40172.
118. Wree A, Broderick L, Canbay A, Hoffman HM, Feldstein AE. From NAFLD to NASH to cirrhosis-new insights into disease mechanisms. *Nat Rev Gastroenterol Hepatol.* 2013;10(11):627-636.
119. Neuschwander-Tetri BA. Hepatic lipotoxicity and the pathogenesis of nonalcoholic steatohepatitis: the central role of nontriglyceride fatty acid metabolites. *Hepatology.* 2010;52(2):774-788.
120. Magee N, Zou A, Zhang Y. Pathogenesis of Nonalcoholic Steatohepatitis: Interactions between Liver Parenchymal and Nonparenchymal Cells. *Biomed Res Int.* 2016;2016:5170402.
121. Ikura Y, Ohsawa M, Suekane T, et al. Localization of oxidized phosphatidylcholine in nonalcoholic fatty liver disease: impact on disease progression. *Hepatology.* 2006;43(3):506-514.
122. Dunning S, Hannivoort RA, De Boer JF, Buist-Homan M, Faber KN, Moshage H. Superoxide anions and hydrogen peroxide inhibit proliferation of activated

rat stellate cells and induce different modes of cell death. *Liver International.* 2009;29(6):922-932.
123. Zhan SS, Jiang JX, Wu J, et al. Phagocytosis of apoptotic bodies by hepatic stellate cells induces NADPH oxidase and is associated with liver fibrosis in vivo. *Hepatology.* 2006;43(3):435-443.
124. Puri P, Mirshahi F, Cheung O, et al. Activation and dysregulation of the unfolded protein response in nonalcoholic fatty liver disease. *Gastroenterology.* 2008;134(2):568-576.
125. Videla LA, Tapia G, Rodrigo R, et al. Liver NF-kappaB and AP-1 DNA binding in obese patients. *Obesity (Silver Spring).* 2009;17(5):973-979.
126. Brenner DA, Seki E, Taura K, et al. Non-alcoholic steatohepatitis-induced fibrosis: Toll-like receptors, reactive oxygen species and Jun N-terminal kinase. *Hepatol Res.* 2011;41(7):683-686.
127. Crespo J, Cayón A, Fernández-Gil P, et al. Gene expression of tumor necrosis factor α and TNF-receptors, p55 and p75, in nonalcoholic steatohepatitis patients. *Hepatology.* 2001;34(6):1158-1163.
128. Ruan H, Miles PD, Ladd CM, et al. Profiling gene transcription in vivo reveals adipose tissue as an immediate target of tumor necrosis factor-alpha: implications for insulin resistance. *Diabetes.* 2002;51(11):3176-3188.
129. Musso G, Gambino R, De Michieli F, Durazzo M, Pagano G, Cassader M. Adiponectin gene polymorphisms modulate acute adiponectin response to dietary fat: Possible pathogenetic role in NASH. *Hepatology.* 2008;47(4):1167-1177.
130. Marra F, Aleffi S, Bertolani C, Petrai I, Vizzutti F. Adipokines and liver fibrosis. *Eur Rev Med Pharmacol Sci.* 2005;9(5):279-284.
131. Kolodziejczyk AA, Zheng D, Shibolet O, Elinav E. The role of the microbiome in NAFLD and NASH. *EMBO Molecular Medicine.* 2019;11(2):e9302.
132. Friedman SL. Mechanisms of disease: Mechanisms of hepatic fibrosis and therapeutic implications. *Nat Clin Pract Gastroenterol Hepatol.* 2004;1(2):98-105.
133. Lee UE, Friedman SL. Mechanisms of hepatic fibrogenesis. *Best Practice & Research Clinical Gastroenterology.* 2011;25(2):195-206.
134. Friedman SL. Evolving challenges in hepatic fibrosis. *Nature Reviews Gastroenterology & Hepatology.* 2010;7(8):425-436.
135. Gressner AM, Weiskirchen R, Breitkopf K, Dooley S. Roles of TGF-beta in hepatic fibrosis. *Frontiers in Bioscience-Landmark.* 2002;7(4):793-807.
136. Shek FW, Benyon RC. How can transforming growth factor beta be targeted usefully to combat liver fibrosis? *European journal of gastroenterology & hepatology.* 2004;16(2):123-126.
137. Heldin CH, Miyazono K, ten Dijke P. TGF-beta signalling from cell membrane to nucleus through SMAD proteins. *Nature.* 1997;390(6659):465-471.
138. Breitkopf K, Godoy P, Ciuclan L, Singer MV, Dooley S. TGF-beta/Smad signaling in the injured liver. *Z Gastroenterol.* 2006;44(1):57-66.
139. Yang L, Pang Y, Moses HL. TGF-beta and immune cells: an important regulatory axis in the tumor microenvironment and progression. *Trends Immunol.* 2010;31(6):220-227.
140. de Winter P, Leoni P, Abraham D. Connective tissue growth factor: structure-function relationships of a mosaic, multifunctional protein. *Growth factors.* 2008;26(2):80-91.

141. Arnott JA, Lambi AG, Mundy C, et al. The role of connective tissue growth factor (CTGF/CCN2) in skeletogenesis. *Critical reviews in eukaryotic gene expression.* 2011;21(1):43-69.
142. Abreu JG, Ketpura NI, Reversade B, De Robertis EM. Connective-tissue growth factor (CTGF) modulates cell signalling by BMP and TGF-beta. *Nature cell biology.* 2002;4(8):599-604.
143. Wahab NA, Weston BS, Mason RM. Modulation of the TGFbeta/Smad signaling pathway in mesangial cells by CTGF/CCN2. *Experimental cell research.* 2005;307(2):305-314.
144. Ren J, Wang X, Parry SN, et al. Targeting CCN2 protects against progressive non-alcoholic steatohepatitis in a preclinical model induced by high-fat feeding and type 2 diabetes. *Journal of Cell Communication and Signaling.* 2022;16(3):447-460.
145. Lo L, McLennan SV, Williams PF, et al. Diabetes is a progression factor for hepatic fibrosis in a high fat fed mouse obesity model of non-alcoholic steatohepatitis. *J Hepatol.* 2011;55(2):435-444.
146. Pinzani M, Gesualdo L, Sabbah GM, Abboud HE. Effects of platelet-derived growth factor and other polypeptide mitogens on DNA synthesis and growth of cultured rat liver fat-storing cells. *J Clin Invest.* 1989;84(6):1786-1793.
147. Wong L, Yamasaki G, Johnson RJ, Friedman SL. Induction of beta-platelet-derived growth factor receptor in rat hepatic lipocytes during cellular activation in vivo and in culture. *J Clin Invest.* 1994;94(4):1563-1569.
148. Pinzani M, Gentilini A, Caligiuri A, et al. Transforming growth factor-beta 1 regulates platelet-derived growth factor receptor beta subunit in human liver fat-storing cells. *Hepatology.* 1995;21(1):232-239.
149. Borkham-Kamphorst E, van Roeyen CR, Ostendorf T, Floege J, Gressner AM, Weiskirchen R. Pro-fibrogenic potential of PDGF-D in liver fibrosis. *J Hepatol.* 2007;46(6):1064-1074.
150. Gentilini A, Marra F, Gentilini P, Pinzani M. Phosphatidylinositol-3 kinase and extracellular signal-regulated kinase mediate the chemotactic and mitogenic effects of insulin-like growth factor-I in human hepatic stellate cells. *J Hepatol.* 2000;32(2):227-234.
151. Pinzani M, Marra F, Carloni V. Signal transduction in hepatic stellate cells. *Liver.* 1998;18(1):2-13.
152. Pages G, Lenormand P, L'Allemain G, Chambard JC, Meloche S, Pouyssegur J. Mitogen-activated protein kinases p42mapk and p44mapk are required for fibroblast proliferation. *Proceedings of the National Academy of Sciences of the United States of America.* 1993;90(18):8319-8323.
153. Marra F, Arrighi MC, Fazi M, et al. Extracellular signal-regulated kinase activation differentially regulates platelet-derived growth factor's actions in hepatic stellate cells, and is induced by in vivo liver injury in the rat. *Hepatology.* 1999;30(4):951-958.
154. Dent P, Yacoub A, Fisher PB, Hagan MP, Grant S. MAPK pathways in radiation responses. *Oncogene.* 2003;22(37):5885-5896.
155. Derijard B, Raingeaud J, Barrett T, et al. Independent human MAP-kinase signal transduction pathways defined by MEK and MKK isoforms. *Science.* 1995;267(5198):682-685.
156. Tournier C, Whitmarsh AJ, Cavanagh J, Barrett T, Davis RJ. Mitogen-activated protein kinase kinase 7 is an activator of the c-Jun NH2-terminal kinase.

Proceedings of the National Academy of Sciences of the United States of America. 1997;94(14):7337-7342.
157. Schnabl B, Bradham CA, Bennett BL, Manning AM, Stefanovic B, Brenner DA. TAK1/JNK and p38 have opposite effects on rat hepatic stellate cells. *Hepatology.* 2001;34(5):953-963.
158. Ono K, Han J. The p38 signal transduction pathway: activation and function. *Cellular signalling.* 2000;12(1):1-13.
159. Herlaar E, Brown Z. p38 MAPK signalling cascades in inflammatory disease. *Molecular medicine today.* 1999;5(10):439-447.
160. Lavoie JN, L'Allemain G, Brunet A, Muller R, Pouyssegur J. Cyclin D1 expression is regulated positively by the p42/p44MAPK and negatively by the p38/HOGMAPK pathway. *J Biol Chem.* 1996;271(34):20608-20616.
161. Schwabe RF, Bataller R, Brenner DA. Human hepatic stellate cells express CCR5 and RANTES to induce proliferation and migration. *American journal of physiology Gastrointestinal and liver physiology.* 2003;285(5):G949-958.
162. Wasmuth HE, Lammert F, Zaldivar MM, et al. Antifibrotic effects of CXCL9 and its receptor CXCR3 in livers of mice and humans. *Gastroenterology.* 2009;137(1):309-319, 319.e301-303.
163. Marra F, Bertolani C. Adipokines in liver diseases. *Hepatology.* 2009;50(3):957-969.
164. Ikejima K, Okumura K, Kon K, Takei Y, Sato N. Role of adipocytokines in hepatic fibrogenesis. *J Gastroenterol Hepatol.* 2007;22 Suppl 1:S87-92.
165. Leclercq IA, Farrell GC, Schriemer R, Robertson GR. Leptin is essential for the hepatic fibrogenic response to chronic liver injury. *J Hepatol.* 2002;37(2):206-213.
166. Wedemeyer I, Bechmann LP, Odenthal M, et al. Adiponectin inhibits steatotic CD95/Fas up-regulation by hepatocytes: therapeutic implications for hepatitis C. *J Hepatol.* 2009;50(1):140-149.
167. Malhi H, Gores GJ. Cellular and molecular mechanisms of liver injury. *Gastroenterology.* 2008;134(6):1641-1654.
168. Sohail MA, Hashmi AZ, Hakim W, et al. Adenosine induces loss of actin stress fibers and inhibits contraction in hepatic stellate cells via Rho inhibition. *Hepatology.* 2009;49(1):185-194.
169. Ray K. Liver: Activation of NF-kappaB signaling in hepatocytes induces liver fibrosis. *Nat Rev Gastroenterol Hepatol.* 2012;9(5):244.
170. Bedossa P, Paradis V. Liver extracellular matrix in health and disease. *The Journal of pathology.* 2003;200(4):504-515.
171. Roeb E. Matrix metalloproteinases and liver fibrosis (translational aspects). *Matrix Biology.* 2018;68-69:463-473.
172. Hemmann S, Graf J, Roderfeld M, Roeb E. Expression of MMPs and TIMPs in liver fibrosis – a systematic review with special emphasis on anti-fibrotic strategies. *Journal of Hepatology.* 2007;46(5):955-975.
173. Yoshiji H, Kuriyama S, Yoshii J, et al. Tissue inhibitor of metalloproteinases-1 attenuates spontaneous liver fibrosis resolution in the transgenic mouse. *Hepatology.* 2002;36(4 Pt 1):850-860.
174. Murphy FR, Issa R, Zhou X, et al. Inhibition of apoptosis of activated hepatic stellate cells by tissue inhibitor of metalloproteinase-1 is mediated via effects on matrix metalloproteinase inhibition: implications for reversibility of liver fibrosis. *J Biol Chem.* 2002;277(13):11069-11076.

175. Musso G, Cassader M, Rosina F, Gambino R. Impact of current treatments on liver disease, glucose metabolism and cardiovascular risk in non-alcoholic fatty liver disease (NAFLD): a systematic review and meta-analysis of randomised trials. *Diabetologia.* 2012;55(4):885-904.
176. Hallsworth K, Adams LA. Lifestyle modification in NAFLD/NASH: Facts and figures. *JHEP Rep.* 2019;1(6):468-479.
177. Lassailly G, Caiazzo R, Buob D, et al. Bariatric Surgery Reduces Features of Nonalcoholic Steatohepatitis in Morbidly Obese Patients. *Gastroenterology.* 2015;149(2):379-388.
178. Lassailly G, Caiazzo R, Ntandja-Wandji L-C, et al. Bariatric Surgery Provides Long-term Resolution of Nonalcoholic Steatohepatitis and Regression of Fibrosis. *Gastroenterology.* 2020;159(4):1290-1301.e1295.
179. Chavez-Tapia NC, Tellez-Avila FI, Barrientos-Gutierrez T, Mendez-Sanchez N, Lizardi-Cervera J, Uribe M. Bariatric surgery for non-alcoholic steatohepatitis in obese patients. *Cochrane Database of Systematic Reviews.* 2010(1).
180. Pais R, Aron-Wisnewsky J, Bedossa P, et al. Persistence of severe liver fibrosis despite substantial weight loss with bariatric surgery. *Hepatology.* 2022;76(2):456-468.
181. Mullish BH. Further Insights Into the Impact of Bariatric Surgery on the Progression of Nonalcoholic Fatty Liver Disease. *Gastroenterology.* 2022;163(2):528-529.
182. Sanyal AJ, Chalasani N, Kowdley KV, et al. Pioglitazone, vitamin E, or placebo for nonalcoholic steatohepatitis. *N Engl J Med.* 2010;362(18):1675-1685.
183. Musso G, Gambino R, Cassader M, Pagano G. A meta-analysis of randomized trials for the treatment of nonalcoholic fatty liver disease. *Hepatology.* 2010;52(1):79-104.
184. Tiniakos DG, Anstee QM, Burt AD. Fatty Liver Disease. In: Burt ADBMMDFFFFF, Ferrell LDMD, Hübscher SGMF, eds. *MacSween's Pathology of the Liver.*2018:308-371.
185. Boettcher E, Csako G, Pucino F, Wesley R, Loomba R. Meta-analysis: pioglitazone improves liver histology and fibrosis in patients with non-alcoholic steatohepatitis. *Aliment Pharmacol Ther.* 2012;35(1):66-75.
186. Albhaisi SAM, Sanyal AJ. New drugs for NASH. *Liver International.* 2021;41(S1):112-118.
187. Ekstedt M, Franzén LE, Holmqvist M, et al. Alcohol consumption is associated with progression of hepatic fibrosis in non-alcoholic fatty liver disease. *Scand J Gastroenterol.* 2009;44(3):366-374.
188. Dai W, Ye L, Liu A, et al. Prevalence of nonalcoholic fatty liver disease in patients with type 2 diabetes mellitus: A meta-analysis. *Medicine.* 2017;96(39):e8179-e8179.
189. Hossain N, Afendy A, Stepanova M, et al. Independent Predictors of Fibrosis in Patients With Nonalcoholic Fatty Liver Disease. *Clinical Gastroenterology and Hepatology.* 2009;7(11):1224-1229.e1222.
190. Adams LA, Angulo P. Recent concepts in non-alcoholic fatty liver disease. *Diabetic Medicine.* 2005;22(9):1129-1133.
191. Day CP, James OFW. Steatohepatitis: A tale of two “hits”? *Gastroenterology.* 1998;114(4):842-845.
192. Ali R, Cusi K. New diagnostic and treatment approaches in non-alcoholic fatty liver disease (NAFLD). *Annals of Medicine.* 2009;41(4):265-278.

193. Shimomura I, Bashmakov Y, Horton JD. Increased levels of nuclear SREBP-1c associated with fatty livers in two mouse models of diabetes mellitus. *J Biol Chem.* 1999;274(42):30028-30032.
194. Bril F, McPhaul MJ, Caulfield MP, et al. Performance of Plasma Biomarkers and Diagnostic Panels for Nonalcoholic Steatohepatitis and Advanced Fibrosis in Patients With Type 2 Diabetes. *Diabetes Care.* 2020;43(2):290-297.
195. Gracen L, Hayward KL, Irvine KM, Valery PC, Powell EE. Low accuracy of FIB-4 test to identify people with diabetes at low risk of advanced fibrosis. *Journal of Hepatology.* 2022;77(4):1219-1221.
196. Barb D, Repetto EM, Stokes ME, Shankar SS, Cusi K. Type 2 diabetes mellitus increases the risk of hepatic fibrosis in individuals with obesity and nonalcoholic fatty liver disease. *Obesity (Silver Spring).* 2021;29(11):1950-1960.
197. Boursier J, Hagström H, Ekstedt M, et al. Non-invasive tests accurately stratify patients with NAFLD based on their risk of liver-related events. *Journal of Hepatology.* 2022;76(5):1013-1020.
198. Pina A, Meneses MJ, Ribeiro RT, Raposo JF, Macedo MP. Fibrosis nonalcoholic steatohepatitis index validation and applicability considering glycaemic severity and T2D duration. *Liver Int.* 2022;42(11):2577-2580.
199. European Association for the Study of the L, European Association for the Study of D, European Association for the Study of O. EASL–EASD–EASO Clinical Practice Guidelines for the management of non-alcoholic fatty liver disease. *Diabetologia.* 2016;59(6):1121-1140.
200. American Diabetes Association. 4. Comprehensive Medical Evaluation and Assessment of Comorbidities: Standards of Medical Care in Diabetes—2019. *Diabetes Care.* 2018;42(Supplement_1):S34-S45.
201. Cusi K, Isaacs S, Barb D, et al. American Association of Clinical Endocrinology Clinical Practice Guideline for the Diagnosis and Management of Nonalcoholic Fatty Liver Disease in Primary Care and Endocrinology Clinical Settings: Co-Sponsored by the American Association for the Study of Liver Diseases (AASLD). *Endocrine Practice.* 2022;28(5):528-562.
202. Armstrong MJ, Gaunt P, Aithal GP, et al. Liraglutide safety and efficacy in patients with non-alcoholic steatohepatitis (LEAN): a multicentre, double-blind, randomised, placebo-controlled phase 2 study. *The Lancet.* 2016;387(10019):679-690.
203. Kuchay MS, Krishan S, Mishra SK, et al. Effect of dulaglutide on liver fat in patients with type 2 diabetes and NAFLD: randomised controlled trial (D-LIFT trial). *Diabetologia.* 2020;63(11):2434-2445.
204. Newsome PN, Buchholtz K, Cusi K, et al. A Placebo-Controlled Trial of Subcutaneous Semaglutide in Nonalcoholic Steatohepatitis. *New England Journal of Medicine.* 2020;384(12):1113-1124.
205. ClinicalTrials.gov. Research Study on Whether Semaglutide Works in People With Non-alcoholic Steatohepatitis (NASH) (ESSENCE) (NTC04822181). https://clinicaltrials.gov/ct2/show/NCT04822181. Accessed 28/10/2022.
206. Shimizu M, Suzuki K, Kato K, et al. Evaluation of the effects of dapagliflozin, a sodium-glucose co-transporter-2 inhibitor, on hepatic steatosis and fibrosis using transient elastography in patients with type 2 diabetes and non-alcoholic fatty liver disease. *Diabetes Obes Metab.* 2019;21(2):285-292.
207. Kuchay MS, Krishan S, Mishra SK, et al. Effect of Empagliflozin on Liver Fat in Patients With Type 2 Diabetes and Nonalcoholic Fatty Liver Disease: A

Randomized Controlled Trial (E-LIFT Trial). *Diabetes Care.* 2018;41(8):1801-1808.
208. Lai L-L, Vethakkan SR, Nik Mustapha NR, Mahadeva S, Chan W-K. Empagliflozin for the Treatment of Nonalcoholic Steatohepatitis in Patients with Type 2 Diabetes Mellitus. *Digestive Diseases and Sciences.* 2020;65(2):623-631.
209. Hartman ML, Sanyal AJ, Loomba R, et al. Effects of Novel Dual GIP and GLP-1 Receptor Agonist Tirzepatide on Biomarkers of Nonalcoholic Steatohepatitis in Patients With Type 2 Diabetes. *Diabetes Care.* 2020;43(6):1352-1355.
210. ClinicalTrials.gov. A Study of Tirzepatide (LY3298176) in Participants With Nonalcoholic Steatohepatitis (NASH) (SYNERGY-NASH) (NTC04166773). https://clinicaltrials.gov/ct2/show/NCT04166773. Accessed 28/10/2022.
211. Haczeyni F, Yeh MM, Ioannou GN, et al. Mouse models of non-alcoholic steatohepatitis: A reflection on recent literature. *Journal of Gastroenterology and Hepatology.* 2018;33(7):1312-1320.
212. Farrell G, Schattenberg JM, Leclercq I, et al. Mouse Models of Nonalcoholic Steatohepatitis: Toward Optimization of Their Relevance to Human Nonalcoholic Steatohepatitis. *Hepatology.* 2019;69(5):2241-2257.
213. Ipsen DH, Lykkesfeldt J, Tveden-Nyborg P. Animal Models of Fibrosis in Nonalcoholic Steatohepatitis: Do They Reflect Human Disease? *Advances in Nutrition.* 2020;11(6):1696-1711.
214. Marí M, Caballero F, Colell A, et al. Mitochondrial free cholesterol loading sensitizes to TNF- and Fas-mediated steatohepatitis. *Cell Metab.* 2006;4(3):185-198.
215. Ioannou GN. The Role of Cholesterol in the Pathogenesis of NASH. *Trends in Endocrinology & Metabolism.* 2016;27(2):84-95.
216. Ginsberg HN. Is the slippery slope from steatosis to steatohepatitis paved with triglyceride or cholesterol? *Cell Metab.* 2006;4(3):179-181.
217. Matsuzawa N, Takamura T, Kurita S, et al. Lipid-induced oxidative stress causes steatohepatitis in mice fed an atherogenic diet. *Hepatology.* 2007;46(5):1392-1403.
218. Charlton M, Krishnan A, Viker K, et al. Fast food diet mouse: novel small animal model of NASH with ballooning, progressive fibrosis, and high physiological fidelity to the human condition. *American Journal of Physiology-Gastrointestinal and Liver Physiology.* 2011;301(5):G825-G834.
219. Asgharpour A, Cazanave SC, Pacana T, et al. A diet-induced animal model of non-alcoholic fatty liver disease and hepatocellular cancer. *J Hepatol.* 2016;65(3):579-588.
220. Nakae D, Mizumoto Y, Andoh N, et al. Comparative changes in the liver of female Fischer-344 rats after short-term feeding of a semipurified or a semisynthetic L-amino acid-defined choline-deficient diet. *Toxicol Pathol.* 1995;23(5):583-590.
221. Nakae D, Yoshiji H, Maruyama H, Kinugasa T, Denda A, Konishi Y. Production of both 8-hydroxydeoxyguanosine in liver DNA and gamma-glutamyltransferase-positive hepatocellular lesions in rats given a choline-deficient, L-amino acid-defined diet. *Jpn J Cancer Res.* 1990;81(11):1081-1084.
222. Kodama Y, Kisseleva T, Iwaisako K, et al. c-Jun N-terminal Kinase-1 From Hematopoietic Cells Mediates Progression From Hepatic Steatosis to

Steatohepatitis and Fibrosis in Mice. *Gastroenterology.* 2009;137(4):1467-1477.e1465.
223. Min-DeBartolo J, Schlerman F, Akare S, et al. Thrombospondin-I is a critical modulator in non-alcoholic steatohepatitis (NASH). *PLOS ONE.* 2020;14(12):e0226854.
224. Abe N, Kato S, Tsuchida T, et al. Longitudinal characterization of diet-induced genetic murine models of non-alcoholic steatohepatitis with metabolic, histological, and transcriptomic hallmarks of human patients. *Biol Open.* 2019;8(5).
225. Weber LW, Boll M, Stampfl A. Hepatotoxicity and mechanism of action of haloalkanes: carbon tetrachloride as a toxicological model. *Critical reviews in toxicology.* 2003;33(2):105-136.
226. Oh Y, Park O, Swierczewska M, et al. Systemic PEGylated TRAIL treatment ameliorates liver cirrhosis in rats by eliminating activated hepatic stellate cells. *Hepatology.* 2016;64(1):209-223.
227. Liu F, Chen L, Rao HY, et al. Automated evaluation of liver fibrosis in thioacetamide, carbon tetrachloride, and bile duct ligation rodent models using second-harmonic generation/two-photon excited fluorescence microscopy. *Lab Invest.* 2017;97(1):84-92.
228. Tsuchida T, Lee YA, Fujiwara N, et al. A simple diet- and chemical-induced murine NASH model with rapid progression of steatohepatitis, fibrosis and liver cancer. *J Hepatol.* 2018;69(2):385-395.
229. Tolba R, Kraus T, Liedtke C, Schwarz M, Weiskirchen R. Diethylnitrosamine (DEN)-induced carcinogenic liver injury in mice. *Laboratory Animals.* 2015;49(1_suppl):59-69.
230. Bolzán AD, Bianchi MS. Genotoxicity of streptozotocin. *Mutat Res.* 2002;512(2-3):121-134.
231. Laguens R, Candela S, Hernandez R, Gagliardino J. Streptozotocin-induced liver damage in mice. *Hormone and Metabolic Research.* 1980;12(05):197-201.
232. Radenković M, Stojanović M, Prostran M. Experimental diabetes induced by alloxan and streptozotocin: The current state of the art. *Journal of Pharmacological and Toxicological Methods.* 2016;78:13-31.
233. King AJ. The use of animal models in diabetes research. *Br J Pharmacol.* 2012;166(3):877-894.
234. Saito T, Muramatsu M, Ishii Y, et al. Pathophysiological analysis of the progression of hepatic lesions in STAM mice. *Physiological research.* 2017;66 5:791-799.
235. Larter CZ, Yeh MM. Animal models of NASH: getting both pathology and metabolic context right. *J Gastroenterol Hepatol.* 2008;23(11):1635-1648.
236. Trak-Smayra V, Paradis V, Massart J, Nasser S, Jebara V, Fromenty B. Pathology of the liver in obese and diabetic ob/ob and db/db mice fed a standard or high-calorie diet. *Int J Exp Pathol.* 2011;92(6):413-421.
237. Okumura K, Ikejima K, Kon K, et al. Exacerbation of dietary steatohepatitis and fibrosis in obese, diabetic KK-A(y) mice. *Hepatol Res.* 2006;36(3):217-228.
238. Farooqi IS, Keogh JM, Yeo GS, Lank EJ, Cheetham T, O'Rahilly S. Clinical spectrum of obesity and mutations in the melanocortin 4 receptor gene. *New England Journal of Medicine.* 2003;348(12):1085-1095.
239. Itoh M, Suganami T, Nakagawa N, et al. Melanocortin 4 receptor-deficient mice as a novel mouse model of nonalcoholic steatohepatitis. *Am J Pathol.* 2011;179(5):2454-2463.

240. Brigstock DR. The CCN family: a new stimulus package. *J Endocrinol.* 2003;178(2):169-175.
241. Bork P. The modular architecture of a new family of growth regulators related to connective tissue growth factor. *FEBS Lett.* 1993;327(2):125-130.
242. Pennica D, Swanson TA, Welsh JW, et al. WISP genes are members of the connective tissue growth factor family that are up-regulated in wnt-1-transformed cells and aberrantly expressed in human colon tumors. *Proceedings of the National Academy of Sciences of the United States of America.* 1998;95(25):14717-14722.
243. Perbal B, Tweedie S, Bruford E. The official unified nomenclature adopted by the HGNC calls for the use of the acronyms, CCN1–6, and discontinuation in the use of CYR61, CTGF, NOV and WISP 1–3 respectively. *Journal of Cell Communication and Signaling.* 2018;12(4):625-629.
244. Krupska I, Bruford EA, Chaqour B. Eyeing the Cyr61/CTGF/NOV (CCN) group of genes in development and diseases: highlights of their structural likenesses and functional dissimilarities. *Human Genomics.* 2015;9(1):24.
245. Holbourn KP, Acharya KR, Perbal B. The CCN family of proteins: structure–function relationships. *Trends in Biochemical Sciences.* 2008;33(10):461-473.
246. Lau LF. CCN1/CYR61: the very model of a modern matricellular protein. *Cellular and Molecular Life Sciences.* 2011;68(19):3149.
247. Kim HS, Nagalla SR, Oh Y, Wilson E, Roberts CT, Jr., Rosenfeld RG. Identification of a family of low-affinity insulin-like growth factor binding proteins (IGFBPs): characterization of connective tissue growth factor as a member of the IGFBP superfamily. *Proceedings of the National Academy of Sciences of the United States of America.* 1997;94(24):12981-12986.
248. Zhang J-L, Huang Y, Qiu L-Y, Nickel J, Sebald W. von Willebrand Factor Type C Domain-containing Proteins Regulate Bone Morphogenetic Protein Signaling through Different Recognition Mechanisms *. *J Biol Chem.* 2007;282(27):20002-20014.
249. Tucker RP. The thrombospondin type 1 repeat superfamily. *Int J Biochem Cell Biol.* 2004;36(6):969-974.
250. Chen H, Herndon ME, Lawler J. The cell biology of thrombospondin-1. *Matrix biology : journal of the International Society for Matrix Biology.* 2000;19(7):597-614.
251. Perbal B. CCN proteins: multifunctional signalling regulators. *The Lancet.* 2004;363(9402):62-64.
252. Jun J-I, Lau LF. Taking aim at the extracellular matrix: CCN proteins as emerging therapeutic targets. *Nature Reviews Drug Discovery.* 2011;10(12):945-963.
253. Leask A, Abraham DJ. All in the CCN family: essential matricellular signaling modulators emerge from the bunker. *Journal of Cell Science.* 2006;119(23):4803-4810.
254. Segarini PR, Nesbitt JE, Li D, Hays LG, Yates JR, 3rd, Carmichael DF. The low density lipoprotein receptor-related protein/alpha2-macroglobulin receptor is a receptor for connective tissue growth factor. *J Biol Chem.* 2001;276(44):40659-40667.
255. Gao R, Brigstock DR. Low density lipoprotein receptor-related protein (LRP) is a heparin-dependent adhesion receptor for connective tissue growth factor (CTGF) in rat activated hepatic stellate cells. *Hepatol Res.* 2003;27(3):214-220.

256. Mercurio S, Latinkic B, Itasaki N, Krumlauf R, Smith JC. Connective-tissue growth factor modulates WNT signalling and interacts with the WNT receptor complex. *Development.* 2004;131(9):2137-2147.
257. Wahab NA, Weston BS, Mason RM. Connective Tissue Growth Factor CCN2 Interacts with and Activates the Tyrosine Kinase Receptor TrkA. *Journal of the American Society of Nephrology.* 2005;16(2):340-351.
258. Inoki I, Shiomi T, Hashimoto G, et al. Connective tissue growth factor binds vascular endothelial growth factor (VEGF) and inhibits VEGF-induced angiogenesis. *FASEB journal : official publication of the Federation of American Societies for Experimental Biology.* 2002;16(2):219-221.
259. Chen C-C, Lau LF. Functions and mechanisms of action of CCN matricellular proteins. *The International Journal of Biochemistry & Cell Biology.* 2009;41(4):771-783.
260. Kular L, Pakradouni J, Kitabgi P, Laurent M, Martinerie C. The CCN family: A new class of inflammation modulators? *Biochimie.* 2011;93(3):377-388.
261. Sun C, Zhang H, Liu X. Emerging role of CCN family proteins in fibrosis. *Journal of Cellular Physiology.* 2021;236(6):4195-4206.
262. Jun JI, Lau LF. The matricellular protein CCN1 induces fibroblast senescence and restricts fibrosis in cutaneous wound healing. *Nature cell biology.* 2010;12(7):676-685.
263. Kyriakides TR, Bornstein P. Matricellular proteins as modulators of wound healing and the foreign body response. *Thrombosis and haemostasis.* 2003;90(6):986-992.
264. Bornstein P. Diversity of function is inherent in matricellular proteins: an appraisal of thrombospondin 1. *The Journal of cell biology.* 1995;130(3):503-506.
265. Jun JI, Lau LF. Cellular senescence controls fibrosis in wound healing. *Aging.* 2010;2(9):627-631.
266. Lau LF. CCN1/CYR61: the very model of a modern matricellular protein. *Cell Mol Life Sci.* 2011;68(19):3149-3163.
267. Paradis V, Dargere D, Vidaud M, et al. Expression of connective tissue growth factor in experimental rat and human liver fibrosis. *Hepatology.* 1999;30(4):968-976.
268. Abou-Shady M, Friess H, Zimmermann A, et al. Connective tissue growth factor in human liver cirrhosis. *Liver.* 2000;20(4):296-304.
269. Williams EJ, Gaça MD, Brigstock DR, Arthur MJ, Benyon RC. Increased expression of connective tissue growth factor in fibrotic human liver and in activated hepatic stellate cells. *J Hepatol.* 2000;32(5):754-761.
270. Riser BL, Najmabadi F, Perbal B, et al. CCN3 (NOV) is a negative regulator of CCN2 (CTGF) and a novel endogenous inhibitor of the fibrotic pathway in an in vitro model of renal disease. *Am J Pathol.* 2009;174(5):1725-1734.
271. Yoon PO, Lee MA, Cha H, et al. The opposing effects of CCN2 and CCN5 on the development of cardiac hypertrophy and fibrosis. *Journal of molecular and cellular cardiology.* 2010;49(2):294-303.
272. Twigg SM. Regulation and bioactivity of the CCN family of genes and proteins in obesity and diabetes. *J Cell Commun Signal.* 2018;12(1):359-368.
273. McLennan SV, Wang XY, Moreno V, Yue DK, Twigg SM. Connective tissue growth factor mediates high glucose effects on matrix degradation through tissue inhibitor of matrix metalloproteinase type 1: implications for diabetic nephropathy. *Endocrinology.* 2004;145(12):5646-5655.

274. Rachfal AW, Brigstock DR. Connective tissue growth factor (CTGF/CCN2) in hepatic fibrosis. *Hepatol Res.* 2003;26(1):1-9.
275. Paradis V, Perlemuter G, Bonvoust F, et al. High glucose and hyperinsulinemia stimulate connective tissue growth factor expression: a potential mechanism involved in progression to fibrosis in nonalcoholic steatohepatitis. *Hepatology.* 2001;34(4, Part 1):738-744.
276. Paradis V, Dargere D, Bonvoust F, Vidaud M, Segarini P, Bedossa P. Effects and regulation of connective tissue growth factor on hepatic stellate cells. *Lab Invest.* 2002;82(6):767-774.
277. Uchio K, Graham M, Dean NM, Rosenbaum J, Desmouliere A. Down-regulation of connective tissue growth factor and type I collagen mRNA expression by connective tissue growth factor antisense oligonucleotide during experimental liver fibrosis. *Wound repair and regeneration : official publication of the Wound Healing Society [and] the European Tissue Repair Society.* 2004;12(1):60-66.
278. Leask A. TGFbeta, cardiac fibroblasts, and the fibrotic response. *Cardiovascular research.* 2007;74(2):207-212.
279. Kisseleva T, Uchinami H, Feirt N, et al. Bone marrow-derived fibrocytes participate in pathogenesis of liver fibrosis. *J Hepatol.* 2006;45(3):429-438.
280. Strnad P, Lienau TC, Tao GZ, et al. Keratin variants associate with progression of fibrosis during chronic hepatitis C infection. *Hepatology.* 2006;43(6):1354-1363.
281. Sato S, Nagaoka T, Hasegawa M, et al. Serum levels of connective tissue growth factor are elevated in patients with systemic sclerosis: association with extent of skin sclerosis and severity of pulmonary fibrosis. *The Journal of rheumatology.* 2000;27(1):149-154.
282. Tamatani T, Kobayashi H, Tezuka K, et al. Establishment of the enzyme-linked immunosorbent assay for connective tissue growth factor (CTGF) and its detection in the sera of biliary atresia. *Biochemical and biophysical research communications.* 1998;251(3):748-752.
283. Gressner AM, Yagmur E, Lahme B, Gressner O, Stanzel S. Connective tissue growth factor in serum as a new candidate test for assessment of hepatic fibrosis. *Clinical chemistry.* 2006;52(9):1815-1817.
284. Kovalenko E, Tacke F, Gressner OA, et al. Validation of connective tissue growth factor (CTGF/CCN2) and its gene polymorphisms as noninvasive biomarkers for the assessment of liver fibrosis. *Journal of Viral Hepatitis.* 2009;16(9):612-620.
285. Piao RL, Brigstock DR, Zhu J, Zhang ML, Gao RP. Clinical significance of connective tissue growth factor in hepatitis B virus-induced hepatic fibrosis. *World J Gastroenterol.* 2012;18(18):2280-2286.
286. Kim K-H, Chen C-C, Monzon RI, Lau LF. Matricellular Protein CCN1 Promotes Regression of Liver Fibrosis through Induction of Cellular Senescence in Hepatic Myofibroblasts. *Molecular and Cellular Biology.* 2013;33(10):2078-2090.
287. Ju L, Sun Y, Xue H, et al. CCN1 promotes hepatic steatosis and inflammation in non-alcoholic steatohepatitis. *Scientific reports.* 2020;10(1):1-13.
288. Borkham-Kamphorst E, Schaffrath C, Van de Leur E, et al. The anti-fibrotic effects of CCN1/CYR61 in primary portal myofibroblasts are mediated through induction of reactive oxygen species resulting in cellular senescence, apoptosis and attenuated TGF-β signaling. *Biochimica et Biophysica Acta (BBA) - Molecular Cell Research.* 2014;1843(5):902-914.

289. Fontaine DA, Davis DB. Attention to Background Strain Is Essential for Metabolic Research: C57BL/6 and the International Knockout Mouse Consortium. *Diabetes.* 2015;65(1):25-33.
290. Kelmenson P. Cre Lox Breeding for Beginners, Part 1. In. *The JAX Blog*: The Jackson Laboratory; 2011.
291. Rossmeisl M, Rim JS, Koza RA, Kozak LP. Variation in type 2 diabetes--related traits in mouse strains susceptible to diet-induced obesity. *Diabetes.* 2003;52(8):1958-1966.
292. Surwit RS, Feinglos MN, Rodin J, et al. Differential effects of fat and sucrose on the development of obesity and diabetes in C57BL/6J and AJ mice. *Metabolism.* 1995;44(5):645-651.
293. Leiter EH. Multiple low-dose streptozotocin-induced hyperglycemia and insulitis in C57BL mice: influence of inbred background, sex, and thymus. *Proceedings of the National Academy of Sciences of the United States of America.* 1982;79(2):630-634.
294. Ayala JE, Samuel VT, Morton GJ, et al. Standard operating procedures for describing and performing metabolic tests of glucose homeostasis in mice. *Disease Models & Mechanisms.* 2010;3(9-10):525-534.
295. Singh B, Saxena A. Surrogate markers of insulin resistance: A review. *World journal of diabetes.* 2010;1(2):36-47.
296. Matthews DR, Hosker JP, Rudenski AS, Naylor BA, Treacher DF, Turner RC. Homeostasis model assessment: insulin resistance and beta-cell function from fasting plasma glucose and insulin concentrations in man. *Diabetologia.* 1985;28(7):412-419.
297. Katz A, Nambi SS, Mather K, et al. Quantitative insulin sensitivity check index: a simple, accurate method for assessing insulin sensitivity in humans. *J Clin Endocrinol Metab.* 2000;85(7):2402-2410.
298. Lee S, Muniyappa R, Yan X, et al. Comparison between surrogate indexes of insulin sensitivity and resistance and hyperinsulinemic euglycemic clamp estimates in mice. *American Journal of Physiology-Endocrinology and Metabolism.* 2008;294(2):E261-E270.
299. Mather K. Surrogate measures of insulin resistance: of rats, mice, and men. *American Journal of Physiology-Endocrinology and Metabolism.* 2009;296(2):E398-E399.
300. Tinsley FC, Taicher GZ, Heiman ML. Evaluation of a Quantitative Magnetic Resonance Method for Mouse Whole Body Composition Analysis. *Obesity Research.* 2004;12(1):150-160.
301. D'Souza JC, Sultan LR, Hunt SJ, et al. B-mode ultrasound for the assessment of hepatic fibrosis: a quantitative multiparametric analysis for a radiomics approach. *Scientific Reports.* 2019;9(1):8708.
302. Cook MJ. The Anatomy of the Laboratory Mouse: Alimentary canal removed to display lobes of the liver. http://www.informatics.jax.org/cookbook/figures/figure60.shtml. Published 1965. Accessed.
303. Szczypiński PM, Strzelecki M, Materka A, Klepaczko A. MaZda--a software package for image texture analysis. *Comput Methods Programs Biomed.* 2009;94(1):66-76.
304. Müller A, Hochrath K, Stroeder J, et al. Effects of Liver Fibrosis Progression on Tissue Relaxation Times in Different Mouse Models Assessed by Ultrahigh Field Magnetic Resonance Imaging. *Biomed Res Int.* 2017;2017:8720367.

305. Junqueira LC, Bignolas G, Brentani RR. Picrosirius staining plus polarization microscopy, a specific method for collagen detection in tissue sections. *Histochem J.* 1979;11(4):447-455.
306. Bankhead P, Loughrey MB, Fernández JA, et al. QuPath: Open source software for digital pathology image analysis. *Scientific Reports.* 2017;7(1):16878.
307. https://imagej.nih.gov/ij/docs/examples/stained-sections/index.html. Accessed 15/02/2022.
308. Cardiff RD, Miller CH, Munn RJ. Manual hematoxylin and eosin staining of mouse tissue sections. *Cold Spring Harbor Protocols.* 2014;2014(6):655-658.
309. Kleiner DE, Brunt EM, Van Natta M, et al. Design and validation of a histological scoring system for nonalcoholic fatty liver disease. *Hepatology.* 2005;41(6):1313-1321.
310. Sambrook J, Fritsch EF, Maniatis T. *Molecular cloning : a laboratory manual.* 2nd ed ed: Cold Spring Harbor Laboratory Press; 1989.
311. Pfaffl MW. A new mathematical model for relative quantification in real-time RT-PCR. *Nucleic Acids Res.* 2001;29(9):e45.
312. Kawaki H, Kubota S, Suzuki A, et al. Differential roles of CCN family proteins during osteoblast differentiation: Involvement of Smad and MAPK signaling pathways. *Bone.* 2011;49(5):975-989.
313. Adriaenssens T, Mazoyer C, Segers I, Wathlet S, Smitz J. Differences in Collagen Expression in Cumulus Cells after Exposure to Highly Purified Menotropin or Recombinant Follicle-Stimulating Hormone in a Mouse Follicle Culture Model1. *Biology of Reproduction.* 2009;80(5):1015-1025.
314. Casellas A, Salavert A, Agudo J, et al. Expression of IGF-I in pancreatic islets prevents lymphocytic infiltration and protects mice from type 1 diabetes. *Diabetes.* 2006;55(12):3246-3255.
315. Fossati P, Prencipe L. Serum triglycerides determined colorimetrically with an enzyme that produces hydrogen peroxide. *Clinical chemistry.* 1982;28(10):2077-2080.
316. McGowan MW, Artiss JD, Strandbergh DR, Zak B. A peroxidase-coupled method for the colorimetric determination of serum triglycerides. *Clinical chemistry.* 1983;29(3):538-542.
317. Williams KH, Burns K, Constantino M, et al. An association of large-fibre peripheral nerve dysfunction with non-invasive measures of liver fibrosis secondary to non-alcoholic fatty liver disease in diabetes. *J Diabetes Complications.* 2015;29(8):1240-1247.
318. Yu DM, Slaitini L, Gysbers V, et al. Soluble CD26/dipeptidyl peptidase IV enhances human lymphocyte proliferation in vitro independent of dipeptidyl peptidase enzyme activity and adenosine deaminase binding. *Scand J Immunol.* 2011;73(2):102-111.
319. Keane FM, Yao TW, Seelk S, et al. Quantitation of fibroblast activation protein (FAP)-specific protease activity in mouse, baboon and human fluids and organs. *FEBS Open Bio.* 2013;4:43-54.
320. Stefan N, Häring H-U. The Metabolically Benign and Malignant Fatty Liver. *Diabetes.* 2011;60(8):2011-2017.
321. Targher G, Day CP, Bonora E. Risk of Cardiovascular Disease in Patients with Nonalcoholic Fatty Liver Disease. *New England Journal of Medicine.* 2010;363(14):1341-1350.

322. Marengo A, Jouness RI, Bugianesi E. Progression and Natural History of Nonalcoholic Fatty Liver Disease in Adults. *Clin Liver Dis.* 2016;20(2):313-324.
323. Dulai PS, Singh S, Patel J, et al. Increased risk of mortality by fibrosis stage in nonalcoholic fatty liver disease: Systematic review and meta-analysis. *Hepatology.* 2017;65(5):1557-1565.
324. Adams LA, Anstee QM, Tilg H, Targher G. Non-alcoholic fatty liver disease and its relationship with cardiovascular disease and other extrahepatic diseases. *Gut.* 2017;66(6):1138-1153.
325. Angulo P, Hui JM, Marchesini G, et al. The NAFLD fibrosis score: A noninvasive system that identifies liver fibrosis in patients with NAFLD. *Hepatology.* 2007;45(4):846-854.
326. Sterling RK, Lissen E, Clumeck N, et al. Development of a simple noninvasive index to predict significant fibrosis in patients with HIV/HCV coinfection. *Hepatology.* 2006;43(6):1317-1325.
327. Treeprasertsuk S, Björnsson E, Enders F, Suwanwalaikorn S, Lindor KD. NAFLD fibrosis score: a prognostic predictor for mortality and liver complications among NAFLD patients. *World J Gastroenterol.* 2013;19(8):1219-1229.
328. Shah AG, Lydecker A, Murray K, Tetri BN, Contos MJ, Sanyal AJ. Comparison of noninvasive markers of fibrosis in patients with nonalcoholic fatty liver disease. *Clin Gastroenterol Hepatol.* 2009;7(10):1104-1112.
329. Chalasani N, Younossi Z, Lavine JE, et al. The diagnosis and management of nonalcoholic fatty liver disease: Practice guidance from the American Association for the Study of Liver Diseases. *Hepatology.* 2018;67(1):328-357.
330. Australian Institute of Health and Welfare. Diabetes. AIHW. https://www.aihw.gov.au/reports/diabetes/diabetes. Published 2020. Accessed 01/02/2022.
331. Castera L, Forns X, Alberti A. Non-invasive evaluation of liver fibrosis using transient elastography. *J Hepatol.* 2008;48(5):835-847.
332. Wong VW, Vergniol J, Wong GL, et al. Diagnosis of fibrosis and cirrhosis using liver stiffness measurement in nonalcoholic fatty liver disease. *Hepatology.* 2010;51(2):454-462.
333. Sterling RK, Lissen E, Clumeck N, et al. Development of a simple noninvasive index to predict significant fibrosis in patients with HIV/HCV coinfection. *Hepatology.* 2006;43(6):1317-1325.
334. Alberti KGMM, Eckel RH, Grundy SM, et al. Harmonizing the Metabolic Syndrome. *Circulation.* 2009;120(16):1640-1645.
335. Castera L, Friedrich-Rust M, Loomba R. Noninvasive Assessment of Liver Disease in Patients With Nonalcoholic Fatty Liver Disease. *Gastroenterology.* 2019;156(5):1264-1281.e1264.
336. Casey SP, Kemp WW, McLean CA, Topliss DJ, Adams LA, Roberts SK. A prospective evaluation of the role of transient elastography for the detection of hepatic fibrosis in type 2 diabetes without overt liver disease. *Scandinavian Journal of Gastroenterology.* 2012;47(7):836-841.
337. de Lédinghen V, Vergniol J, Gonzalez C, et al. Screening for liver fibrosis by using FibroScan® and FibroTest in patients with diabetes. *Digestive and Liver Disease.* 2012;44(5):413-418.
338. Ciardullo S, Monti T, Perseghin G. High Prevalence of Advanced Liver Fibrosis Assessed by Transient Elastography Among U.S. Adults With Type 2 Diabetes. *Diabetes Care.* 2020;44(2):519-525.

339. Tuong TTK, Tran DK, Phu PQT, Hong TND, Chu Dinh T, Chu DT. Non-Alcoholic Fatty Liver Disease in Patients with Type 2 Diabetes: Evaluation of Hepatic Fibrosis and Steatosis Using Fibroscan. *Diagnostics.* 2020;10(3):159.
340. Mikolasevic I, Domislovic V, Turk Wensveen T, et al. Screening for nonalcoholic fatty liver disease in patients with type 2 diabetes mellitus using transient elastography - a prospective, cross sectional study. *Eur J Intern Med.* 2020;82:68-75.
341. Lai L-L, Wan Yusoff WNI, Vethakkan SR, Nik Mustapha NR, Mahadeva S, Chan W-K. Screening for non-alcoholic fatty liver disease in patients with type 2 diabetes mellitus using transient elastography. *Journal of Gastroenterology and Hepatology.* 2019;34(8):1396-1403.
342. Roulot D, Roudot-Thoraval F, NKontchou G, et al. Concomitant screening for liver fibrosis and steatosis in French type 2 diabetic patients using Fibroscan. *Liver International.* 2017;37(12):1897-1906.
343. Sagara M, Iijima T, Kase M, et al. Serum levels of soluble dipeptidyl peptidase-4 in type 2 diabetes are associated with severity of liver fibrosis evaluated by transient elastography (FibroScan) and the FAST (FibroScan-AST) score, a novel index of non-alcoholic steatohepatitis with significant fibrosis. *Journal of Diabetes and its Complications.* 2021;35(5):107885.
344. Kim K, Oh TJ, Cho HC, et al. Liver fibrosis indices are related to diabetic peripheral neuropathy in individuals with type 2 diabetes. *Scientific Reports.* 2021;11(1):24372.
345. Targher G, Bertolini L, Rodella S, Lippi G, Zoppini G, Chonchol M. Relationship between Kidney Function and Liver Histology in Subjects with Nonalcoholic Steatohepatitis. *Clinical Journal of the American Society of Nephrology.* 2010;5(12):2166-2171.
346. Papademetriou M, Athyros GV, Geladari E, Doumas M, Tsioufis C, Papademetriou V. The Co-Existence of NASH and Chronic Kidney Disease Boosts Cardiovascular Risk: Are there any Common Therapeutic Options? *Current Vascular Pharmacology.* 2018;16(3):254-268.
347. Schuppan D, Surabattula R, Wang XY. Determinants of fibrosis progression and regression in NASH. *Journal of Hepatology.* 2018;68(2):238-250.
348. Kocabay G, Telci A, Tutuncu Y, et al. Alkaline phosphatase: can it be considered as an indicator of liver fibrosis in non-alcoholic steatohepatitis with type 2 diabetes? *Bratisl Lek Listy.* 2011;112(11):626-629.
349. Singh DK, Sakhuja P, Malhotra V, Gondal R, Sarin SK. Independent predictors of steatohepatitis and fibrosis in Asian Indian patients with non-alcoholic steatohepatitis. *Dig Dis Sci.* 2008;53(7):1967-1976.
350. Sato K, Marzioni M, Meng F, Francis H, Glaser S, Alpini G. Ductular Reaction in Liver Diseases: Pathological Mechanisms and Translational Significances. *Hepatology.* 2019;69(1):420-430.
351. Silverman MG, Ference BA, Im K, et al. Association Between Lowering LDL-C and Cardiovascular Risk Reduction Among Different Therapeutic Interventions: A Systematic Review and Meta-analysis. *JAMA.* 2016;316(12):1289-1297.
352. ClinicalTrials.gov. www.ClinicalTrials.gov Accessed 01/02/2022.
353. Myers RP, Pomier-Layrargues G, Kirsch R, et al. Feasibility and diagnostic performance of the FibroScan XL probe for liver stiffness measurement in overweight and obese patients. *Hepatology.* 2012;55(1):199-208.
354. Hagström H, Nasr P, Ekstedt M, Stål P, Hultcrantz R, Kechagias S. Accuracy of Noninvasive Scoring Systems in Assessing Risk of Death and Liver-Related

Endpoints in Patients With Nonalcoholic Fatty Liver Disease. *Clin Gastroenterol Hepatol.* 2019;17(6):1148-1156.e1144.
355. Tapper EB, Hunink MGM, Afdhal NH, Lai M, Sengupta N. Cost-Effectiveness Analysis: Risk Stratification of Nonalcoholic Fatty Liver Disease (NAFLD) by the Primary Care Physician Using the NAFLD Fibrosis Score. *PLOS ONE.* 2016;11(2):e0147237.
356. Crossan C, Majumdar A, Srivastava A, et al. Referral pathways for patients with NAFLD based on non-invasive fibrosis tests: Diagnostic accuracy and cost analysis. *Liver International.* 2019;39(11):2052-2060.
357. Srivastava A, Gailer R, Tanwar S, et al. Prospective evaluation of a primary care referral pathway for patients with non-alcoholic fatty liver disease. *J Hepatol.* 2019;71(2):371-378.
358. Srivastava A, Jong S, Gola A, et al. Cost-comparison analysis of FIB-4, ELF and fibroscan in community pathways for non-alcoholic fatty liver disease. *BMC Gastroenterol.* 2019;19(1):122.
359. Corey KE, Klebanoff MJ, Tramontano AC, Chung RT, Hur C. Screening for Nonalcoholic Steatohepatitis in Individuals with Type 2 Diabetes: A Cost-Effectiveness Analysis. *Digestive Diseases and Sciences.* 2016;61(7):2108-2117.
360. Noureddin M, Jones C, Alkhouri N, et al. Screening for Nonalcoholic Fatty Liver Disease in Persons with Type 2 Diabetes in the United States Is Cost-effective: A Comprehensive Cost-Utility Analysis. *Gastroenterology.* 2020;159(5):1985-1987.e1984.
361. Serra-Burriel M, Graupera I, Torán P, et al. Transient elastography for screening of liver fibrosis: Cost-effectiveness analysis from six prospective cohorts in Europe and Asia. *Journal of Hepatology.* 2019;71(6):1141-1151.
362. Ivkovic S, Yoon BS, Popoff SN, et al. Connective tissue growth factor coordinates chondrogenesis and angiogenesis during skeletal development. 2003.
363. Baguma-Nibasheka M, Kablar B. Pulmonary hypoplasia in the connective tissue growth factor (Ctgf) null mouse. *Developmental Dynamics.* 2008;237(2):485-493.
364. Crawford LA, Guney MA, Oh YA, et al. Connective tissue growth factor (CTGF) inactivation leads to defects in islet cell lineage allocation and β-cell proliferation during embryogenesis. *Molecular endocrinology.* 2009;23(3):324-336.
365. Williams KH, Shackel NA, Gorrell MD, McLennan SV, Twigg SM. Diabetes and nonalcoholic Fatty liver disease: a pathogenic duo. *Endocr Rev.* 2013;34(1):84-129.
366. Wagner L, Klemann C, Stephan M, von Hörsten S. Unravelling the immunological roles of dipeptidyl peptidase 4 (DPP4) activity and/or structure homologue (DASH) proteins. *Clin Exp Immunol.* 2016;184(3):265-283.
367. Itou M, Kawaguchi T, Taniguchi E, Sata M. Dipeptidyl peptidase-4: a key player in chronic liver disease. *World J Gastroenterol.* 2013;19(15):2298-2306.
368. Nagai N, Klimava A, Lee WH, Izumi-Nagai K, Handa JT. CTGF is increased in basal deposits and regulates matrix production through the ERK (p42/p44mapk) MAPK and the p38 MAPK signaling pathways. *Invest Ophthalmol Vis Sci.* 2009;50(4):1903-1910.
369. Nouchi T, Tanaka Y, Tsukada T, Sato C, Marumo F. Appearance of α-smooth-muscle-actin-positive cells in hepatic fibrosis. *Liver.* 1991;11(2):100-105.

370. Deshmane SL, Kremlev S, Amini S, Sawaya BE. Monocyte chemoattractant protein-1 (MCP-1): an overview. *J Interferon Cytokine Res.* 2009;29(6):313-326.
371. Dyson JK, Anstee QM, McPherson S. Non-alcoholic fatty liver disease: a practical approach to diagnosis and staging. *Frontline Gastroenterology.* 2014;5(3):211-218.
372. van der Poorten D, Samer CF, Ramezani-Moghadam M, et al. Hepatic fat loss in advanced nonalcoholic steatohepatitis: Are alterations in serum adiponectin the cause? *Hepatology.* 2013;57(6):2180-2188.
373. Schile A. Slicing and dicing Cre/lox: part 1. In. *The JAX Blog*: The Jackson Laboratory; 2011.
374. Iredale JP. Tissue inhibitors of metalloproteinases in liver fibrosis. *The International Journal of Biochemistry & Cell Biology.* 1997;29(1):43-54.
375. Iredale JP, Benyon RC, Arthur MJ, et al. Tissue inhibitor of metalloproteinase-1 messenger RNA expression is enhanced relative to interstitial collagenase messenger RNA in experimental liver injury and fibrosis. *Hepatology.* 1996;24(1):176-184.
376. Templeman NM, Skovsø S, Page MM, Lim GE, Johnson JD. A causal role for hyperinsulinemia in obesity. *Journal of Endocrinology.* 2017;232(3):R173-R183.
377. Turu MM, Slevin M, Matou S, et al. C-reactive protein exerts angiogenic effects on vascular endothelial cells and modulates associated signalling pathways and gene expression. *BMC Cell Biology.* 2008;9(1):47.
378. Seino Y, Ogawa A, Yamashita T, et al. Application of NT-proBNP and BNP measurements in cardiac care: a more discerning marker for the detection and evaluation of heart failure. *European Journal of Heart Failure.* 2004;6(3):295-300.
379. Mo F-E, Lau LF. The matricellular protein CCN1 is essential for cardiac development. *Circulation research.* 2006;99(9):961-969.
380. Twigg SM. Mastering a mediator: blockade of CCN-2 shows early promise in human diabetic kidney disease. *J Cell Commun Signal.* 2010;4(4):189-196.
381. Riser BL, Najmabadi F, Perbal B, et al. CCN3 (NOV) is a negative regulator of CCN2 (CTGF) and a novel endogenous inhibitor of the fibrotic pathway in an in vitro model of renal disease. *The American journal of pathology.* 2009;174(5):1725-1734.
382. Fan H, Liu Z, Zhang X, et al. Thyroid Stimulating Hormone Levels Are Associated With Genetically Predicted Nonalcoholic Fatty Liver Disease. *The Journal of Clinical Endocrinology & Metabolism.* 2022;107(9):2522-2529.
383. Martínez-Escudé A, Pera G, Costa-Garrido A, et al. TSH Levels as an Independent Risk Factor for NAFLD and Liver Fibrosis in the General Population. *Journal of Clinical Medicine.* 2021;10(13):2907.
384. Guo Z, Li M, Han B, Qi X. Association of non-alcoholic fatty liver disease with thyroid function: A systematic review and meta-analysis. *Dig Liver Dis.* 2018;50(11):1153-1162.
385. Jaruvongvanich V, Sanguankeo A, Upala S. Nonalcoholic Fatty Liver Disease Is Not Associated with Thyroid Hormone Levels and Hypothyroidism: A Systematic Review and Meta-Analysis. *Eur Thyroid J.* 2017;6(4):208-215.
386. Hagan C. When are mice considered old? In. *The JAX Blog*: The Jackson Laboratory; 2017.

387. Rossmeisl M, Rim JS, Koza RA, Kozak LP. Variation in Type 2 Diabetes-Related Traits in Mouse Strains Susceptible to Diet-Induced Obesity. *Diabetes.* 2003;52(8):1958-1966.
388. World Health Organization. Healthy diet. World Health Organisation. https://www.who.int/news-room/fact-sheets/detail/healthy-diet. Published 2020. Accessed 05/12/2022.
389. Centers for Disease Control and Prevention. Health, United States, 2020-2021: Nutrition. Centers for Disease Control and Prevention. https://www.cdc.gov/nchs/hus/topics/nutrition.htm. Published 2022. Accessed 05/12/2022.
390. Speakman JR. Use of high-fat diets to study rodent obesity as a model of human obesity. *International Journal of Obesity.* 2019;43(8):1491-1492.
391. Wang-Fischer Y, Garyantes T. Improving the Reliability and Utility of Streptozotocin-Induced Rat Diabetic Model. *J Diabetes Res.* 2018;2018:8054073.
392. Su EN, Alder VA, Yu DY, Yu PK, Cringle SJ, Yogesan K. Continued progression of retinopathy despite spontaneous recovery to normoglycemia in a long-term study of streptozotocin-induced diabetes in rats. *Graefes Arch Clin Exp Ophthalmol.* 2000;238(2):163-173.
393. Hartmann K, Besch W, Zühlke H. Spontaneous recovery of streptozotocin diabetes in mice. *Exp Clin Endocrinol.* 1989;93(2-3):225-230.
394. Weiss RB. Streptozocin: a review of its pharmacology, efficacy, and toxicity. *Cancer Treat Rep.* 1982;66(3):427-438.
395. Kume E, Fujimura H, Matsuki N, et al. Hepatic changes in the acute phase of streptozotocin (SZ)-induced diabetes in mice. *Experimental and Toxicologic Pathology.* 2004;55(6):467-480.
396. Banerjee A, Chitnis UB, Jadhav SL, Bhawalkar JS, Chaudhury S. Hypothesis testing, type I and type II errors. *Ind Psychiatry J.* 2009;18(2):127-131.
397. Pomplun D, Florian S, Schulz T, Pfeiffer AF, Ristow M. Alterations of pancreatic beta-cell mass and islet number due to Ins2-controlled expression of Cre recombinase: RIP-Cre revisited; part 2. *Horm Metab Res.* 2007;39(5):336-340.
398. Cre-recombinase-associated toxicity highlights limitations of genome editing. *Disease Models & Mechanisms.* 2013;6(6):1299-1300.
399. Loonstra A, Vooijs M, Beverloo HB, et al. Growth inhibition and DNA damage induced by Cre recombinase in mammalian cells. *Proceedings of the National Academy of Sciences of the United States of America.* 2001;98(16):9209-9214.
400. Huh WJ, Mysorekar IU, Mills JC. Inducible activation of Cre recombinase in adult mice causes gastric epithelial atrophy, metaplasia, and regenerative changes in the absence of “floxed” alleles. *American Journal of Physiology-Gastrointestinal and Liver Physiology.* 2010;299(2):G368-G380.
401. Wicksteed B, Brissova M, Yan W, et al. Conditional gene targeting in mouse pancreatic ß-Cells: analysis of ectopic Cre transgene expression in the brain. *Diabetes.* 2010;59(12):3090-3098.
402. Kelmenson P. Cre Lox Breeding for Beginners, Part 2. In. *The JAX Blog*: The Jackson Laboratory; 2011.
403. Ballestri S, Nascimbeni F, Baldelli E, Marrazzo A, Romagnoli D, Lonardo A. NAFLD as a Sexual Dimorphic Disease: Role of Gender and Reproductive Status in the Development and Progression of Nonalcoholic Fatty Liver Disease and Inherent Cardiovascular Risk. *Advances in Therapy.* 2017;34(6):1291-1326.

404. Burra P, Bizzaro D, Gonta A, et al. Clinical impact of sexual dimorphism in non-alcoholic fatty liver disease (NAFLD) and non-alcoholic steatohepatitis (NASH). *Liver International.* 2021;41(8):1713-1733.
405. Turola E, Petta S, Vanni E, et al. Ovarian senescence increases liver fibrosis in humans and zebrafish with steatosis. *Dis Model Mech.* 2015;8(9):1037-1046.
406. Kamada Y, Kiso S, Yoshida Y, et al. Estrogen deficiency worsens steatohepatitis in mice fed high-fat and high-cholesterol diet. *American journal of physiology Gastrointestinal and liver physiology.* 2011;301(6):G1031-1043.
407. Kim B, Kim YY, Nguyen PT-T, Nam H, Suh JG. Sex differences in glucose metabolism of streptozotocin-induced diabetes inbred mice (C57BL/6J). *Applied Biological Chemistry.* 2020;63(1):59.
408. Cho SG, Kim MY, Kim HJ, et al. Chronic hepatitis: in vivo proton MR spectroscopic evaluation of the liver and correlation with histopathologic findings. *Radiology.* 2001;221(3):740-746.
409. Garbow JR, Lin X, Sakata N, Chen Z, Koh D, Schonfeld G. In vivo MRS measurement of liver lipid levels in mice. *J Lipid Res.* 2004;45(7):1364-1371.
410. Peng XG, Ju S, Qin Y, et al. Quantification of liver fat in mice: comparing dual-echo Dixon imaging, chemical shift imaging, and 1H-MR spectroscopy. *J Lipid Res.* 2011;52(10):1847-1855.
411. Ko S-F, Huang T-H, Lin Y-P, Chen Y-L, Yip H-K. Accuracy and precision of 31P-MRS assessment for evaluating the effect of melatonin-pretreated mitochondria transferring on liver fibrosis of rats. *Melatonin Research.* 2022;5(1):18-33.
412. Information paper: The implementation of the 3Rs in Australia. In: National Health and Medical Research Council; 2019.
413. Yokoi H, Mukoyama M, Nagae T, et al. Reduction in Connective Tissue Growth Factor by Antisense Treatment Ameliorates Renal Tubulointerstitial Fibrosis. *Journal of the American Society of Nephrology.* 2004;15(6):1430-1440.
414. Okada H, Kikuta T, Kobayashi T, et al. Connective Tissue Growth Factor Expressed in Tubular Epithelium Plays a Pivotal Role in Renal Fibrogenesis. *Journal of the American Society of Nephrology.* 2005;16(1):133-143.
415. Guha M, Xu ZG, Tung D, Lanting L, Natarajan R. Specific down-regulation of connective tissue growth factor attenuates progression of nephropathy in mouse models of type 1 and type 2 diabetes. *The FASEB Journal.* 2007;21(12):3355-3368.
416. Luo GH, Lu YP, Song J, Yang L, Shi YJ, Li YP. Inhibition of connective tissue growth factor by small interfering RNA prevents renal fibrosis in rats undergoing chronic allograft nephropathy. *Transplant Proc.* 2008;40(7):2365-2369.
417. Ren Y, Du C, Yan L, et al. CTGF siRNA ameliorates tubular cell apoptosis and tubulointerstitial fibrosis in obstructed mouse kidneys in a Sirt1-independent manner. *Drug Des Devel Ther.* 2015;9:4155-4171.
418. Adler SG, Schwartz S, Williams ME, et al. Phase 1 Study of Anti-CTGF Monoclonal Antibody in Patients with Diabetes and Microalbuminuria. *Clinical Journal of the American Society of Nephrology.* 2010;5(8):1420-1428.
419. ClinicalTrials.gov. Study of FibroGen (FG)-3019 in Subjects With Type 2 Diabetes Mellitus and Kidney Disease on ACEi and/or ARB Therapy (NCT00913393). https://clinicaltrials.gov/ct2/show/NCT00913393. Accessed 12/12/2022.
420. Richeldi L, Fernández Pérez ER, Costabel U, et al. Pamrevlumab, an anti-connective tissue growth factor therapy, for idiopathic pulmonary fibrosis

(PRAISE): a phase 2, randomised, double-blind, placebo-controlled trial. *The Lancet Respiratory Medicine.* 2020;8(1):25-33.
421. ClinicalTrials.gov. Zephyrus I: Evaluation of Efficacy and Safety of Pamrevlumab in Patients With Idiopathic Pulmonary Fibrosis (NTC03955146). https://clinicaltrials.gov/ct2/show/NCT03955146. Accessed 12/12/2022.
422. ClinicalTrials.gov. Zephyrus II: Efficacy and Safety Study of Pamrevlumab in Participants With Idiopathic Pulmonary Fibrosis (IPF) (NTC04419558). https://clinicaltrials.gov/ct2/show/NCT04419558. Accessed 12/12/2022.
423. ClinicalTrials.gov. A Study to Evaluate the Effectiveness and Safety of RXI 109 on the Outcome of Scar Revision Surgery in Healthy Adults (NTC02030275). https://clinicaltrials.gov/ct2/show/NCT02030275. Accessed 12/12/2022.
424. ClinicalTrials.gov. A Study to Evaluate the Effectiveness and Safety of RXI-109 on the Outcome of Keloid Excision Surgery in Healthy Adults (NTC02079168). https://clinicaltrials.gov/ct2/show/NCT02079168. Accessed 12/12/2022.
425. Byrne M, Gagne N, Hafiz G, et al. A Phase 1/2 multidose, dose escalation study to evaluate RXI-109 administered by intravitreal injection to reduce the progression of subretinal fibrosis in subjects with advanced neovascular AMD (NVAMD). *Investigative Ophthalmology & Visual Science.* 2017;58(8):3210-3210.
426. Libertine L, Lewis GP, Luna G, et al. RXI-109 Treatment for Proliferative Vitreoretinopathy (PVR) and other Ocular Disorders. *Investigative Ophthalmology & Visual Science.* 2014;55(13):1120-1120.
427. Uchio K, Graham M, Dean NM, Rosenbaum J, Desmoulière A. Down-regulation of connective tissue growth factor and type I collagen mRNA expression by connective tissue growth factor antisense oligonucleotide during experimental liver fibrosis. *Wound Repair and Regeneration.* 2004;12(1):60-66.
428. Li G, Xie Q, Shi Y, et al. Inhibition of connective tissue growth factor by siRNA prevents liver fibrosis in rats. *The Journal of Gene Medicine.* 2006;8(7):889-900.
429. George J, Tsutsumi M. siRNA-mediated knockdown of connective tissue growth factor prevents N-nitrosodimethylamine-induced hepatic fibrosis in rats. *Gene Therapy.* 2007;14(10):790-803.
430. ClinicalTrials.gov. A Study of FG-3019 in Subjects With Liver Fibrosis Due to Chronic Hepatitis B Infection (NCT01217632). https://clinicaltrials.gov/ct2/show/study/NCT01217632. Accessed 12/12/2022.
431. Choi JS, Kim KH, Lau LF. The matricellular protein CCN1 promotes mucosal healing in murine colitis through IL-6. *Mucosal Immunology.* 2015;8(6):1285-1296.
432. Suda T, Kamimura K, Kubota T, et al. Progress toward liver-based gene therapy. *Hepatology Research.* 2009;39(4):325-340.
433. Yu Q, Xiong X, Zhao L, Xu T, Wang Q. Antifibrotic effects of specific siRNA targeting connective tissue growth factor delivered by polyethyleneimine-functionalized magnetic iron oxide nanoparticles on LX-2 cells. *Mol Med Rep.* 2020;21(1):181-190.
434. Kong WH, Park K, Lee M-Y, Lee H, Sung DK, Hahn SK. Cationic solid lipid nanoparticles derived from apolipoprotein-free LDLs for target specific systemic treatment of liver fibrosis. *Biomaterials.* 2013;34(2):542-551.
435. Resovi A, Borsotti P, Ceruti T, et al. CCN-based therapeutic peptides modify pancreatic ductal adenocarcinoma microenvironment and decrease tumor growth in combination with chemotherapy. *Cells.* 2020;9(4):952.

436. Riser BL, Barnes JL, Varani J. Balanced regulation of the CCN family of matricellular proteins: a novel approach to the prevention and treatment of fibrosis and cancer. *Journal of Cell Communication and Signaling.* 2015;9(4):327-339.